THE UNIVERSITY OF QUEENSLAND

AUSTRALIA

Development of a Composite Layered Double Hydroxide-liposomal System for Gene Delivery

Haiyan Dong

ME, BS

A thesis submitted for the degree of Doctor of Philosophy at

The University of Queensland in 2014

Australian Institute for Bioengineering and Nanotechnology

Abstract

In recent years, gene therapy has attracted much attention in treating a wide range of severe diseases, including cancers. Unfortunately, naked genetic materials are rapidly degraded by the ubiquitous nucleases in the body and their negative charge property hinders crossing cell membrane to the cytoplasm. Thus, an efficient delivery system is urgently sought for desired gene therapeutic efficacy.

Up to date, a wide variety of vectors have been examined for gene delivery, including viral and non-viral ones. Non-viral vectors, including polymers, cell penetrating peptides (CPPs), liposomes, and inorganic nanoparticles (NPs), are clinically promising due to their safety. It is well known that every delivery system has its own unique merits and inherent shortfalls, hence hybrid delivery systems are expected to merge their advantages while avoid their drawbacks.

Inorganic layered double hydroxide (LDH) acts as an excellent drug/gene delivery vehicle due to its protection to the loaded drugs/genes and efficient cellular uptake by various mammalian cells. However, aggregation of LDH NPs in serum or culture medium limits the effective application *in vivo*. On the other hand, liposome is a promising lipid-based system which can protect the hydrophilic genes/drugs in the aqueous core or hydrophobic drugs between the lipid bilayers, and it is colloidally stable in the circulatory blood flow. Unfortunately, its disadvantages are also obvious, such as low transfection efficiency and inefficient endosome escape.

This PhD project aims to develop a hybridised delivery system by forming small LDH (sLDH)-liposome composites. Considering encapsulating LDH NPs in the vesicles of lipid bilayers, small Mg-Al-LDH NPs were first prepared by a non-aqueous method with the *Z*-average diameter size of ~ 40 nm. This method requires co-precipitation of magnesium and aluminium nitrate solution with sodium hydroxide in methanol, followed by LDH slurry collection and re-suspension in methanol. The methanol suspension is then heated in an autoclave, followed by separation via centrifugation and thorough washing with deionised water. The NPs are finally dispersed in deionised water into homogeneous aqueous suspension after 4-6 day standing at room temperature. The prepared sLDH NPs have the *Z*-average size of 35-50 nm, the number-average size of 14-30 nm and the polydispersity index (PdI) of 0.19-0.25, with the colloidal suspension stable for at least 1 month when stored at fridge (2-8 °C) or ambient (22-25 °C) temperature.

Engineered sLDH with the *Z*-average size of ~40 nm and normal LDH with the *Z*-average size of ~100 nm (large LDH, denoted as L-LDH in this thesis) were then compared in transfection efficiency to human colon cancer HCT-116 cells. Using fluorescein Isothiocyanate (FITC) to label LDH NPs and as a model anionic drug (where FITC is intercalated in the interlayers of LDH NPs), we found that 40 nm sLDH and 100 nm L-LDH have the similar cellular uptake rate based on the equivalent particle number concentration, which means in the size range of 35 to 100 nm, LDH NP size does not significantly affect the cellular uptake rate. Note worthily, a critical particle number concentration was found for both sLDH and L-LDH, below which the cellular uptake is in linear proportion to the concentration, while above which, the cellular uptake is not further improved.

When delivering genetic materials to cancer cells (where DNA is adsorbed on the surfaces of LDH NPs), sLDH is far superior to L-LDH at low LDH:DNA mass ratio (e.g. 5:1). This is mainly attributed to full loading of DNA by sLDH and higher sLDH particle number concentration. At the high mass ratio (40:1), where both sLDH and L-LDH can completely bind and protect DNA, sLDHs are able to transport 2-fold DNA to the cells just because of the higher sLDH particle concentration.

Finally, sLDH-liposome composites were prepared by the hydration of freeze-dried matrix (HFDM) method. This composite system exhibits good colloidal stability both in water and in cell culture medium, with the *Z*-average particle size ~ 200 nm, which is appropriate for cellular uptake. It is also proved for the composite system to completely bind/protect DNA at LDH:DNA mass ratio = 20:1, no matter how DNA is loaded in the composite system. About 3-time higher efficiency is observed in delivery of DNA to HCT-116 cells by the sLDH-liposome composite system compared to sLDH only.

In general, the sLDH-liposome composite system shows higher cellular delivery efficiency than either sLDH or liposome only, good colloidal stability and low cytotoxicity, so it could be a promising gene delivery system.

Declaration by author

This thesis is composed of my original work, and contains no material previously published or written by another person except where due reference has been made in the text. I have clearly stated the contribution by others to jointly-authored works that I have included in my thesis.

I have clearly stated the contribution of others to my thesis as a whole, including statistical assistance, survey design, data analysis, significant technical procedures, professional editorial advice, and any other original research work used or reported in my thesis. The content of my thesis is the result of work I have carried out since the commencement of my research higher degree candidature and does not include a substantial part of work that has been submitted **to qualify for the award of any** other degree or diploma in any university or other tertiary institution. I have clearly stated which parts of my thesis, if any, have been submitted to qualify for another award.

I acknowledge that an electronic copy of my thesis must be lodged with the University Library and, subject to the General Award Rules of The University of Queensland, immediately made available for research and study in accordance with the *Copyright Act 1968*.

I acknowledge that copyright of all material contained in my thesis resides with the copyright holder(s) of that material. Where appropriate I have obtained copyright permission from the copyright holder to reproduce material in this thesis.

Publications during candidature

Dong, H.; Chen, M.; Rahman, S.; Parekh, H. S.; Cooper, H. M.; Xu, Z. P. Engineering small MgAl-layered double hydroxide nanoparticles for enhanced gene delivery. *Applied Clay Science* **2014**; 100, 66-75; doi: 10.1016/j.clay.2014.04.028

Dong, H.; Parekh, H. S.; Xu, Z. P. Particle size- and number-dependent delivery to cells by layered double hydroxide nanoparticles. *Journal of Colloid and Interface Science* **2015**, 437, 10-16; doi: 10.1016/j.jcis.2014.09.010

Dong, H.; Parekh, H. S.; Xu, Z. P. Enhanced cellular delivery and biocompatibility of a small layered double hydroxide-liposome composite system; *Pharmaceutics* **2014**, *6*(4), 584-598; doi:10.3390/pharmaceutics6040584.

Chen, M.; Xu, Z. P.; **Dong, H.**; Bartlett, P. F.; Cooper, H. M. Intraventricular delivery of siRNA using layered double hydroxide nanoparticles results in neuronal gene knockdown; Peer-reviewed journal article; Submitted in April 2014.

Dong, H.; Parekh, H. S.; Xu, Z. P. Synthesis of small Mg_3Al-layered double hydroxide (sLDH) nanoparticles; *1st International Conference on BioNano Innovation* (2012); Poster presentation

Dong, H.; Parekh, H. S.; Xu, Z. P. Engineering miniaturised Mg_3Al-layered double hydroxide nanoparticles; *Annual Conference of ARC Centre of Functional Nanomaterials* (2012); Oral presentation

Publications included in this thesis

No publications included

Contributions by others to the thesis

No contributions by others

Statement of parts of the thesis submitted to qualify for the award of another degree

None

Acknowledgements

First of all, I would like to extend my sincerest gratitude to my principal supervisor A/Prof Zhi Ping (Gordon) Xu for his brilliant ideas, excellent guidance and never-ending support during my PhD studies. I also express my grateful thanks to my co-supervisor Dr Harendra (Harry) S. Parekh, for his ideas, suggestions, and encouragement. Particularly, kind and great help from Gordon's wife in my everyday life is genuinely appreciated.

My thanks also go to our centre manager Ms Celestien Warnaar-Notschaele, lab manager Ms Cheryl Berquist, and technician officer Mr Chaoqing Lu for their great help during my PhD studies. I also really appreciate Dr Wenyi Gu from Australian Institute for Bioengineering and Nanotechnology and Dr Jiezhong Chen from School of Biomedical Sciences for providing the cell line and their kind suggestions. I would also acknowledge all my fellow researchers in Gordon's group for their kind assistance and useful discussions: Dr Sophia Gu, Dr Li Li, Dr Peng Li, Dr Annie Zhu, Ms Huali Zuo, Miss Shiyu Yan, Mr Yanheng Wu, Miss Jie Tang, and Mr Weiyu Chen. Special acknowledgements are extended to my friends & colleagues Dr Min Chen from Queensland Brain Institute (previously) and Centre of Advanced Imaging (currently), Dr Cynthia Lin and Dr Meihua Yu from our centre for their kind help and encouragement.

I would like to express my thanks to ARC Centre of Excellence for Functional Nanomaterials (now Nanomaterials Centre), Australian Institute for Bioengineering and Nanotechnology, Centre for Microscopy and Microanalysis at the University of Queensland, for providing the research facilities and assistance. My grateful thanks are also extended to the University of Queensland for the UQ International scholarship (Tuition), China Scholarship Council (CSC) scholarship, and AIBN group leader living allowance scholarship for the financial support.

Finally, I would love to show respect and appreciation to my parents and my brother, from my heart, for their everlasting love, support, and encouragement during the whole course of my PhD life. Special thanks go to my previous supervisor Prof Guangren Qian at Shanghai University, for all his help and encouragement.

Keywords

small layered double hydroxide, liposome, composite, cellular delivery

Australian and New Zealand Standard Research Classifications (ANZSRC)

ANZSRC code: 100703, Nanobiotechnology, 40%

ANZSRC code: 100708, Nanomaterials, 30%

ANZSRC code: 100709, Nanomedicine, 30%

Fields of Research (FoR) Classification

FoR code: 1007, Nanotechnology, 100%

Table of Contents

List of Figures

List of Tables

List of Abbreviations used in the thesis

5ASA	5-aminosalicylic acid
5-Fu	Fluorouracil (5-Fluoro-1*H*,3*H*-pyrimidine-2,4-dione)
AMP	Adenosine-5´-monophosphate
APTMS	(3-aminopropyl) trimethoxy silane
asODNs	Antisense Oligodeoxyonucleotides
ATP	Adenosine triphosphate
ATRP	Atom Transfer Radical Polymerization
Au NPs	Gold Nanoparticles
CADY	a secondary amphipathic peptide
CaP	Calcium Phosphate
CCL	Coated Cationic Liposome
CD siRNA	Cell Death siRNA
CHT	Chitosan
CMCDs	Carboxymethyl-β-cyclodextrins
CMP	Cytidine-5´-monophosphate
CNTs	Carbon Nanotubes
CPPs	Cell-Penetrating Peptides
CPT	Camptothecin
CTAB	Cetyltrimethylammonium Bromide
DA	Deoxycholic Acid
DBCs	DNA Block Copolymers
DI water	Deionised water
DLS	Dynamic Light Scattering
DMAEMA	2-(dimethylamino)-ethyl Methacrylate
DMEM	Dulbecco's Modified Eagle Medium
DMFL	Dextran-magnetic Layered double hydroxide-fluorouracil Liposome
DMSO	Dimethyl Sulfoxide
DOPA	1,2-dioleoyl-*sn*-glycero-3-phosphate(sodium salt)
DOTAP	1,2-dioleoyl-3-trimethylammonium-propane (chloride salt)
DOX	Doxorubicin
DPBS	Dulbecco's phosphate-buffered saline
dsDNA	double stranded DNA
dsRNA	double stranded RNA

EA	Elemental Analysis
EGFP	Enhanced Green Fluorescent Protein
ELP	Elastin-Like Polypeptide
EPC	L-α-phosphatidylcholine (Egg, Chicken)
EPR	Enhanced Permeability and Retention
FA	Folic Acid
FACS	Fluorescence Activated Cell Sorting
FBS	Fetal Bovine Serum
FITC	Fluorescein Isothiocyanate
FTIR	Fourier Transform Infrared spectroscopy
FWHM	Full Width at Half Maximum
GM1	Monosialoganglioside
GMP	Guanosine-5´-monophosphate
GSH	Glutathione
HCC	Hepatocellular Carcinoma
HFDM	Hydration of Freeze Dried Matrix
HTlcs	Hydrotalcite-like Compounds
HTLF	Hydration of Thin Lipid Film
IAA	Indole-3-Acetic Acid
ICP-AES	Inductively Coupled Plasma-Atomic Emission Spectrometry
IO NPs	Iron Oxide Nanoparticles
LAP	Lapachone
LDH	Layered Double Hydroxide
L-LDH	Large LDH
LMWH	Low Molecular Weight Heparin
LUV	Large Unilamellar Vesicle
MLVs	Multi-lamellar Vesicles
MPEG	Methoxy PEG
MRI	Magnetic Resonance Imaging
MSNs	Mesoporous Silica Nanoparticles
MTT	3-(4,5-Dimethylthiazol-2-yl)-2,5-Diphenyltetrazolium Bromide
MWNTs	Multi-Walled Nanotubes
NGR	Asn-Gly-Arg
NPs	Nanoparticles
NSAID	Non-steroid-anti-inflammatory Drug

ODNs	Oligonucleotides
OVA	Ovalbumin
PAE	Poly(β-Amino Ester)
PAMAM	Polyamidoamine
PCL	Poly(ε-Caprolactone)
PCS	Photon Correlation Spectroscopy
PCT	Pectin
PDA	Parenteral Drug Association
PEG	Polyethylene Glycol
PEI	Polyethyleneimine
PFA	Paraformaldehyde
PLGA	poly(lactide-co-glycolide) or poly(lactic-co-glycolic acid)
PPI	Polypropylenimine
PPO	Polypropyleneoxide
PTX	Paclitaxel
RBF	Round Bottom Flask
RES	Reticuloendothelial System
RGD	Arg-Gly-Asp
RISC	RNA-Induced Silencing Complex
SEM*	Scanning Electron Microscopy
SEM**	Standard Error of the Mean
SiO_2	Silica
siRNA	small interfering RNA
sLDH	small Layered Double Hydroxides
SMC	Smooth Muscle Cell
SUVs	Small Unilamellar Vesicles
SWNTs	Single-Walled Nanotubes
TAF	Tamoxifen
TBA	Tertiary Butyl Alcohol
TBE	Tris/Borate/EDTA
TEA	Triethanolamine
TEM	Transmission Electron Microscopy
XRD	X-ray Diffraction

Chapter 1 Introduction

1.1 Background

Gene therapy uses genetic material(s) as drug(s) to treat a wide range of severe diseases, genetic disorder/deficiency related diseases, or cancers. A growing body of evidences have proved the effectiveness and efficacy of gene therapy in breast cancer, colon cancer, prostate cancer, cardiovascular disease, immune deficiencies, neurological disorders, Alzheimer's disease, Parkinson's disease, and Huntington's disease. Unfortunately, the success of gene therapy relies on a safe and efficient vector because of various extracellular and intracellular barriers for naked genetic drugs.

So far, a broad spectrum of vectors has been developed for gene delivery, including viral and non-viral ones. Viral vectors are highly efficient due to their native properties, but they are suffering from safety concerns. Non-viral vectors are generally categorised into organic and inorganic ones. Organic vectors include polymers, liposomes, cell penetrating peptides, and inorganic vectors involve metal and metal oxide nanoparticles (NPs), carbon nanotubes, mesoporous silica NPs, calcium phosphate NPs, and layered double hydroxide (LDH) NPs. Each pure system has its own advantages along with its drawbacks, so hybridisation systems have been widely developed and proved to merge the merits from two or more worlds, while overcoming their limitations.

1.2 Research hypothesis and specific objectives

Inorganic layered double hydroxide (LDH) nanoparticles (NPs) have been well developed for drug and gene delivery. LDH NPs are easily prepared in the lab by co-precipitation of mixed salt solution with certain ratio of sodium hydroxide followed by purification, with tailored particle size, high loading capacity and protection for the payload. They also have beneficial properties such as low cytotoxicity, efficient cellular uptake, controlled cargo release and endosome escape. Unfortunately, the aggregation of LDH NPs in serum/blood circulation is a big hurdle for its *in vivo* application.

On the other hand, liposomes are colloidally stable in blood circulation especially after modified by poly(ethylene glycol) (PEG), and they are the most biocompatible organic delivery vehicles for genes and drugs because it consists of cell membrane constitutes lipids, protects hydrophilic drugs and genetic materials in the aqueous core of liposomal

vesicles, hydrophobic drugs between the lipid bilayers. Unfortunately, inefficient endosome escape is a crucial drawback for liposomes as an excellent delivery system.

Therefore, we hypothesised to develop a hybridised LDH-liposome composite system by combining the advantages of LDH NPs for high transfection efficiency, low toxicity, good safety, rapid endosome escape, efficient and controlled release of the payload, and liposomes for good colloidal stability, while avoiding their downsides by LDH NPs for aggregation, and liposomes for inefficient endosome escape and cargo release.

To achieve the overall aim stated above, the specific stage-by-stage objectives for this project are:

[1] to develop a procedure for preparing small LDH (sLDH) NPs (*Z*-average diameter size ~ 30 to 50 nm) i.e. ≈1/3 to 1/2 the size of normal LDH NPs (*Z*-average size ~ 100 - 110 nm, denoted as large LDH, L-LDH in this thesis, compared to sLDH), which is appropriate to be encapsulated inside the liposomal vesicles;

[2] to compare the gene loading capacity and delivery efficiency between sLDH and L-LDH NPs, and explore how the LDH particle size affects the cellular delivery;

[3] to prepare LDH-liposome composite and then assess its suspension stability, gene loading capacity, and gene delivery efficiency.

1.3 Thesis outline

Following the specified objectives, the whole thesis is composed of seven chapters and one appendix; each being briefly introduced below.

Chapter 1 is the general introduction. Here, the necessity of developing gene delivery vectors is stated, and then the research hypothesis and specific objectives are presented, followed by the detail thesis structure.

Chapter 2 reviews the recent advances in gene delivery systems, including categories of vectors and their advantages along with drawbacks, strategies to overcome the drawbacks and improve/enhance gene delivery efficiency. Among them, hybridisation of two or more pure systems for a multifunctional composite system is a new research direction which merges the merits from all separate systems, while overcomes their limitations. This

chapter ends with a summary for these delivery systems and further brings forward the project hypothesis.

Chapter 3 is a summary for the materials and the general methods used in this thesis, including some characterisation techniques.

Chapter 4 states the synthesis of small LDH nanoparticles (NPs) by a non-aqueous co-precipitation method, followed by hydrothermal treatment and washing, natural dispersion. Finally obtained well-dispersed sLDH NPs suspension possesses a *Z*-average diameter size ~ 40 nm with narrow size distribution. A wide range of parameters are examined to explore their effects on sLDH particle size and suspension dispersion. Moreover, the mechanism for sLDH NPs formation via non-aqueous co-precipitation method is proposed.

Chapter 5 compares the cellular delivery efficiency of small LDH (sLDH) and large LDH (L-LDH) NPs. Particle size in the range of 35 ~ 100 nm does not obviously affect the cellular uptake rate of LDH NPs, while sLDH NPs show improved gene delivery efficiency because they possess larger specific surface area than L-LDH NPs. The gene materials are mainly adsorbed on the surface of LDH NPs via electrostatic interaction. Meanwhile, at the same mass ratio to genetic materials, sLDH NP suspension exhibits much higher particle number concentration, which is proved to be critical for cellular uptake.

Chapter 6 examines the suspension stability, nucleic acid loading, and cellular delivery efficiency of the LDH-liposome composite system prepared by the hydration of freeze-dried matrix (HFDM) method. LDH-liposome composites possess narrow size distribution with *Z*-average diameter size ~ 200 nm, which is proper for cellular uptake and is determined to be stable in serum. The nucleic acids are fully immobilised by the composite system no matter how nucleic acids are loaded in the system. The sLDH-liposome composite system shows 2-3 times improved cellular delivery efficiency than sLDH, while L-LDH-liposome exhibit no difference from L-LDH only, which might imply encapsulation of sLDH NPs inside liposomal vesicles, but not for L-LDH NPs.

Chapter 7 gives the final conclusions and the future directions following this thesis. More efforts could be dedicated for investigating the mechanisms for sLDH-liposome composite formation, which would guide to develop new method(s) or formulations to further improve the encapsulation efficiency of sLDH in the composite. The cellular uptake behaviour and endosome escape pathway of this composite system could also be explored; this would pave a way for further enhancing the cellular delivery. Following modification of the

composite system such as PEGylation or linking targeting ligands could be considered for better stability in blood circulation and targeting delivery of genetic materials. Combination therapy could be developed for the new composite system, loading hydrophilic anionic drugs or genes by LDH, and carrying hydrophobic drugs by liposomes. Functional gene therapeutic materials such as functional siRNA could be attempted for the practical application of this new delivery system.

Chapter 2 Literature Review

2.1 Introduction

Although gene therapy has proved to be superior to traditional chemotherapy for some severe diseases, cancers, and genetic deficiency related diseases, its therapeutic efficiency is highly dependent on a safe and efficient delivery vehicle. Vectors developed so far are divided into two major categories, viral vectors and non-viral vectors.

Generally, viral vectors can deliver genetic materials into the targeted cells with high transfection efficiency due to their naturally evolved property, overcoming cellular barriers easily. Normal viral vectors include adenovirus, retrovirus, and lentivirus (Figure 2-1).

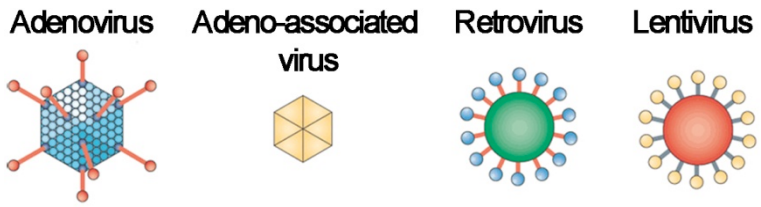

Figure 2-1 Viral vectors for gene therapy, reproduced from Ref. 1

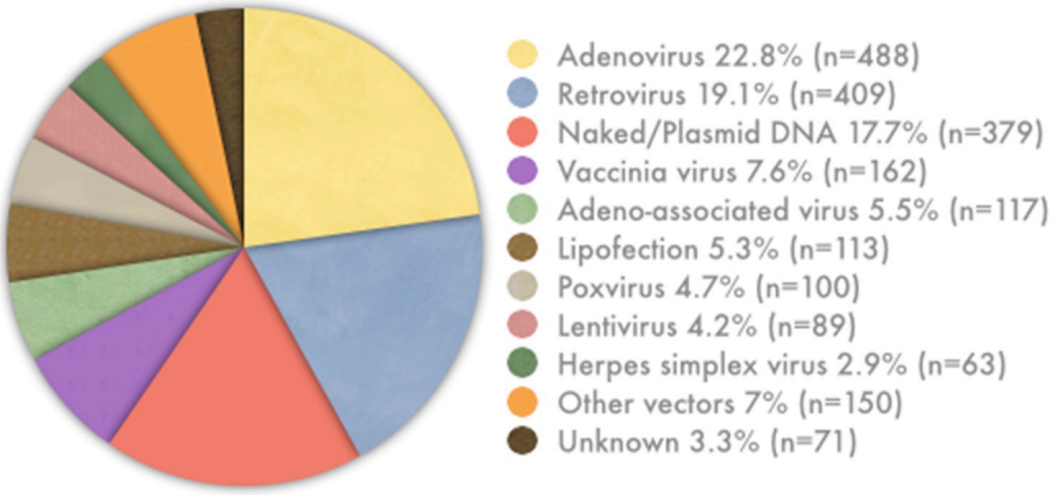

Figure 2-2 Vectors used in gene clinical trials, The journal of Gene Medicine ©2014 John Wiley and Sons Ltd, www.wiley.co.uk/genmed/clinical

Moreover, most of the approved gene therapy clinical trials are using viral vectors (Figure 2-2). However, they have major drawbacks. Viruses can be cleared in the blood-stream by

pre-existing antibodies and can activate complement or coagulation factors. They can also induce neutralising antibody responses that prevent repeated administration. Dys-regulation of gene expression in the target cell by insertion is a major safety issue, and some viruses integrate only in dividing cells.[2] Substantial safety concerns are also resulted from their high risk for immunogenic responses and mutagenicity, viral vectors therefore should be restricted strictly in the clinical practice.

Non-viral vectors are good alternatives to viral ones for their safety, simplicity and capacity for packing large nucleic acids. They are studied extensively in recent decades as they are non-immunogenic, non-mutagenic, and easy for scale-up production. Generally, non-viral vectors can be categorised into organic and inorganic systems.

2.2 Organic vectors with a wide range of variety

Normally used organic materials for gene delivery include polymers, dendrimers, liposomes, cell penetrating peptides, etc.

2.2.1 Polymers

Polymers are the most investigated organic materials for drug/gene delivery. The most widely used polymers such as PLGA (poly(lactide-*co*-glycolide) or poly(lactic-*co*-glycolic acid)), PEI (polyethyleneimine), PEG (polyethylene glycol), chitosan, and their hybrids, had been applied for delivering a broad range of drugs, microRNA, and small interfering RNA (siRNA), as reviewed by Devulapally and Paulmurugan recently.[3]

PLGA is a biodegradable and biocompatible polymer, which has been approved by FDA (Food and Drug Administration). PLGA has been widely used for drug delivery due to its low systematic toxicity and immune-modulatory effects, because it is rapidly hydrolysed in the body to biodegradable monomers lactic acid and glycolic acid (Figure 2-3).[3] Most chemotherapeutic drugs are also toxic to the healthy cells, tissues, and organs, but by encapsulating the drugs using PLGA-based NPs, the adverse effects of chemotherapeutic drugs can be avoided.

PEGylated PLGA nanoparticles (NPs) are one of the most popular polymer hybrids for drug and gene delivery. By PEGylation, the drugs/genes encapsulation, complexes circulation time, and bioavailability are improved, because PLGA polymers are

hydrophobic, but PEG is well-established hydrophilic. Hydrophilic PEG also protects the complexes from the immune clearance.

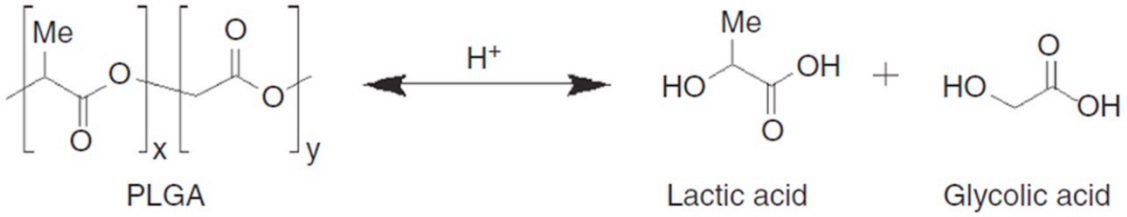

Figure 2-3 Hydrolysis of PLGA in the body into biodegradable lactic acid and glycolic acid, reproduced from Ref. 3

Another widely studied polymer is PEI, which is also considered with highest gene transfection efficiency. PEI was firstly used as gene delivery in 1995 by Boussif et al.[4] It is an organic macromolecule with the highest cationic-charge-density potential. This property provides PEI to condense and compact DNA into tight complexes, so that DNA is protected from degradation. The amino group (-NH-) in the PEI chain (Figure 2-4) can be protonated, which renders PEI a substantial buffering capacity at any virtual pH, provides PEI-DNA complexes an escape mechanism via endosomal/lysosomal swelling and rupture, so called 'proton sponge' effect. Figure 2-4 shows the diagram for linear and branched PEI structures, formation of PEI-gene materials complexes, surface modifications of PEI-based complexes for targeted delivery. Boussif et al. also found the cytotoxicity of PEI was low and only noted well above the required concentrations for optimal transfection. Since then, PEI has been widely used as gene delivery vectors.[5-9] After the superiority of siRNA has been recognised, PEI has also been quickly used for siRNA delivery.[10-12]

Cytoplasmic delivery of siRNA after endocytosis of the particles is achieved through the 'proton sponge' effect of PEI, which results in endosomal rupture. While any rupture or leakage of the endosomal or lysosomal membrane will lead to cell stress, inflammasome activation associated with apoptosis, which precludes prolonged use of PEI *in vivo*. In general, PEI-RNA complexes accumulate in the liver, lung, spleen and kidney, limiting their utility for other tissues.

Chitosan is another commonly used polymer for drug/gene delivery, which is a positively charged, biodegradable, linear polysaccharide composed of β-(1-4)-linked D-glucosamine (deacetylated unit) and N-acetyl-D-glucosamine (acetylated unit) (Figure 2-5). The primary

amines on it become protonated at pH<8.5, which is beneficial for binding nucleic acids and endosomal escape of chitosan-nucleic acid complexes through 'proton-sponge' effect.

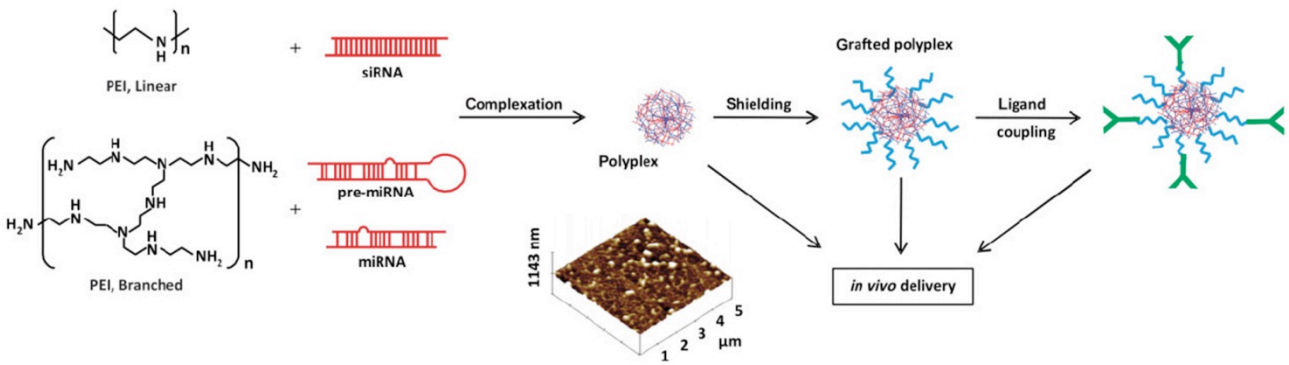

Figure 2-4 Schematic illustration of PEI structures, complex formation, and surface modifications, reproduced from Ref. 13

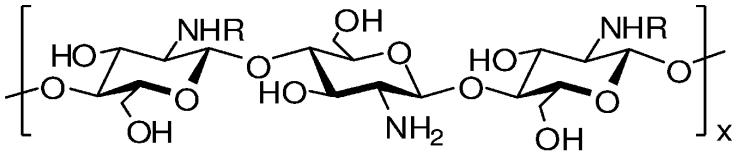

R = H or $COCH_3$

Figure 2-5 Chemical structure of chitosan

Chitosan was introduced for siRNA delivery by Alpar's group and Howard's group because of its low toxicity, biodegradability and biocompatibility.[14, 15] Howard's group also found that the physicochemical properties (size, zeta potential, morphology and complex stability) are strongly dependent on the chitosan molecular weight and degree of deacetylation, which affect the *in vitro* gene silencing of chitosan/siRNA nanoparticles.[16]

Recently, combination of polymeric materials has been intensively explored for improved therapeutic efficacy. For instance, MPEG-PLA-PAE copolymer (methoxy PEG-PLA-poly(β-amino ester)) was found to be more stable in plasma than MPEG-PLA micelles, with improved cellular uptake by MCF-7 cells, longer circulation time, and enhanced tumour growth inhibition with anticancer drug curcumin.[17] It has also been reported that hy-PEI-PCL-mPEG copolymers (mono-methoxyl-poly(ethylene glycol)-block-poly(ε-caprolactone) (mPEG-PCL) modified hyperbranched PEI copolymers) exhibits higher stability and reduced zeta-potential for siRNA polyplexes.[18]

Besides biodegradability of polymeric materials, which saves post-treatment clearance of polymeric NP waste, ease of surface modification is another superior property for polymeric NP drug delivery system, such as addition of pH/thermal/GSH (glutathione) sensitive linker for external stimuli cargo release or addition of targeting ligand for active targeting delivery. Modification of polymeric nanocarrriers by RGD (Arg-Gly-Asp)- and NGR (Asn-Gly-Arg)-based oligopeptides/HIV-1 Tat peptides/folate/ hyaluronic acid can realise the active targeting to tumour blood vessels.[20-23]

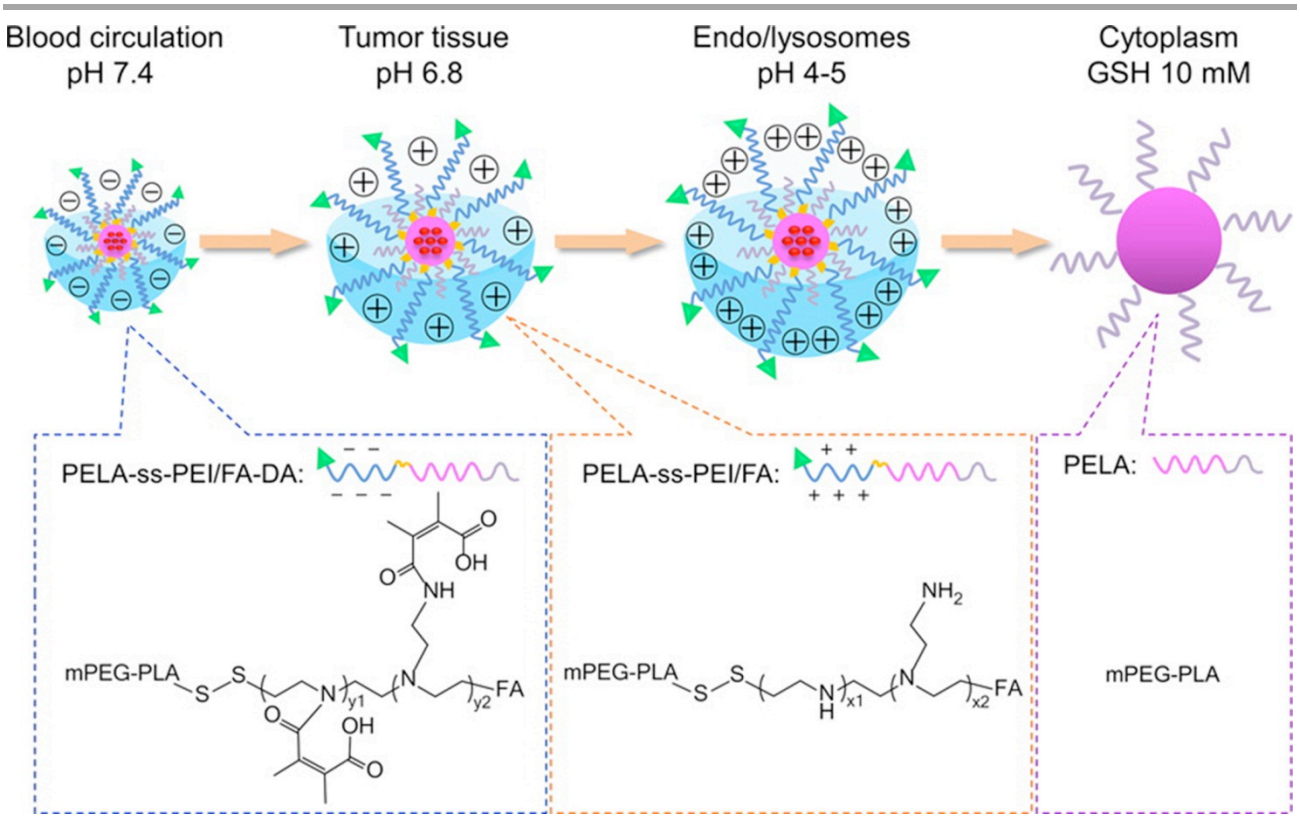

Figure 2-6 Schematic illustration of charge reversal of dual-responsive polymer micelles for tumour extracellular matrix and intracellular GSH-triggered drug release, reproduced from Ref. 19

More complicated delivery systems have been designed by combining external stimuli release with active targeting. For example, Guo et al.[19] developed dual-responsive copolymer micelles with disulphide linker, sheddable PEI and targeting ligand folic acid (FA). The system exhibits prolonged circulation time because of the originally negatively charged surface, and it is ultrasensitive to the tumour extracellular pH with reverse charge property, which greatly enhances cellular uptake via electrostatic interactions. At the same time, the active targeting property of the micelles with FA further improves the selective uptake by the cancer cells. Once the micelles escape from endosome/lysosome, the

disulphide linkage can be cleaved by GSH (glutathione) in the cytoplasm, causing rapid release of encapsulated agent to the nuclei. The charge reversal of this system in tumour extracellular pH condition, and the cleavage of disulphide linkage causing encapsulated agent release are illustrated in Figure 2-6.

Although polymers have shown their capability and advantages in drug/gene delivery because of biodegradability, protection of drugs/genes, accumulation of polymeric NP-drug/gene complexes in tumour sites via enhanced permeability and retention (EPR) effect, ease of surface modification for active targeting, the cytotoxicity of polymeric NP still needs further investigation and strategies to alleviate the toxic property of polymeric NP are still needed to be explored. Schäfer et al.[24] assessed a broad range of lipids modified low molecular weight PEI25 based nucleic acid polyplexes and found that introduction of negative, rigid lipids into polyplexes leads to increased transfection, which is attributed to the enhancement of clathrin-dependent internalisation. Moreover, introduction of liposome to polyplexes decreases the toxicity of polyplexes.

2.2.2 Dendrimers

Dendrimers are a class of globular nano-sized (1-100 nm) macromolecules with a particular ‘tree-like’ highly branched three-dimensional architecture. Different from linear polymers, dendrimers possess precisely controlled architecture with tailor-made surface groups, which can be finely tuned and modified. Figure 2-7 shows the types and chemical structures of different dendrimers. Of them, the most used dendrimers are PAMAM (polyamidoamine) dendrimer and PPI (polypropylenimine) dendrimer.

Dendrimers can be applied in gene delivery field because they are able to condense and compact gene materials to form polyplexes/dendriplexes, so as to protect genetic materials. Triethanolamine (TEA)-core PAMAM denderimer was reported to successfully deliver siRNA to a prostate cancer model *in vitro* and *in vivo*, resulting in potent gene silencing and notable anticancer effect.[25]

Various modifications have been explored by researchers to improve the transfection efficiency of dendrimers while reduce the cytotoxicity. It has been reported that disulphide cross-linked PAMAM dendrimers show improved transfection efficiency and low cytotoxicity, which is comparable to commercial branched PEI.[26] Fluorinated PPI dendrimers have comparable or superior transfection efficacies to six representative

transfection reagents. Moreover, these fluorinated PPI dendrimers exhibit low cytotoxicity on the transfected cells because they achieve excellent transfection at extremely low N/P ratios.[27, 28] Oligoamine linker modified PAMAM dendrimers exhibit significantly improved transfection with low cytotoxicity, and the following siRNA delivery results in ~73% suppression of the target gene.[29]

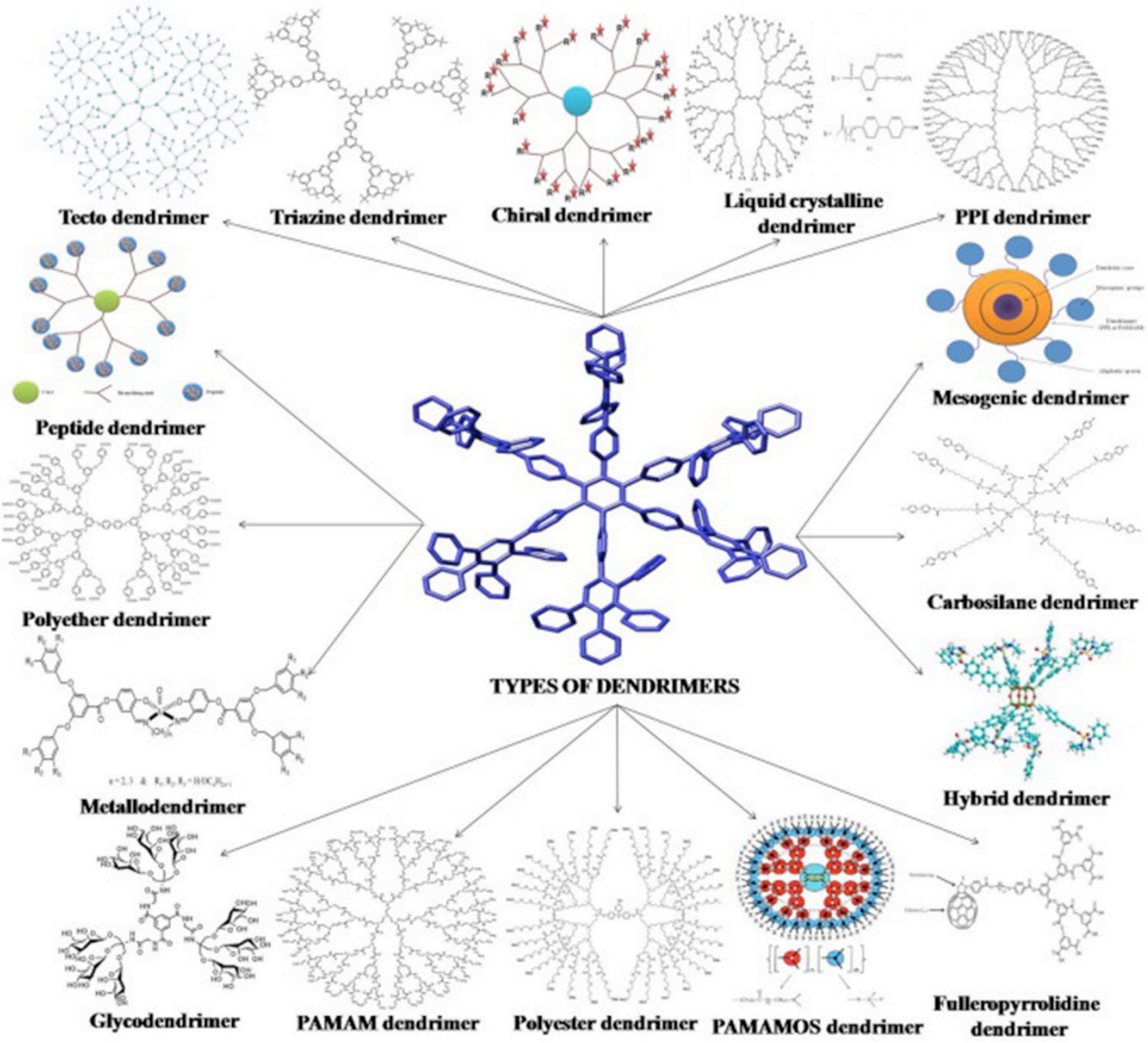

Figure 2-7 Different types of dendrimers, reproduced from Ref. 30

Conjugation with peptide or other NPs has also been explored for improved therapeutic efficacy or for target delivery. For example, arginine, cyclodextrin, PEG conjugated dendrimers showed enhanced transfection efficiency.[31-35] Peptide conjugated dendrimers allow for target delivery of genetic materials.[36-38] Dendrimers with entrapped gold NPs (Au NPs) have significantly higher transfection efficiency than dendrimers only.[39]

2.2.3 Cell-penetrating peptides (CPPs)

Cell penetrating peptides (CPPs) are another class of organic biomolecules (mostly positively charged) which have been used as non-viral vectors. They are a class of short peptides (typically with 5-30 amino acids), which differ from other peptides with specific feature to enter cells via various mechanisms: energy dependent endocytosis (including macropinocytosis, clathrin-dependent endocytosis, caveolae/lipid raft-mediated endocytosis, andclathrin/caveolae-independent endocytosis) and energy independent direct translocation across the membrane bilayer (through toroidal/barrel-stave poremodel or carpet model). The CPP cell entry pathways are summarised in Figure 2-8.

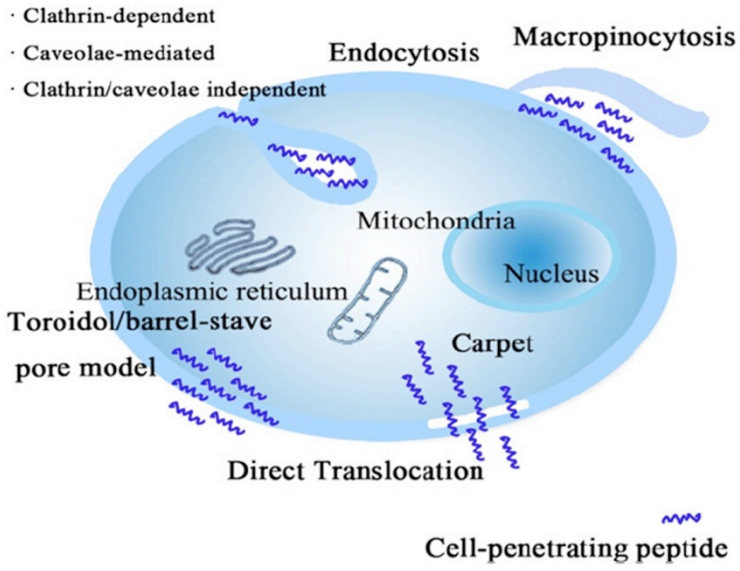

Figure 2-8 Cell entry pathways of cell penetrating peptides, reproduced from Ref. 40

The positive charge property of cationic CPPs renders the spontaneous interaction and complexation between CPPs and gene materials, which enables autonomously cross the plasma membrane and then facilitates the cellular uptake. Since their discovery in 1988, CPPs have been widely used as vectors for siRNA,[41-44] nucleic acid,[45] small molecule therapeutic agents,[46] proteins,[47] QDs,[48] and MRI contrast agents.[49] For example, Crombez et al.[41] designed a secondary amphipathic peptide (CADY) for siRNA delivery, and found CADY forms stable complexes with siRNA, with increased stability and improved cellular delivery. Moreover, CADY mediated siRNA delivery leads to significant knockdown of the target gene at both the mRNA and protein levels and the CADY is proved to be nontoxic. Hoyer and Neundorf[44] demonstrated that CPPs can effectively transport siRNA into HEK-293 and MCF-7 cell lines without inducing cytotoxicity, knocking down the expression of a

G-protein-coupled receptor, the human neuropeptide Y Y1 receptor. The knockdown rates are comparable to those obtained by lipofection. This offers a potential therapy for Y1 receptor disorder, such as osteoporosis.

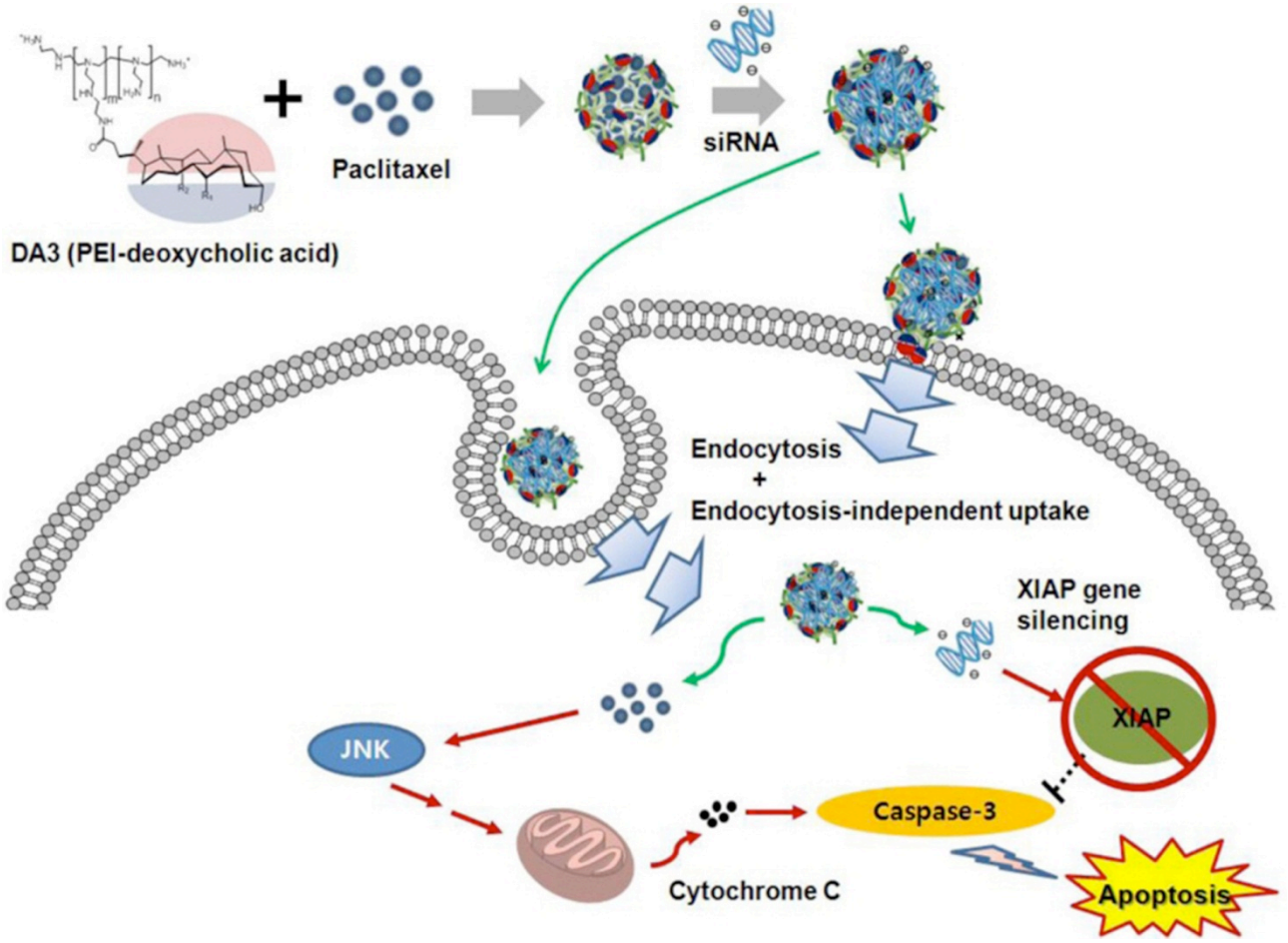

Figure 2-9 Cell penetrating peptide mimicking polymer for codelivery of anticancer drug and siRNA, reproduced from Ref. 50

On the other hand, CPP-modified/functionalised pH-sensitive and thermally sensitive carriers are also extensively explored for drug delivery. For instance, Cohen et al.[51] functionalised acid-degradable polyacrylamide particles with polyarginine CPPs, and found improved cellular uptake by non-phagocytic cells. Walker et al.[52] conjugated three different CPPs to a thermally responsive macromolecular carrier elastin-like polypeptide (ELP), and found clearly enhanced cellular uptake.

More interestingly, Jang et al.[50] synthesised a CPP mimicking conjugate of deoxycholic acid and low molecular weight PEI (DA3) for codelivery of anticancer drug paclitaxel and siRNA, and found higher target gene silencing efficiency with enhanced cancer cell growth

inhibition and tumour growth suppression. Figure 2-9 illustrates the complexes of DA3 with siRNA and paclitaxel taken up by cells via endocytosis and endocytosis independent cell membrane translocation, followed by enhanced inhibition of cancer cells and gene silencing.

2.2.4 Liposomes

Liposomes are artificially-made lipid bilayer vesicles, which was firstly observed and described by Bangham.[53, 54] When Bangham and Horne were testing the institute's new electron microscope by adding negative stain to dry phospholipids, they noticed the lamellar structures formed spontaneously which can sequester solutes. Specifically, when lipids are exposed to excess water or in an aqueous system, the polar heads of lipids align towards the polar, aqueous environment, while the hydrophobic tails minimize their contact with water and tend to cluster together, forming vesicles. Depending on the lipid concentration, this biophysical interaction may result in the formation of micelles, liposomes, where liposomes are lipid bilayer spheres in water or solution with entrapped water or solution inside. Additionally, there can be some reverse micelles formed when lipids are exposed to the mixture of organic solvent or solution.

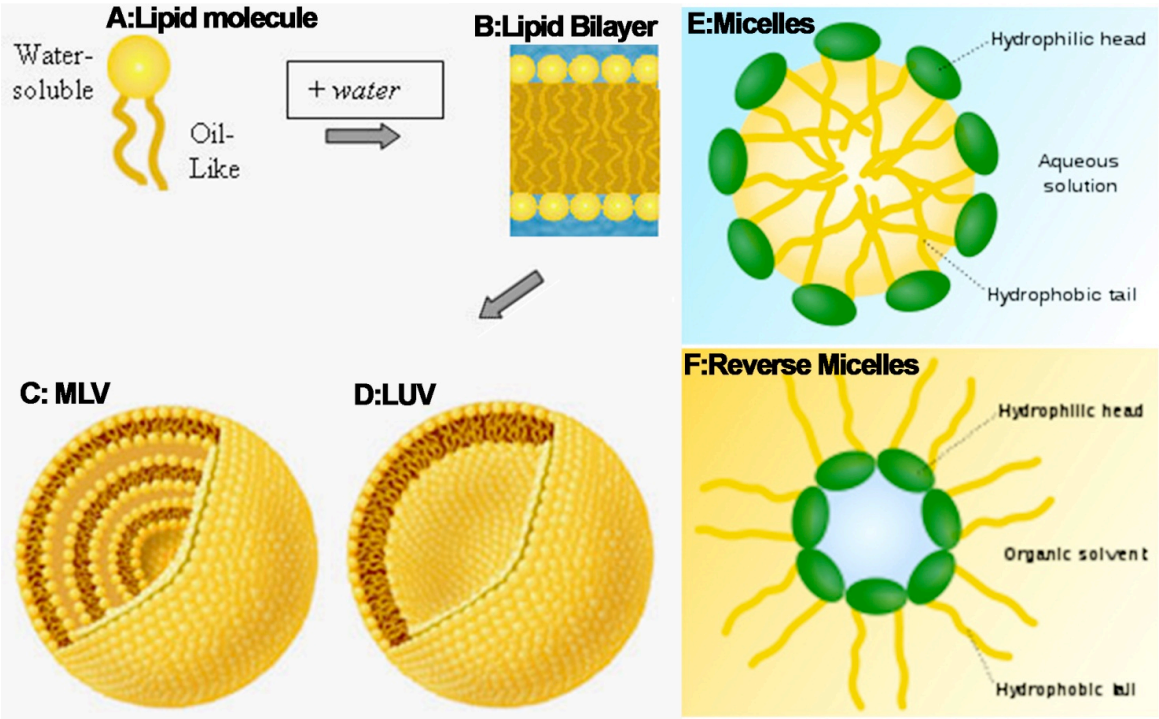

Figure 2-10 Schematic structures of lipid molecule (A), lipid bilayer (B), multilamellar large vesicle (MLV, C), large unilamellar vesicle (LUV, D), micelle (E), and reverse micelle (F)

Liposomes can be classified into multilamellar large vesicle (MLV), large unilamellar vesicle (LUV) and small unilamellar vesicle (SUV) according to their particle size and number of lamellae. MLVs are normally hetereogeneous, with size ranging from 400 to 3500 nm in diameter. LUVs generally range from 200 to 1000 nm with the largest entrapment volume and the highest encapsulation efficiency. SUVs are in the range of 25 to 100 nm with the most uniform size distribution, which can be attained from MLVs and LUVs by size reduction process (such as ultrasonication, gas extrusion). Figure 2-10 shows the schematic structures of lipid molecule, lipid bilayer, liposomes, micelles, and reverse micelles.

Liposomes are composed of natural cell membrane constituents and can be re-utilised by the body as fuel,[55] thus they are biocompatible with non- or very weak immunogenic and intrinsic toxicity. In the past decades, liposomes are widely used for drug delivery for their wide variety of compositions, reduced cytotoxicity compared to viral vectors, well-defined structure compared to linear polymers, narrow size distribution for cellular uptake, high entrapment efficiency for drugs, extended circulation lifetime by PEGylation,[56, 57] accumulation at regional sites,[58] surface-associated targeting,[59, 60] ease for large-scale, and cost-effective artificial synthesis aseptically. The evolution of liposomes are shown in Figure 2-11. However, liposome still faces a few stability issues. Its chemical stability is not high because of hydrolysis of ester bond or oxidation of unsaturated acyl chains. Physically, drug molecules are likely to leak from vesicles and vesicles to aggregate or fuse to larger particles. Furthermore, the endosomal escape mechanism of liposome via forming ion pairs with anionic phospholipids within the endosomal membrane,[61] which is less efficient than the ‘proton sponge’ effect of PEI.

Incorporation of dendrimer in liposome has been found to improve the drug entrapment while slow the release rate, leading to improved therapeutic efficacy.[63, 64] Liposomes coated with synthetic pH/temperature sensitive peptides could release the contents in response to pH/temperature change.[65] pH-sensitive polymer modified liposomes has been explored as antigen delivery carriers for cancer immunotherapy. The modified liposomes are found to be taken up efficiently by dendritic cells, and they are stable at neutral pH, but destabilised in response to acidic pH. With loaded ovalbumin (OVA), the tumour growth is significantly suppressed in mice model.[66, 67]

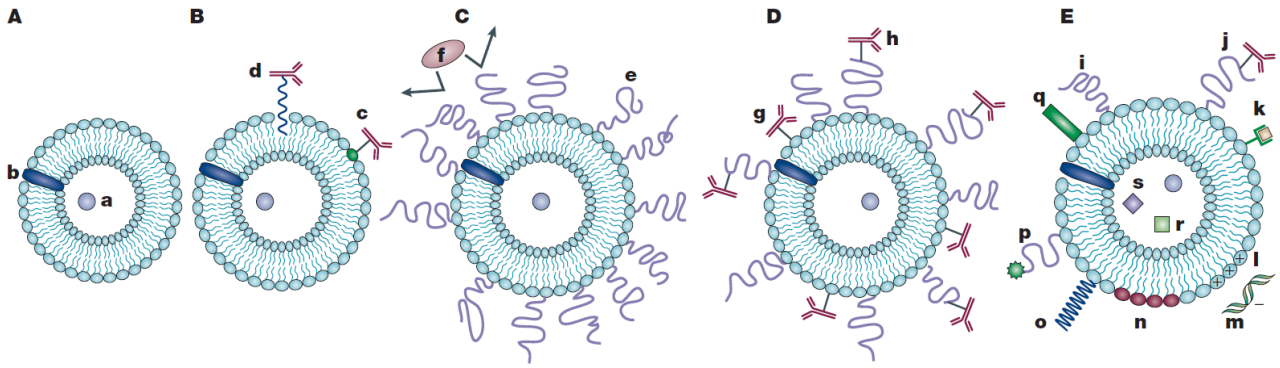

Figure 2-11 Evolution of liposomes. (A) Early traditional phospholipids 'plain' liposomes with water soluble drug (a) entrapped into the aqueous liposome interior and water-insoluble drug (b) incorporated into the liposomal membrane. (B) Antibody-targeted immunoliposome with antibody covalently coupled (c) to the reactive phospholipids in the membrane, or hydrophobically anchored (d) into the liposomal membrane after preliminary modification with a hydrophobic moiety. (C) Long-circulating liposome grafted with a protective polymer (e) such as PEG, which shields the liposome surface from the interaction with opsonising proteins (f). (D) Long-circulating immunoliposome simultaneously bearing both protective polymer and antibody, which can be attached to the liposome surface (g) or, preferably, to the distal end of the grafted polymeric chain (h). (E) New-generation liposome, the surface of which can be modified (separately or simultaneously) by different ways. Among these modifications are: the attachment of protective polymer (i) or protective polymer and targeting ligand, such as antibody (j); the attachment/incorporation of the diagnostic label (k); the incorporation of positively charged lipids (l) allowing for the complexation with DNA (m); the incorporation of stimuli-sensitive lipids (n); the attachment of stimuli-sensitive polymer (o); the attachment of cell-penetrating peptide (p); the incorporation of viral components (q). In addition to a drug, liposome can loaded with magnetic particles (r) for magnetic targeting and/or with colloidal gold or silver particles (s) for electron microscopy. Reproduced from Ref. 62

Very specifically, successful incorporation of single-stranded DNA block copolymers (DNA-*b*-polypropyleneoxide, DNA-*b*-PPO) to the lipid bilayers of liposomes helps achieve the target delivery of liposomes via the specific recognition of oligonucleotides (ODNs) by hybridisation with their complementary strands, while the oxidation of PPO chains or the highly unsaturated lipids effectively mediates the release of drugs/genes loaded in liposome vesicles.[68] Figure 2-12 shows the incorporation of DNA block copolymers (DBCs) to liposome vesicles, hybridisation of single-stranded DNA from DBCs with complementary

DNA sequence, and the light irritation triggering release of payload from liposomes. Lipid (monolayer/bilayer) coated other delivery materials, such as polymeric NPs, mesoporous silica NPs as drug delivery systems are reviewed recently by Raemdonck et al.[69] These hybrids mainly merges the beneficial features of both materials in a single nanocarrier while avoid their limitations, and they are proved to be suitable for combination therapy to enhance therapeutic efficacy and reduce drug resistance. Lipid coated calcium phosphate (CaP) NPs are developed by Huang's group for nontoxic composites with pH responsive cargo release and good stability in blood circulation.[70, 71]

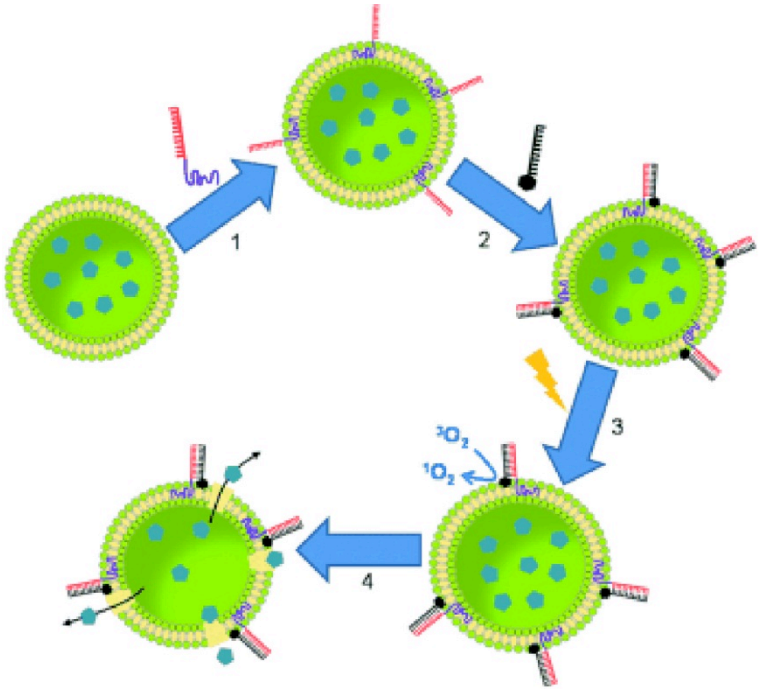

Figure 2-12 Schematic illustration of DNA block copolymer incorporated in liposome vesicle, hybridisation of single-stranded DNA from DBCs with complementary DNA sequence, and light irritation triggered release of payload from liposome vesicle, reproduced from Ref. 68

2.2.5 Polymersomes

Polymersomes are self-assembled polymeric vesicles, which have also been used in nanomedicine recently, as they can encapsulate hydrophilic compounds with the aqueous core and incorporate hydrophobic and amphiphilic molecules within the bilayers like liposomes, while they are more stable than liposomes. Figure 2-13 illustrates the schematic structures of liposome, polymersome and dendrimersome.

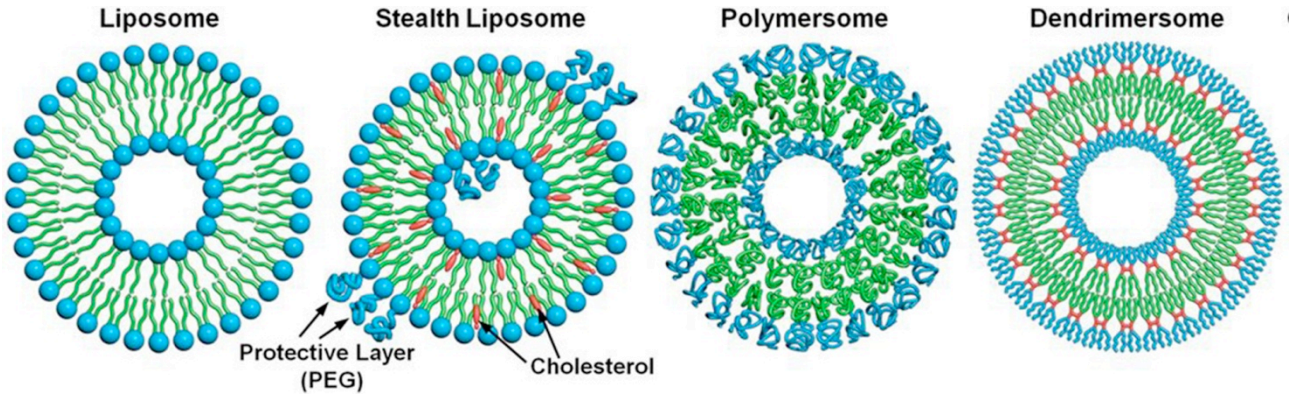

Figure 2-13 Schematic structures of liposome, polymersome, and dendrimersome, reproduced from Ref. 73

Nahire et al.[72] prepared redox sensitive and folate receptor targeted polymersomes from disulphide-linked copolymer PEG-S-S-PLA, and used them for encapsulating anticancer drugs gemcitabine and fluorouracil (5-Fu) simultaneously. They found that the polymersomes can release 80% of the encapsulated drugs within 20 min when incubated in solution with reducing agents at the cytosolic concentration level, while exhibit minimal release in serum levels of reducing agents. Folate-targeted polymersomes show enhanced uptake by folate-receptor overexpressing breast and pancreatic cancer cells and the drug encapsulated polymersomes show significant cytotoxicity to the cancer cells.

As another example, Xu et al.[74] prepared cross-linked polymersomes from temperature-sensitive copolymers, and found the cross-linked polymersomes can encapsulate model protein with loading efficiency > 85 wt%, with remarkable stability against dilution, organic solvent, high salt conditions and change of temperature, while the polymersomes are rapidly dissociated under reducing conditions mimicking intracellular environment.

2.2.5 Niosomes

Niosomes are self-assembled vesicles after hydrating a mixture of single or double alkyl-chain, non-ionic surfactant with cholesterol, which are similar to liposomes in terms of structure and physical properties. They can also be prepared as unilamellar and multilamellar vesicles. The self-assembly of non-ionic surfactant into vesicles was firstly observed and reported in 1979.[75] Since then, they have been extensively explored for application in pharmaceutics, cosmetics, and other fields.

Tavano at al.[76-78] developed a few types of niosomes and demonstrated that they could act as carrier for anticancer drugs doxorubicin (DOX) and 5-Fu, with good encapsulation, controlled release profile, and significant reduction in cancer cell viability. They also reported niosomes could be excellent carriers for antioxidants. When loaded in niosomes, resveratrol, alpha-tocopherol and curcumin lead to promoted ability to reduce free radicals.[79] Marianecci at al.[80] recently comprehensively reviewed niosomes concerning formations and applications in drug delivery and targeting since 80s of last century.

A library of 36 lipodoids are examined for siRNA delivery from lipid-like materials, including six amines, three alkyl-acrylates, and three alkyl-acrylamides.[81] Interestingly, when two ineffective single lipid-like materials are formulated into one delivery vehicle, the binary combination system can induce nearly complete knockdown of firefly luciferase and factor VII in HeLa cells and in mice, respectively.

Chien et al.[82] prepared 'liposome' from synthetic cationic cardiolipin analogue (CCLA) for siRNA delivery. The results show seven-fold higher transfection efficiency in mice than the commercially available 1,2-dioleoyl-3-trimethylammonium-propane (chloride salt) (DOTAP)-based liposome, 62% of growth inhibition in cancer cells, and 73% of tumour growth suppression in SCID mice bearing human breast xenograft tumours.

Monodisperse 'liposomal' particles made from di-alkylated amino acids based upon arginine DiLA2 compounds were prepared by Adami et al.[83] with particle size of 100 nm. Their pH dependent phase transition to hexagonal phase facilitates efficient siRNA release from endosome to cytosol. They also noted the improved long term tolerability, ease of manufacture, potential for metabolism and high *in vivo* delivery efficiency of this system.

2.3 Inorganic nanoparticles with low cytotoxicity

Widely explored inorganic gene carriers include metals and metal oxides, silica-based NPs, carbon-based NPs, calcium phosphate NPs, and layered double hydroxide NPs.

2.3.1 Metals and metal oxides

Gold nanoparticles (Au NPs) are the most popular metal NPs applied in nanomedicine for centuries. Faraday[84] firstly reported Au NPs in 1857, attributing the red colour to its colloidal nature, and a half century later, Mie[85] rationalised the visible absorption of colloidal Au NPs, which depends on the adsorption and reflection of metal. Au NPs can be

synthesised in the lab with the size ranging from 1 to 150 nm and a variety of shapes like spheres, rods, shells, cages, prisms, triangles, tetrapods, dogbones and cubes. Au NPs can be stabilised by a wide range of ligands, surfactants, polymers, dendrimers and biomolecules, etc. The most robust Au NPs is stabilised by thiolates via the strong Au-S bond, which was firstly disclosed by Giersig and Mulvaney.[86]

Hydrophobic drugs can be incorporated inside the ligand shell surrounding Au NPs by a non-covalent way to achieve controlled delivery. Kim et al.[87] prepared Au NPs-payload conjugates (AuNPZwit-Bodipy, TAF, and LAP) by a solvent replacement method from Au NPs core (AuNPZwit) and three hydrophobic guest compounds: e.g. 4,4-difluoro-4-bora-3a,4a-diaza-s-indacene (Bodipy) as a fluorescent probe and the highly hydrophobic therapeutics tamoxifen (TAF) and lapachone (LAP) as drugs. They found this delivery system can stably entrap drugs in the hydrophobic pocket of Au NPs and efficiently deliver dyes/drugs into MCF-7 cells without uptake of carrier NPs by membrane-mediated diffusion. The drugs loading and cellular delivery are illustrated in Figure 2-14.

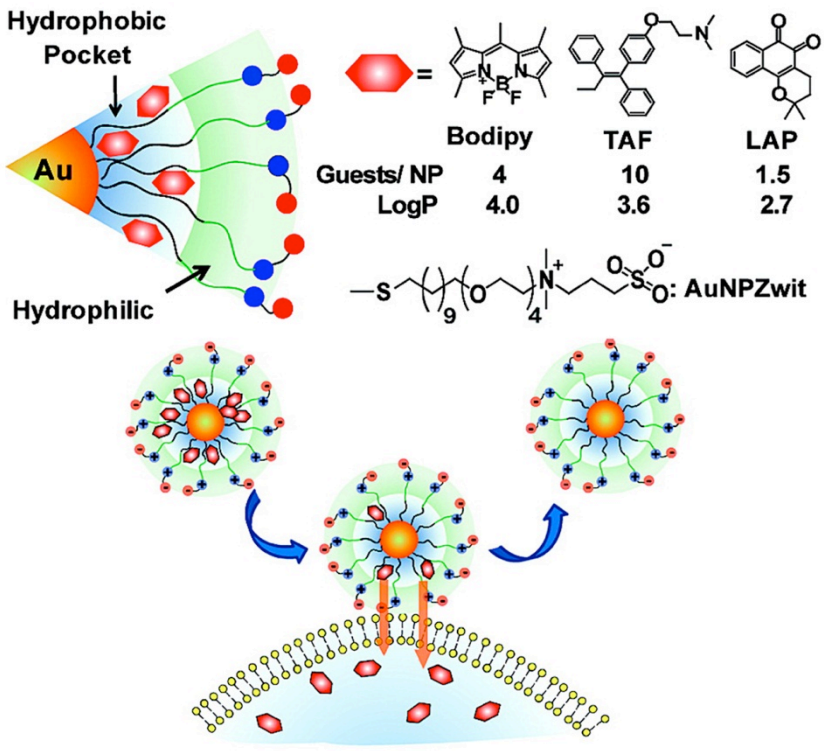

Figure 2-14 Structure of Au NPs with loaded hydrophobic drugs and its cellular delivery through monolayer-membrane interactions, reproduced from Ref. 87

By subsequent biomolecular substitution of a thiolate ligand, oligonucleotides, peptides and PEGs are easily attached to Au NPs. Rosi et al.[88] conjugated antisense

oligodeoxyonucleotides (asODNs) to the Au NPs surface with thiol groups, and found the Au NPs-asODNs composites readily enter C166, HeLa, NIH-3T3, and MDCK cells (>99% uptake). They also found the bound asODNs remain undigested by DNAse after 48 h of incubation in the cellular environment, and the enhanced green fluorescent protein (EGFP) expression reduced. This has proved the protection of nucleic acids by Au NPs via condensing the gene materials (Figure 2-15).

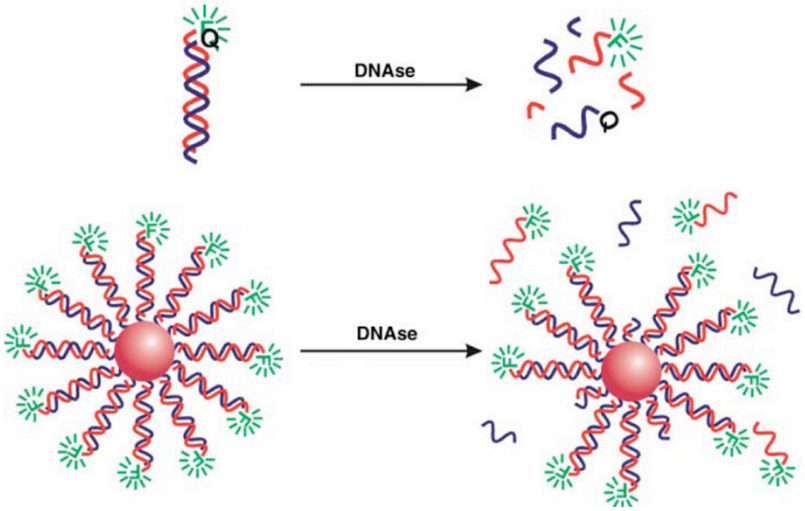

Figure 2-15 asODNs protected by Au NPs from enzyme degradation, reproduced from Ref. 88

Oishi et al.[89] developed a smart PEGylated Au NPs for siRNA delivery by complexing poly(ethylene glycol)-block-poly(2-(N,N-dimethylamino)ethyl methacrylate) copolymer (PEG–PAMA) and Au NPs, and then conjugating thiolated siRNA. The PEGylated Au NPs with thiolated siRNA achieve an effective RNAi activity with 65 % gene knockdown, which is similar to the commercial Oligofectamine (60 % inhibition).

2.3.2 Silica-based nanoparticles

Mesoporous silica nanoparticles (MSNs) were firstly introduced by Beck and coworkers in 1992 and the first family of MSNs was named as M41s.[90, 91] Later on, highly ordered MSNs and SBA-15 MSNs were also synthesised and intensively investigated. MSNs have drawn much attention in nanomedicine because of its large surface area, high pore volume, tunable pore structure as well as particle size, low mass density, good biocompatibility, and ease of surface functionalisation. In 2001, MSN material was firstly reported as a drug

delivery system.[92] Recently, Yu's group explored MSNs with rough surfaces (mimicking viruses), and found enhanced cellular delivery of curcumin to KHOS cells.[93, 94]

To overcome the limitations of pure MSNs, magnetism and luminescence functionalised MSNs help for drug targeting and tracking, and various silica pore-blocking caps are used to develop MSN-based drug delivery system with external stimuli triggered release to prevent "zero-premature release", including NPs, organic molecules, and supra-molecular assemblies. The stimuli-responsive strategies are also diverse, such as chemical, pH, electrostatic interaction, enzymatic, redox, temperature, and photo-irradiation. Yang et al.[95] extensively summarised the functionalised MSNs-based drug delivery systems and illustrated the major types, as shown in Figure 2-16.

Figure 2-16 Functionalised MSNs-based sustained/controlled drug delivery systems, reproduced from Ref. 95

Recently, Zhou et al.[97] developed a DNA-gated multifunctional MSN-based delivery system, which is multi-responsive to disulphide reducing agents, elevated temperature, and DNase for co-delivery of genes and drugs with controlled release (Figure 2-17). Zhang et al.[98] developed traceable and targeted MSN-based nanocarrier by capping MSN coated QDs with DNA hybrid, and the drug release can be triggered by overexpressed endogenous miR-21 in pathological cells which competitively hybridises with DNA. This also provides the possibility for co-delivering drugs and genes. Zhang et al.[99] engineered a more complicated multifunctional MSN-based nanocarrier by incorporating polymer PEG on MSNs, functionalising with cyclodextrin by disulphide bond bridging for pH and glutathione triggered release, and folate ligand for targeting. Xiao et al.[100] designed a dual-

responsive MSN-based drug carrier by functionalising MSN surface with peptide ligand via disulphide bonds, with the peptide being then PEGylated and protected by methoxy PEG (MPEG) with benzoic-imine bond. The multi-functionalised NPs can be easily taken up by tumour cells because of the peptide targeting ligand, while the loaded drug is released by hydrolysis of benzoic-imine bond and cleavage of disulphide bond in tumour site.

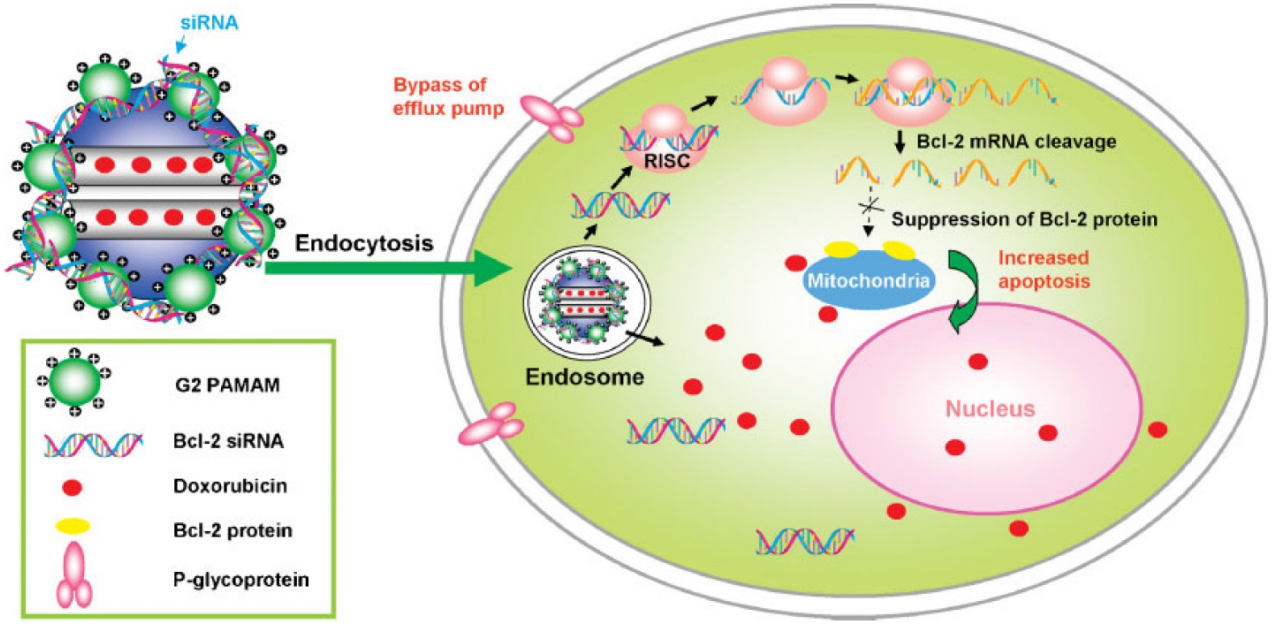

Figure 2-17 Schematic diagram of a co-delivery system based on MSNs to deliver Dox and Bcl-2 target siRNA simultaneously to A2780/AD human ovarian cancer cells, reproduced from Ref. 96

Quite a few groups have also reported loading DNA/siRNA in PEI modified MSNs, providing protection to DNA/siRNA from enzyme degradation, and resulting in enhanced gene delivery.[101-105] Simultaneous co-delivery of drug and nucleic acids has also been reported by researchers, and effective silencing activity and enhanced anticancer action (even in the multidrug resistant cancer cell) were found.[96, 106, 107] Figure 2-17 shows the schematic diagram for MSNs as a co-delivery system for Dox and siRNA. Dendrimer-capped mesoporous silica showed higher transfection efficiency than commercial transfection reagent PolyFect, SuperFect, and Metafectene.[108]

2.3.3 Carbon-based nanoparticles

It is widely accepted that carbon nanotubes (CNTs) were firstly discovered by Iijima in 1991; however there were several earlier reports which introduced similar carbon

structures by Radushkevich and Lukyanovich in 1952, Bacon in 1960, and Oberlin et al. in 1976.[109-112] Two years later, Iijima and Ichihashi reported single shell CNTs in 1 nm diameter size.[113] CNTs are long cylinders of covalently bonded carbon atoms, which have gained much interest as drug delivery vehicles, owing to the high surface area, enhanced cellular uptake and facile conjugation with much therapeutics. The basic structure of CNTs is shown in Figure 2-18.

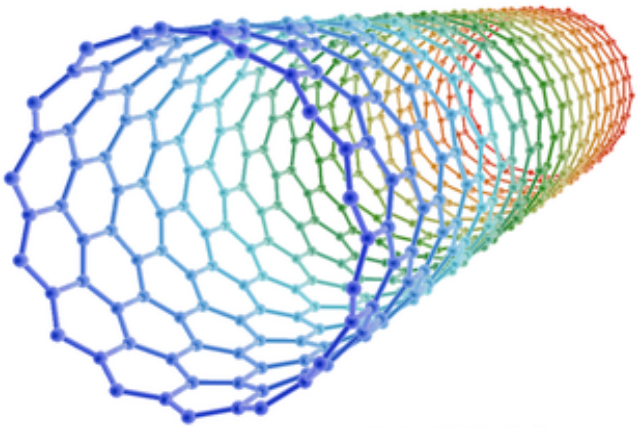

Figure 2-18 The basic structure of CNTs

Wong et al.[114] reviewed CNTs as a type of nanocarrier for small molecule drugs in 2013, including anticancer drugs: topoisomerase inhibitors, antimetabolites, antimicrotubules, and non-anticancer drugs: antimicrobials, anti-inflammatories, antihypertensives, antioxidants, etc. CNTs as vectors for gene delivery were reviewed by Bates and Kostarelos[115] in 2013, including single-walled nanotubes (SWNTs) and multi-walled nanotubes (MWNTs), concerning the delivery of plasmid DNA, siRNA and mRNA, ODN and aptamer DNA/RNA.

Wang et al.[116] prepared PEI functionalised SWNTs to deliver siRNA to PC-3 cells, and found severe apoptosis and strong suppression *in vitro*. After conjugated with a tumour target peptide NGR, they also found significant tumour cell growth inhibition. Wu and co-workers[117] grafted MWNTs with PEI and further conjugated to prostate stem cell antigen monoclonal antibody (mAb) (Figure 2-19), and found the resultant NPs can specifically target the cancer cells and suppress tumour growth with great potential as a targeted ultrasound contrast agent.

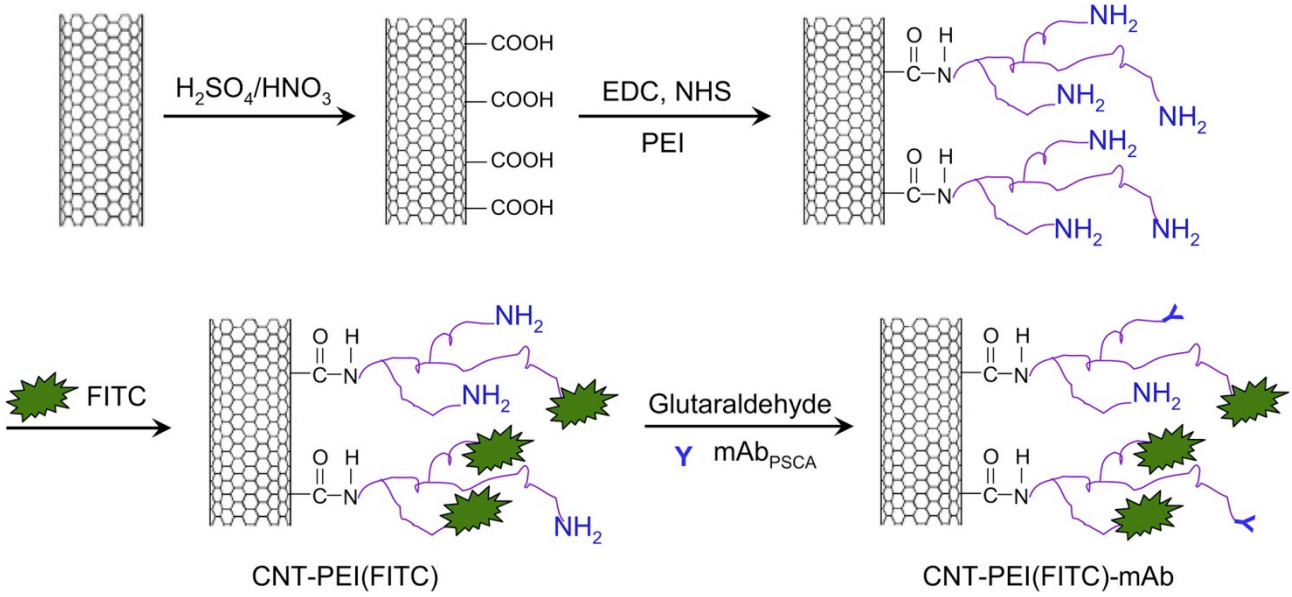

Figure 2-19 Schematic diagram of synthesis process for CNT-PEI-mAb, reproduced from Ref. 117

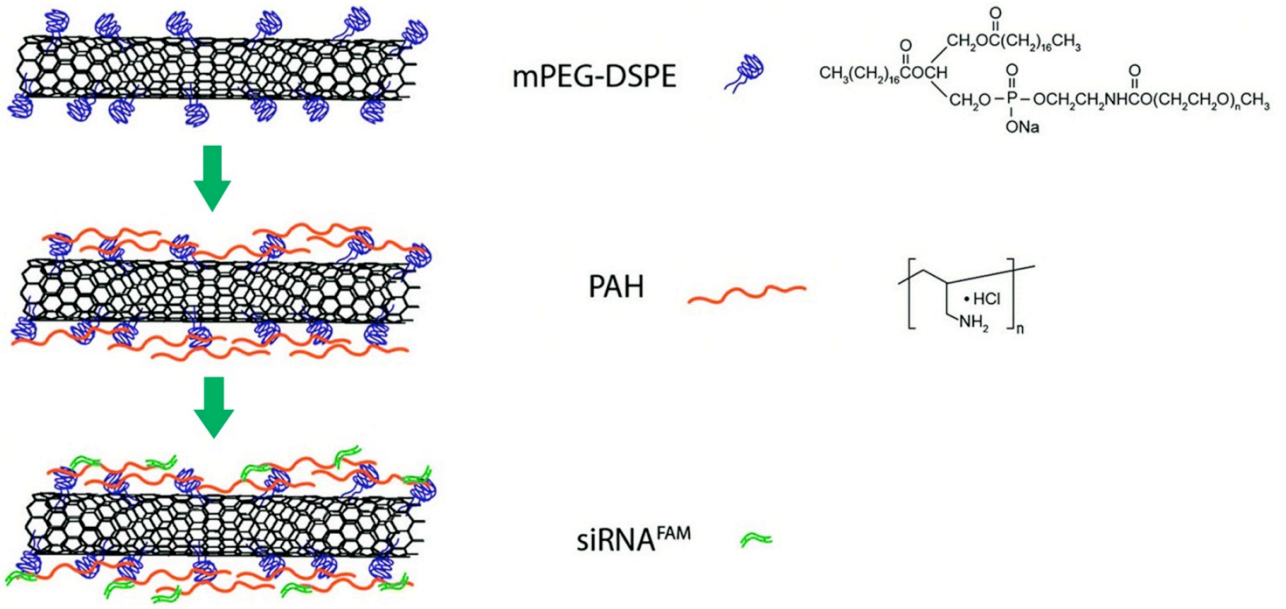

Figure 2-20 Schematic illustration of functionalised SWNTs for loading siRNA, reproduced from Ref. 118

Anderson et al.[118] functionalised SWNTs with mPEG-DSPE, then coated with cationic polymer PAH, and loaded siRNA via electrostatic interactions (Figure 2-20). Successful internalisation of the SWNT/siRNA nanoplexes by pancreatic cancer cells was observed, resulting in down regulation of the target gene, and the functionalised SWNTs are proved

to be highly biocompatible. Dendrimer modified CNTs are also found having higher gene transfection efficiency.[119]

2.3.4 Calcium phosphate

Calcium phosphate (CaP) is a family of minerals containing calcium ions (Ca^{2+}) and orthophosphates (PO_4^{3-}), metaphosphates or pyrophosphates ($P_2O_7^{4-}$), occasionally with hydrogen or hydroxide ions, which includes monocalcium phosphate $Ca(H_2PO_4)_2$, dicalcium phosphate $CaHPO_4$, tricalcium phosphate $Ca_3(PO_4)_2$ (sometimes referred to simply as calcium phosphate or calcium orthophosphate), hydroxyapatite $Ca_5(PO_4)_3(OH)$, apatite $Ca_{10}(PO_4)_6(OH, F, Cl, Br)_2$, and octacalcium phosphate $Ca_8H_2(PO_4)_6.5H_2O$.

CaP has been used for gene delivery because of its safety, good biocompatibility, and a relatively facile and cost-effective preparation. Conventional CaP-DNA/siRNA composite particles can be obtained typically by a microemulsion method, mixing a phosphate ion emulsion and a calcium ion emulsion supplemented with DNA/siRNA under neutral pH in a controlled Ca/P ratio. DNA/siRNA is compacted and protected by CaP in these composites and the composites can be easily taken up by cells. Furthermore, the composites can successfully escape from the endosomes by the ‘proton sponge’ effect, where CaP is easily dissolved in an acidic environment, causing high osmotic pressure in endosomal vesicles and influx of much water, and then rupture of endosomal vesicles.

In general, the critical disadvantages of CaP-based gene delivery system are their insufficient transfection efficiency and poor reproducibility compared with other nonviral systems. Recently, Huang’s group proposed a new CaP-based gene delivery system by coating lipids around the CaP particles,[70, 71, 120] where lipids interact with Ca ions covalently to form stable inner lipid coating. Later, by traditional thin lipid film hydration method, the outer layer of lipid is formed around the CaP-lipid particles. Since the inner and outer layer of lipids are coated in separate steps, the stability and charge property of CaP-lipid particles can be controlled by choosing neutral or negatively/positively charged lipids. Moreover, PEGylated lipids can also be incorporated in this system to further improve the circulation lifetime of this composite system. The CaP-lipid composites have proved to induce ~ 40 fold higher siRNA delivery than the lipid based formulation. The preparation of CaP-siRNA-lipid particles and the interaction between calcium ions and lipid head groups are illustrated in Figure 2-21.

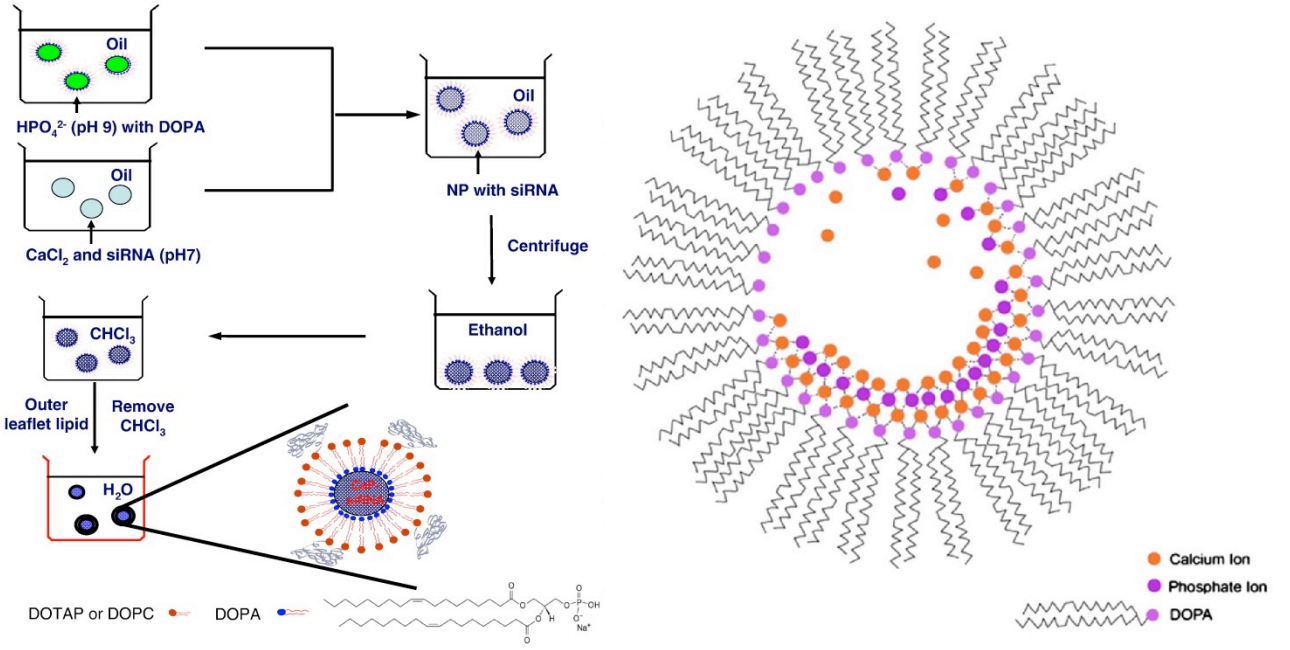

Figure 2-21 Schematic diagram for preparing CaP-lipid composites for siRNA delivery from microemulsion method and the interaction between calcium ions and lipid head groups which facilitates CaP-lipid particles formation, reproduced from Ref. 71

2.3.5 Layered double hydroxides

Layered double hydroxides (LDHs), also known as anionic clays or hydrotalcite-like compounds (HTlcs), are a family of inorganic layered materials, which can be found naturally as minerals or can be easily synthesised in the lab with controlled compositions. LDH composition can be expressed in a general formula $[M^{2+}_{1-x} M^{3+}_{x}(OH)_2]$ $(A^{n-}_{x/n}\cdot mH_2O)$, where M^{2+} can be most divalent ions, such as Mg^{2+}, Ca^{2+}, Cu^{2+}, Zn^{2+}, Co^{2+}, Ni^{2+}, Fe^{2+}; M^{3+} can be most trivalent ions, such as Al^{3+}, Fe^{3+}, Cr^{3+}; x=0.2-0.33, which means the M^{2+}/M^{3+} molar ratio is 2.0-4.0; x also means the positive charge density of LDH; A^{m-} represents any type of anions, and the common ones are CO_3^{2-}, Cl^-, NO_3^-, OH^-, SO_4^{2-}, CrO_4^{2-}; m=1-3x/2.

The schematic 3-D structure of LDH is shown in Figure 2-22. In every single layer, every divalent metal cation is located in the center of the octahedron constructed by six hydroxyl groups. These octahedra are connected one another by edge-sharing, forming the two-dimensionally infinite sheet (or layer), which is similar to the basic structure of brucite $Mg(OH)_2$. Partial substitution of divalent ions in the brucite-like hydroxide layer by trivalent ions leads to the positive charge sheets, which is balanced by the negative charged anions intercalated in the interlayer. Then the brucite-like layers can stack upon one another via electrostatic interactions between the layers, forming the three dimensional structure.

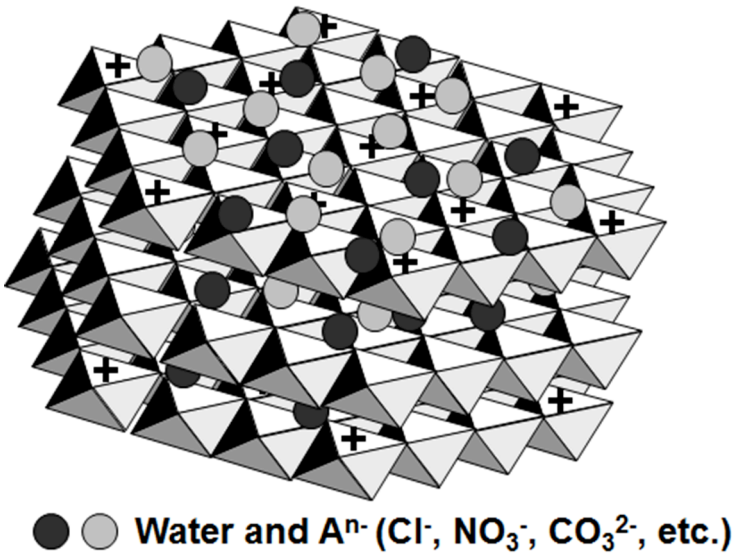

Figure 2-22 Schematic 3-D structure of LDH, reproduced from Ref. 121

2.3.5.1 Pure LDH NPs for drug/gene delivery

The partial substitution of magnesium ions in the brucite-like hydroxide layer by aluminium ions leads to the positive-charged property of the hydroxide sheets. This enables incorporation and protection of negatively charged biomolecules, such as CMP (cytidine-5´-monophosphate), AMP (adenosine-5´-monophosphate) and GMP (guanosine-5´-monophosphate), ATP (adenosine triphosphate), amino acids, peptides, DNA, and siRNA onto LDH via electrostatic interactions. The exchangeable interlayer can also accommodate negatively charged anions and small molecule drugs by ion-exchange or one-step synthesis (e.g. coprecipitation). The LDH-biomolecules hybrids gain extra stabilisation energy due to electrostatic interactions between cationic hydroxide layers and anionic biomolecules. The charge neutralisation facilitates the penetration of LDH-nucleic acid hybrids into cells through endocytosis, since this hybrid greatly reduces the electrostatic repulsive interactions between negatively charged cell membranes and naked anionic biomolecules.

Recently, Rives et al.[122] reviewed LDH for drug delivery and its controlled release. A large variety of drugs are included in this review, such as antibiotics, anticancer agents, vitamins, amino acids and peptides, anticardiovascular agents, diabetes treatment drugs, antifibrinolytic agents, antihypertensives, antimycotic agents, anticoagulants, osteoporosis, antioxidants, and immunosuppressant corticosteroids.

Gu and co-workers used LDH as a carrier for anti-restenotic pharmaceutical reagent low molecular weight heparin (LMWH), finding a sustained release of LMWH from LDH-LMWH hybrids in the physiological condition, enhanced cellular uptake of LMWH-LDH hybrids by smooth muscle cells (SMCs), improved ability of LMWH to inhibit SMC proliferation and migration. This shows LDH a promising delivery system for anti-restenotic drug LMWH.[123-125] Figure 2-23 shows the schematic structure of LDH-LMWH.

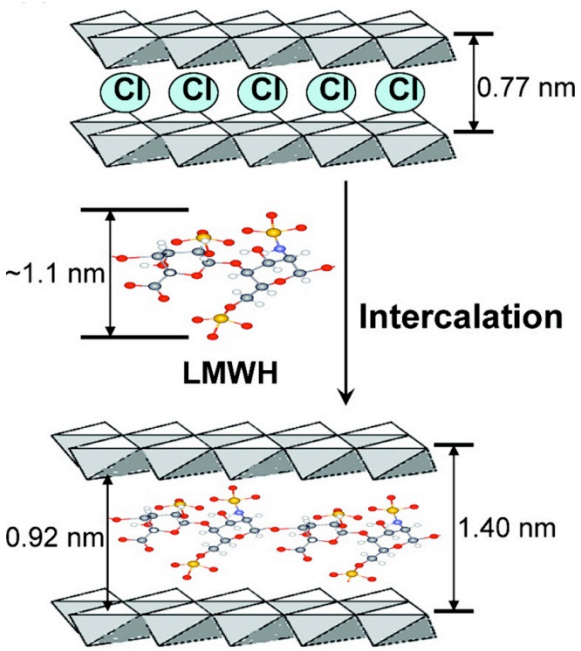

Figure 2-23 Schematic illustration of LMWH intercalated in MgAl-Cl-LDH, reproduced from Ref. 123

In 1999, Choy's group firstly reported the biomolecule-LDH hybrids, including AMP-LDH, CMP-LDH, GMP-LDH, and DNA-LDH. The biomolecules are protected and stabilised by LDH, and moreover they can be recovered in acid conditions without loss of chemical and biological integrity.[126] This work pioneered the research for using LDH as the gene material reservoir. In the following few years, the cellular uptake behaviour of LDH-biomolecule and cytotoxicity of LDH were studied by the same research group and the results show LDH can be a good gene delivery vector.[127-129]

In 2004, Tyner et al.[130] delivered a full gene encoding green fluorescent protein to a variety of cell types, e.g. 9L glioma cells, JEG3 choriocarcinoma placental cells, and cardiac myocytes, and found all cells can internalise and tolerate the LDH-DNA nanocomposites, express the gene with 70 % to 90% transfection efficiency after 48 h of incubation. In 2009, Masarudin et al.[131] transfected the same gene into African monkey kidney (Vero3)

cells using MgAl-LDH as a nanocarrier. They found LDH can provide protection to the plasmid DNA from degradation and the transfected cells exhibit fluorescence 12 h post treatment. In our research group, Ladewig et al.[132, 133] associated plasmid DNA with LDH nanoparticles and achieved successful transfection in adherent cell lines HEK 293T, NIH 3T3, COS-7 and CHO-K1, although the aggregation between LDH and plasmid DNA were observed. In 2011, Li et al.[134] found LDH-plasmid DNA complex has high transfection efficiency *in vivo* and the complex enhances the *in vivo* anti-melanoma immune response significantly. These indicate further that LDH can be a promising vector for gene delivery.

In recent years, using LDH NPs as vector for siRNA has been explored by researchers. Our research group attempted to use LDH NPs for delivering siRNA to mammalian cells, which induced 99% of cellular uptake (even better than commercial transfection agent Lipofectamine®). Furthermore, marked down-regulation of protein expression in HEK 293T cells and primary cultured neurons was also observed, which demonstrates LDH NPs can be adopted as an efficient delivery vehicle for siRNA.[132, 135-139] Co-delivery of anticancer drug and siRNA by LDH has also been explored by our group. By loading anticancer drug 5-fluorouracil (5-Fu) and cell death siRNA (CD-siRNA) simultaneously on LDH NPs, significantly enhanced cytotoxicity to cancer cells MCF-7, U2OS and HCT-116 was observed.[140] This provides a better cancer treatment solution than chemotherapy or gene therapy only.

Remarkably, MgAl-LDH shows no discernible cytotoxic effect because of its physicochemical nature.[124, 137, 139, 141] The hydroxide layer will be dissolved gradually in the weakly acidic condition, such as in endosome or lysosome. This dissolution releases the loaded gene/drug, but simultaneously gives some magnesium and aluminium ions that are physiologically-friendly and can be excreted through ion tunnels. For example, the escape of LDH-drug/siRNA hybrid from endosome is via “increasing endosomal osmotic pressure”. After LDH-drug/siRNA is taken up via endocytosis, H^+ influxes into endosome partially dissolves the hydroxide layer of LDH, which results in a higher concentration of Mg^{2+} and Al^{3+}, and then a higher osmotic pressure in endosome. The higher osmotic pressure thus causes more water influx in endosome, which finally causes the rupture of endosome, releasing LDH-drug/siRNA or drug/siRNA into cytoplasma.[136, 142] The proposed cellular uptake and payload release mechanisms are shown in Figure 2-24.

Thus, LDH nanoparticles possess many advantages as an excellent gene delivery system. However, the LDH-gene complexes form aggregates in the blood flow, which possibly clot

the blood flow and cause animal to die. This is a big barrier for LDH nanoparticles to be an efficient *in vivo* vector. LDH-based hydridisation systems have been developed by researchers for enhanced therapeutic efficacy, hindering LDH NPs forming aggregation, and widening the spectrum of payloads.

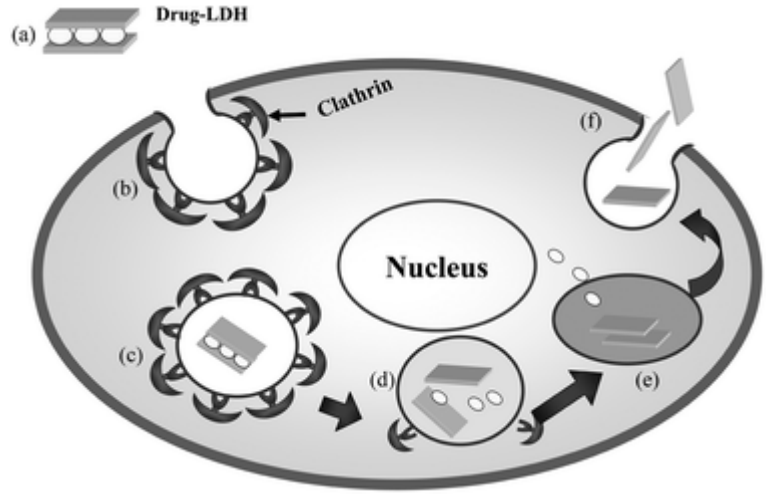

Figure 2-24 Proposed cellular uptake and payload release mechanism of LDH, (a) Drug-LDH nanohybrids approach cell membrane, (b) drug-LDH nanohybrids are internalised via clathrin-mediated endocytosis, (c) nanohybrids are transported inside the cell through early endosome, (d) in late endosome, LDHs are partially dissolved due to the slight acidity, (e) in lysosome, drugs are released, (f) LDHs are externalized via exocytosis, reproduced from Ref. 143

2.3.5.2 LDH hybridised with inorganic vector(s)

Wang and co-workers[144] developed a Gd-doped Mg-Al-LDH/Au nanocomposite, which has high loading capacity for non-anionic anticancer drug DOX with pH-responsive DOX release profile in PBS at varied pH conditions. The composite also efficiently transports DOX into HeLa cells; releases DOX in the acidic cytoplasm and then causes cell death. On the other hand, this nanocomposite shows superior performance for CT-MR imaging both *in vitro* and *in vivo* than the commercial MRI and CT contrast agents. Moreover, the composite shows negligible cytotoxicity and no detectable tissue damage.

Zhang et al.[145] prepared core-shell structure of magnetic nanohybrids by coating MgAl-LDH on magnesium ferrite magnetic cores with intercalated ibuprofen by one-step co-precipitation method. In the absence of external magnetic field, the drug release from the magnetic nanohybrids can be tuned by the magnetic core content in the nanohybrids,

while under external magnetic field in consecutive “ON-OFF” mode, magnetically controlled pulsatile release profile was observed. They proposed this magnetic LDH hybrid could be a promising drug targeting and magnetically tunable delivery system.

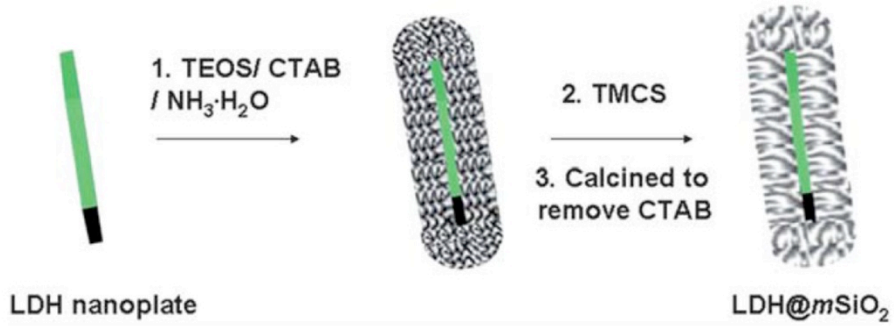

Figure 2-25 Illustration of core@shell LDH@SiO2 NP synthesis and structure, reproduced from Ref. 146

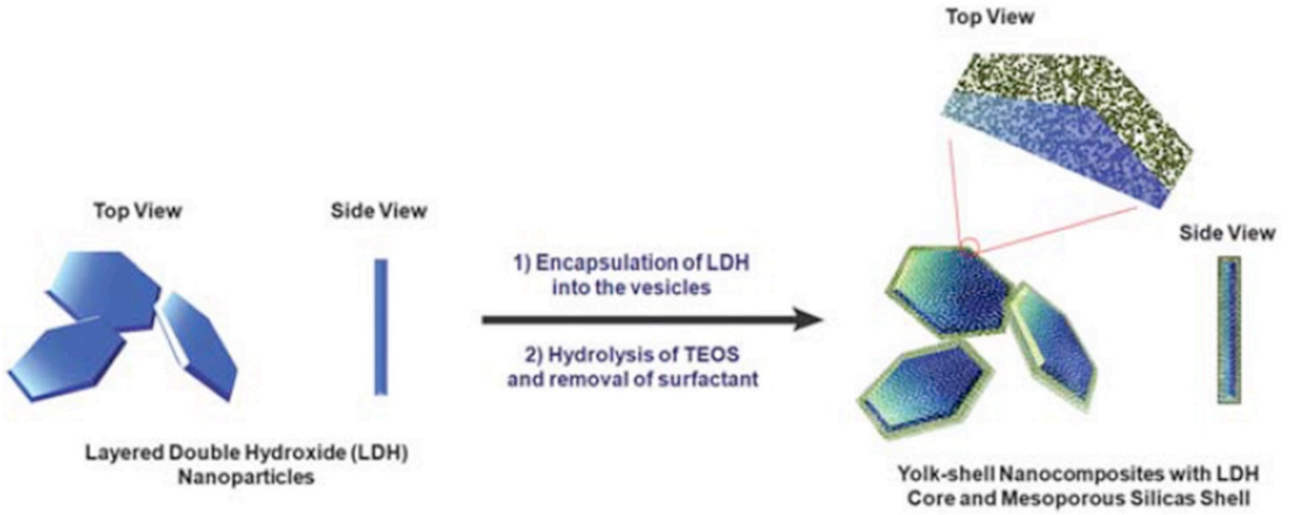

Figure 2-26 Schematic diagram for preparing LDH-MSN nanorattles with LDH core and MSN shell, reproduced from Ref. 147

Bao et al.[146] synthesised core@shell structure of LDH@SiO_2 and used it for loading ibuprofen. The nanocomposite shows slower release of ibuprofen in PBS compared to MSN, which is only due to the LDH core. The synthesis procedure and LDH@SiO_2 structure is shown in Figure 2-25. In the same year, Liu et al.[147] synthesised an LDH-MSN hybrid system by coating silica on LDH surface, forming LDH-MSN nanorattles, and they used the hybrid system for delivering model fluorophore FITC. Aside from pH triggered release of payload, the LDH-MSN hybrids possess several advantages over conventional

carriers, such as high loading amounts, high surface area, ease of functionalisation and controllable particle size and void size, interstitial space between core and shell that can be used for encapsulation of molecules or NPs. Figure 2-26 shows the schematic procedure for preparing LDH-MSN nanorattles with LDH core and MSN shell.

Zheng et al.[148] also developed LDH-MSN hybrid system encapsulating the guest molecules $Ru(bpy)_3Cl_2$, where LDH nanosheets are adsorbed on the surface of MSNs by electrostatic interaction. This hybrid system combines the pH-responsive payload release property of LDH and advantage of MSNs for encapsulating molecules inside nanopores, while it avoids the tedious surface modification of MSNs for pH-triggered release of guest molecules, hinders LDH NPs forming aggregation, and widens the spectrum of payloads. Figure 2-27 shows the procedures for synthesising LDH nanosheets capped MSNs as a pH-responsive release system.

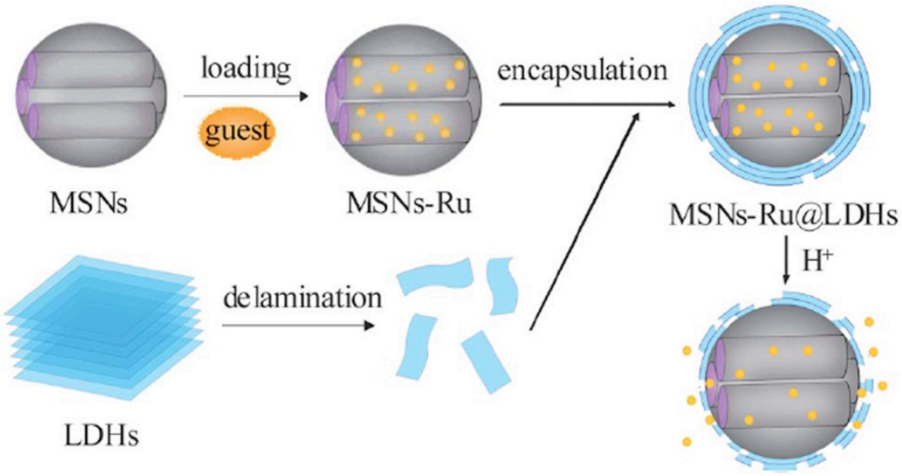

Figure 2-27 Schematic diagram for preparing LDH-MSNs hybrids, reproduced from Ref. 148

Core-shell LDH-MSN hybrid is also used as an adjuvant for DNA vaccine, where much higher transfection efficiency and expression of IFN-γ, IL-6, CD86, and MHC II were observed than LDH and SiO_2 only.[149]

2.3.5.3 LDH hybridised with polymer(s)

Ribeiro and co-workers[150] developed a new pectin-coated chitosan-LDH nanocomposite for delivering the most used non-steroid-anti-inflammatory drug (NSAID, also known as 5-aminosalicylic acid, 5ASA). This composite profits from the mucoadhesiveness of

chitosan, while pectin provides protective coating for chitosan and LDH to keep the system resistant to pH changes (low pH in the stomach when oral administration is used), and LDH host offers opportunity for controlled drug release. Figure 2-28 shows the proposed structure of pectin coated chitosan-LDH nanocomposite loaded with drug 5ASA.

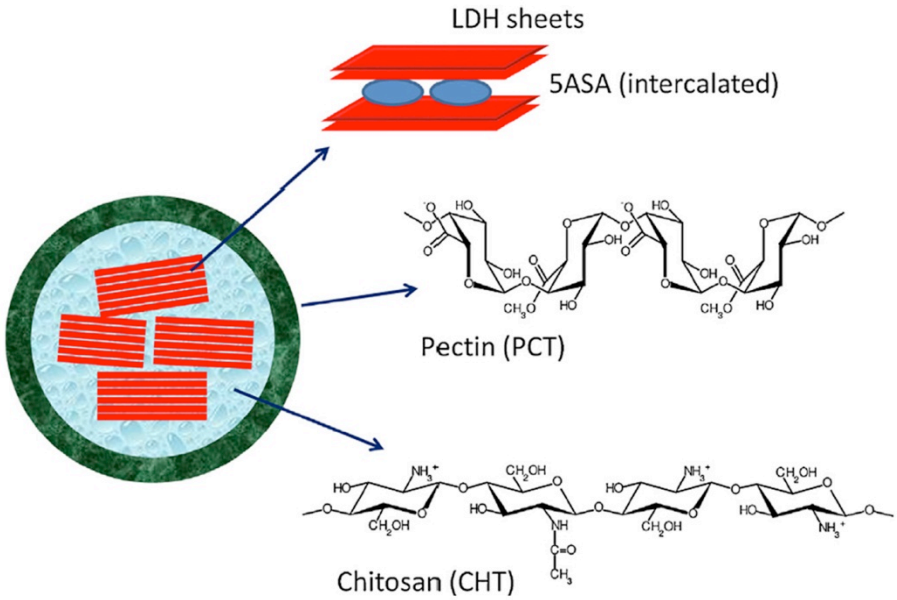

Figure 2-28 Schematic structure of pectin coated chitosan-LDH nanocomposite loaded drug 5ASA, reproduced from Ref. 150

Mahkam and coworkers[151] combined pH-sensitive drug host Zn-Al-LDH and pH-sensitive polymer alginate (a polysaccharide widely used for drug encapsulation) to form a new hybrid material. Acting as crosslinker in the hybrid, LDH restricts the mobility of pH-sensitive polysaccharide chains, and then slows down their swelling and dissolution rates. The LDH-alginate hybrid shows sustained drug release either in the presence or absence of glucose phosphate.

Hu et al.[152] grafted LDH surfaces by 2-(dimethylamino)-ethyl methacrylate (DMAEMA) using surface-initiated atom transfer radical polymerization (ATRP) technique. A series of well-defined cationic LDH-PDs consisting of LDH and disulphide-linked cationic P(DMAEMA) brushes with different lengths were obtained with better ability to condense plasmid DNA, enhanced cellular uptake, and higher gene delivery to COS7 and HepG2 cells. Figure 2-29 shows the schematic diagram illustrating the process for grafting P(DMAEMA) on LDH surfaces.

Ciobanu et al.[153] successfully intercalated carboxymethyl-β-cyclodextrins (CMCDs) into interlayers of LDH via reconstruction method. The resultant hybrid could encapsulate various organic guests, and prolong their release time compared to LDH host only. This is because the organic guests can be included in the cavity of CMCDs. Figure 2-30 shows the schematic illustration for intercalating CMCDs into LDH interlayers and following organic guest encapsulation.

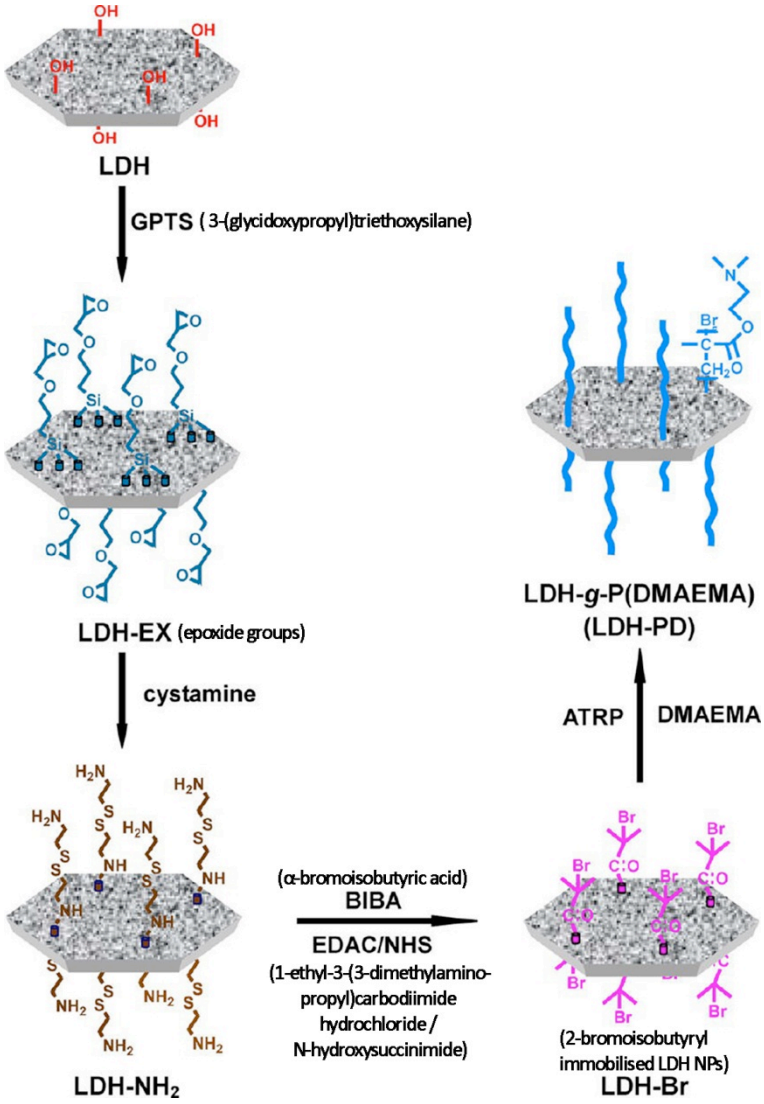

Figure 2-29 Schematic illustration of P(DMAEMA)-grafted LDH hybrid preparation process, reproduced from Ref. 152

San Román et al.[154] prepared LDH-drug-PLA nanocomposite by dispersing LDH-drug in semicrystalline PLA, formed a composite with LDH-drug supported on PLA. Much slower drug release from the nanocomposite than from LDH only was observed which related to the base-catalysed decomposition of PLA.

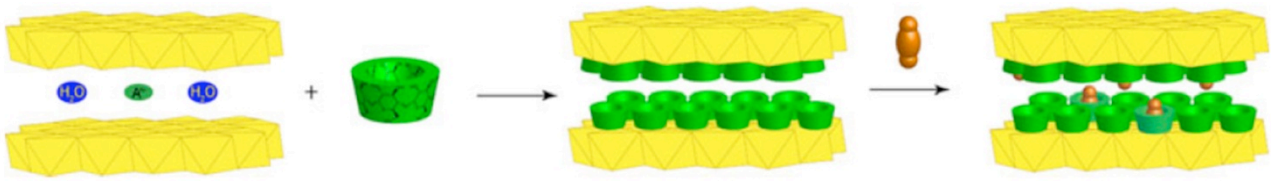

Figure 2-30 Schematic diagram illustrating intercalation of CMCDs into LDH and encapsulating organic guests, reproduced from Ref. 153

Xia et al.[155] modified LDH NPs with PEG and FA for disguise function and targeting, using (3-aminopropyl) trimethoxy silane (APTMS) as linker agent. The modified particles show good dispersibility due to the space steric effect of the modified layers, so they could be used in drug delivery.

Alcântara et al.[156] prepared a nanocomposite beads from LDH (with drug ibuprofen intercalated in the interlayers), a polysaccharide alginate, and a highly hydrophobic protein zein. The resultant composites show a more sustained release of drug than only loaded in LDH because it requires the diffusion of water inside the matrix to LDH, while the hydrophobicity of protein lowered the water uptake of the composites. Figure 2-31 shows the schematic diagram of LDH-alginate-zein nanocomposites loaded with ibuprofen.

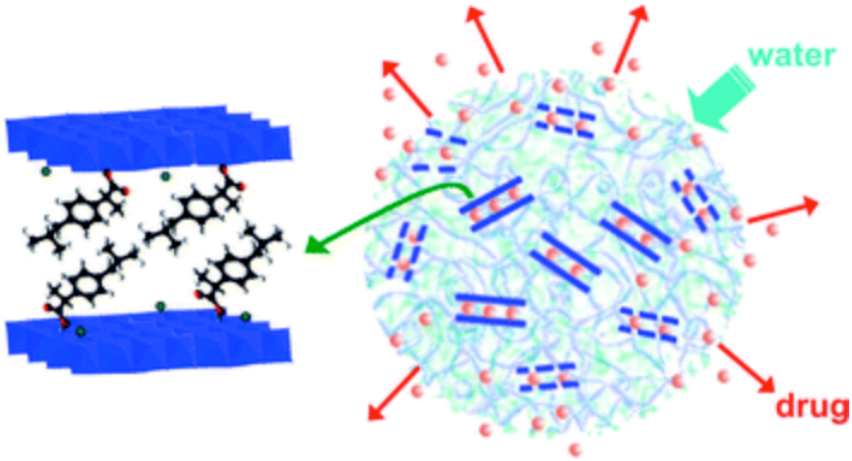

Figure 2-31 Schematic illustation of LDH-alginate-zein nanocomposites loaded with drug ibuprofen for more sustained release, reproduced from Ref. 156

2.3.5.4 LDH hybridised with lipid(s) or lipid-like surfactant(s)

Tyner et al.[157] incorporated poorly water soluble drug camptothecin (CPT) in micelles derived from negatively charged surfactant, and then encapsulated micelles into the interlayer of LDH by ion exchange process. This method increases three-fold solubility of CPT. Figure 2-32 shows the schematic diagram for LDH-micelle formation.

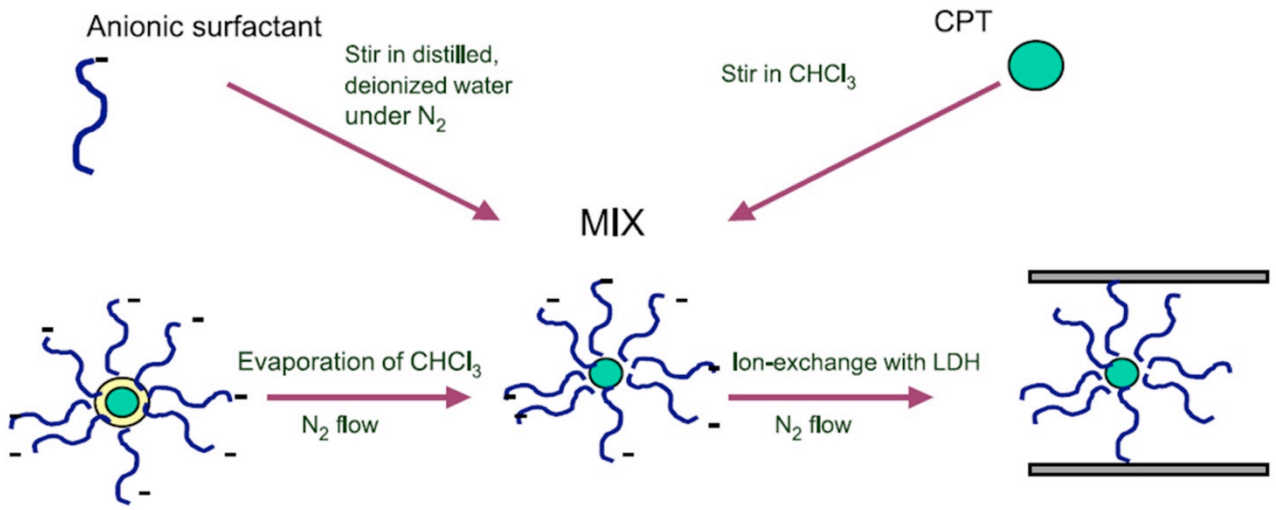

Figure 2-32 Schematic illustration of LDH-micelle hybrid formation, reproduced from Ref. 157

Bégu et al.[158] reported a hybrid system for sustained lipophilic drug delivery prepared from self-assembled unilamellar anionic liposome intercalated in interlayer of LDH. This also provides a possibility to deliver non-ionic water soluble drugs by LDH.

Hou's group[159-161] developed a class of hybrid systems by inducing surfactant derived liposome formation using LDH. They confirmed the liposomal vesicle formation with entrapped LDH particles by TEM and they believed this system is a promising vector for drug delivery.

Huang and co-workers[162, 163] prepared a dextran-magnetic layered double hydroxide-fluorouracil liposome (DMFL) system by reverse evaporation method. They found hexagonal skeleton of dextran-magnetic layered double hydroxide-fluorouracil (DMF) can be encapsulated by lipid bilayer on TEM images, and the encapsulation efficiency of fluorouracil (FU) is determined to be ~ 85%. The average diameter size of DMFL is ~ 160 nm, and the release of FU from DMFL in PBS shows a sustained profile. Moreover, DMFL

shows higher cytotoxicity to human ovarian adenocarcinoma cancer cells (SKOV3) than other FU formulations at the same concentrations and intervention time.

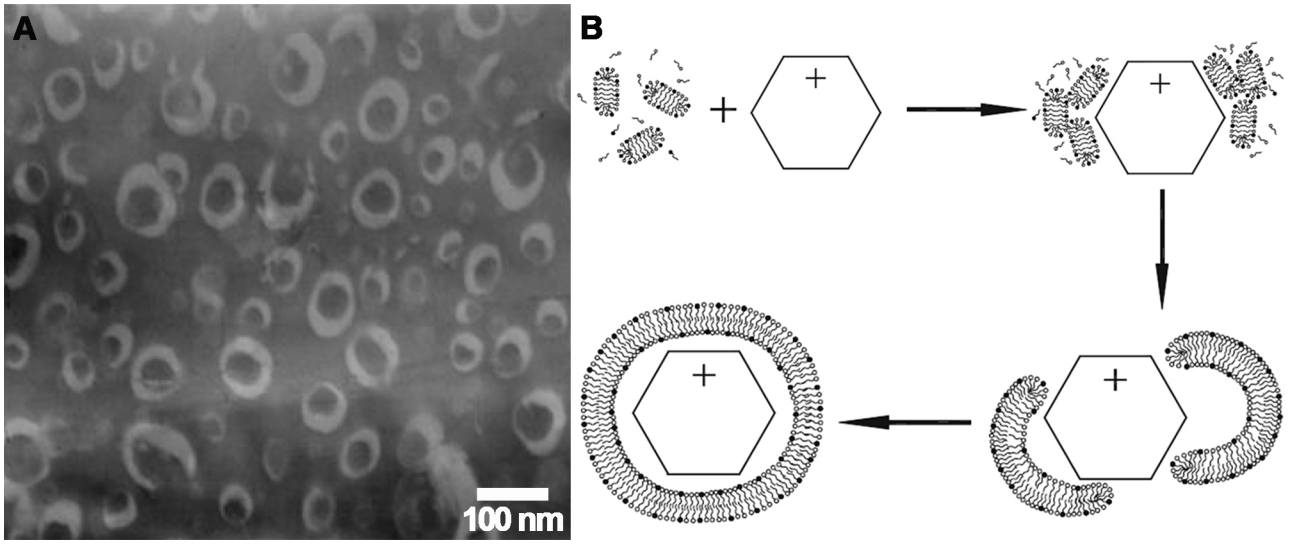

Figure 2-33 Negative stained TEM image of Mg_3Al-LDH-SDS/DTAB composites (A) and schematic illustration for the vesicle formation mechanism (B), reproduced from Ref. 160

2.4 Summary

A broad range of non-viral vectors have been developed for improving the therapeutic efficiency of gene therapy, including polymers, liposomes, and cell penetrating peptides (CPPs), inorganic metal and metal oxide nanoparticles (NPs), carbon nanotubes (CNTs), mesoporous silica nanoparticles (MSNs), calcium phosphate (CaP) NPs and layered double hydroxide (LDH) NPs. However, each pure delivery system has been noted to have its drawback(s).

Some hybridisation systems have shown promising in efficient drug/gene delivery by merging the advantages of two or more worlds, while overcoming their limitations. Thus this PhD project aims to develop a composite system from most biocompatible organic delivery vehicles liposomes and highly efficient, friendly inorganic LDH NPs. The resulted composite system is expected to combine the advantages from LDH NPs for high gene loading capacity, efficient transfection and endosomal escape, and from liposomes for good colloidal stability, while avoid the downsides of LDH for aggregation in blood circulation and liposomes for inefficient endosomal escape and payload release.

References

1. Sheridan, C. Gene therapy finds its niche. *Nature Biotechnology* **29**, 121-128 (2011).

2. Verma, I.M. & Somia, N. Gene therapy - promises, problems and prospects. *Nature* **389**, 239-242 (1997).

3. Devulapally, R. & Paulmurugan, R. Polymer nanoparticles for drug and small silencing RNA delivery to treat cancers of different phenotypes. *Wiley Interdisciplinary Reviews-Nanomedicine and Nanobiotechnology* **6**, 40-60 (2014).

4. Boussif, O. et al. A versatile vector for gene and oligonucleotide transfer into cells in culture and *in vivo*: Polyethylenimine. *Proceedings of the National Academy of Sciences of the United States of America* **92**, 7297-7301 (1995).

5. Goula, D. et al. Polyethylenimine-based intravenous delivery of transgenes to mouse lung. *Gene Therapy* **5**, 1291-1295 (1998).

6. Thomas, M. & Klibanov, A.M. Enhancing polyethylenimine's delivery of plasmid DNA into mammalian cells. *Proceedings of the National Academy of Sciences of the United States of America* **99**, 14640-14645 (2002).

7. Kim, S.J. et al. Gene delivery system based on highly specific recognition of surface-vimentin with N-acetylglucosamine immobilized polyethylenimine. *Biomaterials* **32**, 3471-3480 (2011).

8. Gabrielson, N.P. & Pack, D.W. Acetylation of polyethylenimine enhances gene delivery via weakened polymer/DNA interactions. *Biomacromolecules* **7**, 2427-2435 (2006).

9. Gabrielson, N.P. & Pack, D.W. Efficient polyethylenimine-mediated gene delivery proceeds via a caveolar pathway in HeLa cells. *Journal of Controlled Release* **136**, 54-61 (2009).

10. Grayson, A.C.R., Doody, A.M. & Putnam, D. Biophysical and structural characterization of polyethylenimine-mediated siRNA delivery in vitro. *Pharmaceutical Research* **23**, 1868-1876 (2006).

11. Shim, M.S. & Kwon, Y.J. Acid-responsive linear polyethylenimine for efficient, specific, and biocompatible siRNA delivery. *Bioconjugate Chemistry* **20**, 488-499 (2009).

12. Alshamsan, A. et al. The induction of tumor apoptosis in B16 melanoma following STAT3 siRNA delivery with a lipid-substituted polyethylenimine. *Biomaterials* **31**, 1420-1428 (2010).

13. Hobel, S. & Aigner, A. Polyethylenimines for siRNA and miRNA delivery in vivo. *Wiley Interdisciplinary Reviews-Nanomedicine and Nanobiotechnology* **5**, 484-501 (2013).

14. Katas, H. & Alpar, H.O. Development and characterisation of chitosan nanoparticles for siRNA delivery. *Journal of Controlled Release* **115**, 216-225 (2006).

15. Howard, K.A. et al. RNA interference *in vitro* and *in vivo* using a chitosan/siRNA nanoparticle system. *Molecular Therapy* **14**, 476-484 (2006).

16. Liu, X. et al. The influence of polymeric properties on chitosan/siRNA nanoparticle formulation and gene silencing. *Biomaterials* **28**, 1280-1288 (2007).

17. Yu, Y., Zhang, X. & Qiu, L. The anti-tumor efficacy of curcumin when delivered by size/charge-changing multistage polymeric micelles based on amphiphilic poly(beta-amino ester) derivates. *Biomaterials* **35**, 3467-3479 (2014).

18. Liu, Y., Samsonova, O., Sproat, B., Merkel, O. & Kissel, T. Biophysical characterization of hyper-branched polyethylenimine-graft-polycaprolactone-block-mono-methoxyl-poly(ethylen e glycol) copolymers (hy-PEI-PCL-mPEG) for siRNA delivery. *Journal of Controlled Release* **153**, 262-268 (2011).

19. Guo, X. et al. Dual-responsive polymer micelles for target-cell-specific anticancer drug delivery. *Chemistry of Materials* (2014).

20. Yamano, S. et al. Long-term efficient gene delivery using polyethylenimine with modified Tat peptide. *Biomaterials* **35**, 1705-1715 (2014).

21. Kunjachan, S. et al. Passive versus active tumor targeting using RGD- and NGR-modified polymeric nanomedicines. *Nano Letters* **14**, 972-981 (2014).

22. Xu, S. et al. Preparation and Ccharacterization of folate-chitosan-gemcitabine core-shell nanoparticles for potential tumor-targeted drug delivery. *Journal of Nanoscience and Nanotechnology* **13**, 129-138 (2013).

23. Vangara, K.K., Liu, J.L. & Palakurthi, S. Hyaluronic acid-decorated PLGA-PEG nanoparticles for targeted delivery of SN-38 to ovarian cancer. *Anticancer Research* **33**, 2425-2434 (2013).

24. Schäfera, J., Hoel, S., Bakowsky, U. & Aigner, A. Liposome-polyethylenimine complexes for enhanced DNA and siRNA delivery. *Biomaterials* **31**, 6892-6900 (2010).

25. Liu, X. et al. Efficient delivery of sticky siRNA and potent gene silencing in a prostate cancer model using a generation 5 triethanolamine-core PAMAM dendrimer. *Molecular Pharmaceutics* **9**, 470-481 (2011).

26. Liu, H., Wang, H., Yang, W. & Cheng, Y. Disulfide cross-linked low generation dendrimers with high gene transfection efficacy, low cytotoxicity, and low cost. *Journal of the American Chemical Society* **134**, 17680-17687 (2012).

27. Wang, M., Liu, H., Li, L. & Cheng, Y. A fluorinated dendrimer achieves excellent gene transfection efficacy at extremely low nitrogen to phosphorus ratios. *Nature Communications* **5** (2014).

28. Liu, H., Wang, Y., Wang, M., Xiao, J. & Cheng, Y. Fluorinated poly(propylenimine) dendrimers as gene vectors. *Biomaterials* **35** (2014).

29. Bansal, R., Singh, M., Gupta, K.C. & Kumar, P. Oligoamine-tethered low generation polyamidoamine dendrimers as potential nucleic acid carriers. *Biomaterials Science* (2014).

30. Kesharwani, P., Jain, K. & Jain, N.K. Dendrimer as nanocarrier for drug delivery. *Progress in Polymer Science* **39**, 268-307 (2014).

31. Choi, J.S. et al. Enhanced transfection efficiency of PAMAM dendrimer by surface modification with L-arginine. *Journal of Controlled Release* **99**, 445-456 (2004).

32. Kim, T.I., Baek, J.U., Bai, C.Z. & Park, J.S. Arginine-conjugated polypropylenimine dendrimer as a non-toxic and efficient gene delivery carrier. *Biomaterials* **28**, 2061-2067 (2007).

33. Arima, H., Kihara, F., Hirayama, F. & Uekama, K. Enhancement of gene expression by polyamidoamine dendrimer conjugates with alpha-, beta-, and gamma-cyclodextrins. *Bioconjugate Chemistry* **12**, 476-484 (2001).

34. Kihara, F., Arima, H., Tsutsumi, T., Hirayama, F. & Uekama, K. *In vitro* and *in vivo* gene transfer by an optimized alpha-cyclodextrin conjugate with polyamidoamine dendrimer. *Bioconjugate Chemistry* **14**, 342-350 (2003).

35. Luo, D., Haverstick, K., Belcheva, N., Han, E. & Saltzman, W.M. Poly(ethylene glycol)-conjugated PAMAM dendrimer for biocompatible, high-efficiency DNA delivery. *Macromolecules* **35**, 3456-3462 (2002).

36. Ke, W. et al. Gene delivery targeted to the brain using an Angiopep-conjugated polyethyleneglycol-modified polyamidoamine dendrimer. *Biomaterials* **30**, 6976-6985 (2009).

37. Han, L. et al. Plasmid pORF-hTRAIL and doxorubicin co-delivery targeting to tumor using peptide-conjugated polyamidoamine dendrimer. *Biomaterials* **32**, 1242-1252 (2011).

38. Huang, R.Q. et al. Efficient gene delivery targeted to the brain using a transferrin-conjugated polyethyleneglycol-modified polyamidoamine dendrimer. *Faseb Journal* **21**, 1117-1125 (2007).

39. Shan, Y. et al. Gene delivery using dendrimer-entrapped gold nanoparticles as nonviral vectors. *Biomaterials* **33**, 3025-3035 (2012).

40. Wang, F.H. et al. Recent progress of cell-penetrating peptides as new carriers for intracellular cargo delivery. *Journal of Controlled Release* **174**, 126-136 (2014).

41. Crombez, L. et al. A new potent secondary amphipathic cell-penetrating peptide for siRNA delivery Into mammalian cells. *Molecular Therapy* **17**, 95-103 (2009).

42. Ezzat, K. et al. Solid formulation of cell-penetrating peptide nanocomplexes with siRNA and their stability in simulated gastric conditions. *Journal of Controlled Release* **162**, 1-8 (2012).

43. Park, J.W., Bang, E.K., Jeon, E.M. & Kim, B.H. Complexation and conjugation approaches to evaluate siRNA delivery using cationic, hydrophobic and amphiphilic peptides. *Organic & Biomolecular Chemistry* **10**, 96-102 (2012).

44. Hoyer, J. & Neundorf, I. Knockdown of a G protein-coupled receptor through efficient peptide-mediated siRNA delivery. *Journal of Controlled Release* **161**, 826-834 (2012).

45. Bai, H. et al. Antisense inhibition of gene expression and growth in gram-negative bacteria by cell-penetrating peptide conjugates of peptide nucleic acids targeted to rpoD gene. *Biomaterials* **33**, 659-667 (2012).

46. Lindgren, M. et al. Overcoming methotrexate resistance in breast cancer tumour cells by the use of a new cell-penetrating peptide. *Biochemical Pharmacology* **71**, 416-425 (2006).

47. Liu, B., Liou, J.-S., Chen, Y.-J., Huang, Y.-W. & Lee, H.-J. Delivery of nucleic acids, proteins, and nanoparticles by arginine-rich cell-penetrating peptides in rotifers. *Marine Biotechnology* **15**, 584-595 (2013).

48. Santra, S. et al. Rapid and effective labeling of brain tissue using TAT-conjugated CdS[ratio]Mn/ZnS quantum dots. *Chemical Communications*, 3144-3146 (2005).

49. Lewin, M. et al. Tat peptide-derivatized magnetic nanoparticles allow in vivo tracking and recovery of progenitor cells. *Nature Biotechnology* **18**, 410-414 (2000).

50. Jang, Y.L. et al. Cell-penetrating peptide mimicking polymer-based combined delivery of paclitaxel and siRNA for enhanced tumor growth suppression. *International Journal of Pharmaceutics* **434**, 488-493 (2012).

51. Cohen, J.L. et al. Enhanced cell penetration of acid-degradable particles functionalized with cell-penetrating peptides. *Bioconjugate Chemistry* **19**, 876-881 (2008).

52. Walker, L., Perkins, E., Kratz, F. & Raucher, D. Cell penetrating peptides fused to a thermally targeted biopolymer drug carrier improve the delivery and antitumor efficacy of an acid-sensitive doxorubicin derivative. *International Journal of Pharmaceutics* **436**, 825-832 (2012).

53. Bangham, A.D., Standish, M.M. & Watkins, J.C. Diffusion of univalent ions across the lamellae of swollen phospholipids. *Journal of Molecular Biology* **13**, 238-252, IN26-IN27 (1965).

54. Bangham, A.D. & Horne, R.W. Negative staining of phospholipids and their structural modification by surface-active agents as observed in the electron microscope. *Journal of Molecular Biology* **8**, 660-668, IN2-IN10 (1964).

55. Rudolph L, J. Liposomes as a drug delivery system. *Trends in Pharmacological Sciences* **2**, 39-42 (1981).

56. Klibanov, A.L., Maruyama, K., Torchilin, V.P. & Huang, L. Amphipathic polyethyleneglycols effectively prolong the circulation time of liposomes. *FEBS Lett* **268**, 235-7 (1990).

57. Woodle, M.C. Controlling liposome blood clearance by surface-grafted polymers. *Advanced Drug Delivery Reviews* **32**, 139-152 (1998).

58. Maeda, H., Sawa, T. & Konno, T. Mechanism of tumor-targeted delivery of macromolecular drugs, including the EPR effect in solid tumor and clinical overview of the prototype polymeric drug SMANCS. *Journal of Controlled Release* **74**, 47-61 (2001).

59. Blume, G. et al. Specific targeting with poly(ethylene glycol)-modified liposomes: coupling of homing devices to the ends of the polymeric chains combines effective target binding with long circulation times. *Biochim Biophys Acta* **1149**, 180-4 (1993).

60. Lu, Y. & Low, P.S. Folate-mediated delivery of macromolecular anticancer therapeutic agents. *Advanced Drug Delivery Reviews* **54**, 675-93 (2002).

61. Guo, S.T. & Huang, L. Nanoparticles escaping RES and endosome: Challenges for siRNA delivery for cancer therapy. *Journal of Nanomaterials* (2011).

62. Torchilin, V.P. Recent advances with liposomes as pharmaceutical carriers. *Nature Reviews Drug Discovery* **4**, 145-160 (2005).

63. Khopade, A.J., Caruso, F., Tripathi, P., Nagaich, S. & Jain, N.K. Effect of dendrimer on entrapment and release of bioactive from liposomes. *International Journal of Pharmaceutics* **232**, 157-162 (2002).

64. Papagiannaros, A., Dimas, K., Papaioannou, G.T. & Demetzos, C. Doxorubicin–PAMAM dendrimer complex attached to liposomes: Cytotoxic studies against human cancer cell lines. *International Journal of Pharmaceutics* **302**, 29-38 (2005).

65. Su, C. et al. Liposomes physically coated with peptides: Preparation and characterization. *Langmuir* **30**, 6219-6227 (2014).

66. Yuba, E. et al. Dextran derivative-based pH-sensitive liposomes for cancer immunotherapy. *Biomaterials* **35**, 3091-3101 (2014).

67. Yoshizaki, Y. et al. Potentiation of pH-sensitive polymer-modified liposomes with cationic lipid inclusion as antigen delivery carriers for cancer immunotherapy. *Biomaterials* **35**, 8186-96 (2014).

68. Rodriguez-Pulido, A. et al. Light-triggered sequence-specific cargo release from DNA block copolymer-lipid vesicles. *Angewandte Chemie-International Edition* **52**, 1008-1012 (2013).

69. Raemdonck, K., Braeckmans, K., Demeester, J. & De Smedt, S.C. Merging the best of both worlds: hybrid lipid-enveloped matrix nanocomposites in drug delivery. *Chemical Society Reviews* **43**, 444-472 (2014).

70. Li, J., Chen, Y.-C., Tseng, Y.-C., Mozumdar, S. & Huang, L. Biodegradable calcium phosphate nanoparticle with lipid coating for systemic siRNA delivery. *Journal of Controlled Release* **142**, 416-421 (2010).

71. Li, J., Yang, Y. & Huang, L. Calcium phosphate nanoparticles with an asymmetric lipid bilayer coating for siRNA delivery to the tumor. *Journal of Controlled Release* **158**, 108-114 (2012).

72. Nahire, R. et al. Multifunctional polymersomes for cytosolic delivery of gemcitabine and doxorubicin to cancer cells. *Biomaterials* **35**, 6482-97 (2014).

73. Zhang, S. et al. Self-assembly of amphiphilic Janus dendrimers into uniform onion-like dendrimersomes with predictable size and number of bilayers. *Proceedings of the National Academy of Sciences of the United States of America* **111**, 9058-9063 (2014).

74. Xu, H., Meng, F. & Zhong, Z. Reversibly crosslinked temperature-responsive nano-sized polymersomes: synthesis and triggered drug release. *Journal of Materials Chemistry* **19**, 4183-4190 (2009).

75. Baillie, A.J., Florence, A.T., Hume, L.R., Muirhead, G.T. & Rogerson, A. The preparation and properties of niosomes--non-ionic surfactant vesicles. *Journal of Pharmacy and Pharmacology* **37**, 863-868 (1985).

76. Tavano, L. et al. Doxorubicin loaded magneto-niosomes for targeted drug delivery. *Colloids and Surfaces B-Biointerfaces* **102**, 803-807 (2013).

77. Tavano, L., Aiello, R., Ioele, G., Picci, N. & Muzzalupo, R. Niosomes from glucuronic acid-based surfactant as new carriers for cancer therapy: Preparation, characterization and biological properties. *Colloids and Surfaces B-Biointerfaces* **118**, 7-13 (2014).

78. Tavano, L. et al. Transferrin-conjugated pluronic niosomes as a new drug delivery system for anticancer therapy. *Langmuir* **29**, 12638-12646 (2013).

79. Tavano, L., Muzzalupo, R., Picci, N. & de Cindio, B. Co-encapsulation of lipophilic antioxidants into niosomal carriers: Percutaneous permeation studies for cosmeceutical applications. *Colloids and Surfaces B-Biointerfaces* **114**, 144-149 (2014).

80. Marianecci, C. et al. Niosomes from 80s to present: The state of the art. *Advances in Colloid and Interface Science* **205**, 187-206 (2014).

81. Whitehead, K.A. et al. Synergistic silencing: Combinations of lipid-like materials for efficacious siRNA delivery. *Molecular Therapy*, 1-7 (2011).

82. Chien, P.-Y. et al. Novel cationic cardiolipin analogue-based liposome for efficient DNA and small interfering RNA delivery in vitro and in vivo. *Cancer Gene Therapy* **12**, 321-328 (2004).

83. Adami, R.C. et al. An amino acid-based amphoteric liposomal delivery system for systemic administration of siRNA. *Molecular Therapy* **19**, 1141-1151 (2011).

84. Faraday, M. The Bakerian lecture: Experimental relations of gold (and other metals) to light. *Philosophical Transactions of the Royal Society of London* **147**, 145-181 (1857).

85. Mie, G. Contributions to the optics of turbid media, especially colloidal metal solutions. *Annalen der Physik (Weinheim, Germany)* **25**, 377-445 (1908).

86. Giersig, M. & Mulvaney, P. Preparation of ordered colloid monolayers by electrophoretic deposition. *Langmuir* **9**, 3408-3413 (1993).

87. Kim, C.K. et al. Entrapment of hydrophobic drugs in nanoparticle monolayers with efficient release into cancer cells. *Journal of the American Chemical Society* **131**, 1360-1361 (2009).

88. Rosi, N.L. et al. Oligonucleotide-modified gold nanoparticles for intracellular gene regulation. *Science* **312**, 1027-1030 (2006).

89. Oishi, M., Nakaogami, J., Ishii, T. & Nagasaki, Y. Smart PEGylated gold nanoparticles for the cytoplasmic delivery of siRNA to induce enhanced gene silencing. *Chemistry Letters* **35**, 1046-1047 (2006).

90. Beck, J.S. et al. A new family of mesoporous molecular sieves prepared with liquid crystal templates. *Journal of the American Chemical Society* **114**, 10834-10843 (1992).

91. Kresge, C.T., Leonowicz, M.E., Roth, W.J., Vartuli, J.C. & Beck, J.S. Ordered mesoporous molecular sieves synthesized by a liquid-crystal template mechanism. *Nature* **359**, 710-712 (1992).

92. Vallet-Regi, M., Rámila, A., del Real, R.P. & Pérez-Pariente, J. A new property of MCM-41: Drug delivery system. *Chemistry of Materials* **13**, 308-311 (2001).

93. Niu, Y. et al. Nanoparticles mimicking viral surface topography for enhanced cellular delivery. *Advanced Materials* **25**, 6233-6237 (2013).

94. Xu, C. et al. Rod-like mesoporous silica nanoparticles with rough surfaces for enhanced cellular delivery. *Journal of Materials Chemistry B* **2**, 253-256 (2014).

95. Yang, P., Gai, S. & Lin, J. Functionalized mesoporous silica materials for controlled drug delivery. *Chemical Society Reviews* **41**, 3679-3698 (2012).

96. Chen, A.M. et al. Co-delivery of doxorubicin and Bcl-2 siRNA by mesoporous silica nanoparticles enhances the efficacy of chemotherapy in multidrug-resistant cancer cells. *Small* **5**, 2673-2677 (2009).

97. Zhou, S., Du, X., Cui, F. & Zhang, X. Multi- responsive and logic controlled release of DNAGated mesoporous silica vehicles functionalized with intercalators for multiple delivery. *Small* **10**, 980-988 (2014).

98. Zhang, P. et al. DNA-hybrid-gated multifunctional mesoporous silica nanocarriers for dual-targeted and microRNA-responsive controlled drug delivery**. *Angewandte Chemie-International Edition* **53**, 2371-2375 (2014).

99. Zhang, Q. et al. Biocompatible, uniform, and redispersible mesoporous silica nanoparticles for cancer- targeted drug delivery *in vivo*. *Advanced Functional Materials* **24**, 2450-2461 (2014).

100. Xiao, D. et al. A dual-responsive mesoporous silica nanoparticle for tumor-triggered targeting drug delivery. *Small* **10**, 591-598 (2014).

101. Xia, T.A. et al. Polyethyleneimine coating enhances the cellular uptake of mesoporous silica nanoparticles and allows safe delivery of siRNA and DNA constructs. *Acs Nano* **3**, 3273-3286 (2009).

102. Hom, C. et al. Mesoporous silica nanoparticles facilitate delivery of siRNA to shutdown Sisgnaling pathways in mammalian cells. *Small* **6**, 1185-1190 (2010).

103. Li, X., Xie, Q.R., Zhang, J.X., Xia, W.L. & Gu, H.C. The packaging of siRNA within the mesoporous structure of silica nanoparticles. *Biomaterials* **32**, 9546-9556 (2011).

104. Lee, H., Sung, D., Veerapandian, M., Yun, K. & Seo, S.W. PEGylated polyethyleneimine grafted silica nanoparticles: enhanced cellular uptake and efficient siRNA delivery. *Analytical and Bioanalytical Chemistry* **400**, 535-545 (2011).

105. Buchman, Y.K. et al. Silica nanoparticles and polyethyleneimine (PEI)-mediated functionalization: A new method of PEI covalent attachment for siRNA delivery applications. *Bioconjugate Chemistry* **24**, 2076-2087 (2013).

106. Bhattarai, S.R. et al. Enhanced gene and siRNA delivery by polycation-modified mesoporous silica nanoparticles loaded with chloroquine. *Pharmaceutical Research* **27**, 2556-2568 (2010).

107. Meng, H.A. et al. Engineered design of mesoporous silica nanoparticles to deliver doxorubicin and P-glycoprotein siRNA to overcome drug resistance in a cancer cell line. *Acs Nano* **4**, 4539-4550 (2010).

108. Radu, D.R. et al. A polyamidoamine dendrimer-capped mesoporous silica nanosphere-based gene transfection reagent. *Journal of the American Chemical Society* **126**, 13216-13217 (2004).

109. Iijima, S. Helical microtubules of graphitic carbon. *Nature* **354**, 56-58 (1991).

110. Radushkevich, L.V. & Lukyanovich, V.M. O strukture ugleroda, obrazujucegosja pri termiceskom razlozenii okisi ugleroda na zeleznom kontakte. *Zurn Fisic Chim (Soviet Journal of Physical Chemistry)* **26**, 88-95 (1952).

111. Oberlin, A., Endo, M. & Koyama, T. Filamentous growth of carbon through benzene decomposition. *Journal of Crystal Growth* **32**, 335-349 (1976).

112. Bacon, R. Growth, structure, and properties of graphite whiskers. *Journal of Applied Physics* **31**, 283-290 (1960).

113. Iijima, S. & Ichihashi, T. Single-shell carbon nanotubes of 1-nm diameter. *Nature* **363**, 603-605 (1993).

114. Wong, B.S. et al. Carbon nanotubes for delivery of small molecule drugs. *Advanced Drug Delivery Reviews* **65**, 1964-2015 (2013).

115. Bates, K. & Kostarelos, K. Carbon nanotubes as vectors for gene therapy: Past achievements, present challenges and future goals. *Advanced Drug Delivery Reviews* **65**, 2023-2033 (2013).

116. Wang, L. et al. Synergistic anticancer effect of RNAi and photothermal therapy mediated by functionalized single-walled carbon nanotubes. *Biomaterials* **34**, 262-274 (2013).

117. Wu, H. et al. Prostate stem cell antigen antibody-conjugated multiwalled carbon nanotubes for targeted ultrasound imaging and drug delivery. *Biomaterials* **35**, 5369-80 (2014).

118. Anderson, T., Hu, R., Yang, C., Yoon, H.S. & Yong, K.-T. Pancreatic cancer gene therapy using an siRNA-functionalized single walled carbon nanotubes (SWNTs) nanoplex. *Biomaterials Science* (2014).

119. Qin, W.L. et al. Improved GFP gene transfection mediated by polyamidoamine dendrimer-functionalized multi-walled carbon nanotubes with high biocompatibility. *Colloids and Surfaces B-Biointerfaces* **84**, 206-213 (2011).

120. Zhang, Y. 193 (The University of North Carolina at Chapel Hill, Ann Arbor, 2013).

121. Auerbach, S.M., Carrado, K.A. & Dutta, P.K. (eds.) Handbook of layered materials (Marcel Dekker, Inc, New York, 2004).

122. Rives, V., del Arco, M. & Martin, C. Intercalation of drugs in layered double hydroxides and their controlled release: A review. *Applied Clay Science* **88-89**, 239-269 (2014).

123. Gu, Z., Thomas, A.C., Xu, Z.P., Campbell, J.H. & Lu, G.Q. *In vitro* sustained release of LMWH from MgAl-layered double hydroxide nanohybrids. *Chemistry of Materials* **20**, 3715-3722 (2008).

124. Gu, Z. et al. Enhanced effects of low molecular weight heparin intercalated with layered double hydroxide nanoparticles on rat vascular smooth muscle cells. *Biomaterials* **31**, 5455-5462 (2010).

125. Gu, Z. (The University of Queensland, Queensland, Australia, 2011).

126. Choy, J.-H., Kwak, S.-Y., Park, J.-S., Jeong, Y.-J. & Portier, J. Intercalative nanohybrids of nucleoside monophosphates and DNA in layered metal hydroxide. *Journal of the American Chemical Society* **121**, 1399-1400 (1999).

127. Choy, J.-H., Kwak, S.-Y., Jeong, Y.-J. & Park, J.-S. Inorganic layered double hydroxides as nonviral vectors. *Angewandte Chemie International Edition* **39**, 4041-4045 (2000).

128. Choy, J.H., Kwak, S.Y., Park, J.S. & Jeong, Y.J. Cellular uptake behavior of gamma-P-32 labeled ATP-LDH nanohybrids. *Journal of Materials Chemistry* **11**, 1671-1674 (2001).

129. Kwak, S.-Y., Jeong, Y.-J., Park, J.-S. & Choy, J.-H. Bio-LDH nanohybrid for gene therapy. *Solid State Ionics* **151**, 229-234 (2002).

130. Tyner, K.M. et al. Intercalation, delivery, and expression of the gene encoding green fluorescence protein utilizing nanobiohybrids. *Journal of Controlled Release* **100**, 399-409 (2004).

131. Masarudin, M.J., Yusoff, K., Rahim, R.A. & Hussein, M.Z. Successful transfer of plasmid DNA into *in vitro* cells transfected with an inorganic plasmid-Mg/Al-LDH nanobiocomposite material as a vector for gene expression. *Nanotechnology* **20** (2009).

132. Ladewig, K. (The University of Queensland, Queensland, Australia, 2009).

133. Ladewig, K., Niebert, M., Xu, Z.P., Gray, P.P. & Lu, G.Q. Controlled preparation of layered double hydroxide nanoparticles and their application as gene delivery vehicles. *Applied Clay Science* **48**, 280-289 (2010).

134. Li, A. et al. The use of layered double hydroxides as DNA vaccine delivery vector for enhancement of anti-melanoma immune response. *Biomaterials* **32**, 469-477 (2011).

135. Wong, Y. (The University of Queensland, Queensland, Australia, 2009).

136. Ladewig, K., Niebert, M., Xu, Z.P., Gray, P.P. & Lu, G.Q.M. Efficient siRNA delivery to mammalian cells using layered double hydroxide nanoparticles. *Biomaterials* **31**, 1821-1829 (2010).

137. Wong, Y. et al. Efficient delivery of siRNA to cortical neurons using layered double hydroxide nanoparticles. *Biomaterials* **31**, 8770-8779 (2010).

138. Wong, Y.Y. et al. Efficiency of layered double hydroxide nanoparticle-mediated delivery of siRNA is determined by nucleotide sequence. *Journal of Colloid and Interface Science* **369**, 453-459 (2012).

139. Chen, M., Cooper, H.M., Zhou, J.Z., Bartlett, P.F. & Xu, Z.P. Reduction in the size of layered double hydroxide nanoparticles enhances the efficiency of siRNA delivery. *Journal of Colloid and Interface Science* **390**, 275-281 (2013).

140. Li, L., Gu, W., Chen, J., Chen, W. & Xu, Z.P. Co-delivery of siRNAs and anti-cancer drugs using layered double hydroxide nanoparticles. *Biomaterials* **35**, 3331-3339 (2014).

141. Kriven, W.M., Kwak, S.-Y., Wallig, M.A. & Choy, J.-H. Bio-resorbable nanoceramics for gene and drug delivery. *MRS bulletin* **29**, 33-37 (2004).

142. Gu, Z. et al. Cellular trafficking of low molecular weight heparin incorporated in layered double hydroxide nanoparticles in rat vascular smooth muscle cells. *Biomaterials* **32**, 7234-7240 (2011).

143. Oh, J.-M., Biswick, T.T. & Choy, J.-H. Layered nanomaterials for green materials. *Journal of Materials Chemistry* **19**, 2553-2563 (2009).

144. Wang, L. et al. A Gd-doped Mg-Al-LDH/Au nanocomposite for CT/MR bimodal imagings and simultaneous drug delivery. *Biomaterials* **34**, 3390-3401 (2013).

145. Zhang, H., Pan, D. & Duan, X. Synthesis, characterization, and magnetically controlled release behavior of novel core-shell structural magnetic ibuprofen-intercalated LDH nanohybrids. *The Journal of Physical Chemistry C* **113**, 12140-12148 (2009).

146. Bao, H. et al. Synthesis of well-dispersed layered double hydroxide core@ordered mesoporous silica shell nanostructure (LDH@mSiO_2) and its application in drug delivery. *Nanoscale* **3**, 4069-4073 (2011).

147. Liu, J. et al. Synthesis of nanorattles with layered double hydroxide core and mesoporous silica shell as delivery vehicles. *Journal of Materials Chemistry* **21**, 10641-10644 (2011).

148. Zheng, Q. et al. A pH-responsive controlled release system using layered double hydroxide (LDH)-capped mesoporous silica nanoparticles. *Journal of Materials Chemistry B* **1**, 1644-1648 (2013).

149. Wang, J. et al. The enhanced immune response of hepatitis B virus DNA vaccine using SiO_2@LDH nanoparticles as an adjuvant. *Biomaterials* **35**, 466-478 (2014).

150. Ribeiro, L.N.M. et al. Pectin-coated chitosan LDH bionanocomposite beads as potential systems for colon-targeted drug delivery. *International Journal of Pharmaceutics* **463**, 1-9 (2014).

151. Mahkam, M., Davatgar, M., Rezvani, Z. & Nejati, K. Preparation of pH-sensitive polymers/layered double hydroxide hybrid beads for controlled release of insulin. *International Journal of Polymeric Materials and Polymeric Biomaterials* **62**, 57-60 (2013).

152. Hu, H., Xiu, K.M., Xu, S.L., Yang, W.T. & Xu, F.J. Functionalized layered double hydroxide nanoparticles conjugated with disulfide-linked polycation brushes for advanced gene delivery. *Bioconjugate chemistry* **24**, 968-978 (2013).

153. Ciobanu, A. et al. Cyclodextrin-intercalated layered double hydroxides for fragrance release. *Journal of Inclusion Phenomena and Macrocyclic Chemistry* **75**, 333-339 (2013).

154. San Roman, M.S., Holgado, M.J., Salinas, B. & Rives, V. Drug release from layered double hydroxides and from their polylactic acid (PLA) nanocomposites. *Applied Clay Science* **71**, 1-7 (2013).

155. Xia, Z.-Y., Du, N., Liu, J.-Q. & Hou, W.-G. Surface modification of layer double hydroxide particles by poly (ethylene glycol) and folic acid. *Chemical Journal of Chinese Universities-Chinese* **34**, 596-600 (2013).

156. Alcântara, A.C.S., Aranda, P., Darder, M. & Ruiz-Hitzky, E. Bionanocomposites based on alginate-zein/layered double hydroxide materials as drug delivery systems. Journal of Materials Chemistry 20, 9495-9504 (2010).

157. Tyner, K.M., Schiffman, S.R. & Giannelis, E.P. Nanobiohybrids as delivery vehicles for camptothecin. *Journal of Controlled Release* **95**, 501-514 (2004).

158. Bégu, S. et al. New layered double hydroxides/phospholipid bilayer hybrid material with strong potential for sustained drug delivery system. *Chemistry of Materials* **21**, 2679-2687 (2009).

159. Du, N., Hou, W.-G. & Song, S.-E. A novel composite: Layered double hydroxides encapsulated in vesicles. *The Journal of Physical Chemistry Part B* **111**, 13909-13913 (2007).

160. Nie, H.-Q. & Hou, W.-G. Vesicle formation induced by layered double hydroxides in the catanionic surfactant solution composed of sodium dodecyl sulfate and dodecyltrimethylammonium bromide. *Colloid and Polymer Science* **289**, 775-782 (2011).

161. Nie, H., Song, S. & Hou, W. Vesicles formation induced by layered double hydroxides in mixture of lauryl sulfonate betaine and sodium dodecyl benzenesulfonate. *Chinese Journal of Chemistry* **29**, 1373-1379 (2011).

162. Huang, J. et al. Preparation and characterization of "dextran- magnetic layered double hydroxide- fluorouracil" targeted liposomes. *International Journal of Pharmaceutics* **450**, 323-330 (2013).

163. Huang, J., Xue, B. & Gou, G.-j. in China Functional Materials Technology and Industry Forum (eds. Zhao, G., Lu, L., Long, B. & Nie, Z.) 526-528 (2013).

Chapter 3 Materials and Methods

3.1 Materials

Normal chemicals were used as bought from suppliers, including (sorted alphabetically): chloroform ($CHCl_3$, Merck); aluminium chloride hexahydrate ($AlCl_3 \cdot 6H_2O$, Fluka, ≥99.0%); aluminium nitrate nonahydrate ($Al(NO_3)_3 \cdot 9H_2O$, Fluka, ≥98.0%); DMSO (Sigma-Aldrich, BioReagent, ≥99.9%); DOPA (1,2-dioleoyl-*sn*-glycero-3-phosphate(sodium salt), Avanti polar lipids); egg PC (L-α-phosphatidylcholine (Egg, Chicken), Avanti polar lipids); FITC (fluorescein isothiocyanate isomer I, Sigma-Aldrich); magnesium chloride hexahydrate ($MgCl_2 \cdot 6H_2O$, Sigma-Aldrich, 99.0-102.0%); magnesium nitrate hexahydrate ($Mg(NO_3)_2 \cdot 6H_2O$, Fluka, ≥99.0%); methanol (Fluka, ≥99.0%); nitric acid (ACS reagent, 70%, Sigma-Aldrich); sodium hydroxide (NaOH, Fluka, ≥97.0%, pellets); *tert*-butanol (tertiary butyl alcohol, TBA, Sigma-Aldrich); Triton™ X-100 (Sigma-Aldrich).

Biological reagents used in this thesis include (sorted alphabetically): 25 bp dsDNA ladder (Invitrogen™); agarose powder (molecular grade, Bioline); DMEM (Dulbecco's Modified Eagle Medium, L-glutamine, Gibco®); DNA-Cy3 (PAGE purity, Sigma-Aldrich); DPBS (Dulbecco's phosphate-buffered saline, Gibco®); dsDNA DCC1 (sequencing/PCR purity, geneworks); FBS (Fetal Bovine Serum, Gibco®); gel loading dye (Invitrogen™); gel-Red (Invitrogen™); MTT reagent (5 mg/mL in PBS buffer, 3-(4,5-dimethylthiazol-2-yl)-2,5-diphenyltetrazolium bromide, Molecular Probes®); Oligofectamine™ (Life Technologies); trypsin-0.25%EDTA (Gibco®); UltraPure™ TBE Buffer (Invitrogen™). FBS was treated in 56 °C water bath for 30 min before use for heat inactivation.

3.2 Preparation of various nanoparticles (NPs)

3.2.1 LDH and LDH-FITC NPs

sLDH NPs were prepared by non-aqueous precipitation, followed by heat-treatment, purification and dispersion in water (Figure 3-1), which was modified from Pinnavaia's method.[1] Typically, 10 mL methanol solution containing 6 mmol of $Mg(NO_3)_2 \cdot 6H_2O$ and 2 mmol of $Al(NO_3)_3 \cdot 9H_2O$ was added drop-wise to a 40 mL of methanol solution containing 16 mmol NaOH under vigorous stirring. The mixture was stirred for 30-40 min, the precipitate slurry was then collected through centrifugation, redispersed in 40 mL fresh methanol and transferred to a Teflon®-lined autoclave, followed by heat-treatment at 100

°C for 18 h. After cooling the sample to room temperature, the precipitate slurry was collected through centrifugation, and washed twice with deionised water (DI water). The final collected slurry was manually dispersed in 40 mL of DI water, followed by standing at room temperature with occasional hand-shaking. This dispersion became transparent, resulting in a homogeneous LDH suspension after 4-6 days with the LDH mass concentration determined to be 6 to 7 mg/mL (~50% yield), *Z*-average diameter size ~ 40 nm.

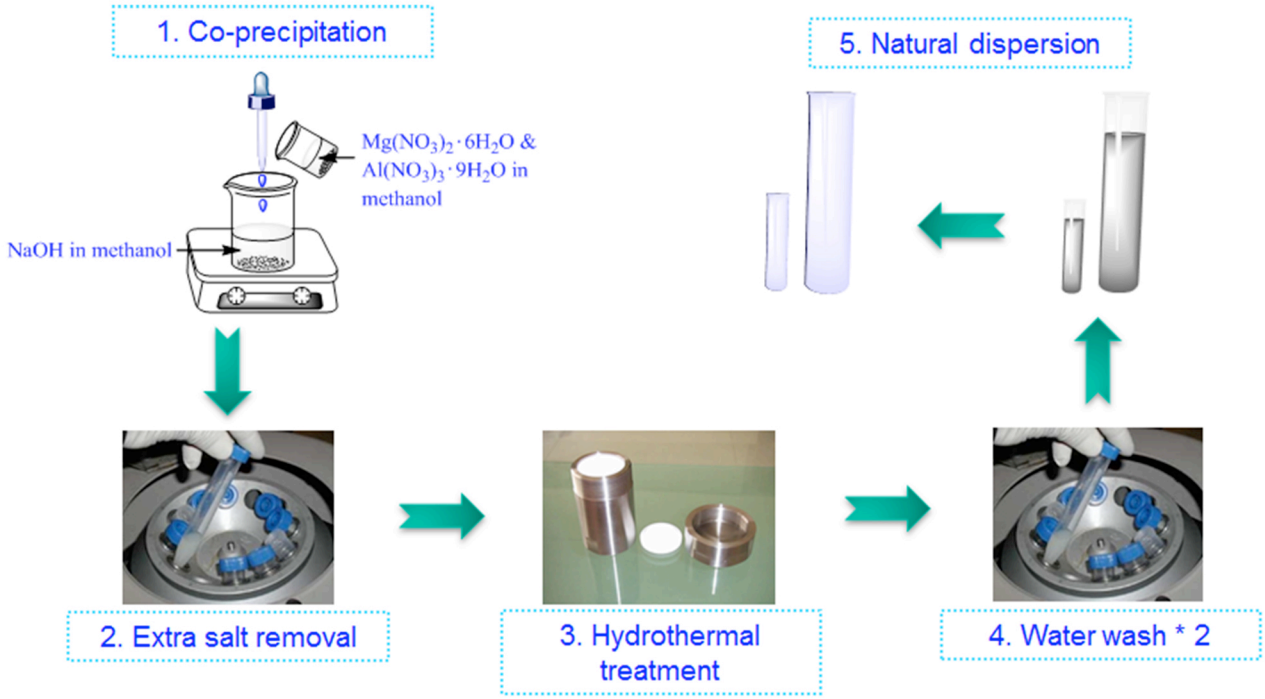

Figure 3-1 Schematic diagram for sLDH synthesis

Large LDH (L-LDH) particles were synthesised by vigorously mixing 10 mL of aqueous solution containing 3.0 mmol of $MgCl_2 \cdot 6H_2O$ and 1.0 mmol of $AlCl_3 \cdot 6H_2O$ with 40 mL of 0.15 M NaOH solution for 10 min at room temperature.[2-4] The LDH slurry was collected by centrifugation and then washed twice with DI water (40 mL), and resuspended in DI water (40 mL), after which the suspension was transferred to a Teflon®-lined autoclave and hydrothermally treated at 100 °C for 16 h. The suspension contained approximately 4 mg/mL of homogeneously dispersed Mg_2Al-LDH nanoparticles, with a *Z*-average diameter particle size ~ 100 nm.

Both small and large LDH-FITC NPs were prepared by ion-exchange method. FITC-Na solution (0.05 mmol) was mixed with 1 mmol of LDH slurry and then shaken on a

reciprocal shaker for 1 h. After ion-exchange, the unchanged FITC and residual $NaNO_3$/NaCl were separated and washed. Small and large LDH-FITC NPs were redispersed in DI water, and then followed by hydrothermal treatment.

3.2.2 LDH-liposome composites

LDH-liposome composites were prepared by two different methods, hydration of thin lipid film (HTLF) method and hydration of freeze dried matrix (HFDM) method.[5-8]

HTLF method: Egg PC (20-100 mg) was dissolved in chloroform (~ 5mL) and dried in a round bottom flask (RBF, 25-100 mL size) on a vacuum rotary evaporation system, then the thin lipid film was hydrated with sLDH suspension (2-10 mL, 6-24 mg/mL). Un-associated sLDH NPs were separated by centrifugation washing.

HFDM method: LDH suspension mixed with sucrose solution at volume ratio of 1:1, and then mixed with EPC in TBA (*tert*-butanol / tertiary butyl alcohol) solution at volume ratio of 7:3. LDH:DNA mass ratio = 20:1, lipid:DNA mass ratio = 20:1, and sucrose:lipid mass ratio = 190 :1 were used in the formulations. A clear solution should be obtained and then snap-frozen in dry ice. This frozen mixture was dried on a freeze-dryer overnight and then hydrated with DI water. A typical process for sLDH-liposome formulation loaded with dsDNA is shown in Figure 3-2 with detailed reagent concentrations and volumes used.

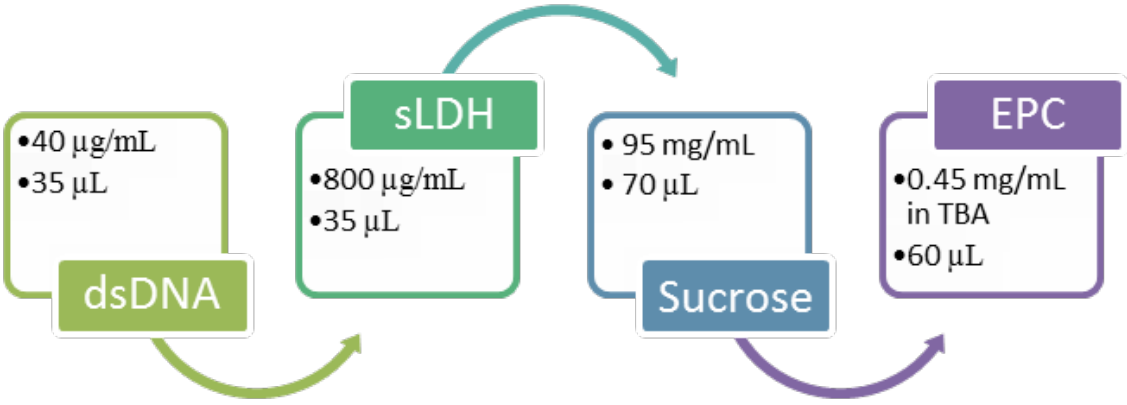

Figure 3-2 A typical process for sLDH-liposome formulation loaded with dsDNA

3.2.3 Nucleic acid complexes

Nucleic acids loaded in LDH NPs were realised by mixing LDH suspension with nucleic acid solution at mass ratio of 2:1, 5:1, 10:1, 20:1, and 40:1.

Nucleic acid loaded in LDH-liposome systems were conducted by three different ways. One way is to form LDH-nucleic acid associates first, then prepare the LDH-nucleic acid-liposome composite (Figure 3-3A). Another way is to add the nucleic acid in lipid/water/TBA three phase mixture before snap freezing (Figure 3-3B). The other is to prepare sLDH-liposome composite first, then mix DNA solution with pre-formed LDH-liposome composite suspension (Figure 3-3C). The resultant composites were denoted as LDH-DNA-Liposome, LDH-Liposome-DNA, and LDH-Liposome+DNA, respectively. The detail procedures for preparing the mixture before freeze-drying process are shown in Figure 3-3.

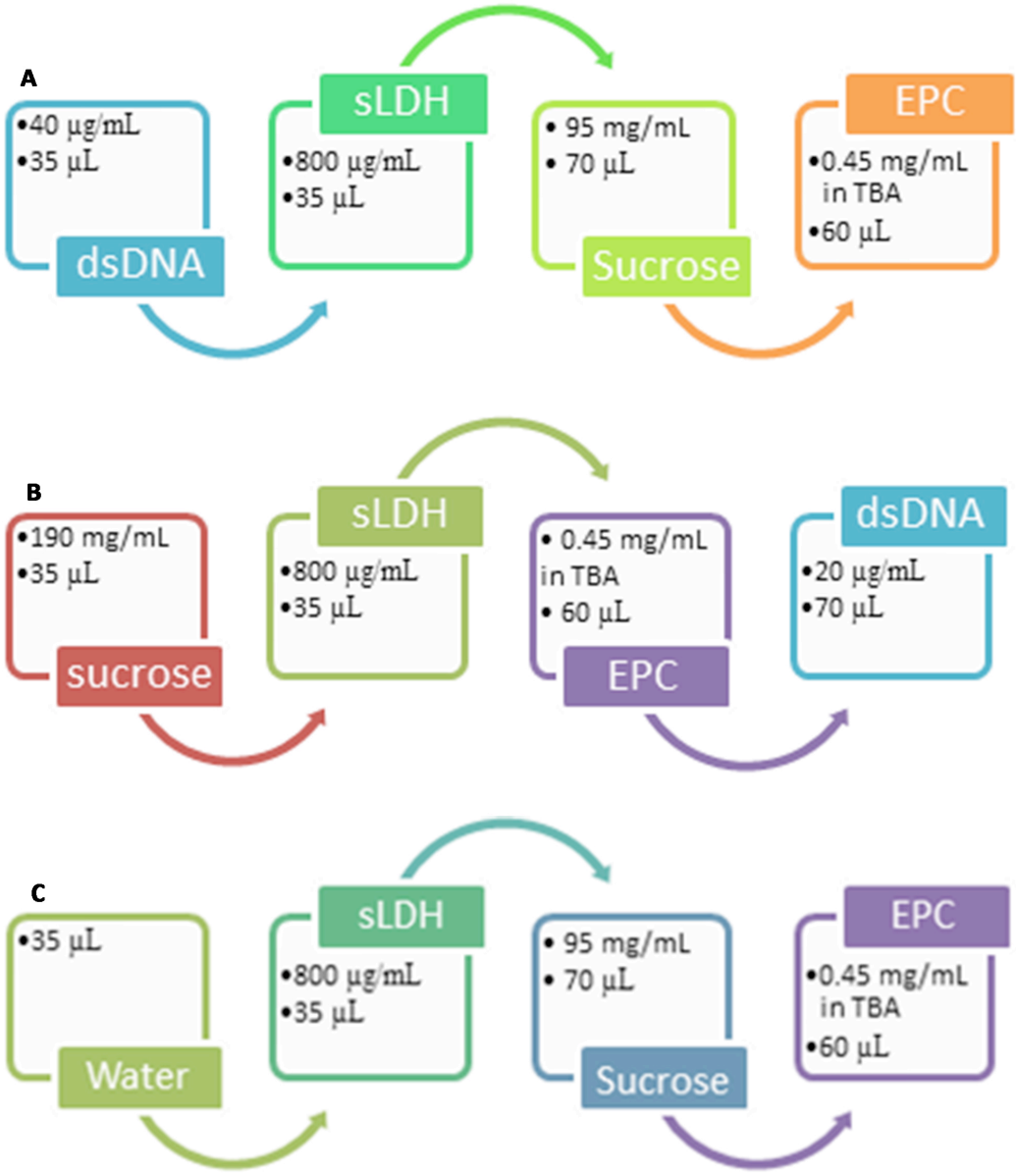

Figure 3-3 Illustrated procedures for loading DNA in LDH-liposome composites by hydration of freeze-dried matrix (HFDM) method

3.3 Characterisations

3.3.1 Dynamic light scattering (DLS)

Particle sizes of LDH NP suspension, LDH-FITC NP suspension, LDH-nucleic acid associates and LDH-liposome composites, LDH-nucleic acid-liposome were measured by dynamic light scattering (DLS, also called photon correlation spectroscopy, PCS) technique on a zetasizer (Zetasizer Nano ZS, Malvern Instruments).

3.3.2 X-ray diffraction (XRD)

LDH suspension was deposited and dried on glass slides for XRD characterisation. Powder LDH was characterised by XRD as a pellet form. A Rigaku Miniflex X-ray diffractometer with Co Kα source (λ = 0.1789 nm) was used in this thesis. The samples were scanned from 2 θ = 2 ° to 60 ° (for suspension) and 80 ° (for powder) with step of 0.02 ° and scanning speed of 2 θ = 2 °/min.

3.3.3 Fourier transform infrared spectroscopy (FTIR)

FTIR spectra of LDH NPs were collected on a FTIR instrument (Nicolet 6700, Thermo Electron Corporation) with smart orbit unit. The samples were scanned 200 times from 4000 cm^{-1} to 400 cm^{-1} at resolution of 1 cm^{-1}.

3.3.4 (cryo-)Transmission electron microscopy (TEM)

LDH NPs were imaged by a TEM machine (JEOL 1011). Liposomes and LDH-liposome composites from hydration of thin lipid film (HTLF) method were imaged by a cryo-TEM facility (FEI, TECNAI F30) in the Centre for Microscopy and Microanalysis (CMM), The University of Queensland.

3.3.5 Elemental analysis (EA)

The carbon, hydrogen and nitrogen contents in powder LDH were characterised by an elemental analyser (FLASH EA 1112 series, Thermo Electron Corporation). Each sample was tested in triplicate.

3.3.6 Inductively coupled plasma-atomic emission spectrometry (ICP-AES)

The magnesium and aluminium contents in LDH NPs and LDH-liposome composites were tested by inductively coupled plasma-atomic emission spectrometry (ICP-AES, Varian VISTA AX Pro) after the LDH NPs or the LDH-liposome NPs were digested by nitric acid with heating at 80 °C.

3.3.7 Ultraviolet–visible spectroscopy (UV-vis)

Concentration of FITC was characterised by measuring absorbance on a UV-vis (Ultraviolet–visible spectroscopy) instrument (UV2450, SHIMADZU). Calibration curve was conducted by a series of known concentration of FITC sodium salt solution (0.5 ppm to 10.0 ppm).

3.4 Biological techniques

3.4.1 Agarose gel electrophoresis

A 2.5 % agarose gel with Gel-Red stain was made and then nuclei acids with/out LDH or LDH-liposome for binding were loaded in the wells (260 ng DNA was used in each well). Gel was imaged by a Bio-Rad imaging system after run at 90 V for 45 min in TBE buffer.

3.4.2 Cell culture

Human colon cancer HCT-116 cells were cultured in DMEM complemented with 10% *v/v* of FBS. The cells were subcultured at the split ratio of 1/4 to 1/8 at confluency 70 ~ 80% and the cell culture medium was changed every other day.

3.4.3 Cell viability

Human colon cancer HCT-116 cells were seeded in 96-well plates at a density of 2,000 cells per well in 200 μL of cell culture media. After 24 h of incubation, cell culture media was replaced by 200 μL of fresh media with desired concentration of LDH or LDH-liposome NPs. After 48, and 72 h further incubation, 20 μL of MTT reagent (5 mg/mL in PBS buffer) was added, followed by 2-4 h of incubation (dependent on cell density). Next, the cell culture media was discarded and 50 μL of DMSO was added to each well, followed by 10 min of incubation. Absorbance was read using a plate reader (Bio-Tek, USA) at 540

nm after 1 min of orbital shaking. A negative control group (only cell culture media, without cells) was used as background. A group without adding NPs was used as control. The cell viability was normalised to control. The experiments were conducted for at least two batches in triplicate. Data are presented as mean ± SEM (standard error of the mean). Two-way ANOVA was used to assess the statistical significance (commercial transfection reagent Oligofectamine™ (life technologies) as control group).

3.4.4 Cellular uptake

Cells were seeded in 6-well plates at density of $1*10^5$ cells per well in 2 mL complete cell culture media. After 24 h of incubation, cell culture media was replaced by 1 mL of fresh media with/out desired concentration of NPs-DNA-Cy3 or LDH-FITC. Another 4 h (0.25 to 8 h used for time-course investigation) of incubation later, cells were detached by trypsin-EDTA from the plates after washed twice by PBS buffer, collected in 2 mL tubes, and washed twice again by PBS buffer, then finally fixed in certain volume of 2% PFA (paraformaldehyde). All treatments were done for at least two batches in triplicate.

3.4.5 Flow cytometry

A BD Accuri™ C6 Flow Cytometer System was used in this thesis and 10,000 cells were counted. Band pass filter 530/30 was used for detecting FITC, and 585/40 for Cy3.

References

1. Gardner, E., Huntoon, K.M. & Pinnavaia, T.J. Direct synthesis of alkoxide-Intercalated derivatives of hydrocalcite-like layered double hydroxides: Precursors for the formation of colloidal layered double hydroxide suspensions and transparent Tthin films. *Advanced Materials* **13**, 1263-1266 (2001).

2. Wong, Y. et al. Efficient delivery of siRNA to cortical neurons using layered double hydroxide nanoparticles. *Biomaterials* **31**, 8770-8779 (2010).

3. Xu, Z.P., Stevenson, G., Lu, C.-Q. & Lu, G.Q. Dispersion and size control of layered double hydroxide nanoparticles in aqueous solutions. *Journal of Physical Chemistry B* **110**, 16923-16929 (2006).

4. Xu, Z.P. et al. Stable suspension of layered double hydroxide nanoparticles in aqueous solution. *Journal of the American Chemical Society* **128**, 36-37 (2006).

5. Wang, T. et al. Preparation of submicron unilamellar liposomes by freeze-drying double emulsions. *Biochimica et Biophysica Acta (BBA) - Biomembranes* **1758**, 222-231 (2006).

6. Li, C. & Deng, Y. A novel method for the preparation of liposomes: Freeze drying of monophase solutions. *Journal of Pharmaceutical Sciences* **93**, 1403-1414 (2004).

7. Wu, S.Y. et al. Development of a novel method for formulating stable siRNA-loaded lipid particles for *in vivo* use. *Pharmaceutical Research* **26**, 512-522 (2009).

8. Cui, J., Li, C., Deng, Y., Wang, Y. & Wang, W. Freeze-drying of liposomes using tertiary butyl alcohol/water cosolvent systems. *International Journal of Pharmaceutics* **312**, 131-136 (2006).

Chapter 4 Synthesis and Characterisation of small Layered Double Hydroxide Nanoparticles

Declaration for Chapter 4

- Most parts of this chapter is published on *Applied Clay Science* **2014**; 100, 66-75; doi: 10.1016/j.clay.2014.04.028
- Thus this chapter is mainly based on the manuscript, with the supplementary tables, figures, and data being inserted into the proper sections. To keep consistency, the AmE spelling in the manuscript has been changed to BrE in this thesis; the format for unit has been changed from $mg \cdot mL^{-1}$ to mg/mL, etc.

Abstract

Small MgAl-layered double hydroxide (sLDH) nanoparticles (NPs) were prepared by a non-aqueous method with the *Z*-average diameter of ~ 40 nm. This method first requires co-precipitation of magnesium and aluminium nitrate solution with sodium hydroxide in methanol, followed by LDH slurry collection and re-suspension in methanol. The methanol suspension is then heated in an autoclave, followed by separation via centrifugation and thorough washing with deionised water (DI water). The NPs are finally dispersed in DI water into homogeneous aqueous suspension after 4-6 day standing at room temperature. In general, sLDH NPs have the *Z*-average size of 35-50 nm, the number-average size of 14-30 nm and the polydispersity index (PdI) of 0.19-0.25. The prepared sLDH suspension is stable for at least 1 month when stored at fridge (2-8 °C) or ambient (22-25 °C) temperature.

4.1 Introduction

In recent years, layered double hydroxide nanoparticles (LDH NPs) have demonstrated good therapeutic-carrier properties as well as highly efficient delivery vehicles for anionic drugs and nucleic acids, due to their favourable physical properties and low cytotoxicity.[1-3] LDHs, also known as anionic clays or hydrotalcite-like compounds (HTlcs), are a broad family of layered inorganic materials, whose composition can be expressed using the general formula $[M^{2+}_{1-x}M^{3+}_{x}(OH)_2](A^{m-}_{x/n})\cdot yH_2O$, where M^{2+} can be typical divalent ions and M^{3+} typical trivalent ions; x represents hydrated anions in the interlayer and can be of any types of anions, such as various inorganic and (bio)organic anions.[4] The lamellar architecture alongside a well-distributed, condensed array of positive charges renders LDH an excellent carrier for a wide range of negatively charged therapeutics.[5-8] Moreover, once the therapeutics are intercalated between LDH interlayers, they are physically protected from degradation. For example, LDH has been used as a DNA vector where intercalation has inferred protection of the gene from DNase-mediated degradation.[9-12]

Given that negatively charged therapeutics do not readily transcend cellular membranes (which are also negatively charged), attempts to overcome this barrier can be effectively addressed by incorporating these anionic therapeutics within the interlayers of LDH, leading to efficient cellular uptake *in vitro*.[3, 13] The high cellular delivery efficiency is also benefited from the innate ability of LDH to actively escape from endosomes (considered a major barrier to effective gene/drug delivery) through LDH-mediated endosomal buffering, which ultimately leads to counter ions and water ingress, rupture of endosomal vesicles, and release of intact therapeutics into the cytoplasm.[14-17] This process thus circumvents the endo-lysosomal pathway[3, 18] and leads to substantial enhancements in delivery efficiency.

Aside from these highly desirable inherent properties of LDH that benefit cellular delivery, the particulate size is another key property that impacts the delivery efficiency. A few reports claim that nanoparticles with size *ca.* 50 nm are more efficiently internalised by a range of cell types, such as HeLa, Caco-2 and HT-29 cells.[18-20] In particular, it was reported that LDH nanoparticles with a number-average size of 50 nm were the most efficient cellular delivery vehicles.[18]

To date, LDH particles reported in most literature have a Z-average (or intensity-average) diameter ≥50 nm, even when hydrothermal treatment has been used in an attempt to tailor

and control the LDH particle size.[21-23] Li et al.[24] reported the so-called smallest CO_3-LDH nanoparticles with a number-average size of ~20 nm (observed in TEM) and an intensity average of ~60 nm (measured with DLS). Using a non-aqueous precipitation method, Gardner et al.[25] prepared a very well dispersed LDH suspension, and further Gunawan and Xu[26] found that the number-average size of their as-prepared LDH particles was 30 nm, while limited knowledge in relation to the growth mechanism has been reported.

On the other hand, aggregation of LDH NPs in blood circulation is a big challenge for LDH applied as a perfect *in vivo* delivery vehicle. Liposomes are widely used biocompatible delivery tools in the recent decades because they are constituted by cell membrane components lipids, which are stable in blood circulation, especially after PEGylation. This projects aims to develop a composite system, which combines the advantages of LDH NPs and liposomes, with efficient cellular uptake, endosomal escape and good stability in blood circulation.

Considering encapsulating LDH NPs in the liposomal vesicles, this chapter aims to decipher how small LDH NPs can be prepared using non-aqueous methodology through systematic investigation of effects of the experimental conditions on the particle size and the size distribution; and then sLDH growth mechanism is proposed.

4.2 Experimental

4.2.1 Materials preparation

sLDH NPs were prepared by non-aqueous precipitation, followed by heat-treatment, purification and dispersion in water, which was modified from Pinnavaia's method.[25] Typically, methanol solution (10 mL) of magnesium nitrate hexahydrate ($Mg(NO_3)_2 \cdot 6H_2O$, 6 mmol) and aluminium nitrate nonahydrate ($Al(NO_3)_3 \cdot 9H_2O$, 2 mmol) was added dropwise to a methanol solution (40 mL) containing sodium hydroxide (NaOH, 16 mmol) under vigorous stirring. The mixture was stirred for 30-40 min, the precipitate slurry was then collected through centrifugation, redispersed in fresh methanol (40 mL) and transferred to a Teflon®-lined autoclave, followed by heat-treatment at 100 °C for 18 h. After cooling the sample to room temperature, the precipitate slurry was collected through centrifugation, and washed twice with deionised water (DI water). The final collected slurry was manually dispersed in 40 mL of DI water, followed by standing at room temperature with occasional hand-shaking. This dispersion became transparent, resulting in a homogeneous LDH suspension after 4-6 days with the LDH mass concentration determined to be 6 to 7

mg/mL (~50% yield). A range of experimental factors, such as LDH mass concentration in the aqueous suspension (Conc6.5 to Conc29), methanol- (MW0 to MW2) and water-washing (WW0 to WW2), the heat-treatment temperature (HT60 to HT100) and duration (HD4 to HD144), co-precipitation temperature with (CPT0HT to CPT50HT) and without hydrothermal treatment (CPT0 to CPT50), were varied to examine their influences on the average particle size and distribution, as summarised in Table 4-2. Note that all experiments were conducted in triplicate, and the standard deviation of triplicate experiments is shown.

Large LDH nanoparticles (L-LDH NPs) were synthesised by vigorously mixing 10 mL of aqueous solution containing magnesium chloride hexahydrate ($MgCl_2 \cdot 6H_2O$, 3.0 mmol) and aluminium chloride hexahydrate ($AlCl_3 \cdot 6H_2O$, 1.0 mmol) with 40 mL of sodium hydroxide (NaOH) solution (0.15 M) for 10 min at room temperature.[13, 27] The LDH slurry was collected by centrifugation and then washed twice with DI water (40 mL), and resuspended in DI water (40 mL), after which the suspension was transferred to a Teflon®-lined autoclave and hydrothermally treated at 100 °C for 16 h. The suspension contained approximately 4 mg/mL of homogeneously dispersed Mg_2Al-LDH nanoparticles, with a Z-average particle size ~ 100 nm.[13]

4.2.2 Materials characterisation

The LDH NP size distribution in aqueous suspension was measured by dynamic light scattering (DLS) (also known as photon correlation spectroscopy, PCS) using a Zetasizer Nano ZS with three runs, from which an average of the Z-average size and the polydispersity index (PdI), also from three runs were calculated. Powder X-ray diffraction (XRD) patterns were recorded on a Rigaku Miniflex X-ray diffractometer with Co Kα source (λ = 0.1789 nm) at a scanning rate of 2.00° min^{-1} (2θ) from 2θ = 2° to 80°. Some XRD patterns were recorded on a thin film of LDH formed by dropping a few droplets of the LDH NP suspension and drying on a glass slide. FTIR spectra were obtained on a Nicolet 6700 (Thermo Electron Corporation) by scanning 200 times from 4000 cm^{-1} to 400 cm^{-1} at a resolution of 1 cm^{-1}. The morphology and size of some typical LDH NPs were examined by Transmission Electron Microscopy (TEM, JEOL 1011) at 80 kV. The concentrations of sLDH and large LDH suspension were calculated from magnesium and aluminium concentrations determined by ICP-AES (Varian VISTA AX Pro) in digested LDH NP solutions. The carbon, hydrogen and nitrogen composition in powdered LDH NPs were

analysed by an elemental analyser (FLASH EA 1112 series, Thermo Electron Corporation).

4.3 Results

4.3.1 Typical features of sLDH NPs

As shown in Figure 4-1A, sLDH NPs typically possess a narrow particle size distribution. All nanoparticles are exclusively in the size range of 15-120 nm, with a Z-average diameter of 42 nm and polydispersity index (PdI) of 0.21. The TEM image (Figure 4-1B) indicates that these sLDH NPs maintain the well-established hexagonal nanosheet morphology, with the lateral dimension of most sheets in the range of 20-80 nm. Such sLDH nanoparticles are nearly half the size of those reported earlier, whose Z-average particle size was ≥ 80 nm.[22] Also of note is the fact that the number-average diameter of as-obtained sLDH nanoparticles is 21.4 nm, which is less than half that of the LDH particles (~50 nm) reported by Oh et al.[23] In comparison, the most widely reported to-date LDH particles prepared in aqueous solution had a Z-average size of 110 nm and a PdI of 0.22,[22, 28] with an empirical formula $Mg_{1.9}Al(OH)_{5.8}Cl_{0.8}(CO_3)_{0.1}\cdot 1.5H_2O$ as reported previously.[29]

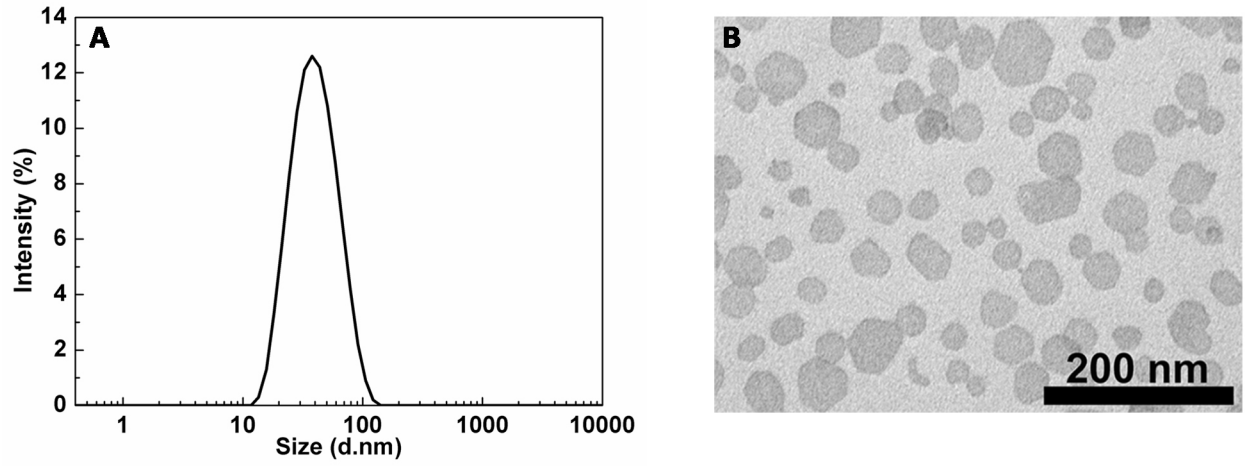

Figure 4-1 Particle size distribution (A) and TEM image (B) of typical sLDH suspension (prepared with 18 h of hydrothermal treatment at 100 °C; sLDH suspension droplet dried on carbon coated copper grid for TEM imaging)

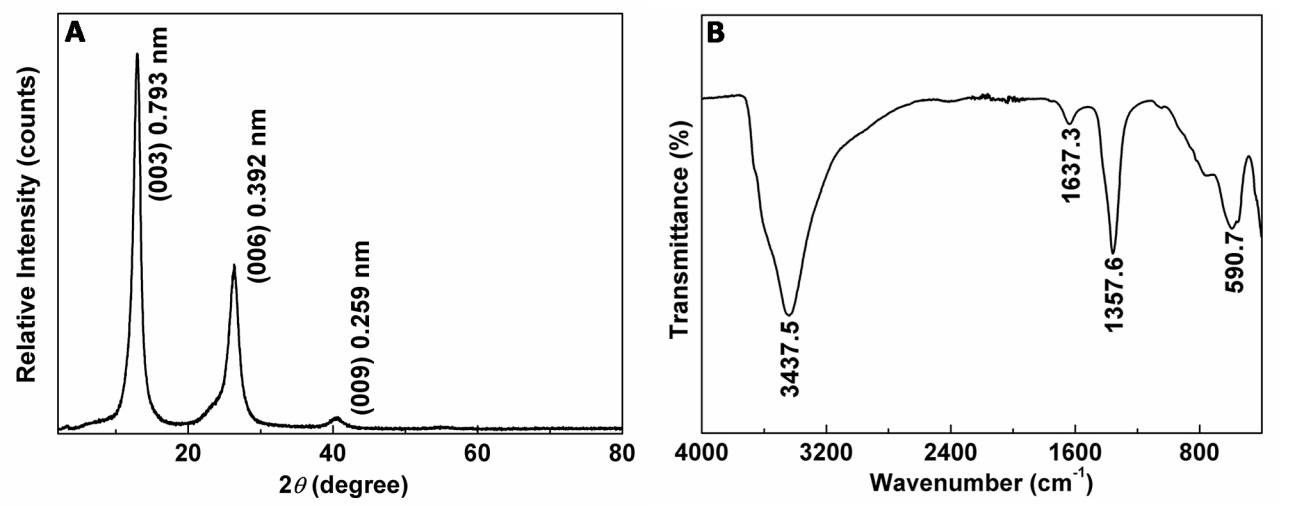

Figure 4-2 XRD pattern (A) and FTIR spectrum (B) of typical sLDH NPs (prepared with 18 h of hydrothermal treatment at 100 °C; suspension dried as a thin film on glass slide for XRD characterisation)

The XRD pattern (Figure 4-2A) shows that sLDH NPs possess the typical lamellar structure, as featured by reflections (003), (006) and (009) in the thin film mode.[16] The *d*-value was 0.79 nm, close to the reported value for Mg_3Al-NO_3-LDH (0.81 nm).[16, 30] Note that the (003) reflection has a full width at half-maximum (FWHM) of 1.2°. This indicates that the thickness in the c-axis is ~7 nm, nearly half the thickness of LDH prepared using the aqueous method.[16, 27] This estimation has also revealed that the aspect ratio of as-prepared sLDH was ~6.

The FTIR spectrum of sLDH (Figure 4-2B) is, as expected, largely identical to that of traditional Mg_3Al-LDH,[30] characteristic of the broad band at 3440 cm^{-1} (stretching vibrations of O-H in brucite-like layer and interlayer H_2O molecules), the peak at 1637 cm^{-1} (the bending vibration of interlayer and adsorbed H_2O molecules), and the bands at around 591 cm^{-1} (M-O and M-O-H stretching vibrations).[31] Of particular note is that the signal at 1358 cm^{-1}, overlapping with the stretching vibration of NO_3^-,[1, 30] is assigned to the stretching vibration of contaminant CO_3^{2-}, which was likely captured from air during the preparation and drying processes. The element analysis (Mg/Al=2.9; 2.6 wt% N; 1.4 wt% C) gave an empirical formula of $Mg_{2.9}Al(OH)_{7.8}(NO_3)_{0.5}(CH_3O)_{0.2}(CO_3)_{0.1}(OH)_{0.1}\cdot 2.0H_2O$.

4.3.2 Parameters affecting LDH NP dispersion

4.3.2.1 Effect of different LDH NP concentration on dispersion

Figure 4-3A shows the change of *Z*-average particle size and polydispersity index (PdI) of sLDH NPs in suspensions with the duration of natural dispersion and the final sLDH concentration (Conc6.5-Conc29 in Table 4-2). After heat-treatment and water-washing, the collected precipitate was manually dispersed in deionised water (DI water), which was then left to stand at room temperature with occasional hand-shaking. The particle size distribution of this suspension was then measured daily. As shown in Figure 4-3A, after 4-6 days of natural dispersion, the *Z*-average particle size of these sLDH NPs was stabilised at ~45 nm. This size corresponds to the lateral size of the sLDH nanosheets (Figure 4-3B), thus revealing that individual sLDH nanosheets in suspension can be obtained after 4-6 days of natural dispersion. A shorter period of dispersion resulted in a *Z*-average particle size of 100-200 nm (at day 1) and 45-65 nm (at day 2). The gradual reduction in *Z*-average particle size over time (day 1 to day 4) indicates that the aggregated precipitate is gradually becoming individually dispersed in DI water. Similarly, the PdI of as-obtained sLDH NPs in suspension reduced in line with the dispersion time (day 1 to day 4) and remained constant thereafter (Figure 4-3B).

Data in Figure 4-3 seemingly indicates that the final sLDH concentration, which was achieved by dispersing water-washed sLDH slurry in a control volume of deionized water, has some influence on the dispersion state (PdI), but not the Z-average particle size. For example, the PdI was ~0.42 at an sLDH concentration of 29 mg/mL, double the value (0.21) in the case of 6.5 mg/mL (Table 4-2 and Figure 4-3B). Although the Z-average sLDH particle sizes were 42-44 nm (Table 4-2) over the entire concentration range (6.5-29 mg/mL), the variation of the Z-average particle size at a higher sLDH concentration was greater (error bar in Figure 4-3A and STDEV in Table 4-2). Both the higher PdI value and larger variation indicate there is some, albeit minor aggregation when higher sLDH concentrations are employed. In addition, the smaller number-average size at higher sLDH concentrations reveals that there is a greater population of much smaller LDH particles (around 10 nm) (Table 4-2, Conc29 generated smallest number-average size) in the high-concentration suspension.

Figure 4-4 shows the *Z*-average and polydispersity index (PdI) changes of sLDH NPs when the sLDH suspension was concentrated by incubation with calcium chloride in a enclosed chamber. Both the *Z*-average particle size and PdI increased gradually with the

sLDH suspension was concentrated. Therefore, this is not a proper way to concentrate the sLDH suspension. Instead, by dispersing sLDH slurry in lower volume of DI water, higher concentration of sLDH suspension with good particle size and acceptable polydispersity index will be obtained (Figure 4-3).

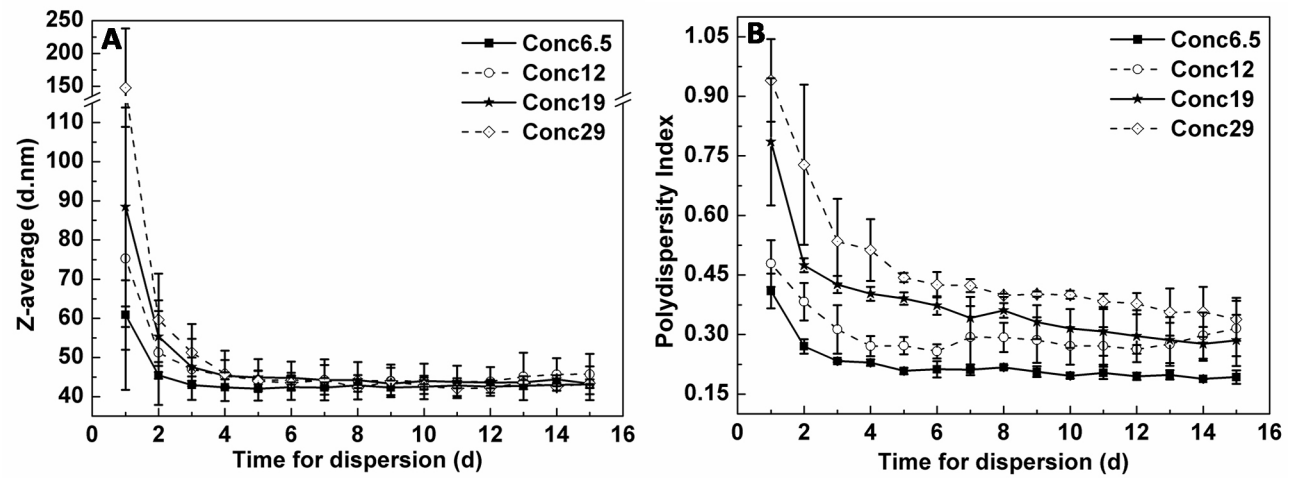

Figure 4-3 sLDH NPs Z-average size (A) and polydispersity index (PdI, B) changes with dispersion time and concentration

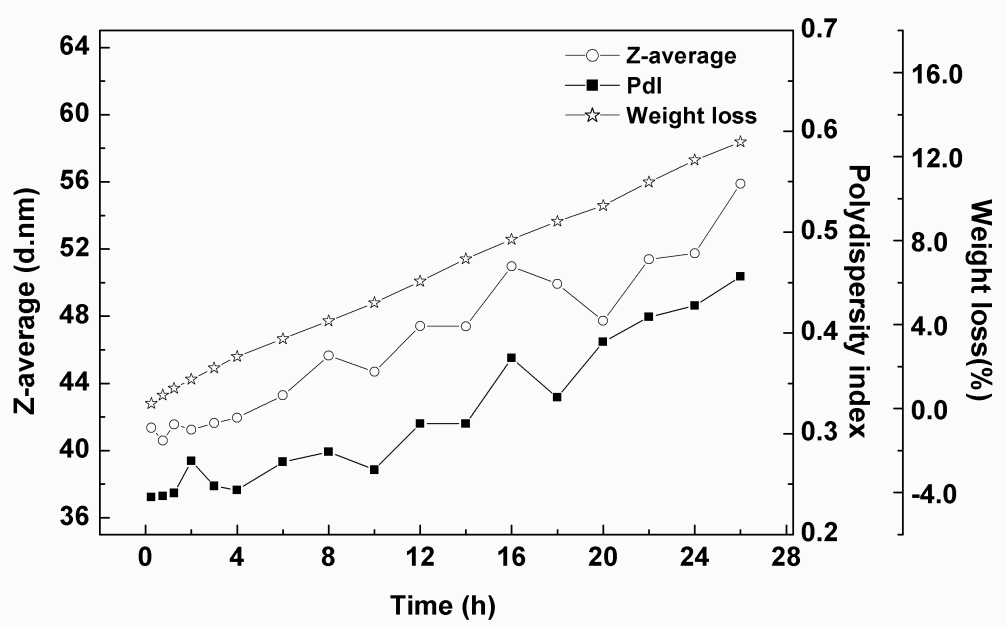

Figure 4-4 *Z*-average particle size and polydispersity index (PdI) changes of sLDH NPs when sLDH NP suspension was concentrated by calcium chloride

4.3.2.2 Effect of ultrasonication on sLDH NPs dispersion

As is seen from Figure 4-5A, bath sonication helps to reduce the LDH particle size from more than 600 nm to around 200 nm when the LDH NPs were freshly prepared. While the sLDH NPs were well dispersed after ~ 4 days, there were no differences between the sLDH NPs with/out bath sonication treatment. As were the polydispersity index data (Figure 4-5B), bath sonication helped the sLDH NPs to be monodispersed in the beginning, but no big differences can be seen for the polydispersity index after the sLDH NPs were well dispersed after ~ 4 days.

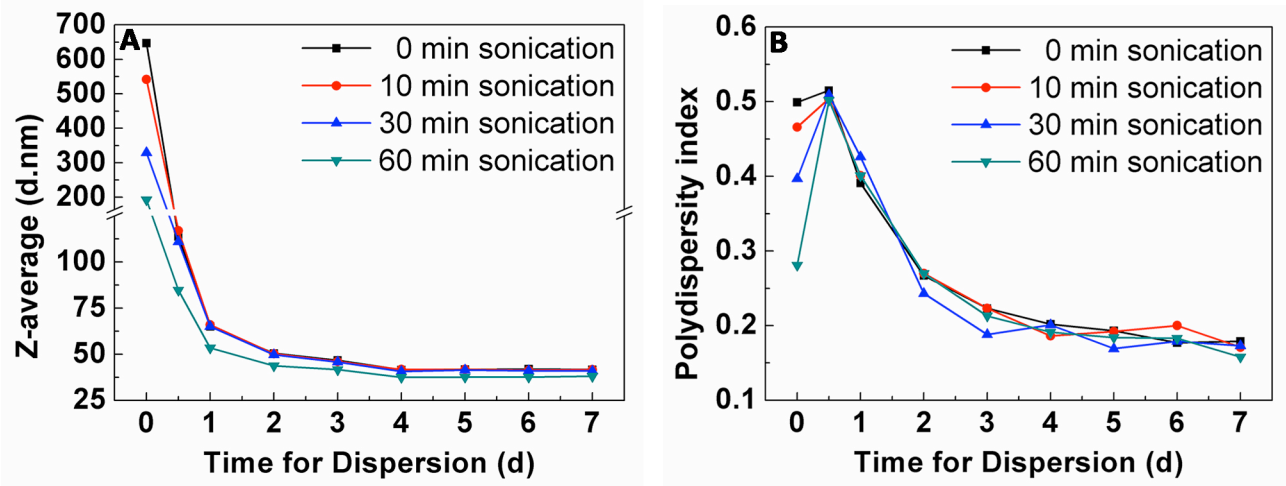

Figure 4-5 (A) *Z*-average particle size (A) and polydispersity index (PdI, B) changes of sLDH NPs with dispersion time and different bath sonication treatments

4.3.2.3 Effect of methanol and water washing on dispersion

Before and after heat-treatment, washing the collected sLDH slurry is a crucial step, which significantly affects the *Z*-average particle size, PdI as well as final product purity. We made three batches of sLDHs that differed merely in terms of the methanol washing time (0, 1, 2) before heat-treatment (MW0-MW2 in Table 4-2). As clearly shown in Figure 4-6A, washing twice with methanol led to the best dispersed suspension with the narrowest size distribution (44.8 nm, PdI of 0.20), while no washing gave a broader distribution with a significantly larger *Z*-average particle size (70 nm) and PdI (0.27), although the XRD patterns in Figure 4-6B demonstrate the similar crystallinity of these sLDHs.

Similarly, the water-washing time (0, 1, 2) also significantly impacts the *Z*-average particle size and PdI (WW0-WW2 in Table 4-2). As shown in Figure 4-7A, the size of sLDH

particles (water washed twice, WW2) had a narrower distribution (PdI 0.21) and a smaller *Z*-average particle size (42.3 nm). When water-washing was omitted, only a small proportion of the collected sLDH aggregate was seen to disperse (WW0 in Figure 4-7A), which could be attributed to the presence of impurity salt $NaNO_3$.[22] The presence of this salt was confirmed by the sharp reflections in the XRD pattern (ICDD PDF card no. 36-1474, WW0 in Figure 4-7B).

Washing only once seemed to partially wash away the impure water-soluble salt $NaNO_3$ (although not detectable by XRD), which is likely responsible for the broad particle size distribution with a much larger Z-average size (Figure 4-7A and Table 4-2). The two small peaks around 2963 and 2850 cm^{-1} in FT-IR spectra (Figure 4-7C), attributed to C-H stretching vibrations of $–CH_3$ in methoxide anion,[32] was weakened after water-washing, indicating that water-washing also assists the removal of methoxide from the sample, as is further explained below.

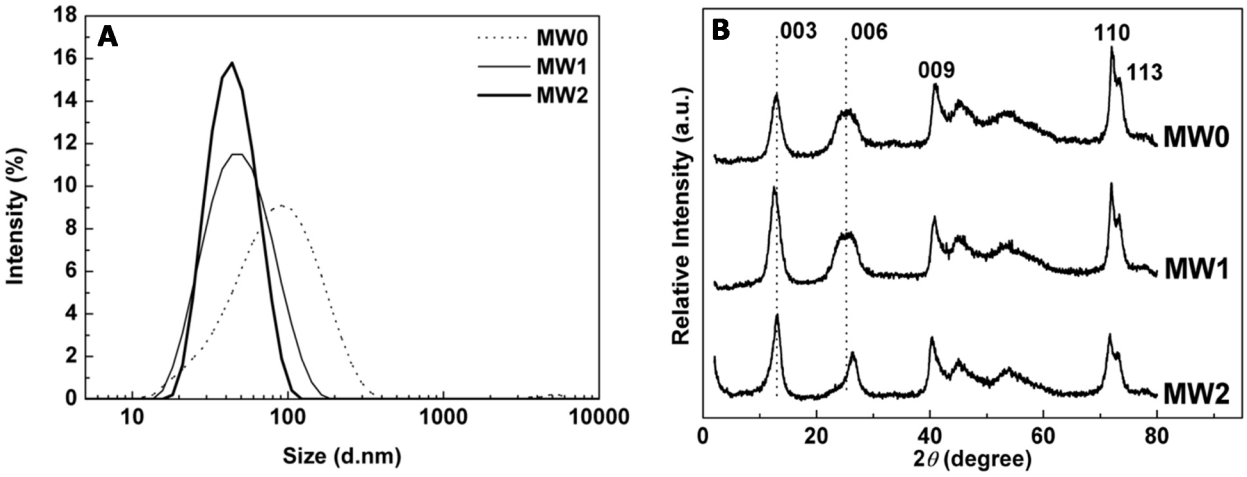

Figure 4-6 Particle size distribution (A) and XRD patterns (B) of sLDH NPs from different methanol washing time(s): MW0, no methanol wash; MW1, methanol-washing once; MW2, methanol-washing twice

The effect of methanol-washing seems to be largely masked by the subsequent water-washing step. This is because the solubility of $NaNO_3$ in water (0.911 g/mL at 25 °C) is much greater than that in methanol (0.00333 g/mL at 25 °C).[33] Therefore it is reasonable to infer that water-washing twice removes all $NaNO_3$ from our LDH slurry and only in the case where methanol wash was omitted (sample MW0 in Figure 4-6) did traces of salt remain, which could be responsible for incomplete dispersion.

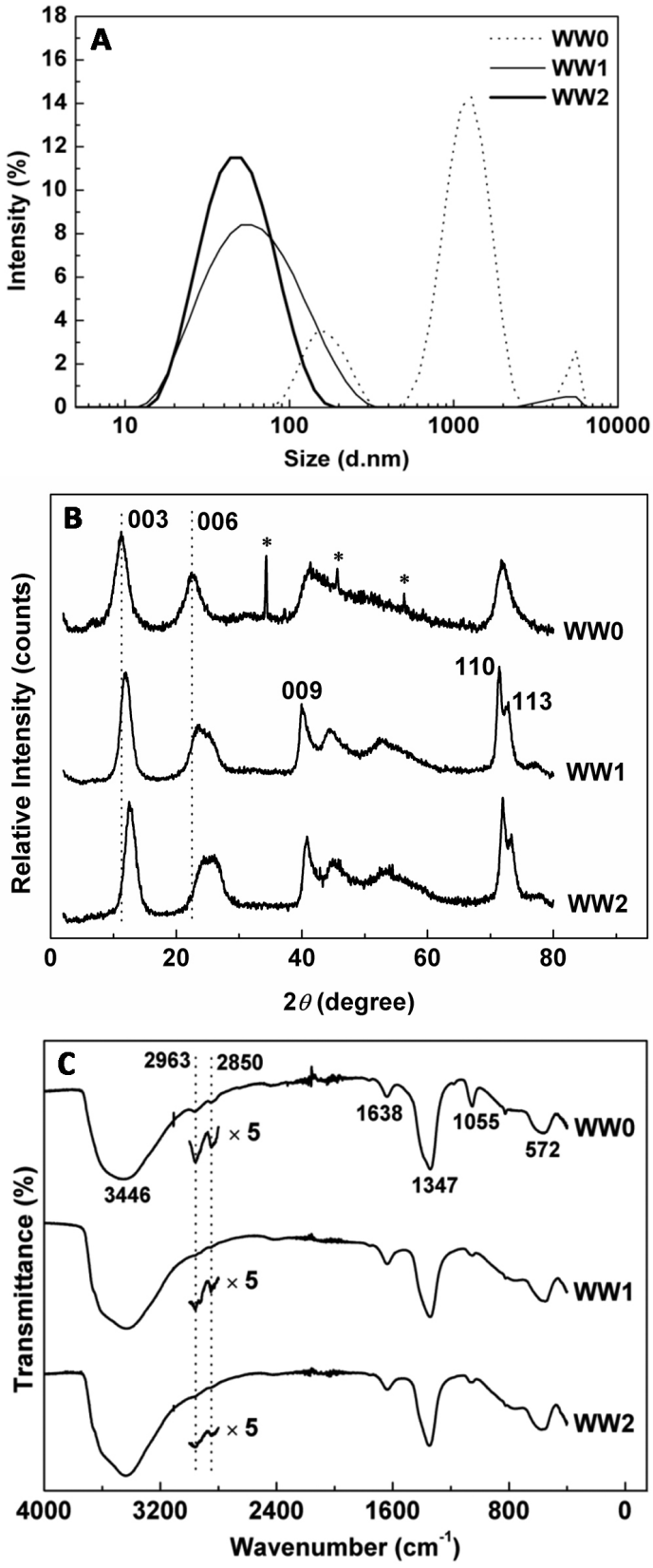

Figure 4-7 Particle size distribution (A), XRD patterns (B), and FT-IR spectra (C) of sLDH NPs from different water washing time(s): WW0, no water wash; WW1, water-washing once; WW2, water-washing twice

4.3.3 Parameters affecting LDH NP size

4.3.3.1 Hydrothermal treatment temperature and duration affect particle size

Figure 4-8 and Figure 4-9 display the effects of heating temperature (60-100 °C) and duration (4-144 h) (over 15 days of natural dispersion) on the *Z*-average particle size and PdI of sLDH NPs. As shown in Figure 4-8A and B, when the treatment temperature was raised from 60 to 100 °C, the Z-average particle size and PdI change was only slight, from 38 to 42 nm and 0.19 to 0.23 after 6 days of dispersion, respectively (HT60-HT100 in Table 4-2). Thus in general, the heat-treatment temperature had a limited impact on the sLDH particle size and distribution.

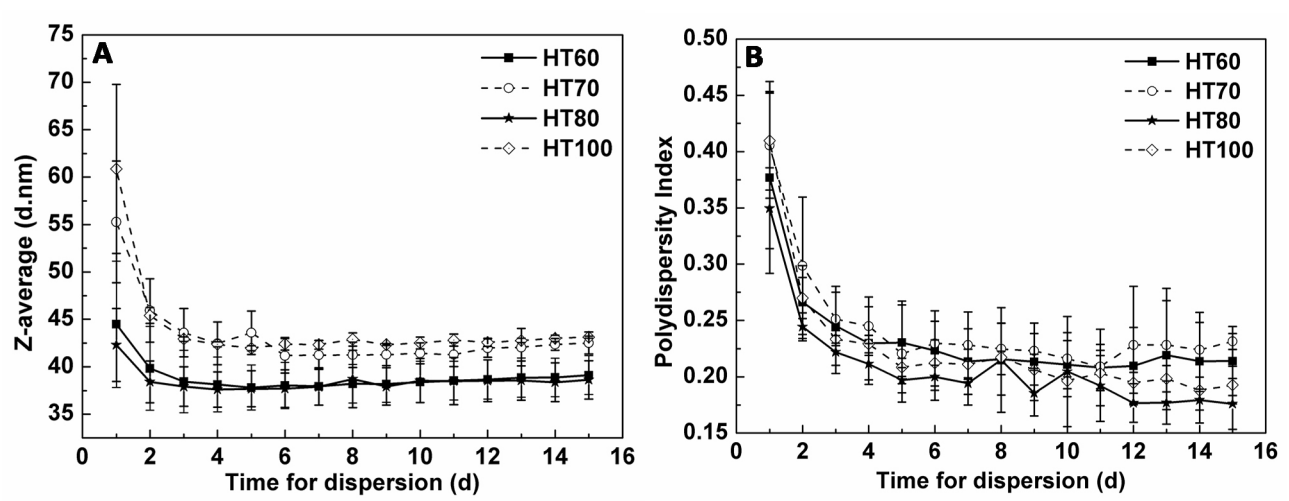

Figure 4-8 sLDH NPs *Z*-average size (A) and polydispersity index (PdI, B) changes with dispersion time and hydrothermal treatment temperatures for 18 h

In contrast, prolonging the heat treatment duration from 4 to 144 h at 100 °C increased the Z-average particle size from ~39 to ~47 nm while the PdI (0.19-0.22) remained unchanged after 6 days of dispersion (Figure 4-9A and B, HD4-HD144 in Table 4-2); this observation demonstrates that extending heating treatment time increased the particle size marginally.

The limited effect of heating temperature and duration on the average particle size and distribution using methanol as solvent is in sharp contrast to that when water is used as solvent. As reported earlier by Oh et al [21] and Xu et al,[22] the average LDH particle size can be tailored in a larger range (from 60-80 up to 300-400 nm) and the particle size distribution (PdI) increases from 0.2 to 0.5 during heating at 80-150 °C over 2-144 h.

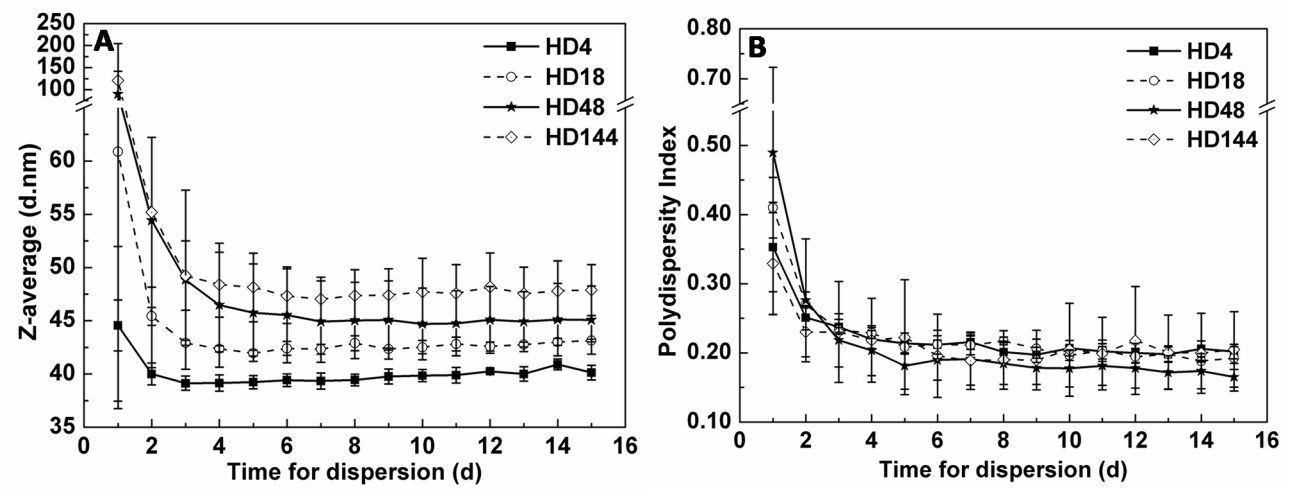

Figure 4-9 sLDH NPs *Z*-average size (A) and polydispersity index (PdI, B) changes with dispersion time and hydrothermal treatment durations at 100 °C

4.3.3.2 Tailoring particle size by controlling extended hydrothermal treatment durations

Table 4-1 shows the *Z*-average particle sizes of original sLDH suspension and sLDH suspension after certain durations of further hydrothermal treatment at 100 °C after the sLDH NPs well dispersed at room temperature. *Z*-average particle size increased from 42.05 nm to 57.11 nm and 73.05 nm after 2 and 4 days of extended hydrothermal treatment, increased by 35.81% and 73.72% (Table 4-1). While after 4 days, it seemed that the particle size growth rate slowed down. The mechanism for particle size growth during hydrothermal treatment will be discussed in *4.4 Discussion of sLDH NPs formation mechanism*.

4.3.3.3 Co-precipitation temperature affects particle size

The co-precipitation step was trialled at temperatures of 0, 23 and 50 ºC by mixing the salt methanol solution with the basic methanol solution. Both solutions were pre-cooled to 0 ºC or pre-heated to 50 ºC before mixing. Stirring was conducted throughout the co-precipitation process and continued for 30 min at the same temperature, followed by methanol washing, heat-treatment at 100 °C for 18 h, and deionised water washing twice (CPT0HT to CPT50HT in Table 4-2). As shown Figure 4-10A and listed in Table 4-2, co-precipitation at 0 and 23 °C yielded sLDH NPs of the similar size with minor fluctuations in their size distribution (44.3 and 42.3 nm with a PdI 0.25 and 0.21), while co-precipitation at

50 ºC generated a slightly larger particles (50.5 nm), indicating that the co-precipitation temperature has a marginal effect on the sLDH NP size.

Table 4-1 Z-average particle size and polydispersity index changes of sLDH NPs with further hydrothermal treatment after well dispersed at room temperature

Further hydrothermal treatment durations at 100 °C	Z-Average (d.nm)	Z-average increase	Polydispersity index	Size Peak (d.nm)
0 d	42.05	/	0.235	43.75
2 d	57.11	35.81%	0.160	68.16
4 d	73.05	73.72%	0.167	85.17
6 d	77.03	83.19%	0.171	88.86
8 d	80.93	92.46%	0.136	94.85

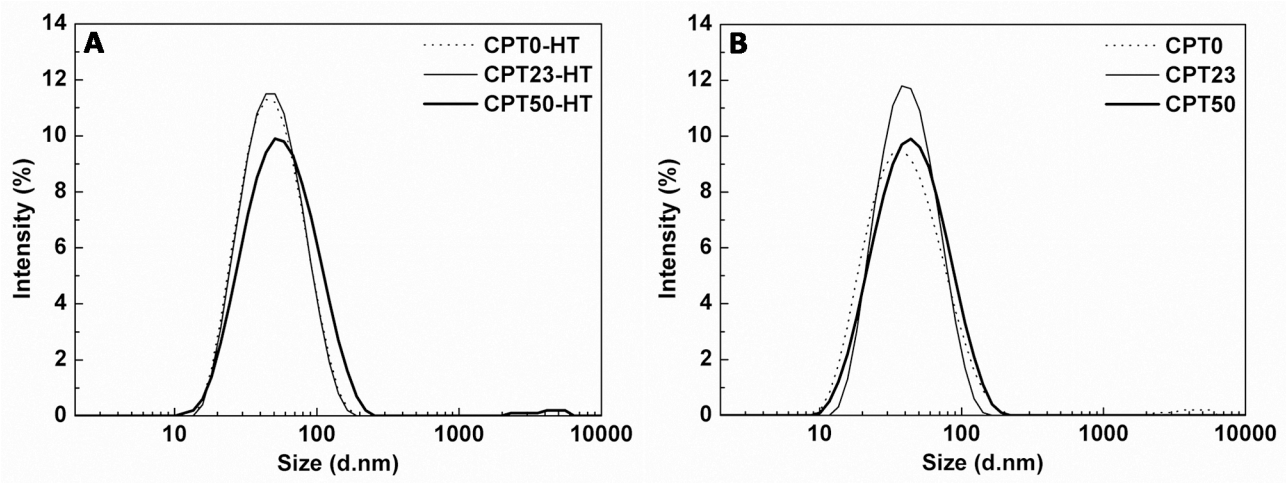

Figure 4-10 Particle size distribution of sLDH NPs prepared at different coprecipitation temperatures followed by hydrothermal treatment at 100 °C for 18 h (A) and without hydrothermal treatment (B)

Furthermore, if heat-treatment was omitted (Figure 4-10B, CPT0 to CPT50 in Table 4-2), the resultant LDH NPs had a smaller Z-average size than those heat-treated. In particular, co-precipitation at 0 °C led to the smallest sLDH size (35.0 nm) with a narrower size distribution (0.21) compared to those at 23 and 50 °C (size of ~40 nm with PdI of ~0.24).

It is worth noting that once prepared, the homogeneous dispersion remained stable for more than one month, regardless of whether the sample was stored at fridge temperature (2-8 °C) or room temperature (22-25 °C) (Figure 4-11).

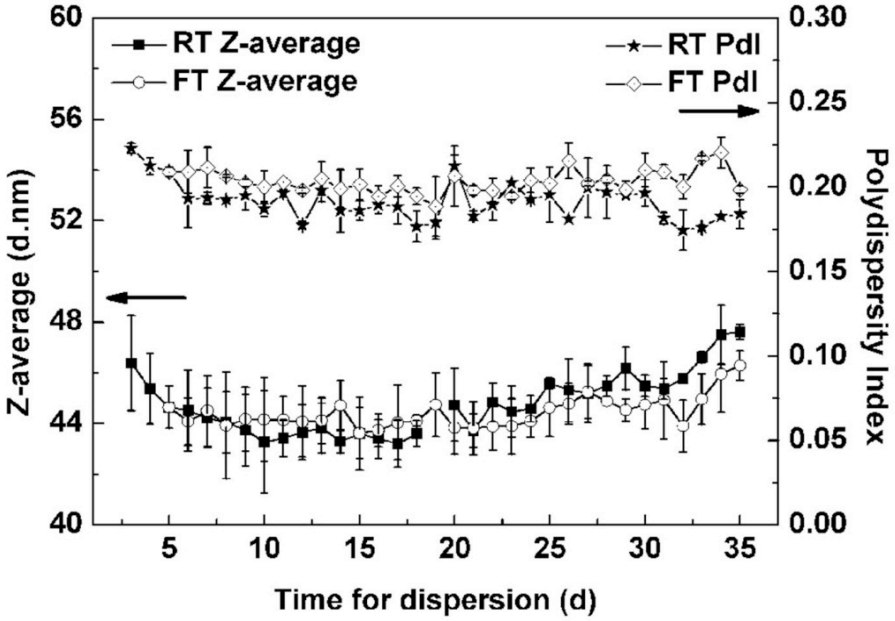

Figure 4-11 sLDH suspension stability study stored at ambient (room) temperature (RT) or fridge temperature (2~8 °C) (FT)

Table 4-2 Summary of preparation condition and the Z-average size and polydispersity index of as-obtained sLDH particles

Sample label	Hydrothermal temperature	Hydrothermal duration	sLDH concentration	Methanol wash	Water wash	Coprecipitation temperature	Z-average size	Number-average size	Polydispersity Index (PdI)
	(°C)	(h)	(mg/mL)	(time)	(time)	(°C)	(d.nm)	(d.nm)	
Conc6.5	100	18	6.5	1	2	23	42.33±0.47	21.38±0.64	0.21±0.01
Conc12			12				44.27±5.27	15.27±3.19	0.29±0.08
Conc19			19				44.20±0.56	16.09±1.90	0.34±0.05
Conc29			29				44.28±3.76	10.84±5.03	0.42±0.02
MW0	100	18	6.5	0	2	23	70.31±8.37	20.79±2.39	0.27±0.01
MW1				1			42.33±0.47	21.38±0.64	0.21±0.01
MW2				2			44.75±1.63	29.51±2.11	0.20±0.03
WW0	100	18	6.5		0	23	--	--	--
WW1					1		59.13±6.56	18.50±3.17	0.31±0.07
WW2					2		42.33±0.47	21.38±0.64	0.21±0.01
HT60	60	18	6.5	1	2	23	37.94±1.98	16.61±3.27	0.21±0.03
HT70	70						41.24±1.52	14.09±6.22	0.23±0.03
HT80	80						37.90±1.94	19.02±0.51	0.19±0.02
HT100	100						42.33±0.47	21.38±0.64	0.21±0.01
HD4	100	4	6.5	1	2	23	39.35±0.75	19.31±1.46	0.22±0.01
HD8		8					39.22±3.76	21.05±1.67	0.19±0.03
HD18		18					42.33±0.47	21.38±0.64	0.21±0.01
HD48		48					44.92±3.82	23.58±1.43	0.19±0.04
HD144		144					47.03±2.07	25.15±1.16	0.19±0.04
CPT0HT	100	18	6.5	1	2	0	44.28±1.15	20.55±2.15	0.25±0.08
CPT23HT						23	42.33±0.47	21.38±0.64	0.21±0.01
CPT50HT						50	50.46±1.61	18.94±4.92	0.23±0.01
CPT0	None	None	6.5	1	2	0	35.02±0.42	14.54±2.63	0.21±0.03
CPT23						23	38.59±2.02	17.75±1.46	0.23±0.03
CPT50						50	39.15±1.17	15.90±1.63	0.24±0.04

4.3.3.4 Compositions of LDH NPs affect particle size

As shown in Table 4-3, MgAl-Cl LDH NPs prepared by non-aqueous method can be well dispersed after 2-3 days of standing at room temperature, while the MgAl-Cl LDH particle size (> 60 nm) is much bigger than the normal MgAl-NO_3 sLDH (~ 40 nm). This is due to the ion radius differences between Cl^- (0.181 nm) and NO_3^- (0.129 nm).

Table 4-3 Particle size and polydispersity index (PdI) changes of MgAl-Cl LDH prepared by non-aqueous method with dispersion time

Dispersion time	Z-Average (d.nm)	PdI	Intensity Mean (d.nm)	Number Mean (d.nm)	Volume Mean (d.nm)	Size Peak (d.nm)
0 h	874.6	0.506	1520	217.1	1981	1516
12 h	241.5	0.974	998.0	24.16	342.0	1350
1 d	80.10	0.286	215.1	35.43	110.1	114.9
2 d	61.71	0.205	78.71	8.622	25.62	79.19
3 d	63.09	0.179	77.71	19.68	38.79	77.71

Figure 4-12 shows the *Z*-average particle size and PdI changes of LDH NPs with dispersion time and different magnesium to aluminium ratios with/out hydrothermal treatment. Both magnesium to aluminium ratios of 2 and 4 gave much larger particle sizes regardless of hydrothermal treatment or not. No much differences can be seen for the polydispersity index data, and they were all in acceptable range (~ 0.20, Figure 4-12B) after 4~6 days of natural dispersion. The good dispersion state of sLDH NPs with magnesium to aluminium ratio of 3 could be attributed to the specific surface charge density.

Figure 4-13 shows the *Z*-average particle size and polydispersity index changes of LDH NPs prepared by non-aqueous method with Co/Ni/Zn-Al at different ratios with/out hydrothermal treatment. All these LDH NPs show much larger particle sizes than the Mg_3Al-sLDH (LDH NPs with Co exhibit particle size ~ 100 nm, smaller than those with Ni or Zn. Moreover, most of these LDH NPs show much bigger polydispersity index, which mean poor dispersion state.

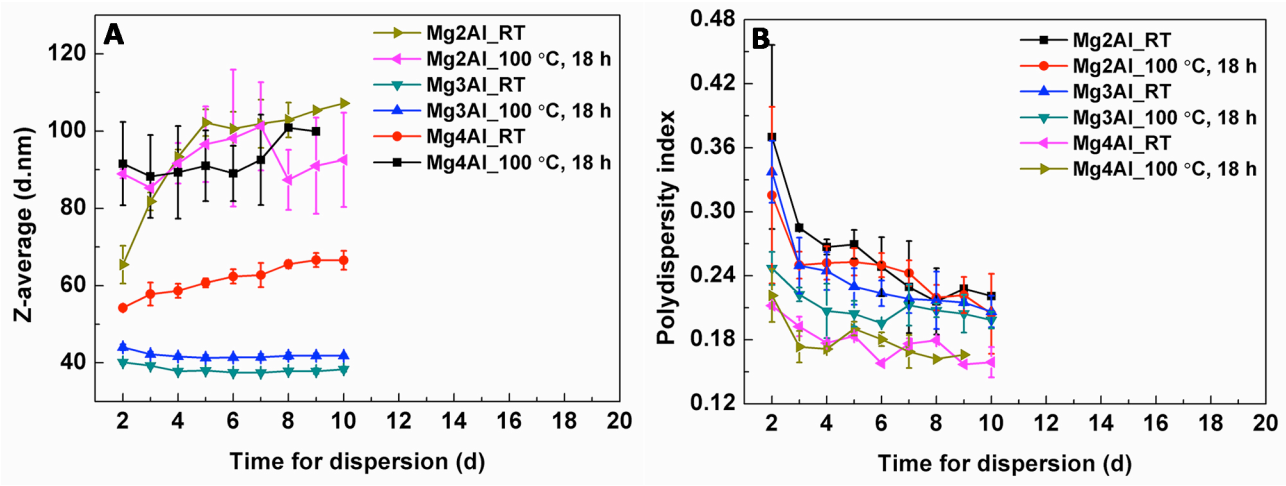

Figure 4-12 Z-average particle size (A) and polydispersity index (PdI, B) change of LDH NPs with dispersion time (LDH NPs prepared by non-aqueous method with different magnesium to aluminium ratios)

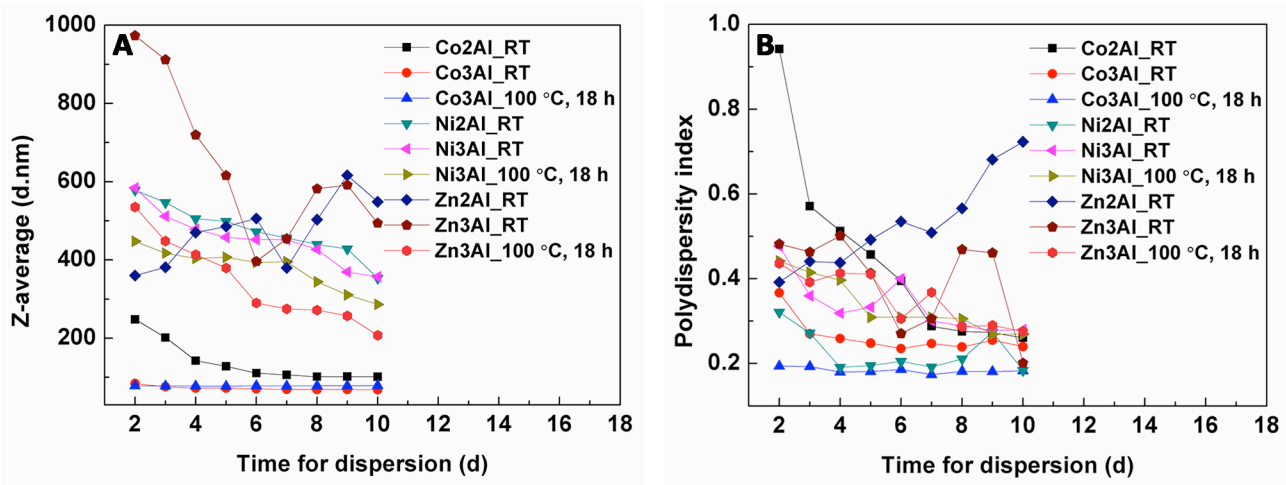

Figure 4-13 Z-average particle size (A) and polydispersity index (PdI, B) changes of LDH NPs with dispersion time (LDH NPs prepared by non-aqueous method with Co, Ni, Zn and different divalent elements to trivalent elements ratios)

Figure 4-14 shows the Z-average particle size and polydispersity index changes of LDH NPs prepared by non-aqueous method with FeAl-Cl and MgFe-Cl at different ratios without hydrothermal treatment. All these LDH NPs also show particle sizes larger than 100 nm and polydispersity index around or more than 0.2.

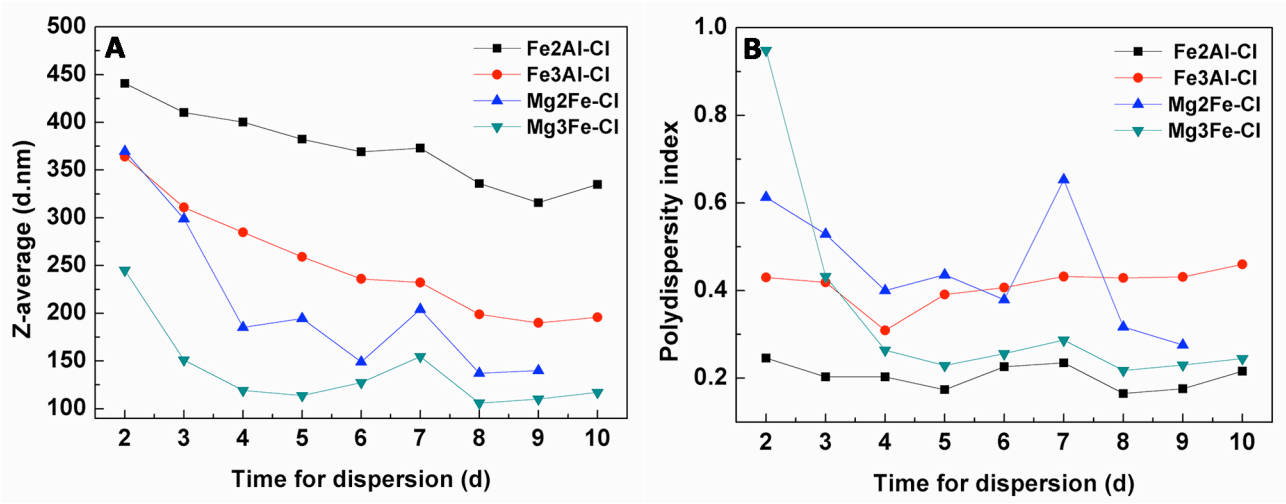

Figure 4-14 *Z*-average particle size (A) and polydispersity index (PdI, B) changes of LDH NPs with dispersion time (LDH NPs prepared by non-aqueous method with FeAl-Cl and MgFe-Cl at different divalent elements to trivalent elements ratios)

4.4 Discussion of sLDH NPs formation mechanism

In summary, non-aqueous preparation, involving co-precipitation and heat-treatment in methanol, and then dispersion in deionised water for 4-6 days, generally produces much smaller LDH NPs that can be individually dispersed into homogeneous aqueous suspensions. Our investigations indicate that the co-precipitation temperature, heating temperature and duration have marginal influences on the *Z*-average particle size of homogenously dispersed sLDH NPs (i.e. the sLDH crystals). Other factors, such as methanol washing, water washing, the duration of natural dispersion and sLDH mass concentration in the final aqueous suspension, merely affect the dispersity of sLDH NPs in suspensions.

It is suggested that when the mixed salts are added into basic methanol solution, the following precipitation takes place to generate LDH nuclei, as in the aqueous case:

$$3Mg(NO_3)_2 \cdot 6H_2O + Al(NO_3)_3 \cdot 9H_2O + (9 - y - 2z)NaOH + xCH_3OH + zNa_2CO_3 \rightarrow Mg_3Al(OH)_8(CH_3O)_x(NO_3)_y(CO_3)_z(OH)_{1-x-y-2z} \cdot mH_2O + (9 - y)NaNO_3 + (27 + x - m)H_2O \quad (1)$$

Table 4-4 XRD lattice and FWHM depending on methanol- and water-washing procedure

Sample label	c (nm)	a (nm)	FWHM (degree)
MW0	2.414	0.304	2.02
MW1	2.463	0.304	1.94
MW2	2.363	0.306	1.82
WW0	2.751	0.306	2.30
WW1	2.609	0.306	2.00
WW2	2.465	0.304	2.00
HT144	2.444	0.304	1.22
CPT0	2.459	0.306	1.54

Following nucleation, nuclei are normally aged at a pre-determined temperature for a given period of time to enable them to disperse and grow into large crystallites. As reported elsewhere, in the case where water is employed as the solvent, the heat treatment can increase the LDH particle size by a factor of 3-5. For example, the particle size can grow from ~90 to ~280 nm (*Z*-average particle size) upon heat treatment at 100 °C from 4 to 144 h, and from ~90 to ~190 nm when heated at temperatures for 16 h at 80 to 150 °C.[27] In other reports (where the size was reported as a number-average value), LDH particle size can be tailored from ~85 to ~120 nm when heated at 100 °C from 12 to 72 h, from ~115 to ~340 nm when heated for 48 h at 100 to 180 °C [21] and from ~50 to ~350 nm when heated at 100-200 °C for 12-48 h.[18] In this research, however, where methanol was employed as the solvent, the sLDH *Z*-average particle size was increased only slightly from 39 from 47 nm when heated at 100 °C from 4 to 144 h, i.e. 20-30% increase. More strikingly, there was only a 10% variation (38-42 nm) in the *Z*-average particle size when heated from 60 to 100 °C for 18 h. The sharp contrast in MgAl-LDH crystallite growth behaviours in methanol and water could be largely attributed to the solubility differences of MgAl-LDH in the two solvents.

During heat treatment, the so-called Ostwald ripening process occurs, i.e. large crystallites grow at the expense of small crystallites, primarily due to the higher solubility of small crystallites in the same solvent as a result of their higher surface energy and specific

surface area. Moreover, such a dissolution/recrystallisation process is highly dependent on the solubility of LDH in that solvent. As reported previously,[18] the solubility of MgAl-Cl-LDH and MgAl-CO_3-LDH in water is 110 and 40 mg/L, respectively, which is consistent with our finding that as-prepared large MgAl-NO_3-LDH possesses a solubility of ~100 mg/L in water at 23 °C. In contrast, we noted the solubility of MgAl-LDH in methanol is only 5-10 mg/L at 23 °C. Therefore, as-formed LDH crystallites are considerably less soluble in methanol than in water. If we suppose that the solubility difference between large and small LDHs in methanol or water is proportional to the solubility in methanol or water, then the growth rate of LDH crystallites in methanol would be much slower than that in water under identical conditions, which would explain why the *Z*-average particle size is not very sensitive to variation in heating temperature and duration in methanol. This may mean that the size of as-prepared sLDH is largely dependent on the size of LDH nuclei formed in methanol. This hypothesis is further supported by the data in Table 4-2 that the *Z*-average size and PdI of sample CPT23 (without heat-treatment, 38.6 nm and 0.23) were very similar to those of samples HT60-HT100 (with heat treatment at 60-100 °C for 18 h, 38-42 nm and 0.19-0.23). Nonetheless, 144 h heating treatment gave better crystallinity (sample HD144), as reflected by the smaller full width at half maximum (FWHM) value (1.22° for 003 reflection, Table 4-4) than that of CPT0 (FWHM = 1.54°) without heat-treatment. Given this relationship, engineering sLDH without any heat treatment and with co-precipitation at 0 °C would be most desirable. This process indeed led to the smallest LDH with the *Z*-average particle size of 35.0 nm and PdI of 0.21 (CPT0 in Table 4-2) in this research.

The dispersion of as-formed sLDH NPs in aqueous suspension can be tightly correlated to temperature as well as impure salt presence and concentration. As reported previously,[22, 27] hydrothermal treatment of manually dispersed LDH aggregates in water at 80-150 °C results in a well-dispersed LDH suspension; this could be attributed to hydrothermal heating, which provides enough thermal energy for some LDH particles to detach from an aggregate and become suspended in the solution. As all LDH NPs carry a positive charge (zeta potential 40-50 mV),[3, 13] so the repulsion between LDH nanoparticles is then expected to keep them stably suspended in solution once disaggregation has occurred. As explained above, the existence of $NaNO_3$ in the current system prohibits complete dispersion of sLDH; this is primarily due to electrolyte ions reducing the thickness of electric double layers, which act as the 'glue' between particles.[34, 35] We also gather from

previous experiments that LDH particles will no longer disperse when the electrolyte concentration reaches a threshold value, for example, at 0.1-0.2 M of NaCl.

In this research, the dispersion of sLDH NPs was conducted at room temperature, without the assistance of heat. Normally 4-6 days of standing with occasional hand-shaking gives rise to a complete dispersion of sLDH NPs in solution. Achieving a relatively small particle size (40-50 nm) is a central aim of this research, and the thermal energy at room temperature is considered sufficient to de-aggregate sLDH NPs from the aggregates. A plausible reason for the smaller particle dispersion could be related to the following exchange reaction occurring during the dispersion process:

$$\begin{aligned} &Mg_3Al(OH)_8(CH_3O)_x(NO_3)_y(OH)_{1-x-y} \cdot mH_2O + (n+x-m)H_2O \rightarrow \\ &Mg_3Al(OH)_8(NO_3)_y(OH)_{1-y} \cdot nH_2O + xCH_3OH \end{aligned} \quad (2)$$

This reaction likely takes place when the LDH slurry is washed with water. As shown in Figure 4-7C, the IR peak intensity of methoxide C-H vibrations decreased from sample WW0 to WW2, indicating that CH_3O^- is gradually eliminated from the interlayer upon water washing. The replacement of a somewhat bulky methoxide by smaller OH^-/NO_3^- ions is also reflected by decrease in the interlayer distance from WW0 (c/3, e.g. 0.92 nm) to WW2 (0.82 nm) (Table 4-4). This is also consistent with the reduction of carbon weight percentage from sample WW0 (2.50 wt %, Table 4-5) to WW2 (1.41 wt %, when more CH_3OH is washed out). It is our belief that the occurrence of this exchange reaction facilitates sLDH dispersion, although this remains under close investigation.

Table 4-5 Elemental analyses of Carbon, Hydrogen and Nitrogen contents in LDH slurry during sLDH NPs preparation with different methanol- and water-washing time(s)

	Carbon %			Hydrogen %			Nitrogen %		
Procedures	WW0	WW1	WW2	WW0	WW1	WW2	WW0	WW1	WW2
MW0	1.89±0.03	2.31±0.01	1.09±0.04	3.07±0.11	2.68±0.12	3.73±0.17	6.43±0.21	6.92±0.14	2.97±0.03
MW1	2.50±0.04	3.27±0.05	1.41±0.07	3.84±0.03	3.78±0.09	3.82±0.02	3.76±0.03	3.88±0.13	2.59±0.02
MW2	2.70±0.12	3.89±0.03	2.02±0.08	4.29±0.11	4.48±0.07	3.96±0.05	2.89±0.09	2.44±0.06	1.56±0.03
Possible products	Theoretical calculations								
$Mg_3Al(OH)_8NO_3•2H_2O$	0			3.60			4.20		
$Mg_3Al(OH)_8OCH_3•2H_2O$	3.97			4.97			0		
$Mg_3Al(OH)_8OH•2H_2O$	0			4.51			0		
$Mg_3Al(OH)_81/2(CO_3)•2H_2O$	1.99			3.99			0		

MW0, MW1, MW2: methanol wash 0, 1, and 2 times; WW0, WW1, WW2: water wash 0, 1, and 2 times

4.5 Conclusions

sLDH particles engineered by this non-aqueous approach possess a Z-average diameter size of 35 to 50 nm, albeit with heat treatment temperatures ranging from 60 to 100 °C and treatment duration up to 144 h, yielding a final sLDH suspension concentration of 6.5-29 mg/mL. Co-precipitation at 0 °C without hydrothermal treatment will generate smallest particle size. Removing salt impurities prior to natural dispersion proves crucial for homogeneous particle dispersion with a narrow particle size distribution. Ultrasonication treatment can reduce the LDH particle size of freshly prepared NPs, but will not affect the final particle size. Once prepared the physical characteristics of our sLDH nanoparticles remain as are, for at least one month. Controlled size of LDH NPs can be obtained by further hydrothermally treating the well-dispersed sLDH NPs.

References

1. Choy, J.-H. et al. Layered double hydroxide as an efficient drug reservoir for folate derivatives. *Biomaterials* **25**, 3059-3064 (2004).

2. Oh, J.-M., Choi, S.-J., Lee, G.-E., Han, S.-H. & Choy, J.-H. Inorganic drug-delivery nanovehicle conjugated with cancer-cell-specific ligand. *Advanced Functional Materials* **19**, 1617-1624 (2009).

3. Ladewig, K., Niebert, M., Xu, Z.P., Gray, P.P. & Lu, G.Q.M. Efficient siRNA delivery to mammalian cells using layered double hydroxide nanoparticles. *Biomaterials* **31**, 1821-1829 (2010).

4. Auerbach, S.M., Carrado, K.A. & Dutta, P.K. (eds.) Handbook of layered materials (Marcel Dekker, Inc, New York, 2004).

5. Nakayama, H., Wada, N. & Tsuhako, M. Intercalation of amino acids and peptides into Mg-Al layered double hydroxide by reconstruction method. *Int. J. Pharm.* **269**, 469-478 (2004).

6. Costantino, U., Ambrogi, V., Nocchetti, M. & Perioli, L. Hydrotalcite-like compounds: Versatile layered hosts of molecular anions with biological activity. *Microporous and Mesoporous Materials* **107**, 149-160 (2008).

7. Costantino, U.a.N., Morena. in Layered Double Hydroxides: Present and Future (ed. Rives, V.) (Nova Science Publisher Inc., New York, 2009).

8. Chakraborti, M., Jackson, J.K., Plackett, D., Brunette, D.M. & Burt, H.M. Drug intercalation in layered double hydroxide clay: Application in the development of a nanocomposite film for guided tissue regeneration. *International Journal of Pharmaceutics* **416**, 305-313 (2011).

9. Choy, J.-H., Kwak, S.-Y., Jeong, Y.-J. & Park, J.-S. Inorganic layered double hydroxides as nonviral vectors. *Angewandte Chemie International Edition* **39**, 4041-4045 (2000).

10. Kwak, S.-Y., Jeong, Y.-J., Park, J.-S. & Choy, J.-H. Bio-LDH nanohybrid for gene therapy. *Solid State Ionics* **151**, 229-234 (2002).

11. Masarudin, M.J., Yusoff, K., Rahim, R.A. & Hussein, M.Z. Successful transfer of plasmid DNA into in vitro cells transfected with an inorganic plasmid-Mg/Al-LDH nanobiocomposite material as a vector for gene expression. *Nanotechnology* **20**, 045602 (2009).

12. Li, A. et al. The use of layered double hydroxides as DNA vaccine delivery vector for enhancement of anti-melanoma immune response. *Biomaterials* **32**, 469-477 (2011).

13. Wong, Y. et al. Efficient delivery of siRNA to cortical neurons using layered double hydroxide nanoparticles. *Biomaterials* **31**, 8770-8779 (2010).

14. Khan, A.I., Lei, L.X., Norquist, A.J. & O'Hare, D. Intercalation and controlled release of pharmaceutically active compounds from a layered double hydroxide. *Chemical Communications*, 2342-2343 (2001).

15. bin Hussein, M.Z., Zainal, Z., Yahaya, A.H. & Foo, D.W.V. Controlled release of a plant growth regulator, alpha-naphthaleneacetate from the lamella of Zn-Al-layered double hydroxide nanocomposite. *Journal of Controlled Release* **82**, 417-427 (2002).

16. Gu, Z., Thomas, A.C., Xu, Z.P., Campbell, J.H. & Lu, G.Q. *In vitro* sustained release of LMWH from MgAl-layered double hydroxide nanohybrids. *Chemistry of Materials* **20**, 3715-3722 (2008).

17. Gasser, M.S. Inorganic layered double hydroxides as ascorbic acid (vitamin C) delivery system-Intercalation and their controlled release properties. *Colloids and Surfaces B: Biointerfaces* **73**, 103-109 (2009).

18. Choi, S.-J. & Choy, J.-H. Layered double hydroxide nanoparticles as target-specific delivery carriers: uptake mechanism and toxicity. *Nanomedicine* **6**, 803-814 (2011).

19. Chithrani, B.D., Ghazani, A.A. & Chan, W.C.W. Determining the Size and Shape Dependence of Gold Nanoparticle Uptake into Mammalian Cells. *Nano Letters* **6**, 662-668 (2006).

20. Maurice, V., Georgelin, T., Siaugue, J.-M. & Cabuil, V. Synthesis and characterization of functionalized core-shell γFe_2O_3-SiO_2 nanoparticles. *Journal of Magnetism and Magnetic Materials* **321**, 1408-1413 (2009).

21. Oh, J.-M., Hwang, S.-H. & Choy, J.-H. The effect of synthetic conditions on tailoring the size of hydrotalcite particles. *Solid State Ionics* **151**, 285-291 (2002).

22. Xu, Z.P. et al. Stable suspension of layered double hydroxide nanoparticles in aqueous solution. *Journal of the American Chemical Society* **128**, 36-37 (2006).

23. Oh, J.-M., Choi, S.-J., Lee, G.-E., Kim, J.-E. & Choy, J.-H. Inorganic metal hydroxide nanoparticles for targeted cellular uptake through clathrin-mediated endocytosis. *Chemistry-An Asian Journal* **4**, 67-73 (2009).

24. Li, S. et al. Cellular uptake and gene delivery using layered double hydroxide nanoparticles. *Journal of Materials Chemistry B* **1**, 61-68 (2013).

25. Gardner, E., Huntoon, K.M. & Pinnavaia, T.J. Direct synthesis of alkoxide-intercalated derivatives of hydrocalcite-like layered double hydroxides: Precursors for the formation of colloidal layered double hydroxide suspensions and transparent thin films. *Advanced Materials* **13**, 1263-1266 (2001).

26. Gunawan, P. & Xu, R. Direct sssembly of anisotropic layered Ddouble hydroxide (LDH) nanocrystals on spherical template for fabrication of drug-LDH hollow Nnanospheres. *Chemistry of Materials* **21**, 781-783 (2009).

27. Xu, Z.P., Stevenson, G., Lu, C.-Q. & Lu, G.Q. Dispersion and size control of layered double hydroxide nanoparticles in aqueous solutions. *Journal of Physical Chemistry B* **110**, 16923-16929 (2006).

28. Chen, M., Cooper, H.M., Zhou, J.Z., Bartlett, P.F. & Xu, Z.P. Reduction in the size of layered double hydroxide nanoparticles enhances the efficiency of siRNA delivery. *Journal of Colloid and Interface Science* **390**, 275-281 (2013).

29. Wong, Y.Y. et al. Efficiency of layered double hydroxide nanoparticle-mediated delivery of siRNA is determined by nucleotide sequence. *Journal of Colloid and Interface Science* **369**, 453-459 (2012).

30. Xu, Z.P. & Zeng, H.C. Abrupt structural transformation in hydrotalcite-like compounds $Mg_{1-x}Al_x(OH)_2(NO_3)_x \cdot nH_2O$ as a continuous function of nitrate anions. *Journal of Physical Chemistry B* **105**, 1743-1749 (2001).

31. Nakamoto, K. Infrared and Raman spectra of inorganic and coordination compounds: Part A (Wiley, Hoboken, NJ, USA 2009).

32. Dijkstra, G., Maas, J.H. & Smit, A. A systematic approach to IR-analysis of methyl groups. *Fresenius' Zeitschrift für analytische Chemie* **264**, 200-204 (1973).

33. Lide, D.R. et al. CRC Handbook of Chemistry and Physics (ed. Haynes, W.M.M.) (CRC Press, 2011-2012).

34. Vincent, B. Early (pre-DLVO) studies of particle aggregation. *Advances in Colloid and Interface Science* **170**, 56-67 (2012).

35. Fornasiero, D. & Grieser, F. The kinetics of electrolyte induced aggregation of carey lea silver colloids. *Journal of Colloid and Interface Science* **141**, 168-179 (1991).

This page was left blank intentionally.

Chapter 5 Particle Size- and Number-dependent Delivery to Cells by Layered Double Hydroxide Nanoparticles

Declaration for Chapter 5

- Manuscript for this chapter is published on *Journal of Colloid and Interface Science* **2015**, 437, 10-16; doi: 10.1016/j.jcis.2014.09.010
- A schematic diagram is shown in the end to illustrate and help understand the particle size, FITC and DNA loading differences between small and large LDH nanoparticles. Some of the grey scale images in the manuscript have been changed to colour ones in this thesis.

Abstract

It is well known that delivery efficiency to cells is highly dependent on the particle size and the dose used in the experiments. However, there is a marked discrepancy in many reports, mainly due to the inconsistence in assessment of various parameters. In this chapter, we designed specific experiments using layered double hydroxide nanoparticles (LDH NPs) to elucidate the effect of particle size, dose and dye loading manner on the cellular uptake. Using the number of LDH NPs taken up by HCT-116 cells as the indicator of delivery efficiency, we found that (1) the size of sheet-like LDH in the range of 40-100 nm did not significantly affect their cellular uptake; (2) cellular uptake of 40 and 100 nm LDH NPs was increased proportionally to the number concentration below a critical value, but kept nearly unchanged beyond the critical value; and (3) the effect of the dye loading manner is mainly dependent on the loading capacity or yield. In particular, the loading capacity is determined by the NP specific surface area. This research may be extended to a larger size range to examine the size effect, but suggests that it is necessary to set up a protocol to evaluate the effects of NP's physicochemical properties on the cellular delivery efficiency.

5.1 Introduction

Recent years have witnessed the enormous progress of nano-sized materials applied for drug/gene delivery, which include various polymeric nanoparticles (NPs), liposomes, metal (such as gold) and metal oxide (such as iron oxide, IO) NPs, mesoporous silica NPs (MSNs), carbon nanotubes (CNTs), layered double hydroxide (LDH) NPs, and their hybrids etc. [1-16]

It is well known that the physicochemical properties, such as the NP size, shape, dose and surface charge, affect the NP delivery efficacy. Of these characteristics, the particle size is a crucial factor which determines NP endocytosis pathway,[17, 18] uptake rate and efficiency,[6, 16, 19-22] in vitro cytotoxicity,[23-28] immune responses,[28-31] and the final localisation.[15, 32, 33] Thus size-dependent uptake of various NPs has been intensively investigated and widely reported. For example, for organic NPs, some researchers claimed smaller NPs resulted in higher cellular uptake,[22, 34] while others reported an optimal size range for highest uptake.[35-38] Ross and Hui[39] even found linearly increasing cellular uptake of lipoplex in the size range of 35 to 2200 nm. For inorganic-based NPs, the similar results were reported. Some researchers reported an optimal particle size for uptake of Au NPs, CNTs, and MSNs (~ 50 nm),[6, 40-42] but some others found smaller Au, silica, and IO NPs had improved cellular uptake than larger ones in a certain size range.[43-46]

Besides the particle size, the NP shape, on the other hand, also affects the cellular uptake behaviours. Chithrani et al.[6] reported HeLa cells took up much more spherical Au NPs than rod-shaped Au NPs with a high aspect ratio. Jin et al.[41] found long and short SWNTs showed lower cellular uptake than those with the medium length. Choi and Choy's group studied the cellular uptake behaviours and mechanisms of LDH NPs (with sheet-like shape), finding 50 nm LDH NPs showed higher cellular uptake than 100-200 nm and 350 nm ones.[47, 48] Recently we found 40 nm LDH NPs can carry 1-4 times more dsDNA than 100 nm ones at LDH:DNA mass ratio of 1:1 and 5:1, contributing to enhanced gene delivery.[49, 50]

In brief, the observations and conclusions differ from research groups, especially the particle size effect, being not so consistent and sometimes confused. This could be caused by several vague items without clear and consistent definition. The first one is the NP size, which is normally characterised as the *Z*-average hydrodynamic diameter

(measured by dynamic light scattering technology)[29, 42, 51] or the number average size (measured and statistically calculated from transmission/scanning electron microscopy images).[6, 28] The second term is the dose of nanoparticles. Someone used the mass concentration while some others used the particle number concentration. The third one is the delivery efficiency, often expressed as the NP number,[6, 16, 44, 52] the mass amount (pg/cell),[16, 42] or the relative amount of labelled fluorescence dye[49, 53] taken up by each cell. In addition, the difference in the shape and surface property from a variety of materials and surface modified functional groups may also cause the inconsistence. It is worth noting that the cell type used in different research groups is often different, which may also contribute to the inconsistence in determining the optimal particle size for the maximum cellular uptake efficiency.

Therefore, this particular research aimed to clearly elucidate effects of the particle size (*Z*-average), the dose (particle number concentration) and the dye loading (bulky or surface) of sheet-like LDH NPs on the uptake efficiency by HCT-116 cells. We found that (1) the cellular uptake efficiency of 40-50 nm NPs was similar to that of 90-100 nm NPs; (2) there was a critical particle number concentration, below which cellular uptake was in linear proportion to the particle number concentration, while beyond which cellular uptake was not improved; (3) dye loading on the surface may also affect cellular uptake depending on the surface loading capacity.

5.2 Experimental

5.2.1 LDH NPs preparation

Small LDH (sLDH) NPs were prepared by a non-aqueous precipitation method.[49, 50] Briefly, 10 mL methanol solution containing 6 mmol of $Mg(NO_3)_2 \cdot 6H_2O$ and 2 mmol of $Al(NO_3)_3 \cdot 9H_2O$ was added drop-wise to a 40 mL of methanol solution containing 16 mmol NaOH under vigorous stirring. The precipitate slurry was collected via centrifugation, then redispersed in 40 mL fresh methanol and transferred to a Teflon®-lined autoclave for heat-treatment at 100°C for 4 h. The final LDH slurry was collected and manually dispersed in 40 mL of deionised water (DI water) after washing twice with DI water. This dispersion resulted in a homogeneous sLDH suspension after 4-6 days with a sLDH mass concentration of 6-7 mg/mL.

Large LDH (L-LDH) NPs were synthesised by mixing 10 mL of aqueous solution containing 3.0 mmol of $MgCl_2 \cdot 6H_2O$ and 1.0 mmol of $AlCl_3 \cdot 6H_2O$ with 40 mL of 0.15

M NaOH solution and vigorously stirring for 10 min at room temperature [54, 55]. The LDH slurry was collected by centrifugation, washed twice with DI water (40 mL), and then resuspended in DI water (40 mL). The suspension was then transferred to a Teflon®-lined autoclave and hydrothermally treated at 100°C for 16 h. The suspension contained approximately 4 mg/mL of homogeneously dispersed L-LDH NPs.

Both small and large LDH-FITC NPs were prepared by ion-exchange method. Here, FITC (fluorescein isothiocyanate isomer I) sodium solution (0.05 or 0.01 mmol) was mixed with 1 mmol of either sLDH or L-LDH slurry and then shaken on a reciprocal shaker for 1 h. After ion-exchange, the unchanged FITC and residual sodium nitrate or sodium chloride ($NaNO_3$/NaCl) were separated. The collected slurry was then redispersed in deionised water and subjected to 2-4 h of hydrothermal and sterilisation treatment.

All NP sizes were determined by dynamic light scattering (DLS, Zetasizer Nano ZS, Malvern Ltd). The *Z*-average size of sLDH was found to be ~40 nm (~54 nm for sLDH-FITC), while L-LDH measured ~100 nm (~90 nm for L-LDH-FITC).

5.2.2 Suspension stability test

LDH NPs were diluted by complete cell culture media (10% (*v/v*) of fetal bovine serum mixed with Dulbecco's Modified Eagle Medium (DMEM, with L-glutamine and 4.5 g/L of glucose) at desired concentrations, then particle size distribution of the suspension mixture was measured using the zetasizer.

5.2.3 Nucleic acid loading and agarose gel electrophoresis

Nucleic acids were loaded on LDH NPs by mixing LDH suspension with nucleic acid solution at the LDH:dsDNA mass ratios of 2:1, 5:1, 10:1, 20:1, and 40:1. A 2.5% agarose gel with Gel-Red stain was made and then nucleic acids with/out LDH for binding were loaded in the wells. For each well, 260 ng double stranded DNA (dsDNA DCC1) was used. Gel was imaged by a Bio-Rad imaging system after run at 90 V for 45 min in TBE (Tris/Borate/EDTA) buffer.

5.2.4 Cellular uptake

HCT-116 cells were seeded in 6-well plates at density of 1×10^5 cells per well in 2 mL complete cell culture media. After 24 h of incubation, cell culture media was replaced by 1 mL of fresh media with/out desired concentration of LDH-FITC NPs or LDH-DNA-Cy3 NPs (40 nM DNA was used). At different time points after further incubation (from 15 min to 8 h), the culture media was removed, cells were washed twice with PBS buffer and then detached from the plates by trypsin-EDTA. The cells were washed twice with PBS buffer and then fixed in a certain volume of 2% PFA (paraformaldehyde) before measurement by flow cytometry (BD Accuri™ C6 Flow Cytometer System, band pass filter 530/30 for detecting FITC, 585/40 for detecting Cy3, 10,000 cells were counted). All treatments were performed for three different batches in duplicate. Data are presented as the mean ± SEM (standard error of the mean).

5.3 Results

5.3.1 System suspension stability

As shown in Figure 5-1, both sLDH and L-LDH NPs are well dispersed in water, having a hydrodynamic diameter ranging from 10 to 100 nm with the *Z*-average size of 40 nm, and from 40 to 250 nm with the *Z*-average size of 100 nm, respectively. Both sLDH and L-LDH NPs have a zeta potential of ~40 mV, which is in agreement with earlier reports for LDH.[49, 55, 56]

When LDH NPs were diluted in complete cell culture media, both sLDH and L-LDH NPs aggregated, and this was found to be concentration- and size-dependent. As shown in Figure 5-2, when the sLDH NP suspension was diluted to a concentration range of 100-800 μg/mL, sLDH formed aggregates with the *Z*-average size of 200-450 nm. Applying the same concentration range to L-LDH NPs, they also aggregated but to a less extent, with the *Z*-average size of 180-300 nm. The *Z*-average size (74 and 107 nm) was in close agreement with that in the original suspension for both sLDH and L-LDH when they were further diluted to 40 μg/mL. The aggregation may affect the cellular uptake as Andersson et al.[57] found NP uptake was strongly dependent on the agglomeration size, not the primary particle size. This proved serendipitous as the concentration of LDH NPs used in cellular uptake studies did not typically exceed 40 μg/mL so as to circumvent unwanted NP aggregation.

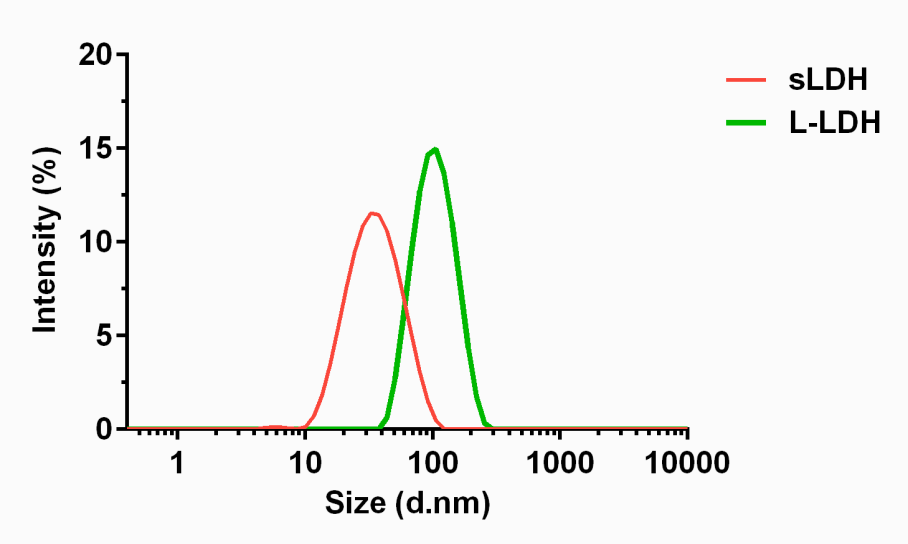

Figure 5-1 Particle size distribution of small and large LDH

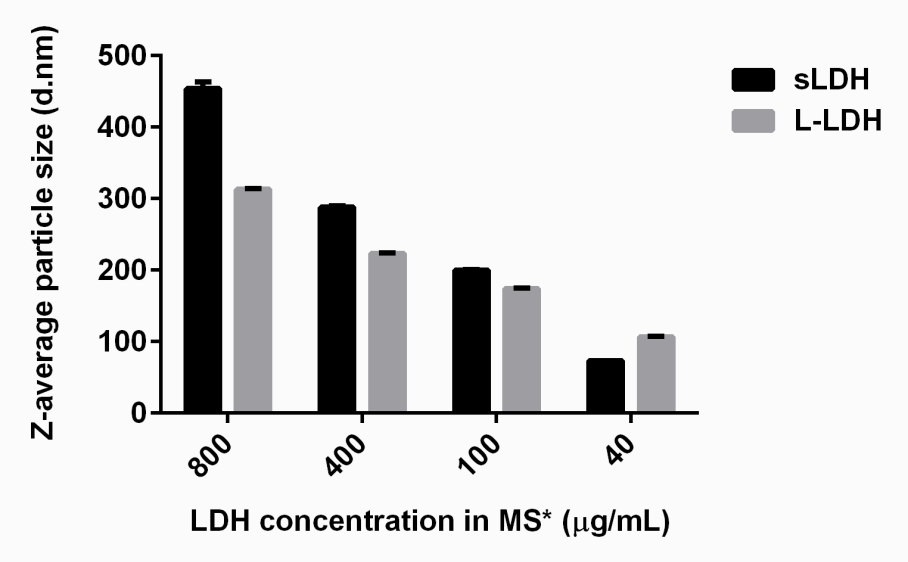

Figure 5-2 Particle size distribution of sLDH and sLDH in cell culture media

Particle aggregation was more pronounced with sLDH in the culture media and this could be attributed to their relative dimensions compared to L-LDH. sLDH possesses a surface area 2.5 times that of L-LDH NPs, and thus its capacity to adsorb proteins (a key driver of aggregation) present in cell culture media is also considered to be 2.5-fold greater than L-LDH. Upon lowering the NP concentration sufficiently (i.e. < 40 μg/mL), sLDH and L-LDH NPs adsorb protein until they reach a relative state of equilibrium, at which point their surface properties are dictated by adsorbed proteins such that aggregation is suppressed. That said, at high NP concentrations, one can expect to reach a point where all available proteins are adsorbed by the NPs, and this triggers surface adsorbed proteins to reach out

and form protein-bridges with neighbouring particles, resulting in aggregation. This latter phenomenon is likely to be more of an issue with sLDH, as L-LDH possesses a smaller surface area and so is able to accommodate far less proteins.

5.3.2 DNA loading

Figure 5-3 to Figure 5-4 show the electrophoretic mobility of dsDNA loaded onto LDH NPs at increasing LDH:dsDNA mass ratios. The first lane for each gel represents a 21-25 bp dsDNA marker, and the bright bands toward the bottom of the gels are free dsDNA. As can be seen in Figure 5-3A, sLDH NPs completely immobilised dsDNA at the mass ratio of ≥ 5:1 in water, while at 2:1 some free dsDNA was present. Similarly, L-LDH NPs completely bound dsDNA at the mass ratio of ≥ 10:1 in water, while the binding was not complete at 5:1 (Figure 5-3B). This difference can again be attributed to the particle size as the larger surface area of sLDH NPs can accommodate a greater load of dsDNA as compared to L-LDH NPs at the equivalent mass concentration.

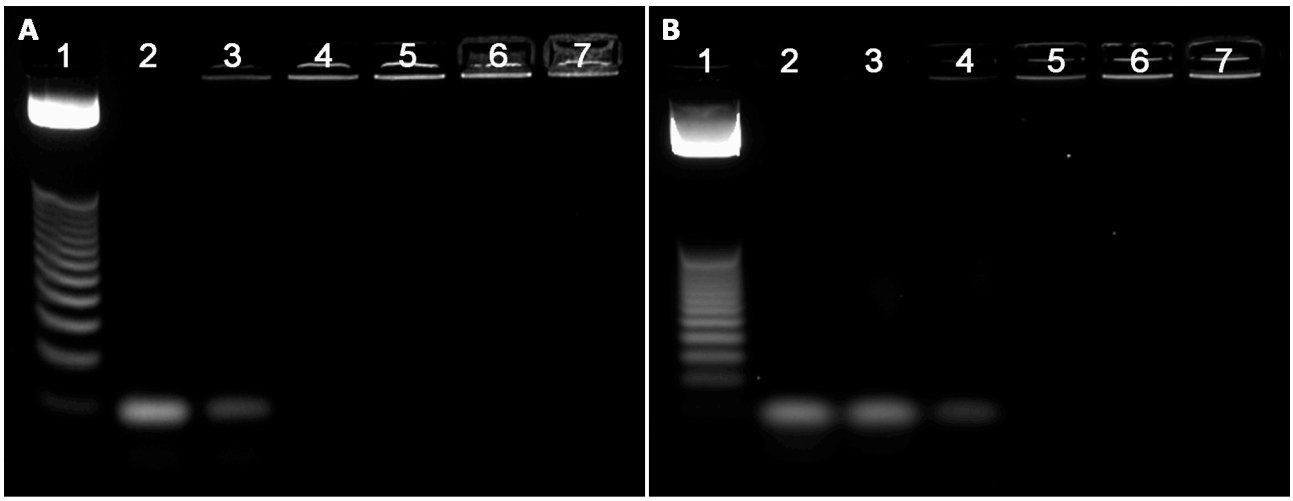

Lane 1: 25 bp ladder
Lane 2: Free dsDNA
Lane 3: sLDH:dsDNA = 2:1
Lane 4: sLDH:dsDNA = 5:1
Lane 5: sLDH:dsDNA = 10:1
Lane 6: sLDH:dsDNA = 20:1
Lane 7: sLDH:dsDNA = 40:1

Lane 1: 25 bp dsDNA ladder
Lane 2: Free dsDNA
Lane 3: L-LDH:dsDNA = 2:1
Lane 4: L-LDH:dsDNA = 5:1
Lane 5: L-LDH:dsDNA = 10:1
Lane 6: L-LDH:dsDNA = 20:1
Lane 7: L-LDH:dsDNA = 40:1

Figure 5-3 Agarose gel electrophoresis test of sLDH (A) and L-LDH (B) loading dsDNA in water at different mass ratios (260 ng dsDNA used, 2.5 % agarose gel run at 90 V for 45 min)

When the LDH-dsDNA complexes were assessed in complete cell culture media, electrophoretic studies revealed less dsDNA immobilised (Figure 5-4) than that in water (Figure 5-3). In the complete cell culture media, only at mass ratios of 20:1 and 40:1 was dsDNA observed to be completely bound by both sLDH and L-LDH NPs. However, the surface area of the respective NPs again yielded subtle differences in binding with dsDNA at the lower (e.g. 5:1) mass ratios.

As alluded to earlier, the significant differences in mass ratios necessary to completely immobilise dsDNA in water versus complete cell culture media can once again be attributed to the competitive adsorption of proteins (in serum) onto the respective NP surfaces. This competition results in a relatively higher mass of LDH NPs needed to fully complex dsDNA in complete cell culture media, and is a phenomenon seen with other vector-DNA complexation studies.[58]

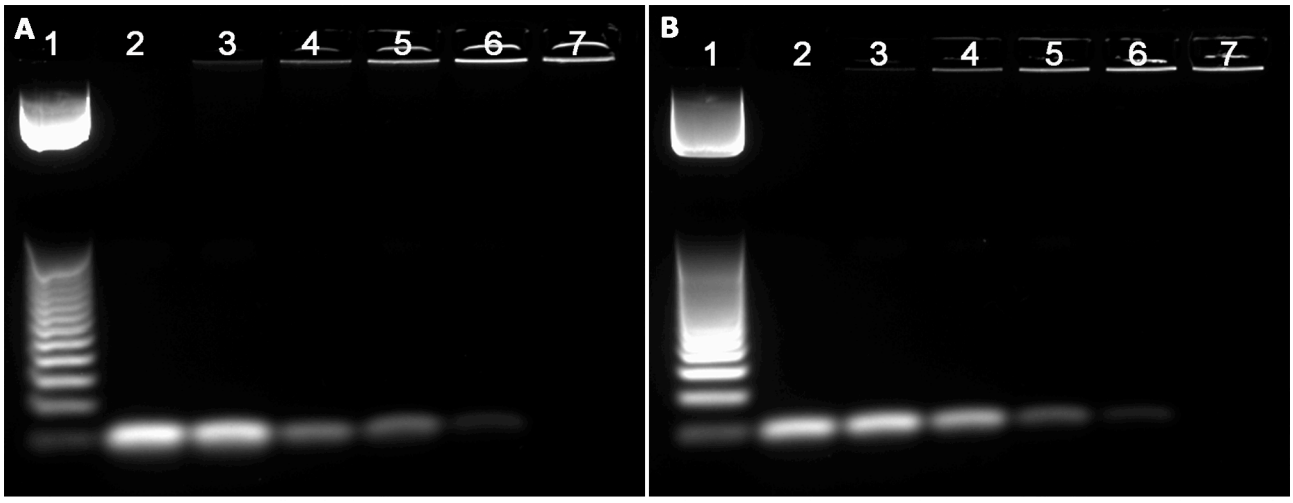

Lane 1: 25 bp dsDNA ladder
Lane 2: Free dsDNA
Lane 3: sLDH:dsDNA = 2:1
Lane 4: sLDH:dsDNA = 5:1
Lane 5: sLDH:dsDNA = 10:1
Lane 6: sLDH:dsDNA = 20:1
Lane 7: sLDH:dsDNA = 40:1

Lane 1: 25 bp dsDNA ladder
Lane 2: Free dsDNA
Lane 3: L-LDH:dsDNA = 2:1
Lane 4: L-LDH:dsDNA = 5:1
Lane 5: L-LDH:dsDNA = 10:1
Lane 6: L-LDH:dsDNA = 20:1
Lane 7: L-LDH:dsDNA = 40:1

Figure 5-4 Agarose gel electrophoresis test of sLDH (A) and L-LDH (B) loading dsDNA in cell culture media at different mass ratios (260 ng dsDNA used, 2.5 % agarose gel run at 90 V for 45 min)

5.3.3 Cellular uptake

5.3.3.1 LDH-FITC uptake

We first tested the cellular uptake of FITC-labelled NPs at different LDH concentrations by HCT-116 cells. The FITC loading capacity within both types of LDH NPs was comparable, being 5% of all intercalated anions (denoted as LDH-5%FITC). We found that > 99% of cells were FITC-positive after incubation with either sLDH-5%FITC or L-LDH-5%FITC at 4 h, and across the concentrations measured (2.5 to 20 μg/mL) (Figure 5-5A and B). The mean fluorescence intensity of cells treated with sLDH-5%FITC at these concentrations did not change (≥ 5.0 μg/mL), indicating that the cellular uptake was saturated under these conditions. Our previous confocal images have confirmed that hexagonal LDH NPs are taken up by various cell types and mostly located in the cytoplasm.[49, 55, 59, 60]

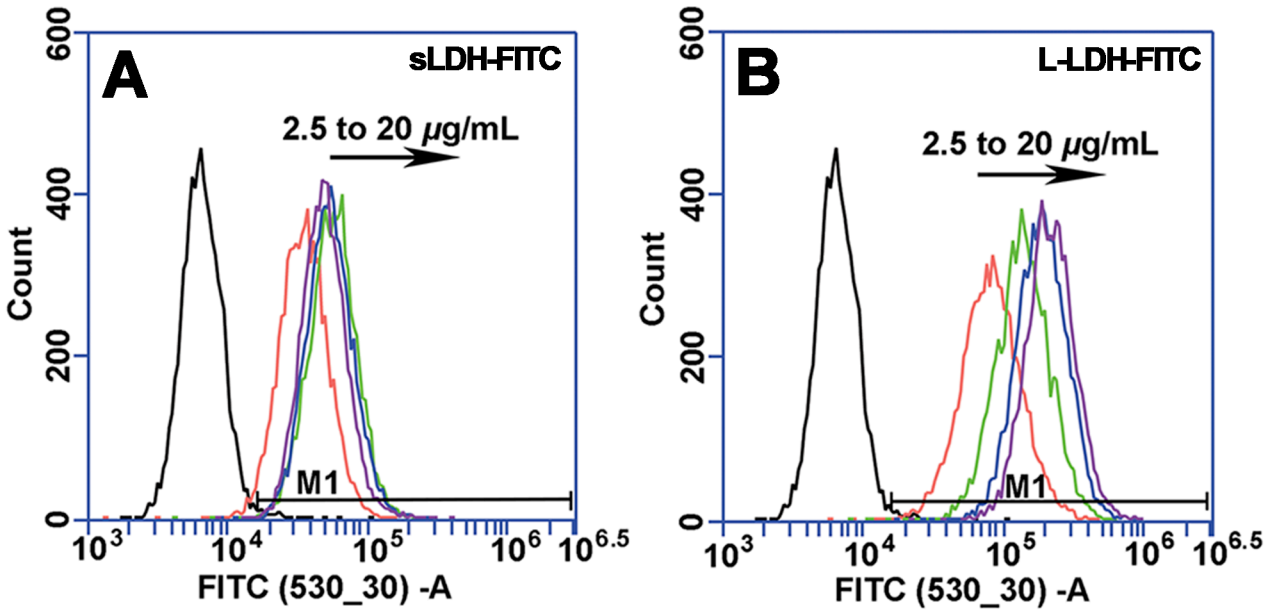

Figure 5-5 Cellular uptake of small (A) and large (B) LDH-5%FITC by HCT-116 cells at concentration of 2.5 to 20 μg/mL

In sharp contrast, the mean fluorescence intensity of cells treated with L-LDH-5%FITC exhibited increasing fluorescence intensity as the LDH concentration was raised (Figure 5-6); this reveals that the cellular uptake of L-LDH-5%FITC continued under the same conditions albeit at a declining rate, indicating the saturated particle concentration for L-LDH-5%FITC is most likely in the region of 20 μg/mL. For sLDH, at the concentration of 1.4 μg/mL, the mean fluorescence intensity was quite low, showing a strong dependence

on the sLDH mass concentration, similar to the dependence seen by L-LDH at 2.5-20 μg/mL (Figure 5-6). Choy et al.[11] also found dose dependent uptake of LDH-FITC NPs by NIH 3T3 cells in the test concentration range (< 45 μM). Li et al.[51] reported concentration dependent uptake of 65 nm CO_3LDH-FITC by NSC 34 cells in the concentration range of 6.25 to 100 μg/mL, where FITC was adsorbed on the surface of CO_3LDH instead of intercalated into the interlayers.

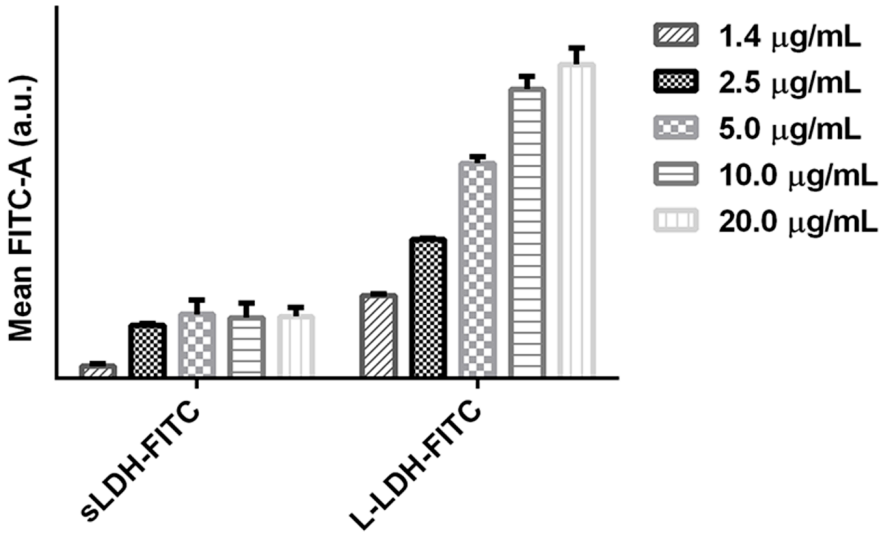

Figure 5-6 Mean FITC intensity in the cells treated by small and Large LDH-FITC NPs at concentration of 1.4 to 20 μg/mL

To explore LDH-5%FITC cell uptake kinetics, time-dependent uptake of small and large LDH-5%FITC at 1.4 and 10.0 μg/mL was investigated. Figure 5-7A shows that almost all cells treated with 1.4 μg/mL of L-LDH-5%FITC were FITC-positive after ≥2 h, although the mean FITC fluorescence intensity kept increasing with incubation time (Figure 5-7B). In comparison, only 25-35% cells were FITC-positive with the mean FITC fluorescence intensity nearly constant when treated with sLDH-FITC at this concentration for ≥ 2 h. Of note was that the mean fluorescence intensity of cells treated with L-LDH was 15-20 times that of sLDH, after 2-8 h of incubation.

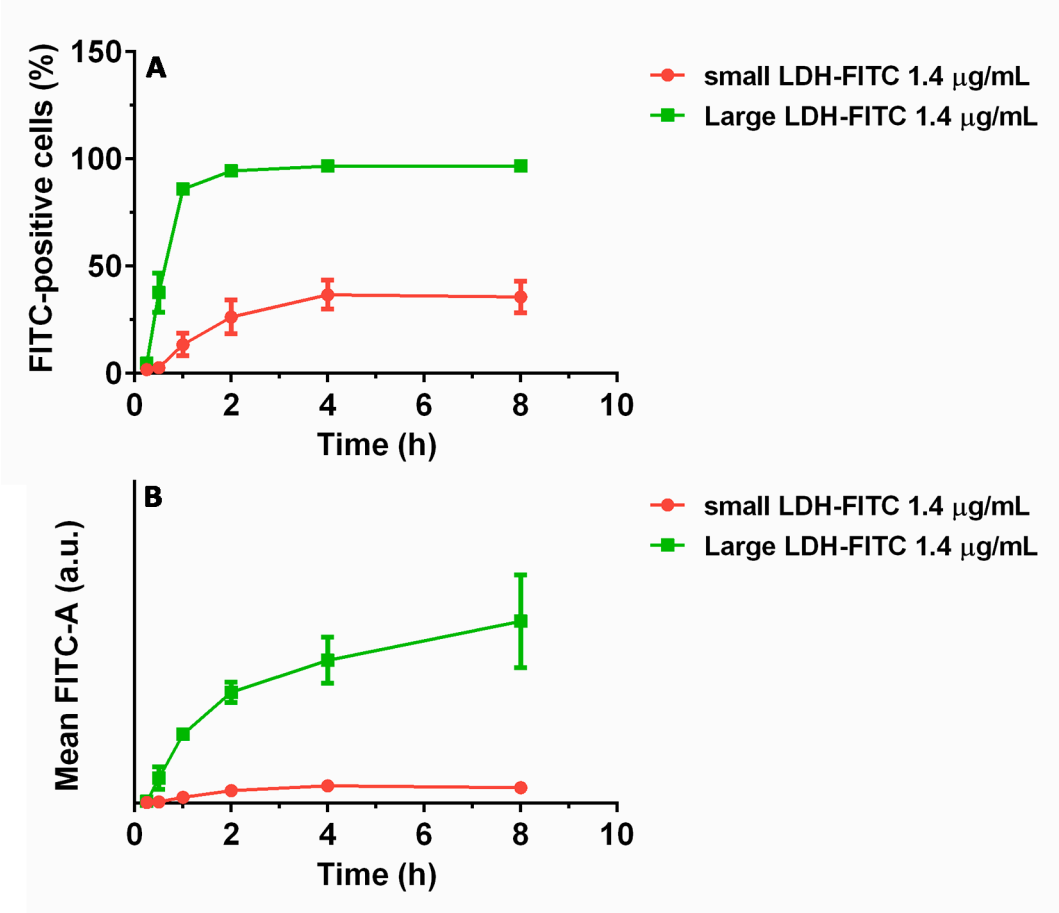

Figure 5-7 Cellular uptake of small and large LDH-FITC at concentration of 1.4 μg/mL

In the case of 10 μg/mL of FITC-labelled LDH NPs, almost all cells were FITC-positive upon treatment with both small and large LDH-5%FITC NPs (Figure 5-8A) after 4 h of incubation. During the 15 min to 4 h incubation window L-LDH-5%FITC led to a marginally higher percentage of FITC-positive cells. This is comparable to what Li et al. [56] reported, where 60-70% of positive cells were observed after incubating MDDC cells with 20 μg/mL FITC-labelled LDH NPs (hydrodynamic number size ~60 nm). The mean FITC intensity continuously increased during the whole uptake process with both sets of NPs (Figure 5-8B). Such a time-dependent uptake of LDH-FITC NPs by NIH 3T3 cells was also reported by Choy et al.[11] Interestingly, the mean FITC fluorescence intensity of the cells treated with 10 μg/mL of L-LDH-5%FITC appeared to be 2-3 times that of the cells treated with 10 μg/mL of sLDH-FITC at each time point.

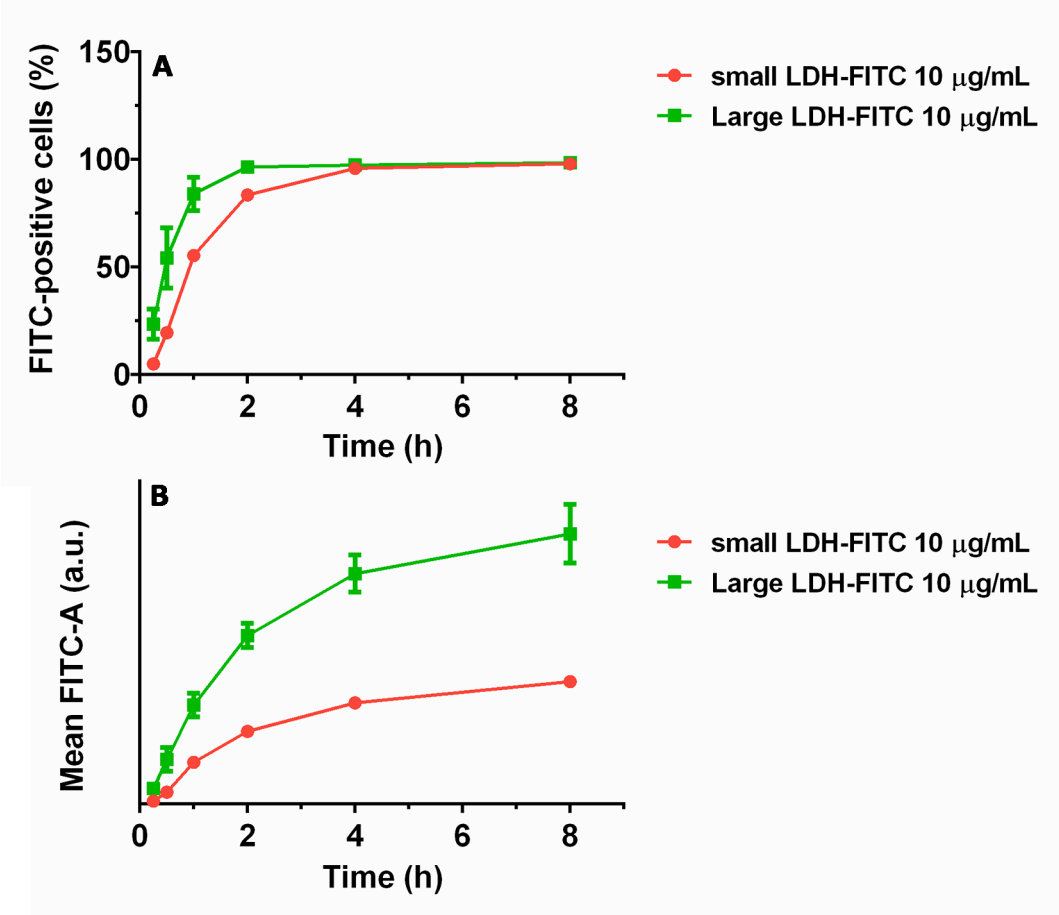

Figure 5-8 Uptake of small and large LDH-FITC at concentration of 10 μg/mL

To elucidate specifically the role of NP size on the rate and efficiency of cellular uptake, we particularly prepared L-LDH NPs containing 1% FITC (L-LDH-1%FITC, ~90 nm) and compared the cellular uptake at 20 μg/mL of L-LDH-1%FITC and 4 μg/mL of sLDH-5%FITC (both being close to saturated particle concentration as discussed earlier). In this series of experiments, each FITC-labelled NP contained an equivalent amount of FITC and the NP number concentration was also the same. Thus, assessment of cellular uptake efficiency would be reflected purely from a NP-size perspective. As shown in Figure 5-9, similar FITC-positive cell percentage and mean FITC intensity were observed in both cases. The subtle difference is that cellular uptake efficiency equilibrated after 2 h of incubation with sLDH-FITC, while L-LDH-FITC NPs uptake kept increasing over the same period, as measured by the percentage of FITC-positive cells and mean FITC fluorescence intensity. This probably reflected a more rapid uptake of sLDH-FITC NPs before 4 h, but sustained and continuous uptake of L-LDH-FITC NPs after 4 h. Rapid internalisation of 50 and 100 nm spheric NPs compared to 200 nm ones was also reported

by Rejman et al.[18] More interestingly, the continuous uptake of larger NPs was also observed and reported for viral NPs,[61] polyplexes,[62] and lipoplexes.[63]

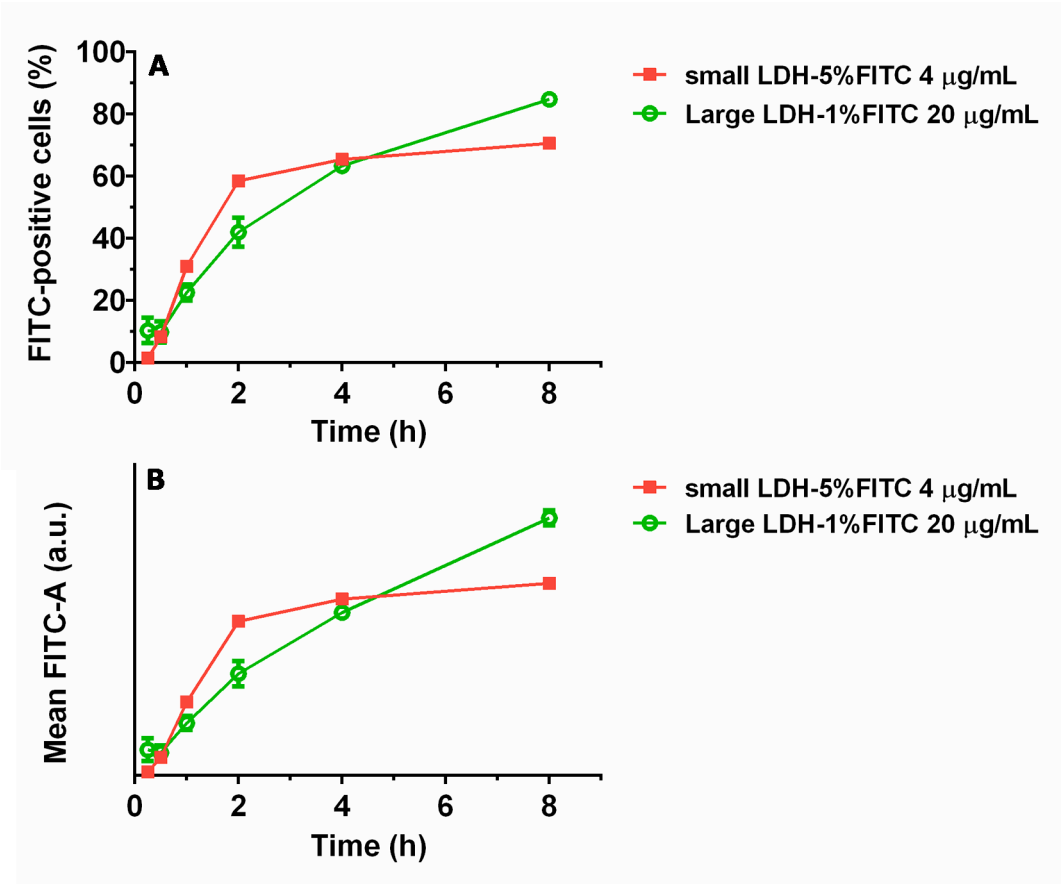

Figure 5-9 Time course cellular uptake of small and large LDH-FITC at identical particle number concentration and FITC loading

5.3.3.2 DNA uptake

We next investigated the cellular uptake of LDH-DNA complexes, where DNA was predominantly adsorbed on the LDH NP surface.[49, 60] The loading capacity of DNA onto LDH was determined by varying the LDH: DNA mass ratios, as discussed previously (Figure 5-3 and Figure 5-4). Based on the observations in Figure 5-3 and Figure 5-4, we chose two LDH: DNA mass ratios, the first of which reflected incomplete LDH-DNA complexation (5:1) while the second reflected complete complexation (40:1), irrespective of NP size. The time-dependent cellular uptake of both sets of LDH NPs with DNA-Cy3 is presented in Figure 5-10 to Figure 5-11.

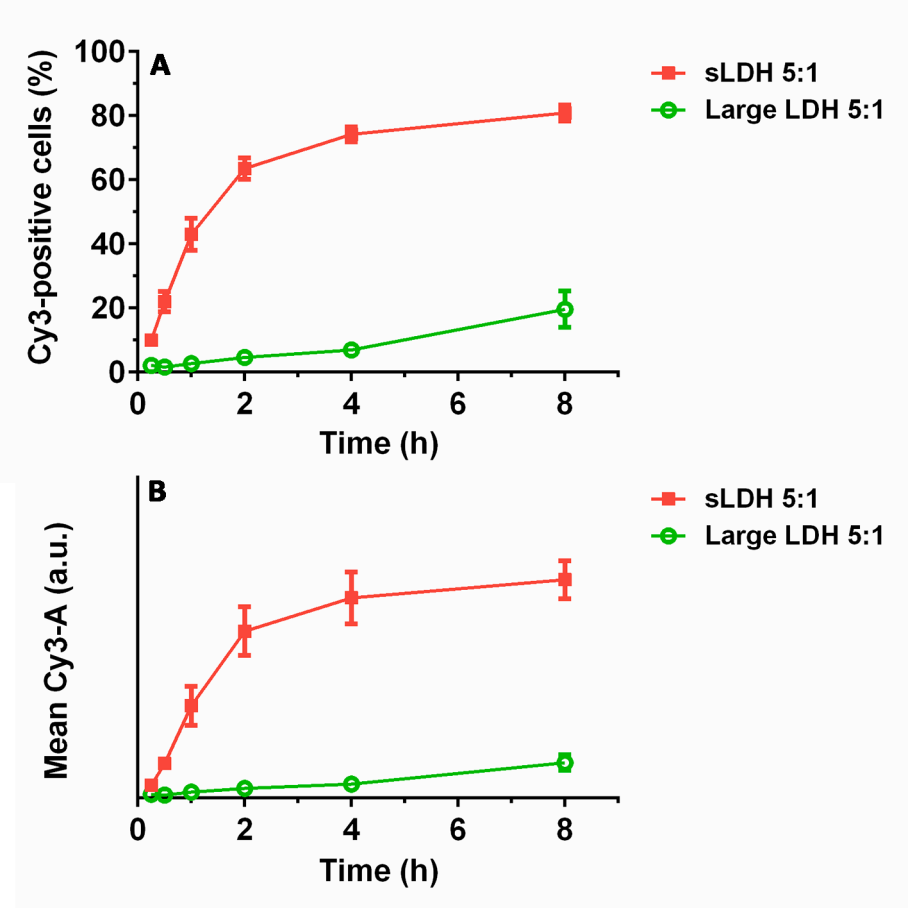

Figure 5-10 Cellular uptake time course of LDH-DNA at mass ratio of 5:1 by HCT-116 cells

At the mass ratio of 5:1 (40 nM DNA-Cy3 and 1.4 μg/mL sLDH), the percentage of Cy3-positive cells quickly increased to 60% after just 2 h incubation, and then slowly increased to 80% over the next 6 h. However, in the case of L-LDH-DNA-Cy3, the percentage of Cy3-positive cells increased steadily over the entire incubation period, reaching a mere 20% after 8 h incubation (Figure 5-10A). The mean Cy3 fluorescence intensity followed a similar trend (Figure 5-10B). Our findings are consistent with our previous observation in HEK-293T cells,[50] suggesting that partial complexation of DNA by L-LDH NPs at this mass ratio is detrimental to gene delivery efficiency. This observation seems to be similar to the report by Elbakry et al.[64] that far more DNA molecules were delivered to one cell by 20 nm Au NPs than 80 ones.

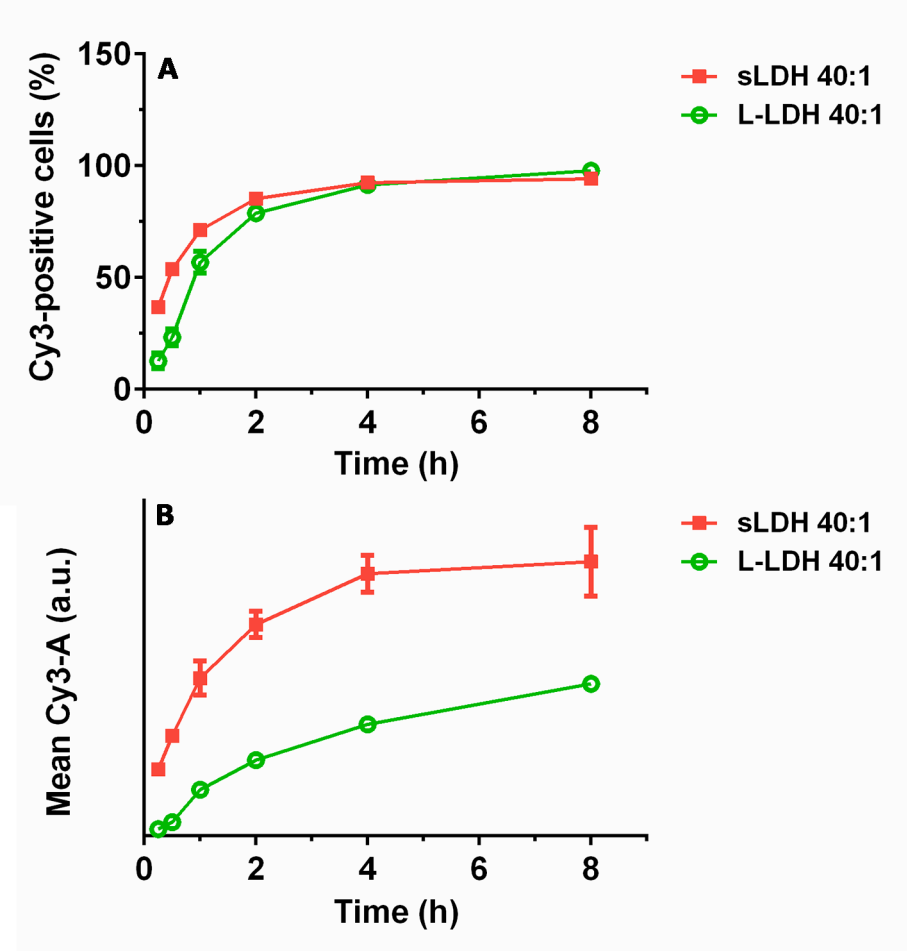

Figure 5-11 Cellular uptake time course of LDH-DNA at mass ratio of 40:1 by HCT-116 cells

At the mass ratio of 40:1 (40 nM DNA-Cy3 and 11 µg/mL LDH), treatment with sLDH and L-LDH led to a similar population of Cy3-positive cells after 2 h of treatment. Prior to this time frame, a higher percentage of Cy3 positive cells was seen with sLDH (Figure 5-11A). The mean Cy3 fluorescence intensity of cells treated with sLDH was twice that of cells treated with L-LDH after 1-8 h of incubation (Figure 5-11B), which indicates that sLDH is able to transport twice the load of DNA as L-LDH, at this mass ratio. This observation appears to be consistent with the following reports: more rapid internalisation of smaller DNA/PEI complexes by K562 cells,[65] and smaller PLGA NPs by COS-7 and HEK-293 cells.[66]

5.4 Discussion

The ease by which therapeutic nanoparticles (e.g. gene-carrier systems) are taken up by their target cell population will directly impact on quantifiable outcomes which ultimately

dictate their 'efficiency', such as the rate and intensity of transfection/fluorescence measured across a population of cells. With this in mind, the key concepts underlying this work presented here aimed to explore and decipher the effects of the LDH particle size, LDH particle number concentration and dye/gene loading by LDH on cellular delivery efficiency, using sLDH and L-LDH as our key NP comparators.

5.4.1 Effect of LDH-NP size on cellular delivery efficiency

To specifically examine the effect of LDH particle size on delivery efficiency, we fixed the particle number concentration of either sLDH or L-LDH particles. Since each L-LDH-FITC particle (90 nm) is about 5 times ($90^3/54^3$ = 4.6) larger than each sLDH-FITC particle (54 nm) from a volume perspective, we employed 4 μg/mL sLDH-5%FITC and 20 μg/mL L-LDH-1%FITC to ensure the presence of a similar particle number concentration alongside an identical load of FITC in each LDH particle. In such an uptake test, the FITC fluorescence intensity observed for each NP type when delivered to a population of cells directly reflects the impact of the particle size on uptake by HCT-116 cells.

Under these 'identical' conditions, HCT-116 cells were shown to internalise a similar amount of FITC irrespective of whether the vector being used was sLDH or L-LDH (Figure 5-9). The only subtle difference was that the cellular uptake of sLDH NPs was seen to be complete in the first 2 h, while L-LDH NPs showed a steady and continual uptake over up to 8 h. Thus, this work shows that the rate of cellular uptake in terms of the particle number was comparable for the 54 nm (sLDH) and 90 nm (L-LDH) NPs. It is reported that internalisation of NPs less than 200 nm involves clathrin-mediated pathway;[17, 18, 67, 68] thus sLDH-FITC (~54 nm) and L-LDH-FITC (~90 nm) used in this work entered HCT-116 cells through the same pathway. That would be the reason why sLDH-FITC and L-LDH-FITC resulted in similar uptake regardless of the particle size difference. This result is consistent with recent *in vitro* and *in silico* correlation studies where NPs ranging in size from 50-100 nm were found to be optimal for cellular delivery.[35] It is also in partial agreement with a cluster of earlier studies where *ca.* 50 nm NPs were more efficiently internalised by a range of cell types.[6, 47, 69]

Clearly, the cellular uptake rate of L-LDH from the particle 'mass' perspective is about 5 times that of sLDH as the volume of one L-LDH particle is nearly 5 times that of one sLDH particle. This translates to the fact that if sLDH-5%FTIC and L-LDH-5%FITC NPs are delivered at an equivalent particle number concentration in cellular uptake studies, the

mean FITC fluorescence intensity of HCT 116 cells treated by L-LDH-5%FITC would be expectedly 5 times that treated by sLDH-5%FTIC, which is really shown by the data in Figure 5-6. The mean fluorescence intensity of cells treated by 10.0-20.0 μg/mL of L-LDH-5%FITC was truly about 5 times that of cells treated by 2.5-5.0 μg/mL of sLDH-5%FITC, where the particle number concentration in the two cases was approximately the same.

5.4.2 Effect of the LDH particle number concentration on cellular delivery efficiency

As shown in Figure 5-6, the amount of FITC delivered by sLDH remained largely unchanged at mass doses ≥ 5.0 μg/mL, while it increased substantially at the lower mass dose range of 1.4 to 5.0 μg/mL. Similarly, the amount of FITC delivered by L-LDH increased steadily at a mass dose from 1.4 to 20.0 μg/mL while the increase was minimal from 10.0 to 20.0 μg/mL (Figure 5-6). It appears that cellular uptake of NPs is dose dependent below a critical mass concentration, while cellular uptake of NPs reaches a plateau at or beyond the critical mass concentration. In the current two cases, the critical mass concentration of sLDH and L-LDH is in the region of 5 and 20 μg/mL, respectively. Interestingly, the corresponding critical particle number concentration in these two cases is very similar, at approximately 1.0×10^{10} particle/mL, which is also supported by the data shown in Figure 5-12. The uptake curves are quite similar for sLDH and L-LDH NPs, with a similar critical particle number concentration. Clearly, cellular uptake in terms of the LDH particle number is almost linearly dependent on the particle number concentration below the critical number concentration (1.0×10^{10} particle/mL). Beyond this critical value, cellular uptake does not improve. Chithrani et al.[6] have also reported dose-dependent phenomena, and moreover, their critical NP number concentration was estimated to be 0.3×10^{10} number/mL for 50 nm Au NPs based on the data provided, which is in close agreement to our critical number concentration. Of course, the critical number concentration of NPs could also be dependent on the cell type and confluency.

As depicted in Figure 5-8B, the amount of FITC delivered by L-LDH was approximately twice that of sLDH after incubation for 1-8 h at the same mass concentration (10 μg/mL). From this we can infer that sLDH particle number taken up by HCT-116 cells was about 2.5 times that of L-LDH, although the number concentration of sLDH particles was 5 times that of L-LDH particles. This uptake rate of sLDH in terms of the particle number is less than that expected (5 times), which could be due to the fact that the mass concentration of

sLDH (10 μg/mL) is beyond the critical mass concentration value (5 μg/mL) while that of L-LDH is below. Therefore, the rate of cellular uptake of L-LDH is relatively slower in this instance.

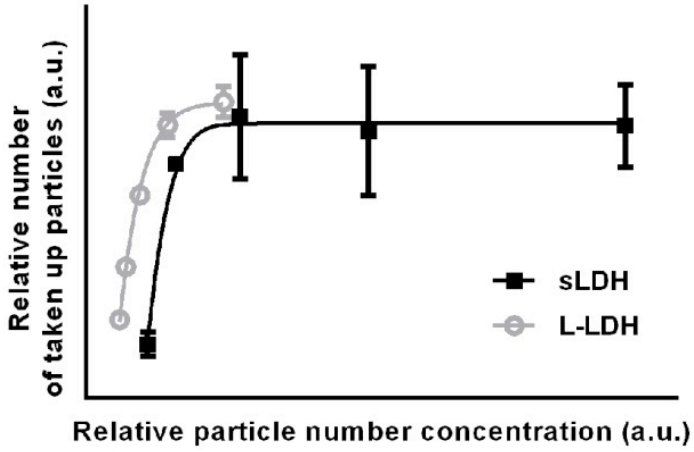

Figure 5-12 Replot of normalised particle number concentration and particle number taken up by cells based on the data in Figure 5-6, including sLDH and L-LDH.

5.4.3 Effect of surface/internal-bulk loading on cellular delivery efficiency

The cellular delivery efficiency can be also determined by the manner of loading on/into the respective NPs. For example, the amount of DNA-Cy3 delivered by sLDHs was 2-3 times that delivered by L-LDH (Figure 5-11B). This is in sharp contrast with the results in Figure 5-8B where the amount of FITC delivered by sLDH was 2 times less than that delivered by L-LDH, which reflects the effect of loading style. It is important to note that DNA was loaded onto LDH in a manner different from FITC, where FITC was intercalated between the interlayers (bulk way), but DNA predominantly adsorbed onto the surface of LDH NPs (surface way). Due to the differences in loading sites on the NP, FITC loading could be controlled through percentage of interlayer anion exchange and correlated to the LDH NP volume, while DNA loading amount was correlated to the LDH surface area.

At the equivalent mass concentration, sLDH with the *Z*-average size of 40 nm has a surface area 2.5 times that of L-LDH with the *Z*-average diameter size of 100 nm. From a loading perspective, this means that sLDH is able to carry 2.5 times the load of DNA as that of L-LDH, at the equivalent mass concentration. This may explain why sLDH bound almost all DNA at the LDH:DNA mass ratio of 2:1 (Figure 5-3A), while a mass ratio of 5:1

was necessary in the case of L-LDH (Figure 5-3B). This may further reflect that the contribution of unassociated DNA at the mass ratio of 5:1 was much lower from sLDH (~10%) than from L-LDH (~50%) in the culture media (Figure 5-4A and Figure 5-4B). Cebrián et al.[70] also found 6 nm PEI-coated Au NPs can load higher quantities of DNA than equivalent mass of 70 nm Au-PEI NPs because of larger external surface area per unit mass. The incomplete complexation of DNA-Cy3 observed with L-LDH at 5:1 in culture media would be expected to reduce the cellular delivery of DNA-Cy3 to 50% of that using sLDH at the same particle number concentration.

Aside from the effect of incomplete complexation, the observed difference in the delivery efficiency of DNA-Cy3 may largely be attributed to LDH particle number concentration changes. Here, as the L-LDH particle number concentration (1.4 and 11 μg/mL) was well below the critical value, cellular uptake of DNA-Cy3 would increase in proportion to the particle number concentration. In comparison, sLDH NP number concentration at 1.4 μg/mL is below the critical value while 11 μg/mL is well over the critical value, so cellular uptake would increase less than in a proportional manner. This understanding, together with the loading yield, goes some way in explaining why the amount of DNA-Cy3 delivered by sLDH was 10-15 times higher than that of L-LDH at the mass ratio of 5:1, decreasing to about 2-3 times higher at the mass ratio of 40:1 (Figure 5-10B and Figure 5-11B).

Figure 5-13 illustrates the relatively particle sizes and particle concentrations for small and large LDH carrying FITC and DNA-Cy3. A and B exhibit same mass concentrations of small and large LDH carrying same percentages of FITC. C and D show same particle concentrations of small and large LDH carrying same amount of FITC in each nanoparticle. E and F are small and large LDH carrying DNA-Cy3 at the same mass ratios and mass concentrations.

5.5 Conclusions

The cellular uptake of LDH NPs is highly dependent on its particle number concentration regardless of particle size in the range of 40 to 100 nm. Under the critical particle number concentration, cellular uptake was in linear proportion to the particle number concentration, while above this critical value, the cellular uptake was not further improved. This research further found that the size of sheet-like LDH particles in the range of 40-100 nm could not significantly affect the cellular uptake in terms of the particle number, and that the surface loading capacity of LDH NPs may significantly affect the delivery efficiency.

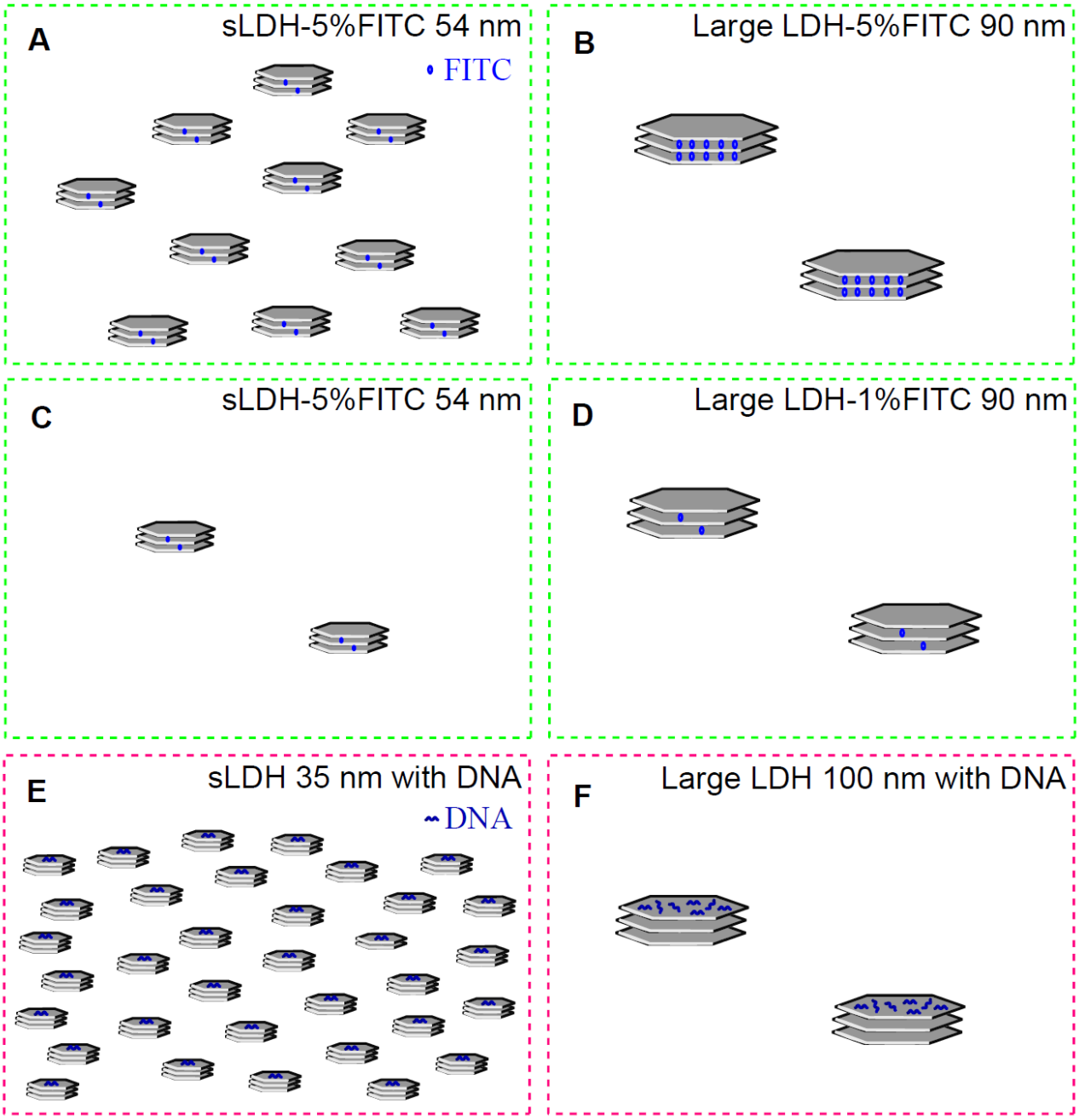

Figure 5-13 Schematic illustration of small and large LDH NPs carrying FITC and DNA

References

1. Gref, R. et al. Biodegradable long-circulating polymeric nanospheres. *Science* **263**, 1600-1603 (1994).

2. Boussif, O. et al. A versatile vector for gene and oligonucleotide transfer into cells in culture and *in vivo*: Polyethylenimine. *Proceedings of the National Academy of Sciences of the United States of America* **92**, 7297-7301 (1995).

3. Liu, H., Wang, Y., Wang, M., Xiao, J. & Cheng, Y. Fluorinated poly(propylenimine) dendrimers as gene vectors. *Biomaterials* **35** (2014).

4. Hughes, J., Yadava, P. & Mesaros, R. in Liposomes : Methods and Protocols, Volume 1: Pharmaceutical Nanocarriers (ed. Weissig, V.) 445-459 (Humana Press, 2009).

5. Rosi, N.L. et al. Oligonucleotide-modified gold nanoparticles for intracellular gene regulation. *Science* **312**, 1027-1030 (2006).

6. Chithrani, B.D., Ghazani, A.A. & Chan, W.C.W. Determining the size and shape dependence of Ggold nanoparticle uptake into mammalian cells. *Nano Letters* **6**, 662-668 (2006).

7. Gupta, A.K. & Gupta, M. Synthesis and surface engineering of iron oxide nanoparticles for biomedical applications. *Biomaterials* **26**, 3995-4021 (2005).

8. Huang, X., Teng, X., Chen, D., Tang, F. & He, J. The effect of the shape of mesoporous silica nanoparticles on cellular uptake and cell function. *Biomaterials* **31**, 438-448 (2010).

9. Gao, Y. et al. Controlled intracellular release of doxorubicin in multidrug-resistant cancer cells by tuning the shell-pore sizes of mesoporous silica nanoparticles. *Acs Nano* **5**, 9788-9798 (2011).

10. Kam, N.W.S., Jessop, T.C., Wender, P.A. & Dai, H.J. Nanotube molecular transporters: Internalization of carbon nanotube-protein conjugates into mammalian cells. *Journal of the American Chemical Society* **126**, 6850-6851 (2004).

11. Choy, J.-H., Kwak, S.-Y., Jeong, Y.-J. & Park, J.-S. Inorganic layered double hydroxides as nonviral vectors. *Angewandte Chemie International Edition* **39**, 4041-4045 (2000).

12. Li, J., Chen, Y.-C., Tseng, Y.-C., Mozumdar, S. & Huang, L. Biodegradable calcium phosphate nanoparticle with lipid coating for systemic siRNA delivery. *Journal of Controlled Release* **142**, 416-421 (2010).

13. Rizzi, S.C. et al. Biodegradable polymer/hydroxyapatite composites: Surface analysis and initial attachment of human osteoblasts. *Journal of Biomedical Materials Research* **55**, 475-486 (2001).

14. Hartono, S.B. et al. Poly-L-lysine Functionalized Large Pore Cubic Mesostructured Silica Nanoparticles as Biocompatible Carriers for Gene Delivery. *Acs Nano* **6**, 2104-2117 (2012).

15. Oh, E. et al. Cellular uptake and fate of PEGylated gold nanoparticles is dependent on both cell-penetration peptides and particle size. *Acs Nano* **5**, 6434-6448 (2011).

16. Huang, J. et al. Effects of nanoparticle size on cellular uptake and liver MRI with polyvinylpyrrolidone-coated iron oxide nanoparticles. *Acs Nano* **4**, 7151-7160 (2010).

17. Canton, I. & Battaglia, G. Endocytosis at the nanoscale. *Chemical Society Reviews* **41**, 2718-2739 (2012).

18. Rejman, J., Oberle, V., Zuhorn, I.S. & Hoekstra, D. Size-dependent internalization of particles via the pathways of clathrin- and caveolae-mediated endocytosis. *The Biochemical Journal* **377**, 159-169 (2004).

19. Zhang, S., Li, J., Lykotrafitis, G., Bao, G. & Suresh, S. Size-dependent endocytosis of nanoparticles. *Advanced Materials* **21**, 419-424 (2009).

20. Osaki, F., Kanamori, T., Sando, S., Sera, T. & Aoyama, Y. A quantum dot conjugated sugar ball and its cellular uptake on the size effects of endocytosis in the subviral region. *Journal of the American Chemical Society* **126**, 6520-6521 (2004).

21. Reichert, S. et al. Size-dependant cellular uptake of dendritic polyglycerol. *Small* **7**, 820-829 (2011).

22. Hu, Y., Xie, J., Tong, Y.W. & Wang, C.-H. Effect of PEG conformation and particle size on the cellular uptake efficiency of nanoparticles with the HepG2 cells. *Journal of Controlled Release* **118**, 7-17 (2007).

23. Yuan, Y., Liu, C., Qian, J., Wang, J. & Zhang, Y. Size-mediated cytotoxicity and apoptosis of hydroxyapatite nanoparticles in human hepatoma HepG2 cells. *Biomaterials* **31**, 730-740 (2010).

24. Xiong, S. et al. Size influences the cytotoxicity of poly (lactic-co-glycolic acid) (PLGA) and titanium dioxide (TiO_2) nanoparticles. *Archives of Toxicology* **87**, 1075-1086 (2013).

25. Gliga, A.R., Skoglund, S., Wallinder, I.O., Fadeel, B. & Karlsson, H.L. Size-dependent cytotoxicity of silver nanoparticles in human lung cells: the role of cellular uptake, agglomeration and Ag release. *Particle and Fibre Toxicology* **11**, 11-11 (2014).

26. Choi, S.-J., Oh, J.-M. & Choy, J.-H. Safety sspect of inorganic layered nanoparticles: Size-dependency *in vitro* and *in vivo*. *Journal of Nanoscience and Nanotechnology* **8**, 5297-5301 (2008).

27. Santos, H.A. et al. In vitro cytotoxicity of porous silicon microparticles: Effect of the particle concentration, surface chemistry and size. *Acta Biomaterialia* **6**, 2721-2731 (2010).

28. Kim, S. et al. Cytotoxicity of, and innate immune response to, size-controlled polypyrrole nanoparticles in mammalian cells. *Biomaterials* **32**, 2342-2350 (2011).

29. Oh, W.-K. et al. Cellular uptake, cytotoxicity, and innate immune response of silica - titania hollow nanoparticles based on size and surface functionality. *Acs Nano* **4**, 5301-5313 (2010).

30. Niikura, K. et al. Gold nanoparticles as a vaccine platform: Influence of size and shape on immunological responses *in vitro* and *in vivo*. *Acs Nano* **7**, 3926-3938 (2013).

31. Wang, X., Li, X., Ito, A., Sogo, Y. & Ohno, T. Particle-size-dependent toxicity and immunogenic activity of mesoporous silica-based adjuvants for tumor immunotherapy. *Acta Biomaterialia* **9**, 7480-7489 (2013).

32. Ohta, S., Shen, P., Inasawa, S. & Yamaguchi, Y. Size- and surface chemistry-dependent intracellular localization of luminescent silicon quantum dot aggregates. *Journal of Materials Chemistry* **22**, 10631-10638 (2012).

33. Schubbe, S. et al. Size-dependent localization and quantitative evaluation of the intracellular migration of silica nanoparticles in Caco-2 cells. *Chemistry of Materials* **24**, 914-923 (2012).

34. Bhattacharjee, S. et al. Cytotoxicity and cellular uptake of tri-block copolymer nanoparticles with different size and surface characteristics. *Particle and Fibre Toxicology* **9** (2012).

35. Xu, A. et al. A physical model for the size-dependent cellular uptake of nanoparticles modified with cationic surfactants. *International Journal of Nanomedicine* **7**, 3547-3554 (2012).

36. Win, K.Y. & Feng, S.S. Effects of particle size and surface coating on cellular uptake of polymeric nanoparticles for oral delivery of anticancer drugs. *Biomaterials* **26**, 2713-2722 (2005).

37. Kulkarni, S.A. & Feng, S.-S. Effects of particle size and surface Mmodification on cellular uptake and biodistribution of polymeric Nnanoparticles for drug delivery. *Pharmaceutical Research* **30**, 2512-2522 (2013).

38. Massignani, M. et al. Controlling cellular uptake by surface chemistry, size, and surface topology at the nanoscale. *Small* **5**, 2424-2432 (2009).

39. Ross, P.C. & Hui, S.W. Lipoplex size is a major determinant of in vitro lipofection efficiency. *Gene Therapy* **6**, 651-659 (1999).

40. Jiang, W., Kim, B.Y.S., Rutka, J.T. & Chan, W.C.W. Nanoparticle-mediated cellular response is size-dependent. *Nature Nanotechnology* **3**, 145-150 (2008).

41. Jin, H., Heller, D.A., Sharma, R. & Strano, M.S. Size-dependent cellular uptake and expulsion of single-walled carbon nanotubes: Single particle tracking and a generic uptake model for nanoparticles. *Acs Nano* **3**, 149-158 (2009).

42. Lu, F., Wu, S.-H., Hung, Y. & Mou, C.-Y. Size effect on cell uptake in well-suspended, Uuniform mesoporous silica nanoparticles. *Small* **5**, 1408-1413 (2009).

43. Shan, Y. et al. Size-dependent endocytosis of single gold nanoparticles. *Chemical Communications* **47**, 8091-8093 (2011).

44. Cho, E.C., Au, L., Zhang, Q. & Xia, Y. The effects of size, shape, and surface functional group of gold nanostructures on their adsorption and internalization by cells. *Small* **6**, 517-522 (2010).

45. Tang, L., Fan, T.M., Borst, L.B. & Cheng, J. Synthesis and biological response of size-specific, monodisperse drug-silica nanoconjugates. *Acs Nano* **6**, 3954-3966 (2012).

46. Matuszewski, L. et al. Cell tagging with clinically approved iron oxides: Feasibility and effect of lipofection, particle size, and surface coating on labeling efficiency. *Radiology* **235**, 155-161 (2005).

47. Choi, S.-J. & Choy, J.-H. Layered double hydroxide nanoparticles as target-specific delivery carriers: uptake mechanism and toxicity. *Nanomedicine* **6**, 803-814 (2011).

48. Chung, H.-E., Park, D.-H., Choy, J.-H. & Choi, S.-J. Intracellular trafficking pathway of layered double hydroxide nanoparticles in human cells: Size-dependent cellular delivery. *Applied Clay Science* **65-66**, 24-30 (2012).

49. Chen, M., Cooper, H.M., Zhou, J.Z., Bartlett, P.F. & Xu, Z.P. Reduction in the size of layered double hydroxide nanoparticles enhances the efficiency of siRNA delivery. *Journal of Colloid and Interface Science* **390**, 275-281 (2013).

50. Dong, H. et al. Engineering small MgAl-layered double hydroxide nanoparticles for enhanced gene delivery. *Applied Clay Science* (2014).

51. Li, S. et al. Cellular uptake and gene delivery using layered double hydroxide nanoparticles. *Journal of Materials Chemistry B* **1**, 61-68 (2013).

52. Wang, S.-H., Lee, C.-W., Chiou, A. & Wei, P.-K. Size-dependent endocytosis of gold nanoparticles studied by three-dimensional mapping of plasmonic scattering images. *Journal of Nanobiotechnology* **8**, 33-33 (2010).

53. He, C., Hu, Y., Yin, L., Tang, C. & Yin, C. Effects of particle size and surface charge on cellular uptake and biodistribution of polymeric nanoparticles. *Biomaterials* **31**, 3657-3666 (2010).

54. Xu, Z.P., Stevenson, G., Lu, C.-Q. & Lu, G.Q. Dispersion and size control of layered double hydroxide nanoparticles in aqueous solutions. *Journal of Physical Chemistry B* **110**, 16923-16929 (2006).

55. Wong, Y. et al. Efficient delivery of siRNA to cortical neurons using layered double hydroxide nanoparticles. *Biomaterials* **31**, 8770-8779 (2010).

56. Li, A. et al. Signalling pathways involved in the activation of dendritic cells by layered double hydroxide nanoparticles. *Biomaterials* **31**, 748-756 (2010).

57. Andersson, P.O. et al. Polymorph- and size-dependent uptake and toxicity of TiO_2 nanoparticles in living lung epithelial cells. *Small* **7**, 514-523 (2011).

58. Shah, N., Steptoe, R.J. & Parekh, H.S. Low-generation asymmetric dendrimers exhibit minimal toxicity and effectively complex DNA. *Journal of Peptide Science* **17**, 470-478 (2011).

59. Xu, Z.P. et al. Subcellular compartment targeting of layered double hydroxide nanoparticles. *Journal of Controlled Release* **130**, 86-94 (2008).

60. Wong, Y.Y. et al. Efficiency of layered double hydroxide nanoparticle-mediated delivery of siRNA is determined by nucleotide sequence. *Journal of Colloid and Interface Science* **369**, 453-459 (2012).

61. KS, M., H, R., A, H. & K, S. Pathway of vesicular stomatitis virus entry leading to infection. *Journal of Molecular Biology* **156**, 609-631 (1982).

62. Godbey, W.T., Wu, K.K. & Mikos, A.G. Tracking the intracellular path of poly(ethylenimine)/DNA complexes for gene delivery. *Proceedings of the National Academy of Sciences of the United States of America* **96**, 5177-5181 (1999).

63. Zuhorn, I.S., Kalicharan, R. & Hoekstra, D. Lipoplex-mediated transfection of mammalian cells occurs through the cholesterol-dependent clathrin-mediated pathway of endocytosis. *Journal of Biological Chemistry* **277**, 18021-18028 (2002).

64. Elbakry, A. et al. Layer-by-layer coated gold nanoparticles: Size-dependent delivery of DNA into cells. *Small* **8**, 3847-3856 (2012).

65. Ogris, M., Steinlein, P., Carotta, S., Brunner, S. & Wagner, E. DNA/polyethylenimine transfection particles: influence of ligands, polymer size, and PEGylation on internalization and gene expression. *AAPS pharmSci* **3**, E21-E21 (2001).

66. Prabha, S., Zhou, W.Z., Panyam, J. & Labhasetwar, V. Size-dependency of nanoparticle-mediated gene transfection: studies with fractionated nanoparticles. *International Journal of Pharmaceutics* **244**, 105-115 (2002).

67. Mayor, S. & Pagano, R.E. Pathways of clathrin-independent endocytosis. *Nature Reviews Molecular Cell Biology* **8**, 603-612 (2007).

68. Vollrath, A. et al. A toolbox of differently sized and labeled PMMA nanoparticles for cellular uptake investigations. *Soft Matter* **9**, 99-108 (2013).

69. Maurice, V., Georgelin, T., Siaugue, J.-M. & Cabuil, V. Synthesis and characterization of functionalized core-shell γFe_2O_3-SiO_2 nanoparticles. *Journal of Magnetism and Magnetic Materials* **321**, 1408-1413 (2009).

70. Cebrián, V. et al. Size-dependent transfection efficiency of PEI-coated gold nanoparticles. *Acta Biomaterialia* **7**, 3645-3655 (2011).

This page was left blank intentionally.

Chapter 6 Enhanced Cellular Delivery and Biocompatibility of a small Layered Double Hydroxide-liposome Composite System

Declaration for Chapter 6

- Manuscript for this chapter is published on *Pharmaceutics* **2014**, *6*(4), 584-598; doi:10.3390/pharmaceutics6040584

Abstract

The various classes of gene delivery vector possess distinct advantages and disadvantages, each of which impacts on cargo loading, delivery, and ultimately its function. With this in mind herein we report on a small layered double hydroxide (sLDH)-liposome composite system, drawing upon the salient features of LDH and liposome classes of vectors, while avoiding their inherent shortfalls when used independently. sLDH-liposome composites were prepared by the hydration of freeze-dried matrix method. These composite systems, with a *Z*-average size of ≈ 200 nm exhibited low cytotoxicity and demonstrated good suspension stability both in water and cell culture medium after rehydration. Our studies demonstrate that short dsDNAs/ssDNAs were completely bound and protected in the composite system at an sLDH:DNA mass ratio of 20:1, regardless of the approach to loading DNA . This composite system delivered DNA to HCT-116 cells with ≈ 3-fold greater efficiency, when compared to sLDH alone. Our findings point towards the sLDH-liposome composite system being an effective and biocompatible gene delivery system.

6.1 Introduction

Gene therapy aims to use genetic materials, namely DNA or RNA as a therapeutic; this approach is expected to lead to effective treatment of a wide range of disorders of genetic origin, most of which are not amenable to curative therapy using conventional 'small molecule' agents.[1, 2] A growing body of evidence points towards the promise of gene therapy as an effective means of treating cancers, as well as genetic and neurodegenerative diseases.[3, 4] That said success of gene therapy trials relies heavily on access to safe and efficient vectors that are able to overcome the various extra- and intracellular barriers faced by genetic materials.[5-8]

Layered double hydroxides (LDHs) otherwise known as anionic clays are either sourced naturally in the form of minerals, or can be synthesised with precise composition and particle size homogeneity.[9-12] Here, magnesium-aluminium-based LDHs (MgAl-LDH) have proved to be excellent gene delivery vehicles, given their intrinsically low cytotoxicity, good biocompatibility, well-defined particle size, and cationic surface properties.[13-20] The positively charged surface of LDH nanoparticles (NPs) allows ready adsorption of negatively charged (genetic) materials, driven by electrostatic attraction, a phenomenon that leads to cargo being protected from degradation by ubiquitous enzymes, while the net cationic charge of LDH-gene complexes facilitates cellular internalisation. Once internalised, the gradual dissolution of LDH NPs in the acidifying conditions of the endosome results in sustained/controlled release of payload, which in turn raises the osmotic pressure in the endosome, and leads to an influx of water, causing swelling and finally rupture of endosomal vesicles.[21, 22] Once the LDH-gene complexes enter the cytosol the LDH system is rapidly disassembled, with the Mg and Al ions eliminated through an abundance of membrane-based ion channels. A major drawback to the use of LDH is the mass aggregation of LDH NPs resulting from interaction with serum proteins abundant in the systemic circulation, a feature which has prevented the wider application of LDH as an *in vivo* compatible gene vector.

Separately, liposomes have long been trialled and accepted as effective drug/gene vectors, given their similarities with the cell membrane, both in structure and composition.[23] Moreover, the surface of PEGylated liposomes has been readily modified with specific ligands for targeted delivery.[24-27] However, a rate-limiting step with many non-viral vectors, including PEGylated liposomes, is their inability to escape endosomes in a timely manner. Hence, researchers have dedicated their efforts to preparing PEGylated liposomes

encompassing various fusogenic lipids (e.g. DOPE), and pH-sensitive polymers, such as polyethylenimine (PEI) to improve endosomal escape and payload release properties.[28, 29]

More recently, lipid-coated hybrid nanoparticles (NPs), such as polymeric NPs, mesoporous silica NPs, and calcium phosphate NPs have found a place in combination therapy, where attempts are being made to enhance therapeutic efficacy while reducing drug resistance and side effects. Such hybrid systems aim to merge the beneficial features from both vectors into one nano-carrier, while mitigating their individual drawbacks.[26, 30-34] These findings motivated us to design a new composite system, comprising of LDH and liposomes, one that would synergistically enhance the colloidal stability and delivery efficiency with reduced side effects. We demonstrated that our novel LDH-liposome composite system possesses good colloidal stability and high rate of gene transfection with consistent dimensions in the low nanometer size range.

6.2 Experimental

6.2.1 Preparation of LDH NPs and LDH-liposome composites

Small LDH (sLDH) and large LDH (L-LDH) NPs were prepared as reported earlier.[35, 36] The LDH-liposome composite system was prepared by the hydration of freeze-dried matrix (HFDM) method, with slight modifications. The minor deviation from the published[37-40] method involved using 30% *v/v* tertiary butyl alcohol (TBA), as opposed to 50% *v/v* TBA.[41] Typically, 70 µL of 400 µg/mL sLDH suspension is mixed with 70 µL of 95 mg/mL sucrose solution, followed by further mixing with 60 µL of 450 µg/mL EPC (chicken egg-derived L-α-lysophosphatidylcholine). The resulting clear TBA/water/EPC three phase mixture was then snap-frozen in dry ice, followed by freeze-drying for 24 h (Christ Alpha 2-4 LD). Finally, the freeze-dried matrix was hydrated with 50-200 µL water and stood at room temperature for 10 min.

6.2.2 Incorporation of DNA into LDH-liposome composite

The complexation of DNA with our LDH-liposome composite was trialed using three different approaches, denoted as ‘LDH-DNA-liposome’, ‘LDH-liposome-DNA’, and ‘LDH-liposome+DNA’. As depicted in Scheme 1 and elaborated on here, the ‘LDH-DNA-liposome’ formulation involved first complexing DNA with LDH in a sucrose solution, followed by mixing in the EPC in TBA solution, then freeze-drying and hydrating the lyophilisate. Similarly, for the ‘LDH-liposome-DNA’ formulation DNA was added to a LDH

suspension containing EPC in TBA, with similar post-treatment. Finally, for 'LDH-liposome+DNA' we first prepared the LDH-liposome composite with DNA added directly to the nanosuspension.

Scheme 1. Sequential schematic outlining the preparation of various composite LDH-liposomal formulations (coloured box widths indicative of the relative volumes employed).

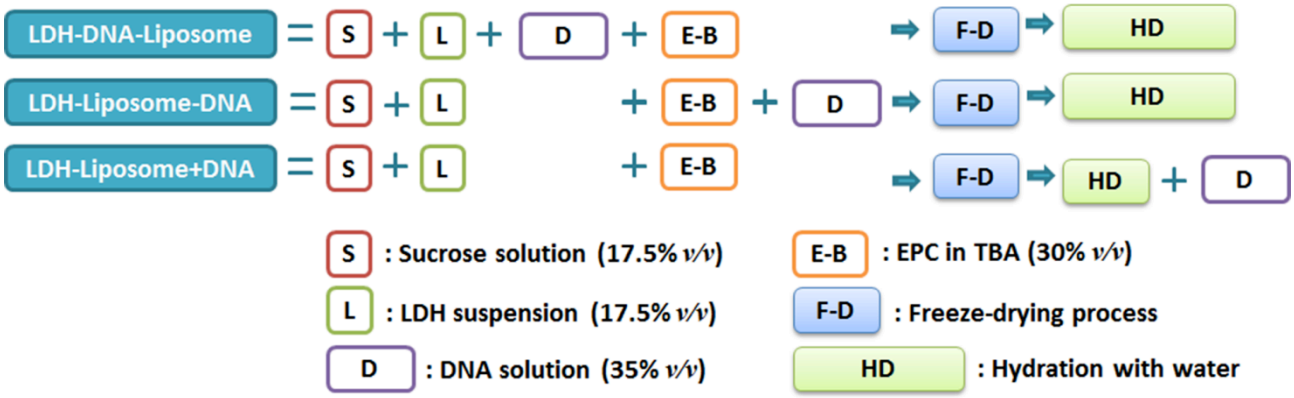

6.2.3 Suspension stability test

All particle size distributions were determined by dynamic light scattering (DLS, Zetasizer Nano ZS, Malvern Instruments) where LDH, LDH-DNA, LDH-liposome, and LDH-liposome with DNA suspensions were diluted with water at a volume ratio of 1:1 before measurement. For their size distribution in cell culture media, they were diluted with complete cell culture media (10% *v/v* of fetal bovine serum mixed with Dulbecco's Modified Eagle Medium (DMEM, with L-glutamine and 4.5 g/L of glucose) at volume ratio of 1:1.

6.2.4 Agarose gel electrophoresis

The dsDNA loaded with LDH NPs and LDH-liposome composites were assessed by agarose gel electrophoresis. A 2.5% agarose gel with Gel-Red stain was made and then dsDNA bound with LDH NPs/LDH-liposome composites were loaded in the wells. For each well, 260 ng dsDNA was used. Gel was imaged by a Bio-Rad imaging system after running at 90 V for 45 min in TBE (Tris/Borate/EDTA) buffer.

6.2.5 Cell viability

Human colon cancer HCT-116 cells were seeded in 96-well plates at a density of 2000 cells per well in 200 µL of cell culture media. After 24 h of incubation, cell culture media was replaced by 200 µL of fresh media with desired concentration of LDH or LDH-liposome NPs. After 48, and 72 h further incubation, 20 µL of MTT reagent (5 mg/mL in PBS buffer) was added, followed by 2-4 h of incubation (dependent on cell density). Next, the cell culture media was discarded, and 50 µL of DMSO (dimethyl sulfoxide) was added to each well, followed by 10 min of incubation. Absorbance was read using a plate reader at 540 nm after 1 min of orbital shaking. A negative control group (only cell culture media, without cells) was used as background. A group without adding NPs was used as control. The cell viability was normalised to control. The experiments were conducted for at least two batches in triplicate. Data are presented as mean ± SEM (standard error of the mean). Two-way ANOVA was used to assess the statistical significance (commercial transfection reagent Oligofectamine™ as control group).

6.2.6 Cellular uptake

HCT-116 cells were seeded in 6-well plates at a density of 1×10^5 cells per well in 2 mL complete cell culture media. After 24 h of incubation, cell culture media was replaced with 1 mL of fresh media containing desired concentration of LDH-DNA-Cy3 NPs (single stranded DNA, 21 base, labeled with Cy3) or LDH-liposomes with DNA-Cy3 NPs (20 nM DNA). After 4 h of further incubation, the culture media was removed; cells were washed twice with PBS buffer and then detached from the plates by trypsin-EDTA. The cells were washed twice with PBS buffer and then fixed in a certain volume of 2% PFA (paraformaldehyde) before measurement by flow cytometry (BD Accuri™ C6 Flow Cytometer System, band pass filter 585/40 was used, 10,000 cells were counted). All treatments were performed for three different batches in duplicate. Data are presented as the mean ± SEM. Two-way ANOVA was used to assess the statistical significance. ****$p<0.0001$.

6.3 Results and discussion

6.3.1 sLDH-liposome composite formation

As shown in Figure 6-1A, sLDH possesses a narrow particle size distribution in the range of 10 to 100 nm with a *Z*-average size of ~40 nm. L-LDH NPs have a particle size in the range of 20 to 200 nm with Z-average size of ~100 nm (data not shown). After mixing with sucrose solution, the LDH suspension particle size increased marginally due to the viscosity of the sucrose solution (Figure 6-1A and Figure 6-2A). While in a homogeneous TBA/water/EPC three phase mixture, the *Z*-average particle size increased considerably to ~200 nm, indicative of the formation of lipidic micelles (Figure 6-1A and Figure 6-2B).

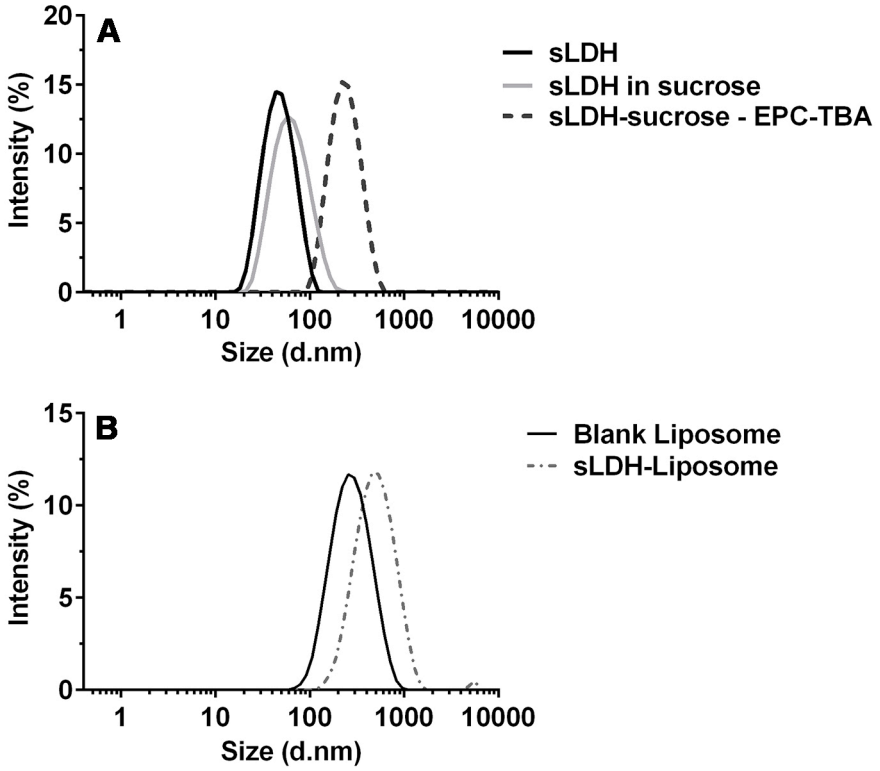

Figure 6-1 Particle size distribution of sLDH in various mixtures (A); Blank liposome and sLDH-liposome prepared by the hydration of freeze-dried matrix (HFDM) method (B).

Upon cooling TBA present within the core of micelles freezes first, given its relatively high freezing point (25.5 °C), this in turn freezes the lipid molecules surrounding the TBA core. The water phase freezes next, albeit more gradually due to the presence of sucrose and its high concentration, which further assists with more uniform distribution of LDH-payload in the water phase of the mixture (Figure 6-2C).[40]

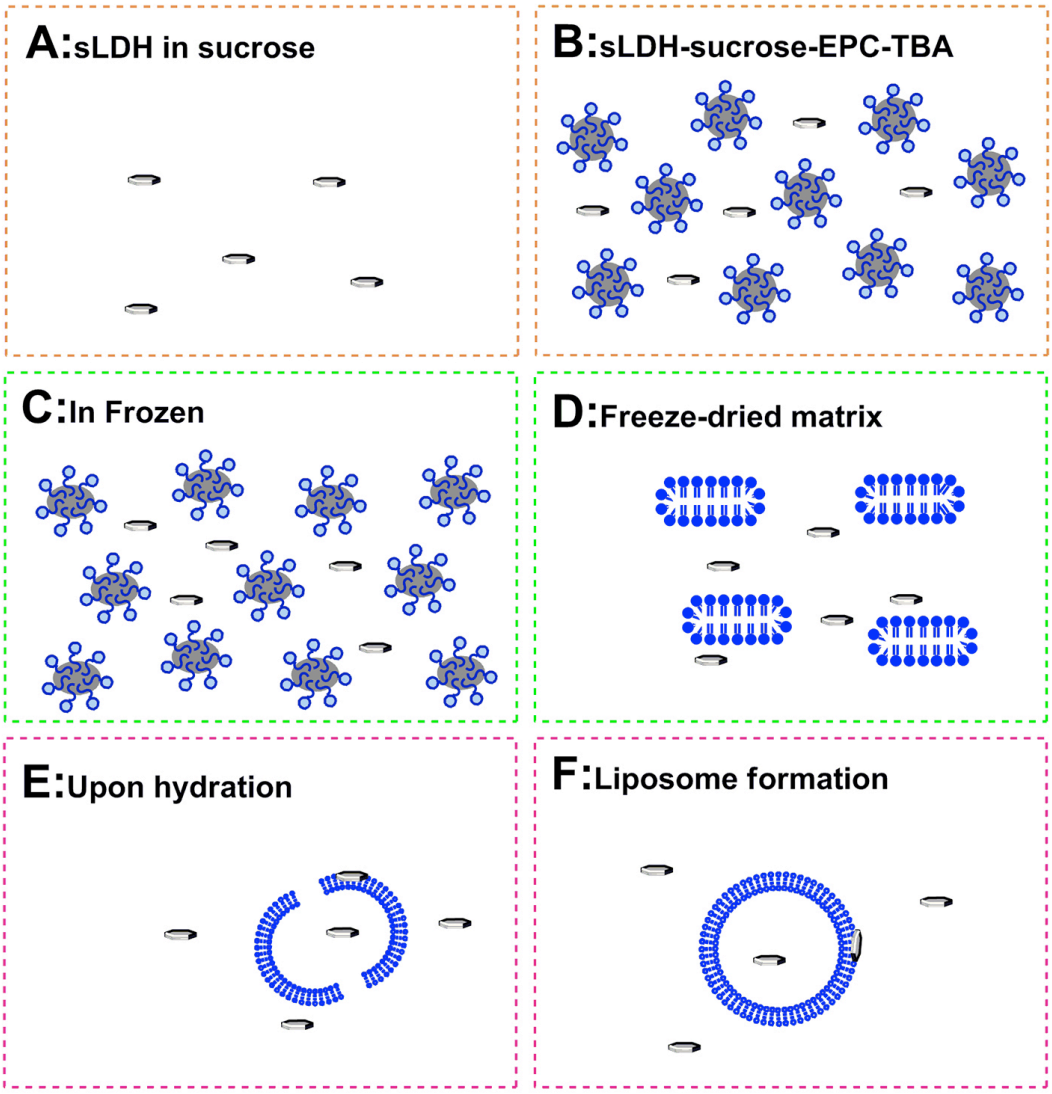

Figure 6-2 Schematic diagram of proposed sLDH-liposome composite formation by the HFDM method (for clarity, sucrose is not shown).

Water and TBA are removed completely during the next freeze drying step. During this process the lipid molecules are expected to re-arrange themselves, forming fragments of lipid bilayers, while sucrose serves to further stabilise these transient structures (Figure 6-2D). Upon hydration, the lipid bilayer fragments spontaneously assemble and seal, forming liposomes (Figure 6-2E and F). Due to the relatively small size of sLDH NPs (~40 nm) compared to the forming liposomes, a proportion of the NPs are encapsulated in the vesicles during lipid-fragment self-assembly into liposomes, although one can indeed expect some sLDH NPs to escape encapsulation (Figure 6-2F). In contrast, when considering this process from the perspective of L-LDH NPs, and their capture into forming

liposomes (Figure 6-2F), one would expect significant challenges, stemming from the considerably larger (~100 nm) size of L-LDH (*c.f.* sLDH), and so they are deemed to be less amenable to composite particle formation.

The process leading to formation of sLDH-liposome composite NPs prepared by the HFDM method is illustrated in Figure 6-2, with the particle size distribution of blank liposome and sLDH-liposome shown in Figure 6-1B. When comparing particle size, the sLDH-liposome composite with a *Z*-average size of ~240 nm was found to be greater than blank liposome (~200 nm); this difference may be attributed to the adsorption of sLDH NPs onto the surface of liposomal vesicles (as shown in Figure 6-2F), and this could well prove advantageous from an endosomal escape perspective (discussed later). Another reason for the particle size difference could be due to the addition of sLDH which affects the formation of liposome structure or the liposome size by encapsulation of sLDH NPs.

6.3.2 Composite stability

Figure 6-3A shows the particle sizes of sLDH and sLDH-liposome formulations loaded with dsDNA in water and in cell culture media at a dsDNA concentration of 10 μg/mL. sLDH-dsDNA has a larger particle size in cell culture media (~90 nm) than in water (~64 nm), which can be attributed to the adsorption of serum proteins onto the surface of sLDH NPs. In contrast, the sLDH-liposome suspension and sLDH-liposome loaded with dsDNA possessed an average particle size between 200-240 nm, which is consistent with the size of cationic liposomes loaded with siRNA reported by Wu et al. [37] and this particle size range is also appropriate for subsequent cellular uptake. Moreover, this observation illustrates that loading dsDNA into the sLDH-liposome composite system does not significantly affect composite size.

In contrast to sLDH, the average particle size of L-LDH-dsDNA composite is smaller in cell culture media than in water (Figure 6-3B) due to the adsorption of proteins onto LDH, which in turn suppresses aggregation between positively charged LDH NPs and negatively charged dsDNA. Similar particle sizes (~200 nm) were observed for L-LDH-liposome formulations loaded with dsDNA (at 10 μg/mL), which is suitable for cellular internalisation. Given that L-LDH NPs do not associate with or are too large for encapsulation within liposomes, and at the equivalent mass concentrations, L-LDH has a much lower particle number concentration than sLDH and liposome vesicles, so the L-LDH-liposome particle

size would be expected to be smaller than that of the sLDH-liposome composite, which is largely attributed to the blank liposome.

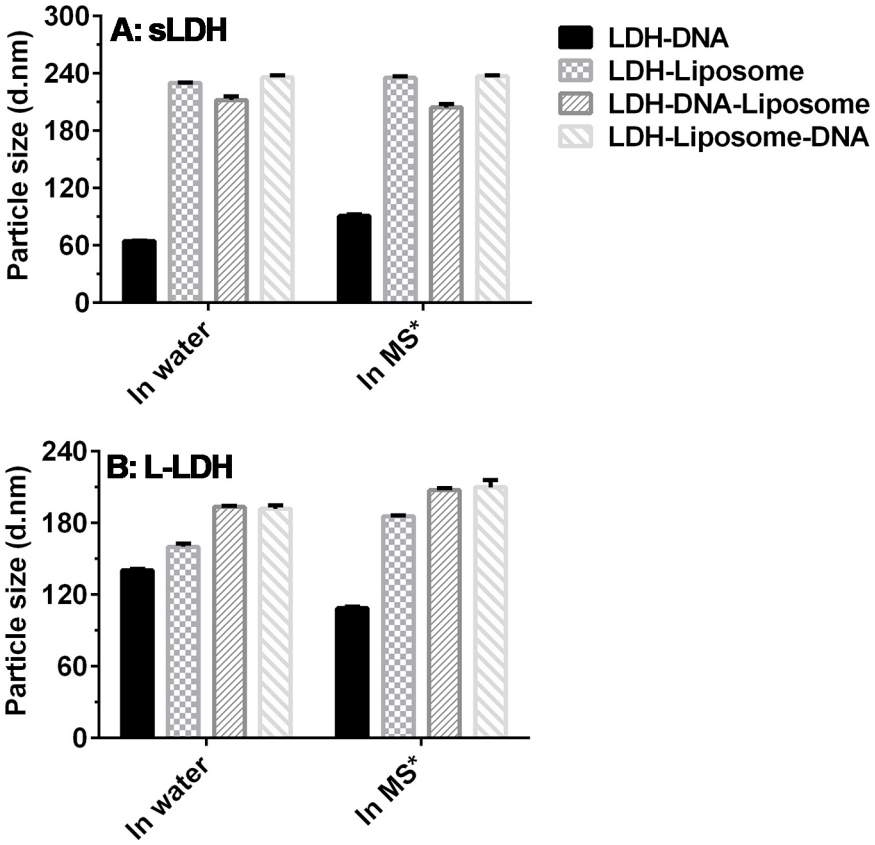

Figure 6-3 The *Z*-average particle sizes of LDH NPs and LDH-liposome formulations loaded with dsDNA (dsDNA = 10 μg/mL, the mass ratio LDH:dsDNA = 20:1, EPC:dsDNA = 20:1, *MS = medium + serum i.e. complete cell culture medium).

6.3.3 Cytotoxicity of LDH and LDH-liposome NPs

LDH and LDH-liposome NPs show negligible cytotoxicity at 72 h even when employing artificially larger concentrations (i.e. 100-200 μg/mL, >10 times the practical concentration), as shown in Figure 6-4, with > 90% cell viability at 48 h, and > 70% cell viability at 72 h at 200 μg/mL of LDH in the systems. In contrast, transfection reagent Oligofectamine™ exhibits significantly higher cytotoxicity at the comparable dose (~45% cell viability at 48 h and ~30 % cell viability at 72 h, $p<0.0001$, and where '1' of Oligofectamine™ equals the minimum recommended dose). Consistent with previous reports the cytotoxicity of LDH [17, 35] and liposomes composed of neutral lipids [42, 43] show moderate levels of cytotoxicity.

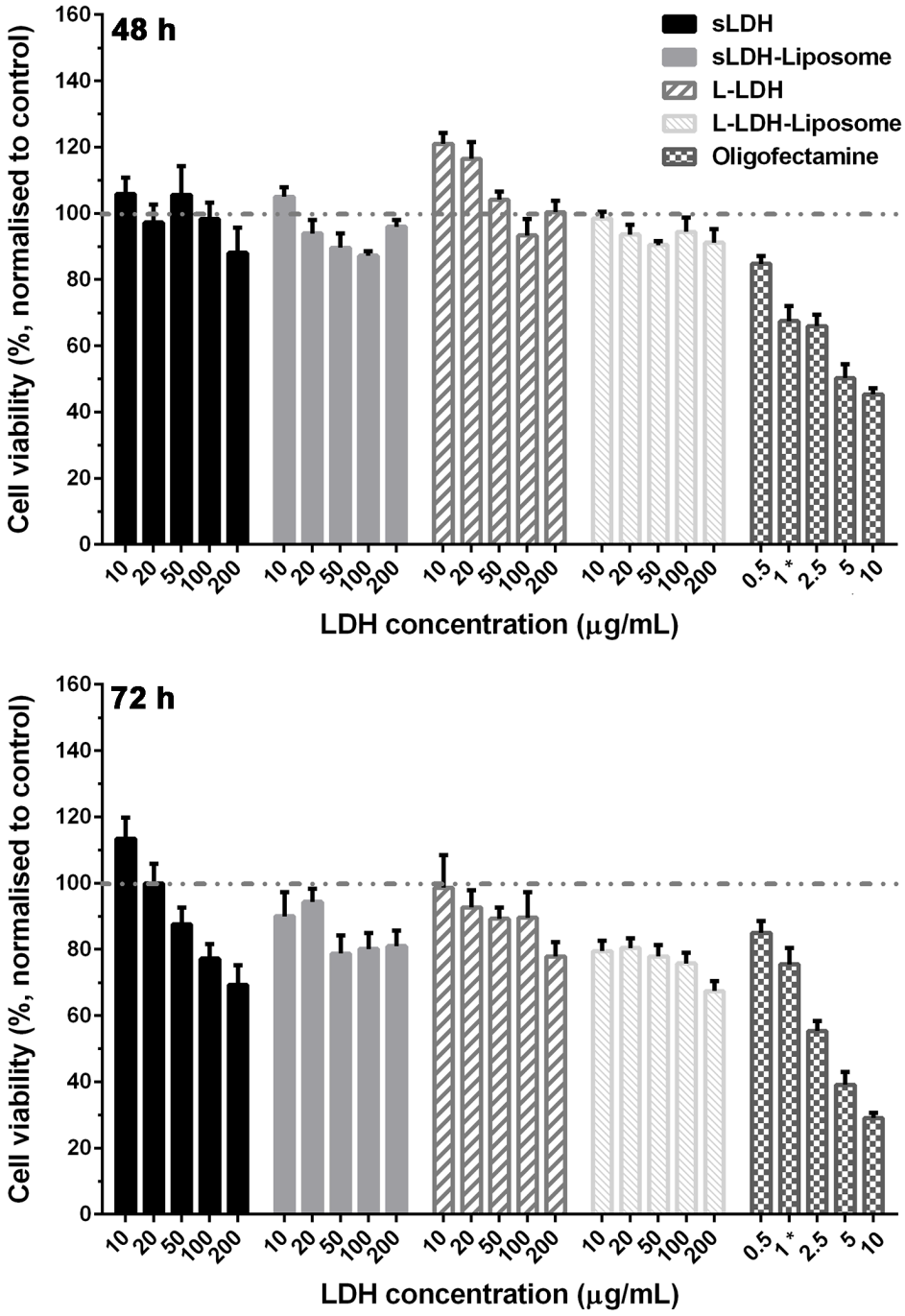

Figure 6-4 Cell viability of LDH and LDH-liposome NPs (MTT assay, in LDH-Liposome formulations LDH:EPC mass ratio = 1:1, transfection reagent Oligofectamine™ was used as positive control, 1* = minimum recommended dose of Oligofectamine™)

6.3.4 Nucleic acid loading

Figure 6-5A shows the electrophoretic mobility of sLDH-liposome composites in the presence of dsDNA. It is evident that sLDH and sLDH-liposome composites completely bind dsDNA, irrespective of the dsDNA loading method (sLDH:dsDNA mass ratio = 20:1,

Lane 3 to Lane 6), driven by the positively charged property of sLDH NPs, which fully immobilises the negatively charged DNA in the wells at this mass ratio. However, neutral liposomes (EPC:dsDNA = 20:1, Lane 7) cannot fully retard dsDNA migration in the well. This difference reveals, as alluded to earlier, that there are likely to be sLDH NPs residing outside the sLDH-liposome composite, which help to immobilise dsDNA in the well (sLDH NPs fully associate dsDNA at mass ratio of 5:1, as reported earlier [36]), as proposed and shown in Figure 6-2F.

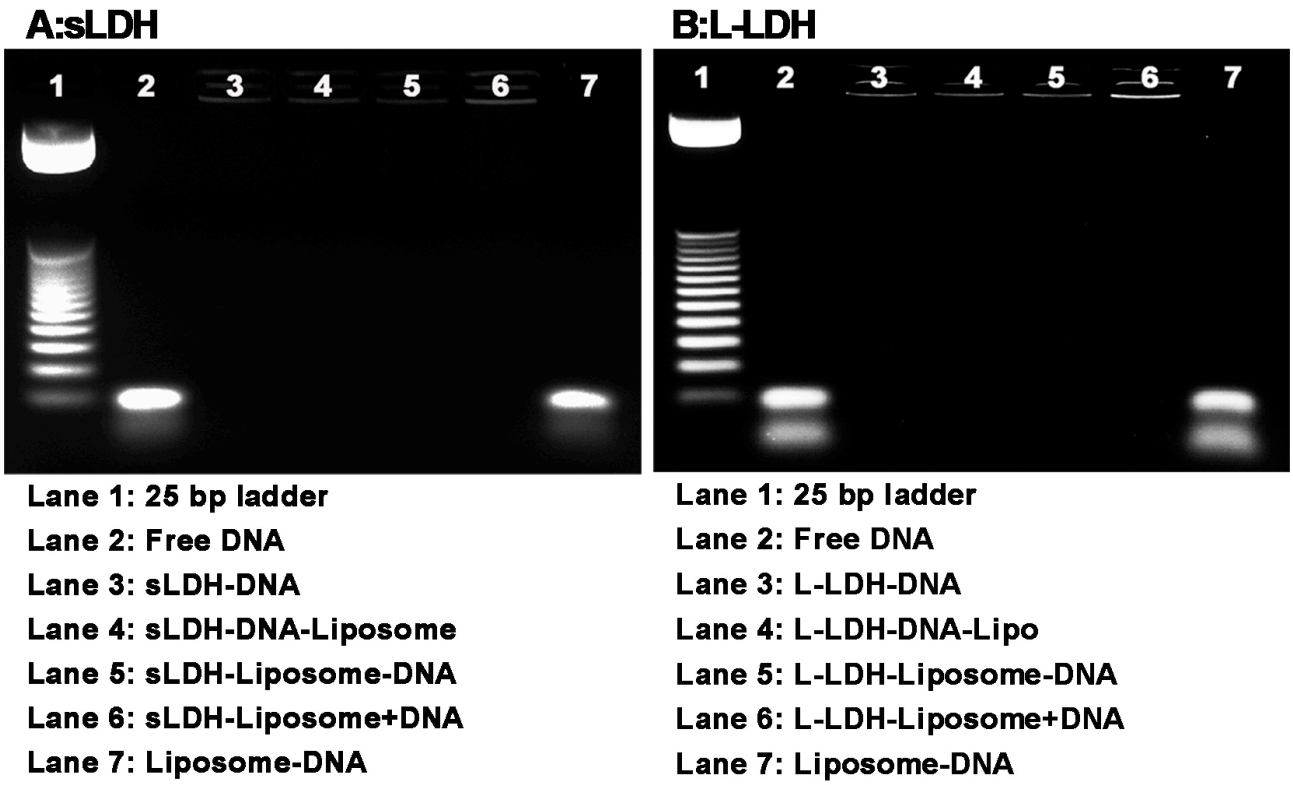

Figure 6-5 Electrophoresis mobility of HFDM LDH-liposome composite for dsDNA loading (LDH:DNA mass ratio = 20:1, EPC:DNA mass ratio = 20:1)

L-LDH and L-LDH-liposome yielded similar profiles for dsDNA immobilisation, as shown in Figure 6-5B. L-LDH and all L-LDH-liposome formulations can fully complex with dsDNA in the wells regardless of the dsDNA loading method (Lane 3 to Lane 6, positively charged L-LDH NPs can also fully combine with DNA at this mass ratio). This also indicates that L-LDH NPs are almost entirely residing outside L-LDH-liposome composites, thus allowing direct interaction with dsDNA. In addition, the two faintest bands in lane 2 and 7 (Figure 6-5B) arise from strand dissociation (to ssDNA), which can occur upon extended storage of dsDNA.

6.3.5 Cellular delivery

In consideration of the high cellular delivery of DNA using LDH NPs only (~100% of positive cells were observed when 40 nM of Cy3-DNA was used with LDH NPs), 20 nM of Cy3-DNA was used here to evaluate the cellular uptake differences between LDH and LDH-liposome composite.

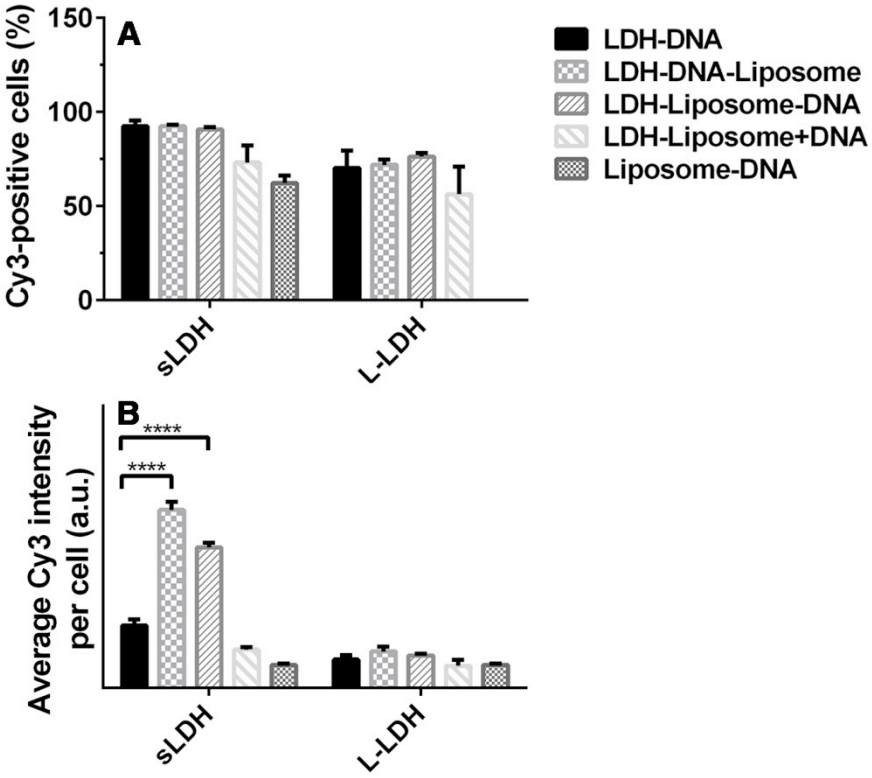

Figure 6-6 Cellular uptake of DNA-Cy3 by HCT-116 cells at 20 nM DNA, LDH:DNA mass ratio = 20:1, EPC:DNA = 20:1, and 4 h incubation.

Cellular uptake of Cy3-DNA (20 nM) delivered using either LDH or LDH-liposome composite after 4 h incubation are shown in Figure 6-6A and B. The LDH-liposome composite led to a similar number of Cy3 positive cell population when compared to (s/L-)LDH alone. Unsurprisingly, the average amount of DNA delivered into each cell by sLDH-DNA-liposome and sLDH-liposome-DNA was 2.9- and 2.2-fold higher, respectively, when compared to that achieved with sLDH alone. In contrast, sLDH-liposome+DNA and liposome-DNA gave a lower relative average Cy3 intensity/cell (= Cy3 intensity of Cy3 positive cells × Cy3 positive cell percentage; the fluorescence of non-Cy3 positive cells was disregarded) than sLDH alone. The reason for the latter observation is most likely due to the lower loading efficiency of dsDNA into liposomes (Figure 6-5), while for the former

this could be due to the competition for internalisation existing between empty sLDH-liposomes, blank liposomes, and sLDH-DNA NPs, more likely, the encapsulated sLDH NPs are redundant in this case.The average Cy3 intensity delivered by L-LDH-liposome composites was much lower than that achieved by sLDH-liposome composites (Figure 6-6B). Moreover, their average Cy3 intensity is very similar in these cases, consistent with the idea that L-LDH largely resides outside L-LDH-liposomes, which leads to a similar internalisation profile of DNA-Cy3 via L-LDH NPs.

6.3.6 Why does the sLDH-liposome composite enhance cellular delivery?

sLDH-liposome composites possess improved cellular delivery properties, and this could be attributed in part to the encapsulation of sLDH NPs inside liposomal vesicles. Firstly, association of sLDH with liposomal vesicles also reduces the risk of aggregation between sLDH NPs and serum proteins, thus improving the in-suspension stability of sLDH(-DNA) NPs, so that the bioavailability and retention of sLDH-DNA NPs in the cell culture media is improved. Other researchers in the field have also related the increased uptake/delivery of cell penetrating peptides, micelles-iron oxide NPs and LDH NPs to their greater stability under physiological conditions.[44-46] Moreover, smaller dimensions of the resulting complexes normally leads to rapid, receptor-mediated internalisation, while larger, aggregated complexes may show less efficient unspecific uptake through adsorptive endocytosis, which is a relatively slower process.[47] Furthermore, with improved composite suspension stability, the system would be expected to perform well in both suspended and adherent cell lines (previously we found transfection of the suspended cell line CHO-S using LDH NPs was not very successful, unlike adherent cell lines such as HEK293T, NIH 3T3, COS-7, and CHO-K1 [16]).

Aside from the key driver to internalisation, which is electrostatic interaction between sLDH NPs and the glycocalyx present on the surface of cells, another crucial factor driving delivery and partitioning is the affinity of phospholipids (from liposomes) for lipids of the cell membrane. This can be confirmed by the > 50% of Cy3 positive cell population achieved with liposomes, while the DNA delivery efficiency obtained was low, due to the poor gene loading capacity (Figure 6-5, lane 7).

Followed by enhanced cellular uptake, efficient cargo release is also crucial for any competent gene delivery vector. The proposed endosomal escape pathway for this sLDH-

liposome composite is outlined in Figure 6-7.[21, 22] Following internalisation of the sLDH-liposome composite, sLDH NPs which are external to the liposomal vesicles or adsorbed onto their surface dissolve gradually under the acidic conditions inside endosomes. This results in increased osmotic pressure inside endosomal vesicles, which causes an influx of water into endosome, and this then swells the endosome (Figure 6-7A to B). Further dissolution of sLDH NPs outside and inside liposomal vesicles leads to even higher osmotic pressures and further swelling of liposomal and endosomal vesicles, which finally leads to rupture of endosomal and liposomal vesicles and cargo release into the cytoplasm (Figure 6-7C). Note that in the case of liposomes, the internalised liposome-DNA complexes cannot escape from endosome in a timely manner, which leads to the bulk of DNA being degraded in the lysosome.

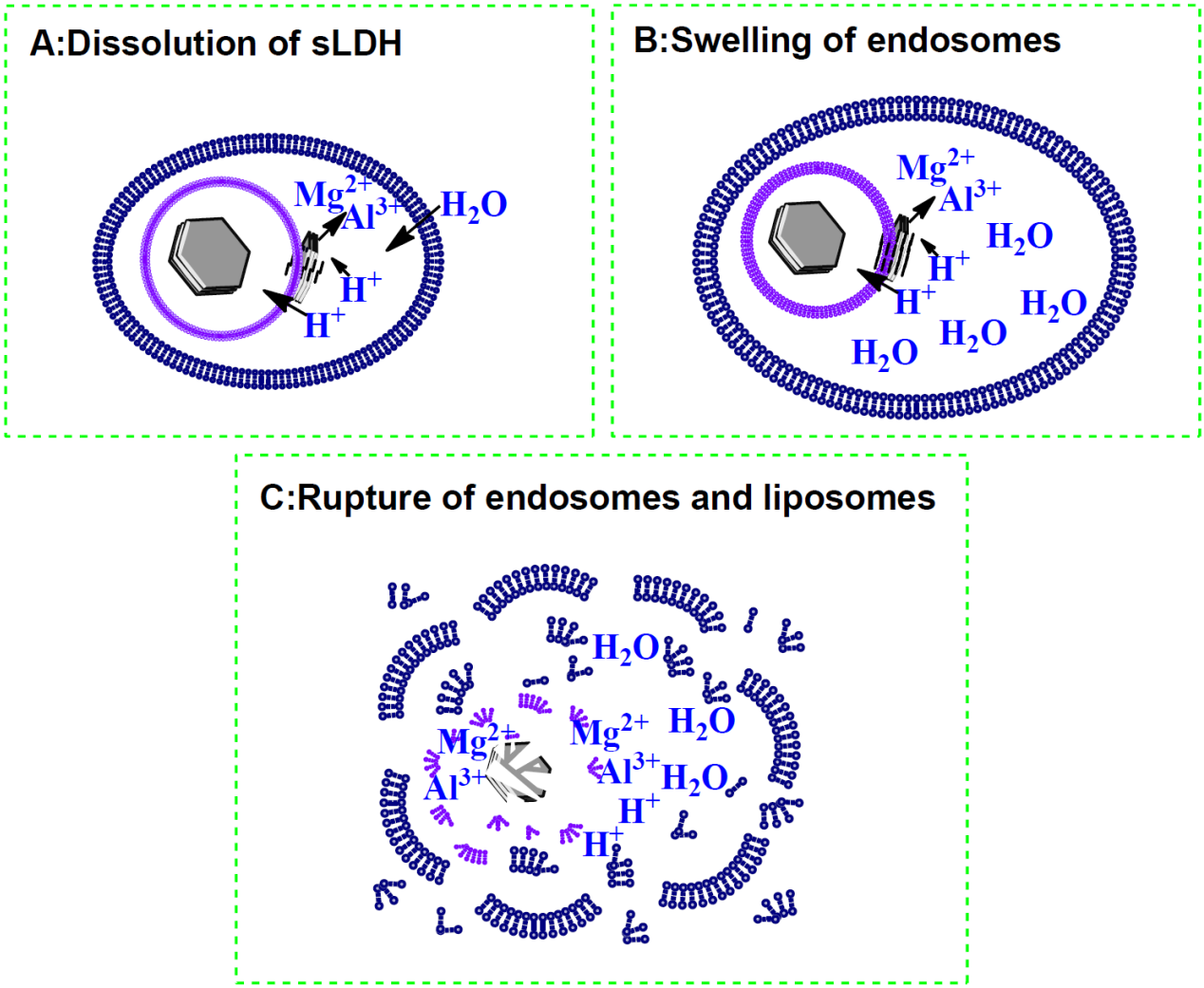

Figure 6-7 Possible endosomal escape pathway for sLDH-liposome composite

6.4 Conclusions

LDH-liposome composites prepared using the HFDM method possess good particle size distribution with *Z*-average size ~200 nm after hydration, and they are suitable for cellular uptake studies. The composite systems are stable in the culture medium with limited cytotoxicity observed. More interestingly, the sLDH-liposome system shows higher cellular delivery efficiency (2-3 times higher) than sLDH alone, while the L-LDH-liposome composite did not exhibit significant differences from L-LDH. The reasons we put forward for these observation are that: (1) sLDH can be easily encapsulated in the aqueous core of liposome because of its small size; (2) some sLDH NPs could attach to the surface of the liposome bilayer, which helps bind and protect DNA, and more importantly, helps its escape from the endosome; (3) the hydrophobicity of liposomes may also facilitate their cellular uptake. Thus, this research has demonstrated that a carefully engineered combination of sLDH and liposome synergises the cellular delivery efficiency, by taking advantages of both systems salient features.

References

1. Mulligan, R.C. The basic science of gene therapy. *Science* **260**, 926-932 (1993).

2. Giacca, M. Gene therapy (Springer Milan, New York, 2010).

3. Panno, J. Gene therapy: treatments and cures for genetic diseases (Facts On File, New York, NY, 2011).

4. Verma, I.M. & Somia, N. Gene therapy -- promises, problems and prospects. *Nature* **389**, 239-242 (1997).

5. Brown, M.D., Schatzlein, A.G. & Uchegbu, I.F. Gene delivery with synthetic (non viral) carriers. *International Journal of Pharmaceutics* **229**, 1-21 (2001).

6. Guo, S. & Huang, L. Nanoparticles escaping RES and endosome: Challenges for siRNA delivery for cancer therapy. *Journal of Nanomaterials* (2011).

7. Wiethoff, C.M. & Middaugh, C.R. Barriers to nonviral gene delivery. *Journal of Pharmaceutical Sciences* **92**, 203-217 (2003).

8. Ruponen, M. et al. Extracellular and intracellular barriers in non-viral gene delivery. *Journal of Controlled Release* **93**, 213-217 (2003).

9. Auerbach, S.M., Carrado, K.A. & Dutta, P.K. (eds.) Handbook of layered materials (Marcel Dekker, Inc, New York, 2004).

10. Xu, Z.P. et al. Stable suspension of layered double hydroxide nanoparticles in aqueous solution. *Journal of the American Chemical Society* **128**, 36-37 (2006).

11. Xu, Z.P., Stevenson, G., Lu, C.-Q. & Lu, G.Q. Dispersion and size control of layered double hydroxide nanoparticles in aqueous solutions. *Journal of Physical Chemistry B* **110**, 16923-16929 (2006).

12. Oh, J.-M., Hwang, S.-H. & Choy, J.-H. The effect of synthetic conditions on tailoring the size of hydrotalcite particles. *Solid State Ionics* **151**, 285-291 (2002).

13. Ladewig, K. (The University of Queensland, Queensland, Australia, 2009).

14. Wong, Y. (The University of Queensland, Queensland, Australia, 2009).

15. Li, L., Gu, W., Chen, J., Chen, W. & Xu, Z.P. Co-delivery of siRNAs and anti-cancer drugs using layered double hydroxide nanoparticles. *Biomaterials* **35**, 3331-3339 (2014).

16. Ladewig, K., Niebert, M., Xu, Z.P., Gray, P.P. & Lu, G.Q. Controlled preparation of layered double hydroxide nanoparticles and their application as gene delivery vehicles. *Applied Clay Science* **48**, 280-289 (2010).

17. Ladewig, K., Niebert, M., Xu, Z.P., Gray, P.P. & Lu, G.Q.M. Efficient siRNA delivery to mammalian cells using layered double hydroxide nanoparticles. *Biomaterials* **31**, 1821-1829 (2010).

18. Wong, Y. et al. Efficient delivery of siRNA to cortical neurons using layered double hydroxide nanoparticles. *Biomaterials* **31**, 8770-8779 (2010).

19. Choy, J.-H., Park, M. & Oh, J.-M. Gene and drug delivery system with soluble inorganic carriers (ed. Shoseyov, O.L.I.) (2008).

20. Choy, J.-H., Kwak, S.-Y., Jeong, Y.-J. & Park, J.-S. Inorganic layered double hydroxides as nonviral vectors. *Angewandte Chemie International Edition* **39**, 4041-4045 (2000).

21. Oh, J.-M., Biswick, T.T. & Choy, J.-H. Layered nanomaterials for green materials. *Journal of Materials Chemistry* **19**, 2553-2563 (2009).

22. Ladewig, K., Xu, Z.P. & Lu, G.Q. Layered double hydroxide nanoparticles in gene and drug delivery. *Expert Opinion on Drug Delivery* **6**, 907-922 (2009).

23. Gregoriadis, G. (ed.) Liposome technology, Vol 2: Entrapment of drugs and other materials into Liposomes (Informa Healthcare, New York, 2007).

24. Gabizon, A. & Papahadjopoulos, D. Liposome formulations with prolonged circulation time in blood and enhanced uptake by tumors. *Proceedings of the National Academy of Sciences of the United States of America* **85**, 6949-6953 (1988).

25. Li, S.-D. & Huang, L. Stealth nanoparticles: High density but sheddable PEG is a key for tumor targeting. *Journal of Controlled Release* **145**, 178-181 (2010).

26. Li, J., Yang, Y. & Huang, L. Calcium phosphate nanoparticles with an asymmetric lipid bilayer coating for siRNA delivery to the tumor. *Journal of Controlled Release* **158**, 108-114 (2012).

27. Qhattal, H.S.S., Hye, T., Alali, A. & Liu, X. Hyaluronan polymer length, grafting density, and surface poly(ethylene glycol) coating influence *in vivo* circulation and tumour targeting of hyaluronan-grafted liposomes. *Acs Nano* **8**, 5423-5440 (2014).

28. Yuba, E. et al. Dextran derivative-based pH-sensitive liposomes for cancer immunotherapy. *Biomaterials* **35**, 3091-3101 (2014).

29. Yoshizaki, Y. et al. Potentiation of pH-sensitive polymer-modified liposomes with cationic lipid inclusion as antigen delivery carriers for cancer immunotherapy. *Biomaterials* **35**, 8186-96 (2014).

30. Raemdonck, K., Braeckmans, K., Demeester, J. & De Smedt, S.C. Merging the best of both worlds: hybrid lipid-enveloped matrix nanocomposites in drug delivery. *Chemical Society Reviews* **43**, 444-472 (2014).

31. Liu, Y. 120 (The University of North Carolina at Chapel Hill, Ann Arbor, 2012).

32. Zhang, Y. 193 (The University of North Carolina at Chapel Hill, Ann Arbor, 2013).

33. Tseng, Y.-C. 101 (The University of North Carolina at Chapel Hill, Ann Arbor, 2013).

34. Li, J., Chen, Y.-C., Tseng, Y.-C., Mozumdar, S. & Huang, L. Biodegradable calcium phosphate nanoparticle with lipid coating for systemic siRNA delivery. *Journal of Controlled Release* **142**, 416-421 (2010).

35. Chen, M., Cooper, H.M., Zhou, J.Z., Bartlett, P.F. & Xu, Z.P. Reduction in the size of layered double hydroxide nanoparticles enhances the efficiency of siRNA delivery. *Journal of Colloid and Interface Science* **390**, 275-281 (2013).

36. Dong, H. et al. Engineering small MgAl-layered double hydroxide nanoparticles for enhanced gene delivery. *Applied Clay Science* (2014).

37. Wu, S.Y. et al. Development of a novel method for formulating stable siRNA-loaded lipid particles for *in vivo* use. *Pharmaceutical Research* **26**, 512-522 (2009).

38. Li, C. & Deng, Y. A novel method for the preparation of liposomes: Freeze drying of monophase solutions. *Journal of Pharmaceutical Sciences* **93**, 1403-1414 (2004).

39. Cui, J., Li, C., Deng, Y., Wang, Y. & Wang, W. Freeze-drying of liposomes using tertiary butyl alcohol/water cosolvent systems. *International Journal of Pharmaceutics* **312**, 131-136 (2006).

40. Gregoriadis, G. (ed.) Liposome technology, Vol 1: Liposome preparation and related techniques (Informa Healthcare, New York, 2007).

41. Kasraian, K. & DeLuca, P.P. Thermal analysis of the tertiary butyl alcohol-water system and its implications on freeze-drying. *Pharmaceutical Research* **12**, 484-490 (1995).

42. Crosasso, P. et al. Preparation, characterization and properties of sterically stabilized paclitaxel-containing liposomes. *Journal of Controlled Release* **63**, 19-30 (2000).

43. Lee, S. et al. DNA amplification in neutral liposomes for safe and efficient gene delivery. *Acs Nano* **8**, 4257-4267 (2014).

44. Crombez, L. et al. A new potent secondary amphipathic cell-penetrating peptide for siRNA delivery into mammalian cells. *Molecular Therapy* **17**, 95-103 (2009).

45. Chandrasekharan, P. et al. Vitamin E (D-alpha-tocopheryl-co-poly(ethylene glycol) 1000 succinate) micelles-superparamagnetic iron oxide nanoparticles for enhanced thermotherapy and MRI. *Biomaterials* **32**, 5663-5672 (2011).

46. Choi, G., Kim, S.Y., Oh, J.M. & Choy, J.H. Drug-Cceramic 2-Dimensional nanoassemblies for drug delivery system in physiological condition. *Journal of the American Ceramic Society* **95**, 2758-2765 (2012).

47. Ogris, M., Steinlein, P., Carotta, S., Brunner, S. & Wagner, E. DNA/polyethylenimine transfection particles: influence of ligands, polymer size, and PEGylation on internalization and gene expression. *AAPS pharmSci* **3**, E21-E21 (2001).

This page was left blank intentionally.

Chapter 7 Conclusions and Future Directions

7.1 Conclusions

The first major contribution of this thesis is the control synthesis of small LDH (sLDH) nanoparticles (NPs) by a non-aqueous co-precipitation method. A methanolic solution containing magnesium and aluminium nitrate is mixed with sodium hydroxide in methanol, followed by removal of side product sodium nitrate and hydrothermal treatment in methanol. The collected precipitate is then washed and finally dispersed in water into homogeneous sLDH NP suspension. The resultant sLDH NPs possess a *Z*-average diameter particle size in the range of 35 ~ 50 nm with good colloidal stability at room temperature for a couple of months. The hydrothermal treatment duration from 0 to 48 h, and the hydrothermal treatment temperature from 60 to 100 °C have slightly influenced the sLDH particle size, but removal of sodium nitrate before hydrothermal treatment is crucial for good dispersion of final sLDH suspension.

Secondly, this research has observed that the most important factor that affects the cellular internalisation rate is the LDH NP number concentration instead of the LDH particle size in the range of 35 ~ 100 nm. A critical particle number concentration has been deduced for both sLDH and normal LDH (denoted as large LDH, L-LDH in this thesis) NPs. Below this value the cellular uptake by human colon cancer (HCT-116) cells is proportional to the particle number concentration, but above the value the cellular uptake is saturated and cannot be improved further. At the same particle number concentration, the cellular uptake profile of sLDH and L-LDH NPs is very similar, indicating that the particle internalisation is not substantially affected by the size in the range (35 ~ 100 nm). The drug/gene loading style and loading capacity have been also noted to affect the efficacy of drug/gene delivery to this cell line.

Lastly, this research suggests that the hydration of freeze-dried matrix (HFDM) method is a proper way to prepare the LDH-liposome composites, although their structure and morphology are not clear at the moment; and moreover, the sLDH-liposome composites facilitate the cellular uptake significantly. sLDH-liposome composites were firstly attempted by the hydration of thin lipid film (HTLF) method, but multilamellar vesicles were obtained and pretty low encapsulation was achieved after size reduction by probe sonication or extrusion. After preparation using HFDM method, the sLDH-liposome composite

suspension has good suspension stability with the *Z*-average diameter size ~ 200 nm, which is suitable for cellular uptake. sLDH-liposome composites are able to transport 2-3 times more DNA to HCT-116 cells than sLDH only, which could be attributed to synergistic combination of sLDH NPs and liposomes. No significant improvement is seen for L-LDH-liposome composites prepared by the same method, which probably suggests that there is no such synergistic combination of L-LDH NPs and liposomes.

7.2 Future directions

Enhanced cellular delivery of nucleic acids has been observed for sLDH-liposome composites; however, more efforts could be made to further improve this hybrid system, such as:

[1] investigating the mechanisms for sLDH-liposome composite formation, and further confirming the hybridisation by encapsulating sLDH NPs inside liposomal vesicles or associating sLDH NPs on the surface of liposomes or the proportion of encapsulation to association; This understanding will help improve the encapsulation efficiency of sLDH in the liposomal vesicles, probably through optimisation or development of new method(s) to prepare liposomal formulations or other liposomal compositions;

[2] examining the cellular uptake behaviour and the endosome escape pathway of sLDH-liposome composites, which would pave a way to further enhance their cellular delivery efficiency;

[3] modifying liposomes with polyethylene glycol (PEG) for further increasing the stability of the composite system and extending its circulation time; linking some antibodies or peptides for specific target delivery of genetic therapeutics;

[4] developing combination therapy for this composite system, for example, using LDH to load hydrophilic anionic drugs and genes, and liposomes to carry hydrophobic drugs.

Appendix Preparation of small Layered Double Hydroxide-liposome Composite by Hydration of Thin Lipid Film Method

Abstract

To encapsulate sLDH NPs inside liposomal vesicles to form sLDH-liposome composites, commonly used liposome preparation method hydration of thin lipid film (HTLF) was used. Micron size of multilamellar vesicles was obtained after hydrated with sLDH suspension with encapsulation efficiency up to 30%. Size reduction of liposomal vesicles was done by both extrusion and sonication methods, however, sLDH-liposome complexes might easily block the filter membrane pores and pretty low amount of sLDH-liposome composites were obtained after extrusion, while sonication led to smaller size of liposomal vesicles with low encapsulation efficiency. In summary, HTLF method might not be a proper method to prepare sLDH-liposome composites with high encapsulation efficiency and good size distribution.

A1 Introduction about liposome preparation

There are quite a few methods for making liposomal formulations, such as hydration of thin lipid film (HTLF), hydration of freeze-dried matrix (HFDM),[1-5] microfluidic jetting,[6] reverse phase evaporation.[7-10] Of them, HTLF is a conventional and easy way to form liposomes. However, liposomes made from this method are normally large/giant multi-lamellar vesicles because of the stacked lipid bilayers in lipid film state. Therefore, following size reduction is always needed. The most commonly used size reduction techniques are extrusion[11-17] and sonication. Figure A1 shows the schematic diagram for preparing liposomes using HTLF method, followed by size reduction via extrusion or sonication.

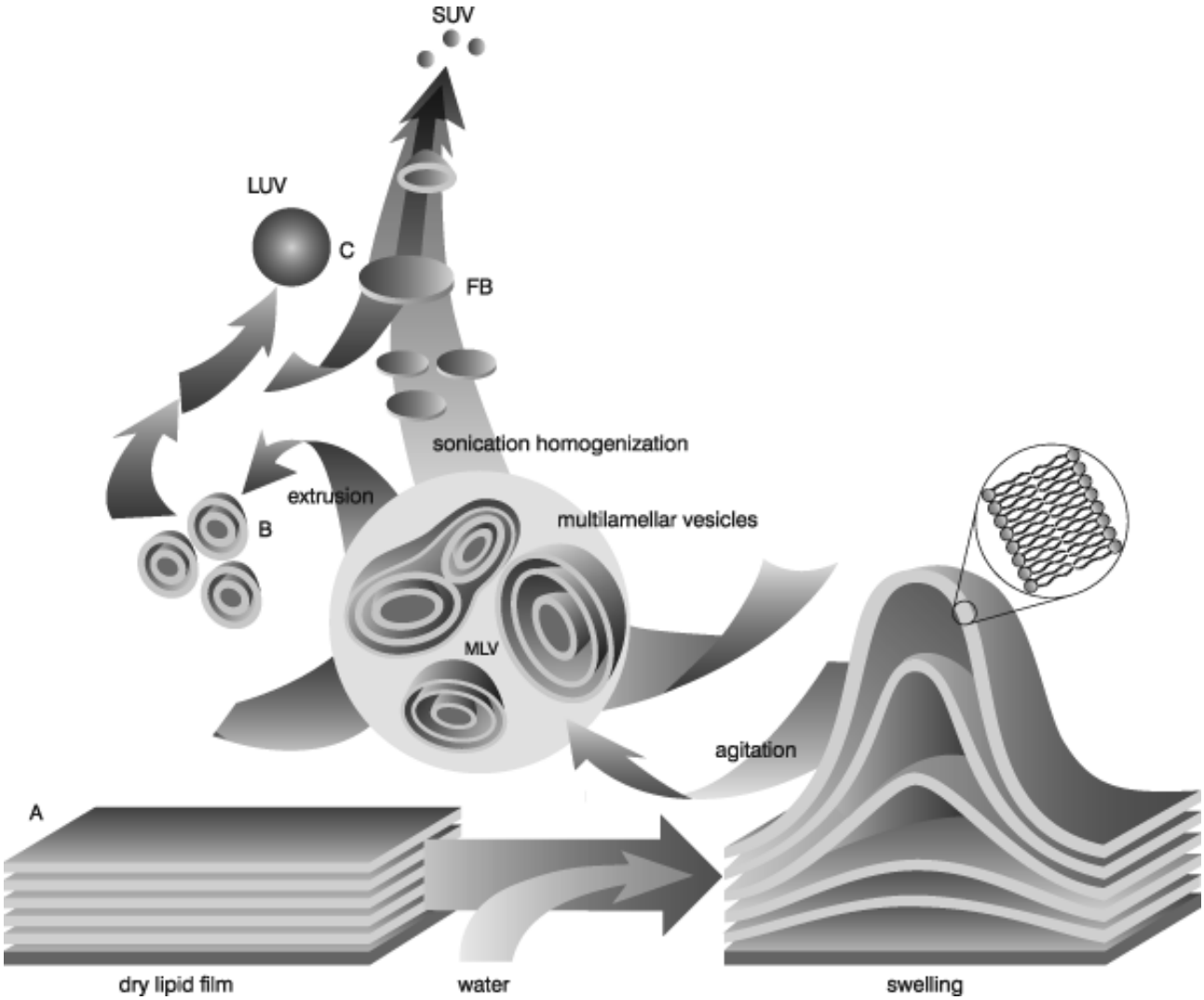

Figure A1 Preparation of liposomes by HTLF method, followed by size reduction via extrusion or sonication; MLV: multilamellar vesicle; LUV: large unilamellar vesicle; SUV: small unilamellar vesicle; http://www.avantilipids.com/

Figure A2 shows the extruder used in our lab (Lipex™ Extruder, manufactured by Northern Lipids (Vancouver, BC, Canada), has a 10 mL capacity and can be operated over a wide range of temperatures when used in combination with a circulating water bath. The quick-release sample port at the top of the unit allows for the rapid cycling of sample through the filters), the particle sizes and polydispersity index (PdI) of liposome suspension, prepared by HTLF method, followed by sequential extrusion.

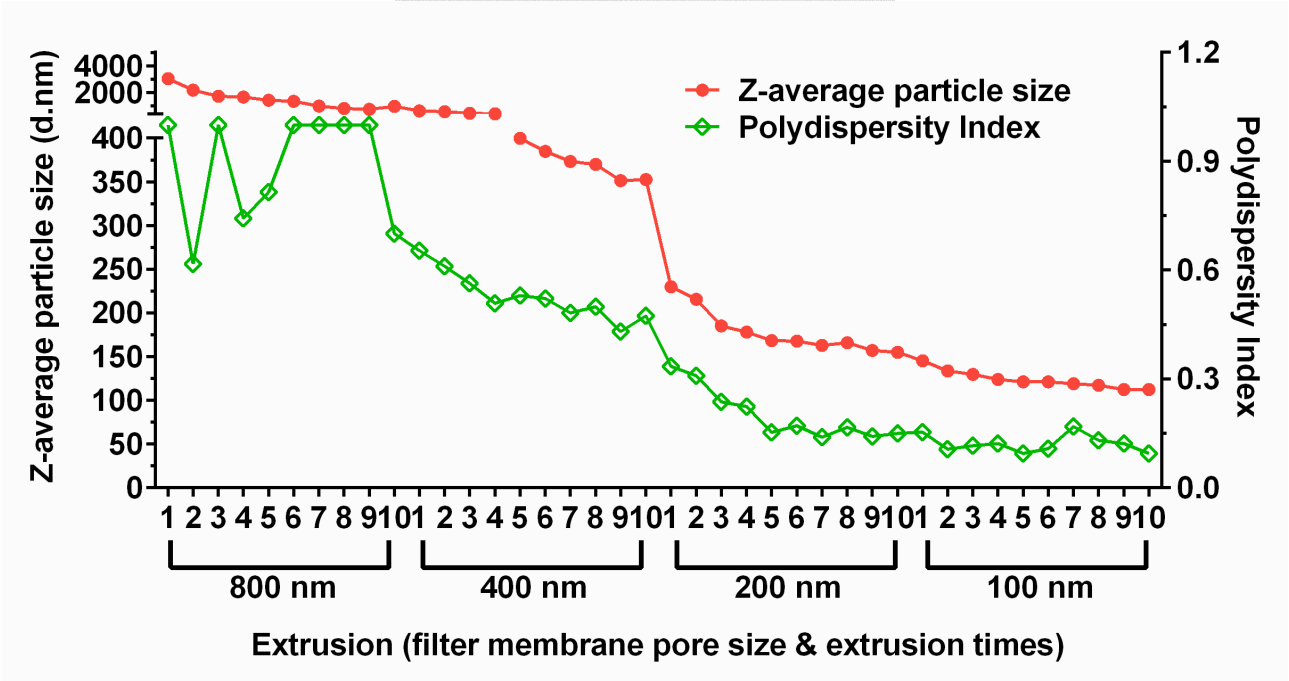

Figure A2 Picture of extruder used (Top) and Z-average particle sizes and polydispersity index values of liposomes after extrusion through polycarbonate membrane(Down); for each pore size of polycarbonate membrane, liposomes were extruded through 10 times

Originally formed liposomes possess sizes in micron range. With extrusion through 800 nm polycarbonate membrane, the particle sizes reduced rapidly from 3 μm to less than 1 μm, but the PdI fluctuated and kept above 0.70. Starting from extrusion through 400 nm membrane, the vesicle sizes reduced gradually together with PdI, ended with *Z*-average size ~ 350 nm and PdI ~ 0.45. *Z*-average size of ~ 150 and ~ 110, and PdI of ~ 0.15 and 0.10 were obtained after sequential extrusion through 200 and 100 nm membranes 10 times, which implied good sizes of liposomes with narrow size distribution were obtained by this method, so called large unilamellar vesicles shown in Figure A1. The final liposome vesicle sizes could be well controlled by the membrane used.

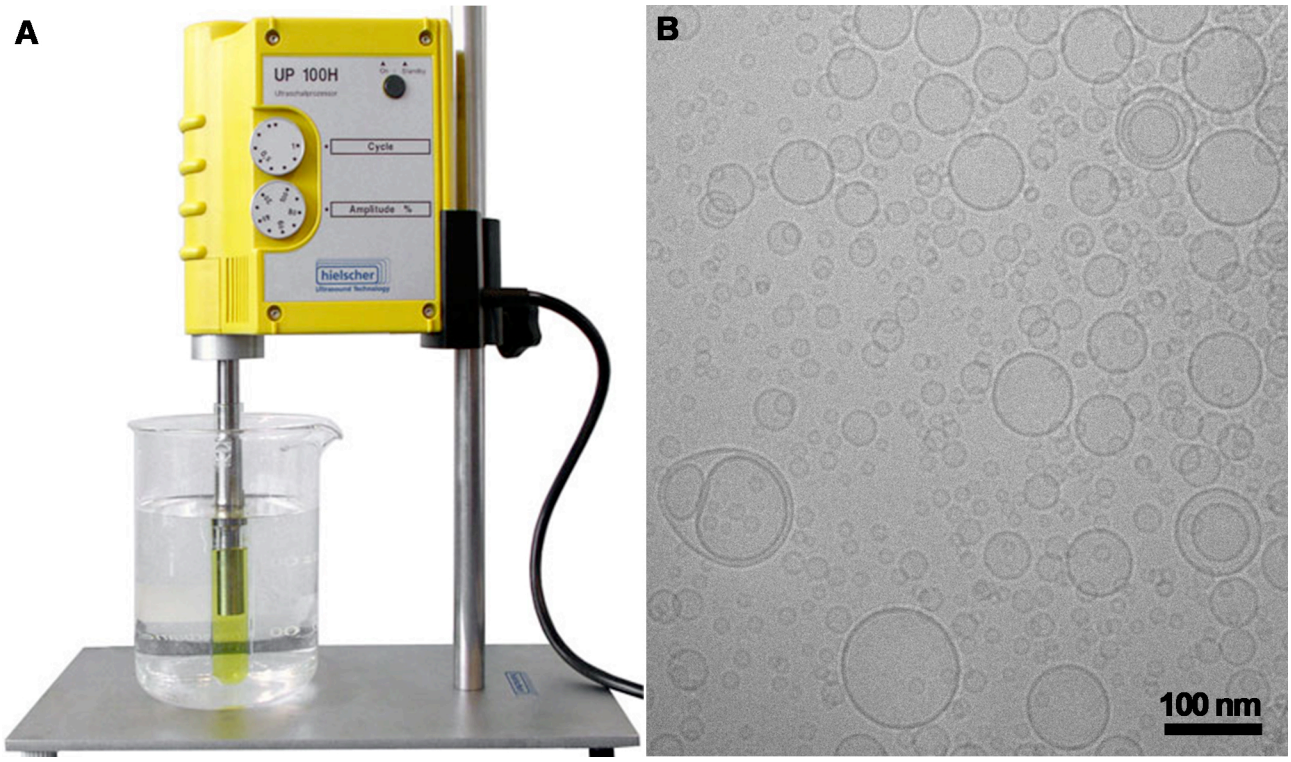

Figure A3 Picture of probe sonicator used for reducing liposome size (A), and cryo-TEM image of blank liposomes, prepared by HTLF method, size reduced by probe sonication (B)

Figure A3 shows the probe sonicator used in our lab, and the cryo-TEM image of liposomes prepared by HTLF method, followed by probe sonication for size reduction. It can be seen that after probe sonication, most of liposomes are unilamellar vesicles, but the sizes of these vesicles are mainly smaller than 100 nm with majority of them ≤ 30 nm, which are so called small unilamellar vesicles as shown in Figure A1.sLDH-liposome composite was then attempted by HTLF method. The amount of sLDH encapsulated

inside liposomal vesicles or attached on liposome surfaces were characterised by centrifugation washing followed by elemental analysis of magnesium and aluminium amounts in the final pellet by ICP-AES. Amounts of sLDH in originally formed composite suspension (MLVs) and smaller sizes of composites (after size reduction by extrusion or sonication) were determined. A range of parameters, such as lipid film thicknesses, liposome concentrations, sLDH concentrations were varied to investigate their impact on the encapsulation efficiency.

A2 Encapsulation of sLDH in multilamellar large vesicles (MLVs)

A2.1 Effect of lipid film thickness on encapsulation

A2.1.1 By changing lipid amount

About 100, 50 and 20 mg of EPC were dissolved in 5 mL of chloroform in 100 mL of round bottom flasks (RBFs), respectively, then chloroform was evaporated by rotary evaporator to form thin lipid film. After that, 5 mL of sLDH suspension (7.26 mg/mL) was added for rehydration by hand-shaking.

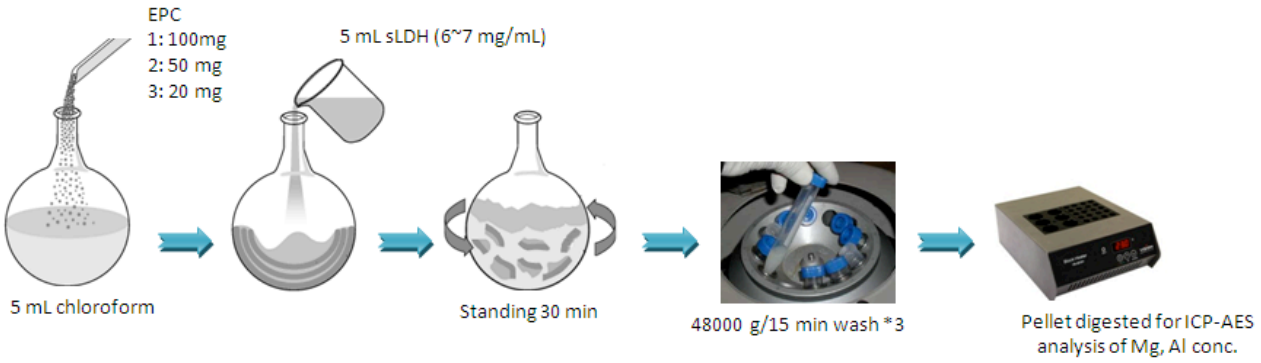

Figure A4 Experimental flowchart for sLDH encapsulation in MLVs (varying lipid amount)

After the liposome suspension was standing at room temperature for 30 min, 1 mL of the sLDH-liposome composite was subjected to centrifugal washing three times by 10 mL of DI water at 48,000 g for 15 min to separate free sLDH particles from sLDH-liposome composite by dilution effect. Final pellet was digested by 10 mL of nitric acid at 80 °C, and then diluted 100 times for ICP-AES test of Mg and Al concentrations. The original sLDH suspension used for rehydration was also digested and diluted by 100 times for ICP-AES test of Mg and Al concentrations. Encapsulation efficiency of sLDH was calculated from

the sLDH amount in composite and the total sLDH amount used for rehydration. The experimental flowchart is shown in Figure A4 and the results are listed in Table A1.

sLDH suspension used for hydration was fixed at 5 mL and 6~7 mg/mL. When the lipid amount increased from 20 mg to 100 mg, the sLDH encapsulation efficiency did not change much, which meant the lipid to sLDH ratio in the final composite was not affected much by liposome concentration.

Table A1 sLDH encapsulated in liposomal vesicles under different liposome concentrations-1 (varying lipid amounts)

Batch	Lipid amount	Mg in composite	Al in composite	Mg in LDH for rehydration	Al in LDH for rehydration	Encapsulation by Mg	Encapsulation by Al
	mg	mg	mg	mg	mg	%	%
1	101	0.56	0.29	8.86	2.78	6.32	10.3
2	52.0	0.48	0.23			5.36	8.09
3	22.5	0.55	0.27			6.15	9.53

A2.1.2 By changing round bottom flask size

Three sizes of RBFs, 100, 50 and 20 mL, were used to form thin lipid film by rotary evaporator, where about 50 mg of EPC was dissolved in 5 mL of chloroform, respectively. After that, 5 mL of sLDH suspension (~24 mg/mL) was added for rehydration by hand-shaking. The following treatments were the same as in *A2.1.1 By changing lipid amount* and the results results are shown in Table A2.

No matter changing lipid amounts in certain volume of round bottom flask or changing round bottom flask volume while using certain amount of lipid, it seems no significant difference for the encapsulation efficiency; therefore it appears that the thickness of lipid film does not affect the encapsulation efficiency much.

Table A2 sLDH encapsulated in liposomal vesicles under different liposome concentrations-2 (varying round bottom flask sizes)

Batch	RBF volume	Mg in composite	Al in composite	Mg in LDH for rehydration	Al in LDH for rehydration	Encapsulation by Mg	Encapsulation by Al
	mL	mg	mg	mg	mg	%	%
1	100	6.50	2.50	31.0	12.0	21.0	20.8
2	50.0	5.50	2.30			17.7	19.2
3	20.0	5.50	2.30			17.7	19.2

A2.2 Effect of liposome concentration on encapsulation

Effect of liposome concentration on the encapsulation efficiency of sLDH NPs in liposomal vesicles were investigated in this project by changing sLDH suspension volume used. Considering concentration dependent encapsulation of silica nanoparticles in the polymersomes reported,[18] two concentrations of sLDH suspension were used in this project.

A2.2.1 sLDH concentration of 22 mg/mL

Three batches of thin lipid film were prepared from about 50 mg of EPC in 5 mL of chloroform by rotary evaporator. Then 2, 5 and 10 mL of sLDH suspension (22.1 mg/mL) were added for rehydration, respectively. The results are listed in Table A3.

It appears that the encapsulation efficiency of sLDH in composites decreased with larger volume of sLDH suspension used, however, 5 mL sLDH led to the highest absolute sLDH amounts in the composites, which might imply a proper sLDH/lipid ratio or hydration volume for encapsulation.

Table A3 sLDH encapsulated in MLVs when different volumes of sLDH suspension used for hydration (sLDH concentration 22 mg/mL)

Batch	sLDH volume	Mg in composite	Al in composite	Mg in LDH for rehydration	Al in LDH for rehydration	Encapsulation by Mg	Encapsulation by Al
	mL	mg	mg	mg	mg	%	%
1	2.00	2.16	0.81	10.3	3.56	21.0	22.6
2	5.00	4.84	2.11	25.7	8.89	18.8	23.7
3	10.0	3.82	1.50	51.4	17.8	7.43	8.42

A2.2.2 sLDH concentration of 12 mg/mL

Three batches of thin lipid film were prepared from about 50 mg of EPC in 5 mL of chloroform by rotary evaporator. Then 2, 5 and 10 mL of sLDH suspension (12 mg/mL) were added for rehydration, respectively. The results are shown in Table A4.

Table A4 encapsulated in MLVs when different volumes of sLDH suspension used for hydration (sLDH concentration 12 mg/mL)

Batch	sLDH volume	Mg in composite	Al in composite	Mg in LDH for rehydration	Al in LDH for rehydration	Encapsulation by Mg	Encapsulation by Al
	mL	mg	mg	mg	mg	%	%
1	2.00	1.80	0.74	6.00	2.40	30.0	30.8
2	5.00	3.30	1.40	15.0	6.00	22.0	23.3
3	10.0	4.20	1.70	30.0	12.0	14.0	14.2

Similar to 22 mg/mL sLDH suspension used, encapsulation efficiency of sLDH in composites decreased with the sLDH volume used for rehydration, and 2 mL of 12 mg/mL sLDH resulted in highest encapsulation ~ 30%. However, the final sLDH to lipid ratio in the purified composite increased with sLDH volume used for rehydration from 0.21:1 (2 mL sLDH) to 0.48:1 (10mL sLDH).

A2.3 Effect of sLDH concentration on encapsulation

Three batches of thin lipid film were prepared from about 50 mg of egg PC in 5 mL of chloroform by rotary evaporator. Then 5 mL of sLDH suspension with concentration of ~6, 12, 24 mg/mL were added for rehydration, respectively. The results are listed in Table A5.

Table A5 sLDH encapsulated in MLVs when different concentration of sLDH used for hydration

Batch	sLDH conc.	Mg in composite	Al in composite	Mg in LDH for rehydration	Al in LDH for rehydration	Encapsulation by Mg	Encapsulation by Al
	mg/mL	mg	mg	mg	mg	%	%
1	6.00	1.50	0.60	7.50	3.00	20.0	20.0
2	12.0	3.50	1.40	15.0	6.00	23.3	23.3
3	24.0	7.30	3.00	31.0	12.0	23.5	25.0

It seems that sLDH concentration has marginal influence on encapsulation efficiency, although the encapsulation efficiency improved a little with sLDH concentration increase. However, sLDH to lipid ratio in the final composite varied a lot, from 0.17:1 (sLDH concentration ~ 6 mg/mL) to 0.40:1 (sLDH concentration ~ 12 mg/mL), 0.83:1 (sLDH concentration ~ 24 mg/mL)

A2.4 Negatively charged lipid was included

To further improve the encapsulation of positively charged sLDH NPs in liposomal vesicles, 10% (molar ratio) of negatively charged lipid (DOPA, 1,2-dioleoyl-***sn***-glycero-3-phosphate (sodium salt), $C_{39}H_{72}O_8PNa$) was included for liposomal formulation, encapsulation efficiency of sLDH in MLVs was significantly improved from less than 30% to around 80% (78.57% by Mg and 80.17% by Al), which was probably due to the strong electrostatic interaction between negatively charged DOPA and positively charged sLDH particles, which caused unfavourable large aggregates.

A3 Encapsulation of sLDH in small unilamellar vesicles (SUVs)

A3.1 MLVs to SUVs by extrusion

About 50 mg of EPC was dissolved in 5 mL of chloroform to form thin lipid film by rotary evaporator, then 10 mL of sLDH suspension (~24 mg/mL) was added to each RBF for rehydration. After liposome suspensions were standing at room temperature for 30 min, the suspension was subjected to 10 cycles of freezing-thawing treatment before extrusion through polycarbonate filter membranes 800, 400 and 200 nm successively. The composite suspensions, before and after freezing-thawing treatment, after each extrusion, were subjected to 3 times of centrifugation at 48,000 g for 15 min, and then all the final pellets and post-extrusion suspension were digested and diluted for ICP-AES test of Mg and Al concentrations. Original sLDH suspension used for rehydration was also digested and diluted for ICP-AES test of Mg and Al concentrations. Encapsulation efficiency was calculated from the sLDH amount remained in composite and total sLDH amount used for rehydration, and then listed in Figure A5.

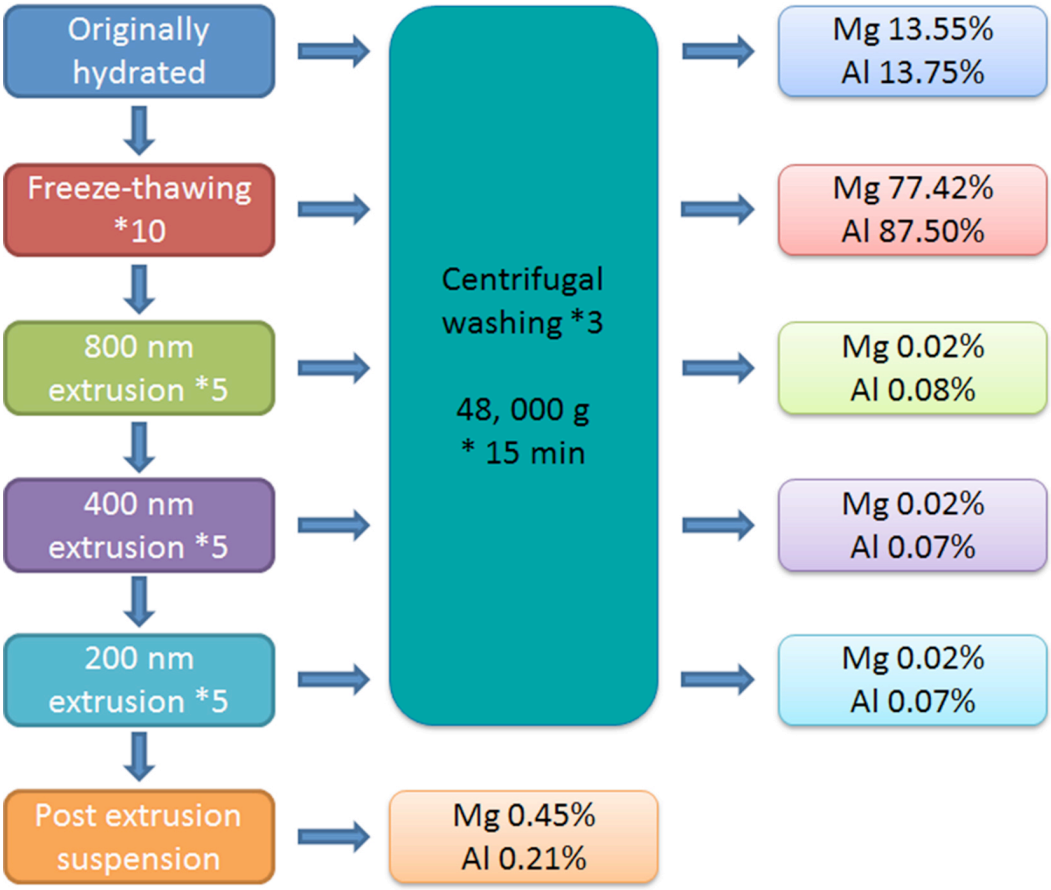

Figure A5 Encapsulation of sLDH in sLDH-liposome composites after sequential extrusion

After freezing-thawing treatment, encapsulation of sLDH in the composite increased to around 80 % from 13.6 %, which confirmed the complexation of sLDH with lipids during freezing-thawing process with time. Similar to the results before, encapsulation after extrusion was lower than 0.5 %, especially after suspensions were subjected to 3 times of centrifugal washing, which also confirmed the complexation of sLDH with lipids during freezing-thawing cycles

A3.2 MLVs to SUVs by probe sonication

About 50 mg of EPC was dissolved in 5 mL of chloroform for forming thin lipid film, then 5 mL of sLDH-1% FITC was added for hydration. After the suspension was standing at room temperature for 30 min, the suspension was treated by probe sonication (100% amplitude) for 27 min in a mode of 20 s ON 20 s OFF to avoid suspension overheat. The liposomal vesicle size is 110 to 130 nm in diameter according to *Z*-average. Then 1 mL of the above suspension was centrifuged and washed by 1 mL of deionised water for 3 times at 16,000 g for 10 min. The supernatant after centrifugation were supernatant 1, 2, 3 and 4 respectively. The final pellet was redispersed in 1 mL of DI water. All the supernatants and final pellet dispersion were analysed by UV-vis for FITC concentration (10% of Trition X-100 was added to final Triton X-100 concentration of 1% to break down the liposomal vesicle structure). The percentages of FITC in each partition indicated the sLDH particle distribution in each partition.

Table A6 Size distribution of liposome-sLDH-FITC particles

Sample Name	Z-Ave	PdI	Intensity Mean	Number Mean	Volume Mean
	d.nm		d.nm	d.nm	d.nm
liposome-sLDH-FITC_15 min sonication	185	0.419	300	45.9	275
liposome-sLDH-FITC_27 min sonication	118	0.242	200	50.2	293
liposome-sLDH-FITC_pellet redispersion	205	0.268	269	112	306

The size distribution of liposome-sLDH-FITC particles is shown in Table A6. After 27 min of probe sonication, the sLDH-FITC-liposome composites with free sLDH-FITC NPs show good size distribution with *Z*-average size around 120 nm. After the suspension was subjected to ce

ntrifugal washing, the redispersed pellet (supposed to only contain sLDH-FITC-liposome composites) also possessed a good size distribution with Z-average size ~ 200 nm.

The FITC indicated sLDH distribution in sLDH-liposome composites was shown in Table A7. More than 70% of FITC was found in the first supernatant separated from sLDH-liposome suspension, which meant most of the sLDH-FITC NPs were free in the suspension, without encapsulated inside liposomal vesicles or attached on the liposomal surfaces. While less and less FITC was detected in the following washing supernatant, 7%-11% in second supernatant, 4%-6% in third supernatant, ~ 2% in fourth supernatant, which might be sLDH-FITC NPs that attached on the surface of liposomal vesicles, so that being washed away gradually. The sLDH-FITC left in the final pellet was ~ 10% (indicated by FITC), which implied ~ 10% of sLDH-FITC NPs were encapsulated inside the liposomal vesicles; this was partly consistent with the results obtained from ICP-AES test of Mg and Al concentrations.

Table A7 sLDH distribution in composite sLDH-liposome system and sLDH encapsulated in SUVs, characterised by FITC using UV-vis spectrometer

	sLDH %	
	Batch 1	Batch 2
Supernatant 1	71.7	76.7
Supernatant 2	7.39	10.5
Supernatant 3	4.40	5.38
Supernatant 4	1.89	2.08
Final pellet	8.89	12.2
Total recovery	94.3	107

Figure A6 shows the cryo-TEM image of sLDH-liposome composites by hydration of thin lipid film (HTLF) method. Few sLDH NPs were seen located inside the liposomal vesicles (which were really encapsulated inside the vesicles or in small probability, in the front or behind the liposomal vesicles), but most of them were attaching on the surface of liposomal vesicles or even piled with liposomal vesicles deformed in between the layers. Many sLDH NPs were observed like standing on the grid as a side view, which is because the grid was upright when sample was dropped on it, and the sLDH NPs tended to

horizonal plate status/shape in the suspension. This is the reason why we always see top view of LDH NPs with hexagonol morphology under normal TEM.

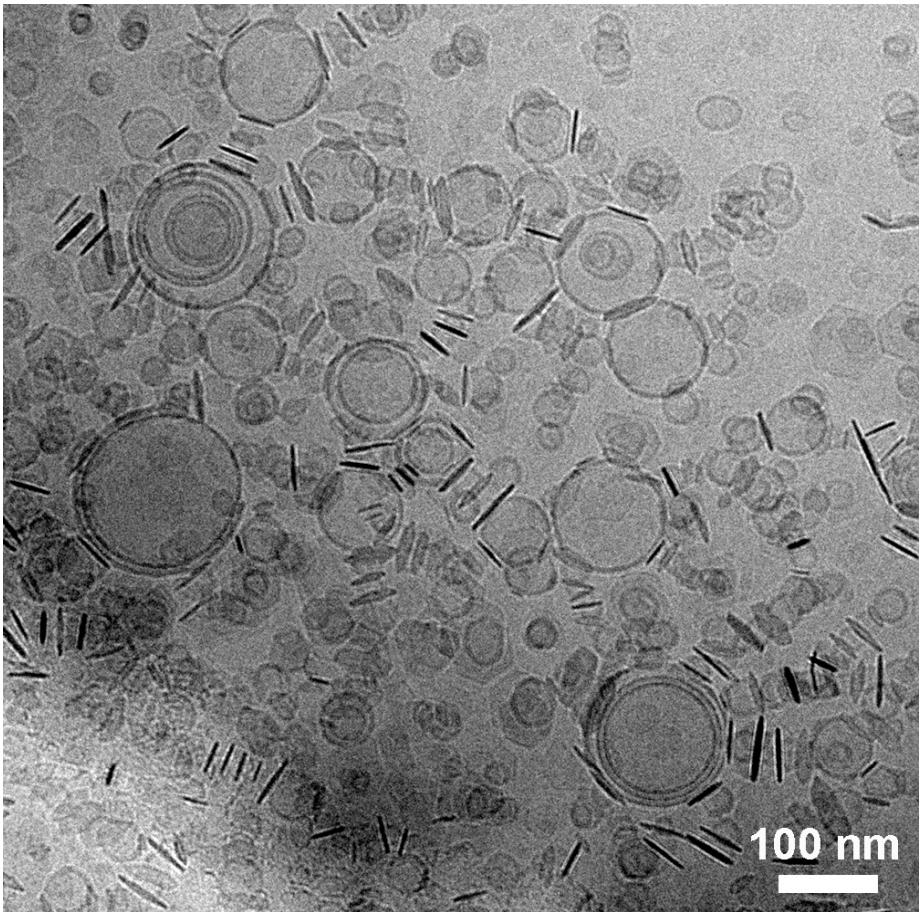

Figure A6 Cryo-TEM image of sLDH-liposome composite by HTLF method, composites washed by centrifugation, followed by size reduction via probe sonication

A4 Summary

sLDH-liposome composites were attempted by hydration of thin lipid film (HTLF) method. Encapsulation of sLDH NPs up to 30% were obtained, and the encapsulation was dependent on sLDH suspension volume and concentration used. However, commonly used extrusion is not a proper way to reduce the size of liposomal vesicles from multilamellar vesicles to unilamellar vesicles, because the sLDH-liposome complexes easily block the pores of filter membranes, especially under high pressure. Probe sonication is an effective and efficient size reduction method, but small vesicles were normally obtained, along with low encapsulation of sLDH NPs.

References

1. Li, C. & Deng, Y. A novel method for the preparation of liposomes: Freeze drying of monophase solutions. *Journal of Pharmaceutical Sciences* **93**, 1403-1414 (2004).

2. Cui, J., Li, C., Deng, Y., Wang, Y. & Wang, W. Freeze-drying of liposomes using tertiary butyl alcohol/water cosolvent systems. *International Journal of Pharmaceutics* **312**, 131-136 (2006).

3. Wang, T. et al. Preparation of submicron unilamellar liposomes by freeze-drying double emulsions. *Biochimica et Biophysica Acta (BBA) - Biomembranes* **1758**, 222-231 (2006).

4. Wang, Z., Deng, Y., Sun, S. & Zhang, X. Preparation of hydrophobic drugs cyclodextrin complex by lyophilization monophase solution. *Drug Development and Industrial Pharmacy* **32**, 73-83 (2006).

5. Wu, S.Y. et al. Development of a novel method for formulating stable siRNA-loaded lipid particles for *in vivo* use. *Pharmaceutical Research* **26**, 512-522 (2009).

6. Stachowiak, J.C. et al. Unilamellar vesicle formation and encapsulation by microfluidic jetting. *Proceedings of the National Academy of Sciences of the United States of America* **105**, 4697-4702 (2008).

7. CORTESI, R. Preparation of liposomes by reverse-phase evaporation using alternative organic solvents. *Journal of Microencapsulation* **16**, 251-256 (1999).

8. Canova-Davis, E., Redemann, C.T., Vollmer, Y.P. & Kung, V.T. Use of a reversed-phase evaporation vesicle formulation for a homogeneous liposome immunoassay. *Clinical Chemistry* **32**, 1687-91 (1986).

9. Pidgeon, C., McNeely, S., Schmidt, T. & Johnson, J.E. Multilayered vesicles prepared by reverse-phase evaporation: liposome structure and optimum solute entrapment. *Biochemistry* **26**, 17-29 (1987).

10. Giulio, A.D. et al. Encapsulation of ampicillin in reverse-phase evaporation liposomes: a direct evaluation by derivative spectrophotometry. *International Journal of Pharmaceutics* **74**, 183-188 (1991).

11. Pupo, E. et al. Preparation of plasmid DNA-containing liposomes using a high-pressure homogenization-extrusion technique. *Journal of Controlled Release* **104**, 379-396 (2005).

12. Magotoshi, M., Abu-Zaid, S.S. & Noriaki, T. Size and permeability of liposomes extruded through polycarbonate membranes. *International Journal of Pharmaceutics* **17**, 215-224 (1983).

13. Jousma, H. et al. Characterization of liposomes. The influence of extrusion of multilamellar vesicles through polycarbonate membranes on particle size, particle size distribution and number of bilayers. *International Journal of Pharmaceutics* **35**, 263-274 (1987).

14. Olson, F., Hunt, C.A., Szoka, F.C., Vail, W.J. & Papahadjopoulos, D. Preparation of liposomes of defined size distribution by extrusion through polycarbonate membranes. *Biochimica et Biophysica Acta (BBA) - Biomembranes* **557**, 9-23 (1979).

15. Mui, B., Chow, L. & Hope, M.J. in Methods in enzymology (ed. Nejat, D.) 3-14 (Academic Press, 2003).

16. Hope, M.J., Bally, M.B., Webb, G. & Cullis, P.R. Production of large unilamellar vesicles by a rapid extrusion procedure. characterization of size distribution, trapped volume and ability to maintain a membrane potential. *Biochimica et Biophysica Acta (BBA) - Biomembranes* **812**, 55-65 (1985).

17. Guo, Y. et al. Dimension control of glycolipid nanotubes by successive use of vesicle extrusion and porous template. *Chemistry of Materials* **18**, 1577-1580 (2006).

18. Jaskiewicz, K. et al. Incorporation of nanoparticles into polymersomes: size and concentration effects. *Acs Nano* **6**, 7254-7262 (2012).